2023-08-01

Growth Of Purple Sulfur Bacteria Allochromatium Vinosum On Solid Phase Metal Sulfides As Sulfur And Electron Sources

Hugo Alarcon
University of Texas at El Paso

GROWTH OF PURPLE SULFUR BACTERIA ALLOCHROMATIUM VINOSUM ON SOLID PHASE METAL SULFIDES AS SULFUR AND ELECTRON SOURCES

HUGO ALARCON

Doctoral Program in Environmental Sciences and Engineering

APPROVED:

Jonathon Mohl, Ph.D., Chair

Jie Xu, Ph.D.

Jorge Gardea-Torresdey, Ph.D.

Jennie McLaren, Ph.D.

Ming-Ying Leung, Ph.D.

Stephen L. Crites, Jr., Ph.D.
Dean of the Graduate School

GROWTH OF PURPLE SULFUR BACTERIA ALLOCHROMATIUM VINOSUM ON SOLID PHASE METAL SULFIDES AS SULFUR AND ELECTRON SOURCES

By

HUGO ALARCON VALENZUELA, PH.D.

DISSERTATION

Presented to the Faculty of the Graduate School of

The University of Texas at El Paso

in Partial Fulfillment

of the Requirements

for the Degree of

DOCTOR OF PHILOSOPHY

ENVIRONMENTAL SCIENCE AND ENGINEERING

THE UNIVERSITY OF TEXAS AT EL PASO

August 2023

Acknowledgments

I would like to take this opportunity to express my heartfelt gratitude to all those who have supported and contributed to my journey toward obtaining my doctoral degree. It is with immense pleasure that I acknowledge the invaluable assistance and unwavering support I have received throughout this challenging yet fulfilling endeavor.

First and foremost, I extend my deepest appreciation to Dr. Jie Xu for her guidance, patience, expertise, and unwavering commitment and support to my academic and personal growth. I wouldn't be here if it weren't for her dedication as an exceptional advisor. Her continuous encouragement, insightful feedback, and commitment to excellence have played a vital role in shaping both my research and my development as a scientist. I am genuinely grateful for her mentorship and the opportunities she has provided me.

I am profoundly grateful to Dr. Jonathon Mohl for his invaluable guidance and support, particularly in the challenging area of bioinformatics where I lacked background knowledge. His expertise and mentorship were instrumental in helping me navigate this complex field and complete my research project. I would also like to express my heartfelt appreciation to my other committee members, Dr. Jorge Gardea-Torresdey, Dr. Jennie McLaren, and Dr. Ming-Ying Leung, for their valuable support and counsel, which significantly contributed to the successful outcome of my doctoral journey.

I am truly grateful for the unwavering emotional support I received from my family throughout the challenging moments of my doctorate. Their love, understanding, and encouragement provided me with the strength to persevere, even when I contemplated leaving the program. During these difficult times, when I faced personal setbacks, health issues, and the added stress of the pandemic, their presence and reassurance were invaluable. Their belief in my abilities

and their constant reminders of my resilience helped me overcome obstacles and regain my determination. I am deeply thankful for their unwavering support, even though I may not have fully shared the extent of the challenges I faced. Their unwavering love and encouragement helped me reach the finish line.

I am indebted to my loving and caring mother, whose love, sacrifices, and unwavering belief in my abilities have been a constant source of motivation. Your endless support and encouragement have been the reasons behind my accomplishments, and I owe my success to your firm belief in me. I thank you for being such a strong and loving individual and wish you the very best in this coming new phase of your life. You fully deserve it; be happy, I would also like to express my heartfelt appreciation to my admirable brother. Despite being the youngest, he has always been a source of inspiration. You have been a beacon of light for me through your fortitude in challenging a hard life, achieving outstanding accomplishments, and for being a loving, protective father. I know you will reach even higher places. I love you very much.

I would also like to thank my dad for guiding me towards higher education and nurturing my passion for life sciences. Thank you for your care and for nurturing our relationship, Dad.

Furthermore, I extend my sincere thanks to all my lab mates and colleagues who have shared this academic journey with me. Your collaboration, intellectual discussions, and camaraderie have enriched my research experience. I am grateful for the knowledge-sharing, support, and friendships that have blossomed within our lab.

Finally, I would like to acknowledge everyone who has offered their assistance and guidance along the way. To all the friends, mentors, administrative staff, and individuals who have supported me in various capacities, I extend my heartfelt appreciation. Your contributions, whether big or small, have played a significant role in shaping both my research and personal growth.

To all those mentioned above and countless others who have touched my life during this journey, please accept my deepest gratitude. Your support, encouragement, and belief in my abilities have been pivotal in reaching this milestone. I am forever indebted to each and every one of you

Abstract

Purple sulfur bacteria (PSB) are photosynthetic microorganisms known for their vital roles in geochemical cycles, especially the sulfur cycle, within anoxic photic environments. PSB are also key contributors to the nitrogen, carbon, and oxygen cycles. This study focuses on the autotrophic growth of *Allochromatium vinosum*, a model strain of PSB, that utilize solid-phase metal sulfides (MS) as both sulfur and electron donors. Through characterizing the growth profiles of *A. vinosum* on pyrite (FeS_2), nickel sulfide (NiS), and iron monosulfide (FeS) nanoparticles, respectively, and investigating the bacteria-MS interaction mechanisms, this work expands our current knowledge of the metabolic capabilities and flexibility of *Allochromatium vinosum*, provides new insight into the mechanisms of bacterial-nanoparticles interactions, and further, possibly opens new research avenues in bacterial extracellular electron transfer and artificial photosynthesis. In this study, growth profiles findings coupled with transcriptome analysis showed that *A. vinosum* could use pyrite and NiS for autotrophic growth, while conflicting findings were found for FeS. Optical density plots of biotic pyrite and NiS showed twice the growth compared to the negative control. IC, ICP-MS, XPS and HR-TEM served as complementary findings providing supporting evidence, along with sulfur oxidation gene profiles, of the transformations experienced by MS results of exposure to *A. vinosum*, as well as providing evidence of an active sulfur oxidation pathway. In the case of FeS, OD did not go beyond growth displayed by the negative control implying that growth in FeS might not go beyond the effects supporting the growth in the negative control. Nonetheless, evidence points to active sulfur oxidation pathway in this metal system through XPS increase of the polysulfide portions compared to the abiotic control, as well as the increase in sulfate concentration to ~400uM on IC. Furthermore, all systems displayed a severe downregulation of photosynthetic genes *puf* and *puc* but comparable expression

values for carotenoid genes to the positive control. Finally, all MS systems displayed a collection of redox active cytochromes and hydrogenases, some of which were associated with the membrane (LXXC), redox activity (CXXCH) and others with secretory pathway (signal peptide). Other genes such as transporters genes, pili and hypothetical proteins were used to generate a more complete assessment of the utilization of MS by *A. vinosum*, as well collection of evidence which proteins are potentially involved in the unidentified electron transfer pathway that allows for utilization of NiS and pyrite, while more studies need to be carried to assess the FeS system.

Table of Contents

List Of Figures

List Of Tables

Chapter 1 Introduction and Literature Review

1.1 Purple sulfur bacteria and their importance in the environment

Purple sulfur bacteria (PSB) are a group of photosynthetic bacteria that are found in aquatic environments such as lakes, ponds, and estuaries. They are called PSB because they contain pigments that absorb light in the green part of the spectrum and reflect light in the purple part of the spectrum. This is a group of gram-negative bacteria belonging to the phylum *Proteobacteria* and are capable of nitrogen fixation (Dincturk *et al.*, 2011). Some members of this group are highly adaptable and although favoring the oxidation of reduced sulfur compounds (i.e., hydrogen sulfide and dissolved sulfide), can utilize a range of electron donors for growth. The electron donors that various PSB can utilize include sulfide, elemental sulfur, thiosulfate, hydrogen, organic acids, ferrous iron, and nitrite (Ehrenreich *et al.*, 1994 and Daldal *et al.*, 2008). Purple sulfur bacteria are widespread in anoxic photic zones and can survive extreme environments like salt marshes and hot springs (Seitz *et al.*, 1991 and Magian *et al.*, 1984). Most commonly, PSB are found in stratified water bodies, thriving in anaerobic layers where light and sulfide meet, but they also have been found in microbial mats where sediment layers protect them from oxygen in the environment, sulfate reducers provide sustenance, and light can still reach them (Hunter *et al.*, 2009). One characteristic of all PSB is the formation of elemental sulfur globules as an obligate intermediate, which are oxidized to sulfate in succeeding metabolic steps. Purple sulfur bacteria may belong to either *Ectothiorhodospiracea* or *Chromaticeae* family, the former of which deposit sulfur globules outside of the cell membrane whereas the latter deposit sulfur globules inside the periplasmic space of the cells.

In the context of primary productivity, PSB are significant due to their ability to perform anoxygenic photosynthesis. Purple sulfur bacteria can utilize reduced sulfur species as electron

donors and harness light energy to drive the generation of organic molecules, ATP, and oxidized sulfur compounds (Dahl *et al.*, 2008). This metabolic process not only supplies energy to the PSB themselves but also plays a vital role in the carbon cycle within the ecosystem. The organic compounds produced by PSB serve as a valuable food source for other organisms, thereby supporting the overall food web dynamics in aquatic environments (Overmann *et al.*, 1997). Furthermore, the oxidation of hydrogen sulfide (H_2S) by PSB has important implications for maintaining the ecological balance in aquatic systems. By converting H_2S into less toxic forms, these bacteria help to reduce the levels of sulfide in their environment, creating a more favorable habitat for other organisms to thrive (Overmann *et al.*, 1997).

Purple sulfur bacteria exhibit metabolic flexibility, allowing them to adapt their growth strategies depending on the availability of substrates in their surroundings. They can engage in both photolithotrophic and photoheterotrophic growth, enabling them to utilize a diverse range of organic and inorganic compounds as energy sources. Purple sulfur bacteria can carry limited photoheterotrophic growth using non-fermentable organic acids, amino acids, carbohydrates, fatty acids, and alcohols. Photoheterotrophic growth can be promoted by the presence of vitamins and yeast extract a common ingredient in PSB media due to rich content of organic compounds (Madigan *et al.*, 2009). This metabolic versatility enhances their ecological success and ability to thrive in various environmental conditions.

1.2 Marine Ecosystems

Purple sulfur bacteria are usually found in euxinic environments where light can reach. Regarding sulfur cycling, PSB often coexist and interact with sulfur-reducing bacteria. Sulfur-reducing bacteria utilize sulfur compounds, including sulfates and sulfur intermediates, as electron acceptors in anaerobic respiration. Because of its role in reducing sulfide-based toxicity, introducing organic carbon and nitrogen, PSB indirectly affect the growth and metabolism of other

microorganisms in the ecosystem. Heterotrophic bacteria are typically associated with the decomposition of organic matter, including the organic compounds produced by PSB. Additionally, PSB may have complex relationships with other microbial groups involved in nutrient cycling and ecosystem dynamics, including nitrogen-fixing bacteria, archaea, and protists. The precise nature and extent of these interactions can vary depending on local environmental conditions and the specific microbial community present.

1.2.1 Intertidal mats and sediment stabilization

Within sediments, PSB thrive in oxygen-depleted environments, actively participating in vital biogeochemical processes. They establish close associations with heterotrophic bacteria, which rely on the organic matter produced by PSB as a valuable carbon source. This relationship ensures the cycling of nutrients and energy within the sediment ecosystem. Furthermore, PSB contribute to the stabilization of intertidal sediments through the secretion of extracellular matrices (Hubas *et al.*, 2013). These organic networks create a favorable environment for the coexistence of diverse organisms, including diatoms, cyanobacteria, and heterotrophic bacteria. In sediment mats with high density, the top oxic layers are approximately 1 mm thick, allowing for the penetration of light while providing a barrier for oxygen diffusion and permitting PSB to be metabolically active in the anoxic layer below. In mats with medium and low density, the thickness of the layers can reach around 1-2 cm, providing suitable conditions for PSB growth (Hubas *et al.*, 2013). PSB have also been spotted in cave systems in aphotic zones where they were found to be involved in nitrogen metabolism (Marques *et al.*, 2019). These complex interactions and ecological roles highlight the significance of PSB in sediment ecosystems. Their participation in biogeochemical processes and their influence on the surrounding microbial community contribute to the overall functioning and stability of sediments, ensuring the efficient cycling of nutrients and the sustained productivity of these environments.

1.3 Lakes

In freshwater lakes, PSB are often found in the hypolimnion, the deeper, cooler, and oxygen-depleted layer. PSB coexist with green sulfur bacteria, which are also photosynthetic bacteria. While PSB utilize sulfur compounds as electron donors, green sulfur bacteria utilize hydrogen and organic acids. Together, they contribute to the carbon and sulfur cycling in lakes. PSB and green sulfur bacteria form stratified layers within the water column, with PSB usually residing deeper due to their preference for lower light intensities. The differential distribution of these bacterial groups is influenced by the availability of light and electron donors. The coexistence of PSB and green sulfur bacteria underscores the intricate dynamics of microbial communities in freshwater lakes.

PSB have also been observed in the chemocline layer of stratified meromictic lakes, such as Lake Cadagno. This lake showcases a diverse bacterial composition, encompassing 15 phyla, 40 classes, and 115 genera. *Proteobacteria, Chlorobi, Verrucomicrobia*, and A*ctinobacteria* are prominent groups in this lake. *Proteobacteria* and *Verrucomicrobia* dominate in the oxygenated surface waters and are involved in sulfur cycling and nutrient cycling, respectively. *Chlorobi*, or green sulfur bacteria, play a role in sulfur cycling in deeper layers of the lake. *Actinobacteria* contribute to the degradation of organic matter and nutrient cycling. *Proteobacteria* exhibit diverse metabolic capabilities, including sulfur cycling, nitrogen fixation, and carbon cycling. *Alphaproteobacteria* prevail in the mixolimnion, while *Gammaproteobacteria* dominate the chemocline and monimolimnion. These bacteria thrive in the anaerobic or microaerophilic conditions present in stagnant contaminated lakes. The bacterial diversity is particularly high in the anoxic chemocline and the bottom layer of Lake Cadagno (Danza *et al.*, 2018).

1.4 Metal sulfides and their role in biogeochemical cycling

Sulfide sediments, which constitute the most abundant sulfur fraction on Earth, hold significant importance in the sulfur cycle and exert considerable influence on other nutrient cycles (Bickle *et al.*, 1994). Among the microorganisms in the world, sulfate reducing bacteria are particularly abundant, given that sulfate ranks as the third most prevalent ion in seawater, following sodium and chloride (Bickle *et al.*, 1994). Sulfate reducing bacteria play a crucial role in catalyzing the conversion of soluble sulfate in the oceans to H2S. This H2S, in turn, interacts favorably with metals to form metal sulfide precipitates (Muyzer *et al.*, 2008; Kobayashi *et al.*, 1983; Utgikar *et al.*, 2002), or alternatively, it can be utilized by sulfur oxidizing bacteria for sulfate production, as observed in PSB (Muyzer *et al.*, 2008).

Sulfur nanoparticles, when considered in the context of environmental sources, arise from diverse origins such as volcanoes, hydrothermal vents, caves, mineral erosion, and anoxic aquatic environments where abiotic sources or sulfate reducing bacteria contribute to the production of metal sulfide nanoparticles (e.g., Gartman *et al.*, 2013). Over time, these nanoparticles gradually aggregate, leading to sedimentation and diagenesis. Sulfides exist in nature as a wide range of minerals, including sphalerite (ZnS), chalcopyrite (CuFeS2), chalcocite (Cu2S), pyrite (FeS2), covellite (CuS), and many others. However, due to the overwhelming abundance of iron, pyrite stands out as the most prevalent sulfidic mineral and is considered the largest sulfur sink in the world. It is estimated that approximately 300 million tons of sulfide are sedimented annually, with 96% of it associated with microbial sulfate reduction in aquatic systems (Rickard *et al.*, 2017). To put the scale of sedimentary sulfide formation in oceans into perspective, the total abundance of sulfate within the sulfur cycle is dwarfed, accounting for only 0.04% (Rickard *et al.*, 2017). The vast extent of sedimentary sulfide formation in oceans has profound and intricate implications for sulfur, as it represents the largest reservoir of trapped sulfide globally. Furthermore, sulfidic

minerals are tightly linked to the carbon cycle, as bacteria have evolved to utilize sulfur compounds, thereby influencing primary production, similar to PSB. Lastly, sedimentary sulfide formation greatly affects the oxygen cycle, as sulfidic minerals are susceptible to oxidation.

The abundance of metal sulfides in oceans serves as a crucial indicator of metal transport in saline, predominantly anoxic aquatic environments. Furthermore, specific metal sulfides have been discovered to exhibit relative stability even in suboxic and oxic environments, thereby comprising a significant component of the metal content in rivers worldwide (Hochella *et al.*, 2008). It is important to note that sulfide and metals, when present individually, can be toxic to biological systems. However, the formation of metal sulfides plays a vital role in sequestering such toxicities, providing a key process for mitigating their adverse effects.

The maintenance of biodiversity in the biosphere relies on the delicate chemical equilibrium of all nutrient cycles. Any significant alterations to these cycles can potentially disrupt environmental conditions to a degree that would lead to the collapse of most life forms. In the case of the sulfur cycle, a drastic impact occurred approximately 252 million years ago during the Permian-Triassic mass extinction event (Wignall *et al.*, 2002). This event was characterized by increased volcanic eruptions, resulting in the combustion of massive coal deposits and the subsequent release of substantial quantities of heavy metals, elevated mobile sulfur levels, and acid rain. The heightened levels of oxidized sulfur led to an increase in H2S levels originating from sulfate-reducing bacteria, further contaminating bodies of water and elevating atmospheric concentrations of H2S (Lee *et al.*, 2005). The elevated atmospheric H2S levels, in turn, contributed to the depletion of the ozone layer (Lee *et al.*, 2005). During this period, the dramatic increase in sulfur and carbon in the atmosphere created toxic environmental conditions that led to a mass extinction event. As the largest fraction of sulfur on Earth, sulfidic minerals play a pivotal role in

maintaining the current redox and chemical composition of the environment, allowing life to thrive.

1.5 Microorganisms that use minerals, solid phases, DIET, EET and other Lithotrophs strategies

1.5.1 Electrochemically active bacteria (EAB bacteria)

Electrochemically active bacteria (EAB) employ diverse mechanisms to utilize solid-phase materials, showcasing their adaptability and versatility. Reductive dissolution involves the microbial reduction of solid electron acceptors, releasing soluble metals and transferring electrons to microbial cells (Liu J *et al.*, 2022). Notably, direct contact between microbial cells and the electron acceptors facilitates electron transfer through outer membrane cytochromes like MtrC and OmcA (Jing X *et al.*, 2020). EAB, such as *Geobacter* and *Shewanella* species, proficiently employ this mechanism to impact metal cycling and environmental biogeochemistry (Ruey-an *et al.*, 2002 and Hu S *et al.*, 2020). On the other hand, mineral respiration involves the microbial reduction of solid minerals as a terminal electron acceptor, and enzymatic reduction is facilitated by specific mechanisms and proteins like reductases (Mitchell *et al.*, 2012 and Richardson *et al.*, 2013). This complex process holds significance for environmental biogeochemistry and potential biotechnological applications. Additionally, DIET, or direct interspecies electron transfer, enables efficient electron exchange between microorganisms, enhancing overall microbial activity and promoting metabolic cooperation through conductive pili, cytochromes, and conductive materials (Wang W, 2021). These mechanisms collectively highlight the unique abilities of EAB to harness energy and participate in crucial biogeochemical processes.

EET, extracellular electron transfer, bacteria are a type of EAB microorganism which utilize inorganic materials as their energy source for metabolism. Within EAB, there are solid

respiration bacteria that derive energy through electron transfer between the cell and solid-phase materials. Two main types of solid respirators are metal-reducing bacteria which transfer electrons from organic molecules to solid-phases (Lovley D *et al.*, 1987), and metal-oxidizing bacteria, which take electrons from solid-phases for energy metabolism (Hallbeck L *et al.*, 1990 and Deng R *et al.*, 2021).

EET, describes microbial bioelectrochemical processes in which electrons are transferred from the cytosol to the exterior of the cell. It is believed that heme-based electron transfer mechanisms are involved (Carlson *et al.*, 2012). Listeria monocytogenes uses a distinctive flavin-based EET mechanism to deliver electrons to iron or an electrode. In their analysis they proposed that specialized NADH dehydrogenase, which catalyzes electron exchange from cytosolic NADH to a membrane-localized lipid-soluble quinone derivative. This eventually leads to secrete flavins that shuttle electrons to acceptors that are not directly contacting the cell. It was found that through EET, bacteria are able to metabolize non-fermentable glycerol (Light *et al.*, 2018). Thus, this could be a strategy that cells use to metabolize extracellular substrates.

Lactiplantibacillus plantarum, a strain of bacteria, has been extensively studied for its ability to perform EET. Researchers investigated mutant strains of *L. plantarum* with deletions in the ndh2 and pplA genes, which are associated with iron reduction and anode reduction. Under EET conditions, these mutants exhibited a 79% increase in ATP production per mole of fermented mannitol, indicating a more efficient production of ATP during EET. This process combines features of both fermentation and respiration, resulting in a more oxidized intracellular redox balance. Additionally, the yield of fermentation products per cell was approximately two-fold greater under EET conditions, suggesting an enhanced production of fermentation products. These findings highlight the potential of L. plantarum for improved energy production and fermentation efficiency in EET-related applications (Tejedor S.H *et al.*, 2022)

In a study focusing on the EET-capable *Bacillus megaterium* strain LLD-1 in microbial fuel cells (MFCs), researchers discovered the presence of flavins in the culture suspension. These flavins were identified as electron shuttles that enhance the transfer of electrons to the electrode. The significance of flavins in EET was further confirmed by observing an increase in voltage and current output in MFCs when exogenous flavins were added to the system, particularly in MFCs inoculated with B. megaterium strain LLD-1. The study highlighted the essential role of flavins, along with S-layer associated c-type cytochromes, in facilitating efficient electron transfer in the context of EET (You L *et al.*, 2018).

1.5.2 EET proposed mechanisms

One of the ways electroactive microorganisms have been proposed to achieved shuttling of the electrons across membrane involved mtr genes. The Mtr pathway in *Shewanella odeinensis* bacteria consists of three key components: MtrA, MtrB, and MtrC. These proteins work together to facilitate the transfer of electrons from the cytoplasmic membrane to the bacterial surface. *MtrA* is a decaheme cytochrome located in the cytoplasmic membrane, while MtrB is a β-barrel protein that spans the outer membrane. MtrC, an outer membrane protein, physically interacts with MtrB and transfers electrons directly to surface iron atoms through its exposed heme iron atom. This pathway enables the bacteria to transfer electrons from the cytoplasmic membrane to minerals or other extracellular electron acceptors, as well as from extracellular electrodes back to the cytoplasmic membrane. The Mtr pathway also plays a role in biofilm formation and the formation of conductive networks called "nanowires," which allow for long-range electron transfer between cells (Shi L *et al.*, 2016).

Another pathway involved the use of flavinated proteins as electron shuttles. Flavin-based EET involves the transfer of electrons from cytosolic NADH to quinone molecules in the cell membrane. These quinones then transfer electrons to secreted Flavins, which act as shuttles to

transfer electrons to acceptor molecules that are not directly in contact with the bacterial cell (Shi L *et al.*, 2016).

The second pathway identified for EET involves outer membrane cytochromes, specifically the OmcA protein and other multi-heme c-type cytochromes. These proteins, found in various microorganisms including *Shewanella* species, are responsible for reducing extracellular electron acceptors, such as Fe(III) minerals, by transferring electrons from the cytoplasmic membrane to the outer membrane. The outer membrane cytochromes play a crucial role in establishing a direct connection between the microbial cell and the extracellular environment. They are thought to form a complex known as a "porin-cytochrome" complex, where the outer membrane cytochromes are embedded in the outer membrane, creating a conduit for electron transfer across the membrane (Shi L *et al.*, 2016).

The porin-cytochrome (Pcc) pathway in *Geobacter sulfurreducens* enables the transfer of electrons from the quinone and quinol pool in the cytoplasmic membrane, across the periplasm, and through the outer membrane to the bacterial surface. This pathway involves multi-heme c-type cytochromes, including OmaB, OmaC, OmcB, and OmcC, which form protein complexes with outer membrane proteins OmbB and OmbC. Interestingly, the proteins involved in the Pcc pathway have evolved independently from those in the Mtr pathway, despite serving similar functions (Shi L *et al.*, 2016).

The phototrophic iron oxidation pathway of *Rhodopseudomonas palustris* utilizes light energy and Fe(II) as an electron source to perform CO2 fixation. The pathway involves the genes *pioA* (similar to *mtrA*), *pioB* (similar to *mtrB*), and *pioC* (encoding an iron-sulfur protein). PioA and PioB are responsible for extracellular oxidation of Fe(II) and transferring the released electrons across the outer membrane to PioC. PioC then relays these electrons to the photoreaction center located in the inner cytoplasmic membrane (Shi L *et al.*, 2016).

The metal-oxidizing pathway of *Sideroxydans lithotrophicus* enables autotrophic growth by utilizing Fe(II) oxidation for energy production. The pathway involves the mto gene cluster, consisting of cymA, mtoA (similar to mtrA), mtoB (similar to mtrB), and mtoD (encoding a mono-haem c-Cyt). MtoA directly oxidizes Fe(II), including Fe(II)-containing minerals, while MtoD serves as a periplasmic c-Cyt that potentially transfers electrons from MtoA in the outer membrane to CymA in the cytoplasmic membrane. These findings suggest that MtoA, MtoB, MtoD, and CymA form a pathway that connects extracellular Fe(II) oxidation with quinone reduction in the cytoplasmic membrane of *S. lithotrophicus* (Shi L *et al.*, 2016).

In summary, EET processes provide bacteria with several advantages. EET allows for energy generation by transferring electrons to external electron acceptors, expanding the range of electron acceptors available for metabolism. It enables survival in low redox environments, where electron acceptors are rare, and promotes interactions between microbial species fostering nutrient cycling and energy exchange. These benefits enhance bacterial adaptation and enable thriving in diverse environments, emphasizing the significance of EET in bacterial physiology and ecology (Shi L *et al.*, 2016).

1.6 Research question and objectives

This research project aims to investigate the interaction between photosynthetic sulfide-oxidizers, specifically PSB, and metal sulfide nanoparticles in aqueous conditions. The study seeks to answer two key questions: (1) whether PSB can utilize various metal sulfides such as FeS, NiS, and pyrite as electron donors, and (2) what underlying mechanisms of interaction drive the bacterial scavenge of the metal sulfides. Demonstrating that PSB can utilize metal sulfides as the sole electron donor would provide evidence for an alternative pathway for sulfur and trace metals to be reintroduced into the water column, thus supporting other bacterial communities. Furthermore, uncovering the mechanism of sulfide release from nanoparticles would offer insights

into potential new sulfur utilization pathways within PSB that have not yet been characterized. The primary goals of my research project are:

1. investigating whether purple sulfur bacteria (PSB) can effectively utilize metal sulfide nanoparticles as the exclusive electron donor;
2. comparing the kinetics of sulfur utilization between soluble and insoluble sulfide sources;
3. exploring the potential pathways involved in the utilization of metal sulfide nanoparticles by bacteria.

By addressing these objectives, we aim to enhance our understanding of the metabolic capabilities of PSB and gain insights into the mechanisms underlying their interaction with metal sulfide nanoparticles.

1.7 Hypothesis

This research project aims to investigate several major hypotheses related to the interaction between *A. vinosum* (purple sulfur bacteria) and metal sulfide nanoparticles. The hypotheses to be tested include:

1. *A. vinosum* can utilize synthetic MS nanoparticles as the sole electron donor for growth (FeS, NiS and Pyrite)
2. *A. vinosum* can interact with the MS nanoparticle interface, leading to the release of metal ions and sulfur into the environment beyond mere dissolution effects (FeS, NiS and Pyrite)
3. The gene expression of *A. vinosum* will exhibit differences when exposed to MS nanoparticles compared to growth under soluble sulfide (FeS, NiS and Pyrite)

Through the investigation of these hypotheses, this study aims to provide insights into the metabolic capabilities and gene expression patterns of *A. vinosum* in relation to the utilization and interaction with metal sulfide nanoparticles.

By delving into the intricacies of the interaction between sulfide nanoparticles and PSB, we have the opportunity to uncover novel sulfur utilization pathways that were previously unknown within these bacterial species. This investigation could lead to a broader comprehension of the metabolic adaptability of PSB and, in turn, pave the way for potential biotechnological applications associated with sulfur-based processes. The discovery of these new pathways has the potential to expand our understanding of PSB's metabolic versatility and open avenues for further exploration and exploitation in various fields.

1.8 Implications of the work

1.8.1 Potential influence of microbes in our understanding of ancient earth

One of the challenges faced by geologists is the presence of inconsistencies in the geological record, which can sometimes contradict current theories (Rickard *et al.* 2017). The dominant approach used to understand ancient environmental conditions and determine rough dating estimates is through thermodynamic modeling (Rickard *et al.*, 2017). However, there are instances where rocks deviate from the expected narrative. For example, during the Great Oxygenation Event (GOE), the increase in atmospheric oxygen was believed to be supported by the presence of sulfates. Nonetheless, there are rock records with lighter sulfur isotopic compositions, which suggest the involvement of biogenic factors rather than relying solely on physical parameters like pressure, temperature, and redox conditions factors (Hurtgen M *et al.*, 2004; Caltech *et al.*, 2023). Another similar example was found in carbonate rock from the Neoproterozoic Era, where extensive carbonate formations emerged. However, isotopic studies conducted on carbonate rocks from this era revealed unexpectedly light carbon isotopic compositions, challenging the prevailing understanding of isotopic fractionation in rocks from that time (Hoffman P *et al.*, 1998). This discrepancy led to alternative hypotheses proposing links between the light isotopic compositions and phenomena like large-scale organic carbon burial and disruptions in the carbon cycle (Hoffman P *et al.*, 1998).

Sulfide sediment-associated minerals, like pyrite, have been used as proxies to infer environmental conditions during different geological eras and their connection to evolution of life (Rickard *et al.* 2017). Phylogenomic reconstructions have indicated shifts in gene presence, such as the transition from sulfite and thiosulfate-related genes in the early Archean to sulfate-related genes in the Neoarchean, which correlates with the hypothesis of significant oxygen levels favoring the prevalence of dissimilatory sulfate reduction (DSR) (Rickard *et al.,* 2017). Pyrite deposits enriched in light stable sulfur isotopes, indicating a biogenic nature involving DSR, were not globally abundant until after the Great Oxidation Event (GOE) (Philippot *et al.,* 2018). The microbial influence on isotopic ratios in rocks may have been underestimated. Microorganisms prefer metabolizing lighter isotopes due to lower energy requirements, which can lead to shifts in the isotope ratios. This interaction between microorganisms and solid-phase materials has significant implications for our understanding of ancient Earth's composition and can impact the accuracy of rock dating assessments (Open Press, 2019). Therefore, studying the co-evolution of microbial life and geological materials is essential for comprehensive interpretations of Earth's history and refining dating methods.

Pyrite is often used to reconstruct ancient environments. Geochemical signatures found in Pyrite are used as indicators of paleoenvironments (pyrite in sedimentary rocks – organics rich conditions for life vs low oxygen environments). One example of this would be relating variation in atmospheric oxygen levels and its relationship with trace elements in sedimentary pyrite. By looking at transition metal solubility and residence times in oxygen rich environments metals like molybdenum (Mo) and selenium (Se) are used to determine oxygen levels in ancient environments. Se/Co ratio was used by Cannel to back calculate marine oxygen concentration (Cannel *et al.,* 2022).

Through the investigation of the interaction between bacteria and metal sulfide

nanoparticles (MS-NP), the utilization of electron microscopy (EM) and crystallographic evidence has the potential to unveil rapid mineralogical changes that occur under milder conditions than previously considered by ancient earth geologists (Rickard, *et al.*, 2017). By observing the crystal structure alterations in MS nanoparticles, distinct characteristics can be identified, serving as valuable biosignatures for understanding the interactions between PSB and metal sulfides. These findings not only contribute to our knowledge of ancient earth but also have practical applications in field studies, enhancing our understanding of past environments and processes.

Furthermore, the increasing evidence of the co-evolution of bacteria and minerals may lead to the progressive re-evaluation of the geological record, reshaping our understanding of ancient earth and changes in geochemical cycles across time. This is very important because by understanding environmental changes in the past and their connection to biogeochemical cycles, scientists aim to predict future events and potentially reverse some effects caused by our increasing impact on these cycles. For example, sulfate levels have increased by 47% since the industrial revolution (Rickard *et al.*, 2017), leading to oxygen-depleted "death zones" poisoned by H2S. This change is mainly driven by global warming, which increases primary productivity, sulfate reduction, and the production of sulfide sediments, revealing a tendency of ocean/atmosphere deoxygenation and a sulfidic future.

1.8.2 Sulfide shift challenge to PSB during Neoproterozoic

The belief that the increased oxygen concentration after the GOE resulted in a shift from sulfidic oceans has raised questions about the environmental challenges faced by PSB during the Neoproterozoic era (Rickard *et al.*, 2017). With a decreasing sulfide pool and an increasing abundance of metal sulfides (MS), PSB would have needed to adapt to survive. This adaptation could potentially involve the utilization of abundant MS as an energy source. The accelerated genetic adaptations observed in bacteria, facilitated by both horizontal gene transfer, where

adaptations are inherited by offspring bacteria, and lateral gene transfer, where genetic adaptations can be shared across different species (OECD, 2010), provide support for the possibility of these adaptations. Species like *Geobacter*, known for their ability to utilize solid-phase materials for energy, already existed during this time. Considering that PSB can utilize solid-phase elemental sulfur globules for energy and are sulfur oxidizers, it is plausible to explore the hypothesis that PSB developed the capability to use MS for energy metabolism.

1.8.3 Significance and scope of the study

The potential revelation that PSB possess the ability to utilize solid-phase sources for energy has wide-ranging implications. If PSB is indeed electrochemically active, it could significantly impact various areas, including industrial applications such as synthesis, biofuel production, energy generation, and precious metal recovery. Additionally, this discovery would hold great scientific significance as it would prompt a reassessment of PSB's role in ecosystems, particularly in terms of their enhanced capacity for nutrient cycling. Moreover, understanding the potential impact of PSB on ancient Earth would further enhance our knowledge of the planet's history.

1.8.3.1 Industrial relevance of EAB bacteria

Microbial electrosynthesis, a process harnessing EET, allows to produce valuable chemicals and fuels from carbon dioxide using electricity as an energy source. This technology holds promise for sustainable bioproduction (Rabaey K *et al.*, 2010 and Lovley DR *et al.*, 2013). In microbial fuel cells, EET plays a crucial role as microorganisms oxidize organic matter and transfer electrons to anodes, generating electricity (Sun Y *et al.*, 2012). While not a major energy source yet, microbial fuel cells have potential applications in low-power devices. This work might reveal another important avenue in which PSB can use solid phases to enable growth. As the end goal of this work is to understand the mechanisms involved in the interaction between solid phases

and bacteria, the results may have critical implication for developing bacterial fuel cells in the future (Sharma *et al.*, 2018).

Additionally, EET pathways enable the recovery of metals from low-grade ores, aiding in the extraction of valuable metals like copper and gold (Shin D *et al.*, 2013). Furthermore, EET can be employed in environmental remediation, facilitating the immobilization of toxic metals, such as uranium, by stimulating the activity of microorganisms for the remediation of contaminated sites (Zou L *et al.*, 2021).

Interspecies electron transfer (IET) has been shown to have potential for industrial applications as affordable alternatives for the formation of methane from organic wastes like wastewater or solid waste, which rate can be enhanced by the addition of conductive materials. For instance, research has shown that magnetite (Fe_3O_4) nanoparticles can serve as conduits for direct interspecies electron transfer (DIET), acting like cables that facilitate electron exchange between cells and accelerating the metabolic rates of microbial communities in natural environments (Chen L *et al.*, 2022). This phenomenon has significant implications for anaerobic digestion processes, as DIET can enhance performance by promoting efficient electron transfer between microorganisms, leading to improved conversion of organic matter into methane. Conductive iron materials, such as biochar and magnetite, have been found to facilitate DIET and effectively increase methane yield in anaerobic digestion systems (Chen L *et al.*, 2022). These findings highlight the potential of nanoparticles to enhance microbial interactions and metabolic processes, offering insights into the optimization of various environmental and industrial applications. Metatranscriptomic and community composition analysis suggested that DIET was the primary mechanism for interspecies electron exchange in anaerobic digesters converting brewery waste to methane (Chen L *et al.*, 2022). Thus, DIET-capable microorganisms are considered an attractive low-cost alternative for methane generation from organic waste (Gahlot

et al., 2021). In addition, the addition of carbon materials, such as biochar and activated carbon, is commonly used to enhance methanogenesis (Wang W *et al.*, 2021).

1.8.3.2 Biomining

Biomining, which involves the use of microorganisms to extract valuable metals from sulfidic ores and minerals, presents a more environmentally friendly and economically viable alternative to conventional mining methods. Sulfidic ores, including pyrite, chalcopyrite, sphalerite, and galena, are abundant sources of metals such as copper, zinc, and lead, which find wide-ranging applications across various industries.

Copper, zinc, lead, and precious metals are valuable metals extracted from sulfidic ores, each playing a crucial role in different industries. Copper's excellent conductivity and corrosion resistance make it essential in electrical and plumbing systems. Zinc is widely used in galvanized steel for construction and alloy production, while lead finds applications in batteries, construction materials, and ammunition. Additionally, sulfidic ores can contain precious metals like silver, gold, and platinum group metals, which have high intrinsic value and find diverse applications in various technologies. These metals contribute significantly to industrial sectors, including electronics, construction, and energy production.

While the scalability of using anaerobic PSB for biomining may be a consideration, their potential to respire metal sulfides offers the possibility of recovering valuable metals from low-grade or complex sulfidic ores at reduced costs. PSB, being photosynthetic, utilize light and carbon dioxide alongside sulfidic minerals for their metabolism. Certain PSB strains, like *Halorhodospira halophila*, thrive in marine environments, enabling the use of seawater as a growth medium and further reducing operational expenses.

The advantages of biomining extend beyond cost-effectiveness. It represents a sustainable and environmentally friendly approach to mineral extraction, minimizing environmentally

damaging practices associated with traditional mining, such as open-pit mining and the use of harmful chemicals. The ability of PSB to selectively oxidize sulfide minerals can aid in the remediation of mine tailings and mitigate environmental issues like acid mine drainage resulting from sulfide mineral oxidation. Furthermore, PSB-mediated biomining has the potential to significantly reduce energy consumption and greenhouse gas emissions typically associated with conventional mining processes.

The possibility of using PSB biomining would hold promise as a sustainable and economically viable alternative method for extracting valuable metals from sulfidic ores. The wide range of metals recoverable from these ores, including copper, zinc, lead, and precious metals, reinforces the economic appeal of biomining. Additionally, the environmental benefits, reduced operational costs, and potential for lower energy consumption make PSB-mediated biomining an attractive alternative to traditional mining practices.

1.8.3.3 Enhanced ecological contribution

Although PSB already hold an important place in aquatic systems contributing by generating organic molecules, reducing toxic sulfide levels and converting them to sulfate a sulfur source for bacteria and to a lesser extend for some PSB species contributing to the nitrogen pool by fixating nitrogen gas. The role of these bacteria may extend what is currently know about them if they are classified as EET capable microorganisms.

Some EET capable microorganisms have been shown to share their electrons with other bacteria which have beneficial results, which the literature has defined as IET. Within IET, there are two main types, DIET and mediated interspecies electron transfer (MIET). Specifically, the difference between DIET and MIET is that the first involves electron sharing with other bacteria from one cell to the next through structures like conductive pili or proteins , while MIET relies on mediator molecules to span the space between them and carry electrons that way. This places

bacteria in our microbiome and in nature with the potential to form complex networks stabilized by extracellular matrix structures with embedded conductive materials like certain minerals, in which bacteria can share electrons resulting in an elegant way to maximize energy harvesting from metabolic processes (Buranaki *et al.*, 2007; Kato *et al.*, 2012).

Although a novel area of study, co-culture studies have shown that coupling IET/EET microorganisms with other species like methanogens has allowed bacteria to use fermentative pathways using molecules that under normal culture conditions cannot be metabolized. One such co-culture study where IET active *Geobacter* promoted the metabolism of a methanogen. Under normal conditions, *Methanosaeta harundinacea* is known to produce methane solely from acetate, utilizing the reduction of carbon dioxide as the primary pathway for methane production. However, when co-cultured with *Geobacter metallireducens*, a different metabolic behavior was observed. The co-culture was found to syntrophically metabolize ethanol via DIET. Interestingly, the co-culture was also capable of utilizing propanol and butanol as energy sources for methanogenesis. This expanded the range of substrates that *M. harundinacea* could utilize for methane production. The specific mechanisms enabling this metabolic versatility were not discussed in the referenced paper. Nonetheless, similar results have been observed in other co-cultures, where a DIET-capable microorganism facilitates the utilization of metabolites that would not be accessible under normal circumstances. For example, co-cultures of *G. metallireducens* and *Methanosarcina barkeri* have been shown to metabolize propanol and butanol (Wang, L *et al.* 2016). The result of expanding their metabolic capabilities through IET is powerful and hints at a key factor in maintaining thriving ecosystems. Thus, IET capable microorganisms either through DIET or MIET could potentially be key members in microbial ecosystems. It's important to highlight that I couldn't find any literature detailing the mechanisms of how IET favored non-EET bacteria's energy

metabolism and enhanced their capacity of utilizing more substrates in what seem to be fermentative pathways.

Cells are extremely efficient at harvesting energy from redox reactions and thus have a heavy collection of cytochromes, hydrogenases, and other reversible redox-capable proteins to undertake these processes. The redox reactions of key molecules, such as glucose and other nutrients, are intricately linked to the synthesis of high-potential energy molecules like ATP, NADH, and FADH2. Adenosine triphosphate (ATP) functions as the primary energy currency in cells. It stores and transports energy within the cell to be utilized for various cellular processes. NADH and FADH2, on the other hand, carry high-energy electrons that are derived from the oxidation of fuel molecules during cellular respiration. NADH, the reduced form of nicotinamide adenine dinucleotide, plays a crucial role in transferring electrons to the electron transport chain. This process generates a proton gradient across the mitochondrial membrane, which is used to synthesize ATP through oxidative phosphorylation. The oxidation of NADH to NAD+ releases energy that is harnessed to drive cellular processes. Similarly, flavin adenine dinucleotide (FADH2), derived from the reduction of flavin adenine dinucleotide (FAD), also participates in the electron transport chain. It transfers electrons to the respiratory chain, contributing to the generation of ATP. By efficiently capturing and utilizing the energy from redox reactions, cells maximize their energy production and ensure the proper functioning of vital biological processes. The interplay between these high-energy molecules allows cells to sustain their energy demands and carry out the complex tasks necessary for cellular function and survival.

In anaerobic bacteria, metabolic pathways such as glycolysis and the TCA cycle play crucial roles in energy production. The glyoxylate pathway enables the conversion of fatty acids to glucose through reverse TCA, serving as an alternative energy source. Anaerobic photosynthesis generates ATP. However, the lack of appropriate electron acceptors can lead to the accumulation

of reduced electron carriers, hindering energy production pathways that rely on key electron acceptors. IET may help modulate intercellular redox conditions, recovering electron acceptors like NAD+ and FADH and sustaining energy metabolism. Additionally, fermentation enables NAD+ renewal, allowing for glycolysis and ATP production to continue. This is particularly important in anaerobic bacterial communities where terminal electron acceptors are scarce.

1.8.3.4 Transition metals and biodiversity

In the environment, various bacterial species actively participate in the formation or breakdown of solid-phase materials. These species play crucial roles in the geochemical cycling of biologically relevant transition metals such as Iron, Copper, Manganese, Cobalt, and Nickel. These transition metals are vital for numerous microbial enzymatic reactions, but their existence in nature as trace elements often renders them limiting factors for microbial growth and diversity, following the principles proposed by Liebig's law. During diagenesis, transition elements become trapped within minerals in both oxygenic and anoxic environments (Nyström E *et al.*, 2021). Hence, erosion rates and chemical weathering processes significantly contribute to determining the availability of transition metals in ecosystems. Microbes have been observed to directly dissolve minerals through facilitating redox reactions of metal counterions or indirectly through the secretion of metabolites like chelating molecules that aid in their solubilization (Klaus *et al.*, 1997). The impact of these bacteria on ecosystems can be substantial, benefiting other members of the ecosystem by increasing the availability of these valuable metals. Sulfidic minerals, which are widespread throughout the Earth, owe their prevalence to the rich sulfide content of ancient reducing environments, which exhibits a high affinity for metals. Additionally, sulfide minerals serve as abundant sources of divalent metals with biological relevance, which are typically scarce in aerobic environments.

1.8.3.5 Landscape formation

The captivating interplay between microbes and minerals have likely driven their co-evolution, leaving a lasting impact on the formation of our present-day landscapes. By introducing nutrient-rich substrates, these interactions fostered the development of a thriving biodiversity, leading to substrate stabilization and influencing the intricate network of water collection systems (Hubas C *et al.,* 2013). Additionally, through the concentration of intracellular metals and the promotion of mineral formation, these microbe-mineral interactions facilitated the accumulation of sediments, ultimately contributing to the formation of land masses (Susanne *et al.*, 1998). These diverse environments, in turn, harbor a multitude of microenvironments with varying chemical and redox conditions, providing a fertile ground for a diverse array of microbial life to flourish. This intricate interaction between microbes and minerals unfolds a profound narrative of interconnectedness that might have shaped our natural world. (Susanne *et al.*, 1998).

1.8.3.6 Geochemical cycling

Sulfides exist in nature as a diverse range of minerals, including sphalerite (ZnS), chalcopyrite ($CuFeS_2$), chalcocite (Cu_2S), pyrite (FeS_2), covellite (CuS), and others. Annually, an estimated 300 million tons of sulfide sedimentation occurs, with microbial sulfate reduction in aquatic systems accounting for 96% of this process (Rickard *et al.*, 2017). The scale of sedimentary sulfide formation in oceans surpasses the total abundance of sulfate within the sulfur cycle, representing a mere 0.04%, yet ranking as the third most abundant ion in the sea (Rickard *et al.*, 2017). Consequently, the impact of sedimentary sulfide formation in oceans extends deep and intricately across the sulfur, carbon, and oxygen cycles, facilitated by the microbial interconnections between sulfate reduction, primary production, and chemical oxidation of sulfide. PSB demonstrate remarkable adaptability, capable of metabolizing a wide array of molecules, including sulfide, elemental sulfur, thiosulfate, hydrogen gas, organic acids, ferrous iron, and

nitrite (Ehrenreich et al, 1994; Daldal *et al.*, 2008). As sulfur oxidizers, if PSB can utilize sulfide minerals, it would significantly influence the cycling of transition metals and establish them as primary contributors within microecosystems. This possibility finds support in the existing adaptation of purple sulfur bacteria to oxidize solid-phase sulfur granules, found either extracellularly outside the cell membrane (Ectothiorhodospiracea) or intracellularly in the periplasmic space (Chromaticeae). Moreover, the extensive scale of sedimentary sulfide formation in oceans profoundly affects the sulfur, carbon, and oxygen cycles through the interconnectedness of microbial sulfate reduction and primary production (Rickard *et al.*, 2017).

Chapter 2 Utilization of Pyrite (FeS2) by Allochromatium vinosum – "Autotrophic Growth of Purple Sulfur Bacteria Enabled by Solid-Phase Metal Sulfide as Sulfur and Electron Donor Source"

2. 1 Abstract

Purple sulfur bacteria (PSB), which are capable of anoxygenic photosynthesis via oxidizing reduced sulfur compounds, have been around for billions of years. While being recognized as key drivers of the sulfur cycle in a range of anoxic environments, PSB are likely underestimated for their full metabolic capability and flexibility. Here we report successful autotrophic growth of *Allochromatium vinosum* using solid-phase pyrite (FeS_2) as the sole sulfur and electron donor. We confirmed different growth patterns of the pyrite-amended cell cultures ("py") compared to their positive controls (containing Na_2S) in terms of doubling time and concentration profiles of dissolved sulfide, sulfate, and iron species. Comparative analysis of transcriptomic sequencing data revealed extensive upregulation in genes related to cytochromes that are likely key constituents of electron transport chains in "py". By contrast, almost all genes encoding light-harvesting complex subunits (i.e., *puf* and *puc* clusters) and bacteriochlorophylls were significantly downregulated, although those related to carotenoid biosynthesis were not. In terms of sulfur metabolism, genes encoding the periplasmic flavocytochrome *c* sulfide dehydrogenase and one of the membrane-bound sulfide: quinone oxidoreductases were dramatically upregulated; the expression of most genes in the *sox* cluster were slightly upregulated, but those related to cytoplasmic proteins (i.e., *dsr* and *apr* clusters) are extensively suppressed. Other most differentially expressed genes include those encoding flagellar/pilin proteins (+), metal efflux proteins (+), outer membrane receptors for ferrienterochelin (-), ribulose-bisphosphate carboxylase (-), and most [NiFe] hydrogenases (+). In "py", we also observed upregulation of key genes related to ferredoxins, iron trafficking proteins, and 4Fe-4S binding proteins, but overall downregulation

related to FeS assembly proteins. Transmission electron microscopic and X-ray photoelectron spectroscopic analyses of the pyrite substrate in the cell cultures indicated the presence of polysulfide and elemental sulfur. These results strongly point to altered pathways in both photosynthesis and sulfur metabolism for the pyrite-supported cell cultures. The findings of this work may directly impact our understanding of PSB's metabolic capability, especially their extracellular electron transfer mechanisms. These findings may also provide new constraints for early-Earth biogeochemical evolutions and new insights into bioelectronics designs.

2.2 Introduction

Purple bacteria are photosynthetic, Gram-negative prokaryotes that convert light energy into chemical energy through the process of anoxygenic photosynthesis (Madigan *et al.* 2009). Anoxic conditions are required for purple bacteria to grow phototrophically, as the biosynthesis of their pigments and complexes is repressed by molecular oxygen (Cohen-Bazire *et al.* 1957). While purple bacteria can utilize a wide range of electron donors to couple their autotrophic CO_2 fixation, a subgroup preferentially oxidize reduced sulfur compounds (i.e., hydrogen sulfide) during their phototrophic growth and are named purple sulfur bacteria (PSB). Almost all identified PSB belong to *Chromatiaceae* or *Ectothiorhodospiraceae* families. A key difference between the two families of PSB lies in the location of the sulfur globules formed during the bacterial growth on reduced sulfur, which occur intracellularly in members of *Chromatiaceae* but extracellularly in those of *Ectothiorhodospiraceae* (Brune *et al.*, 1995). The specific strain studied in this reported work, *Allochromatium vinosum DSM180*, belongs to *Chromatiaceae*. Purple sulfur bacteria can thrive in various freshwater, marine and hypersaline environments that contain hydrogen sulfide and are illuminated, usually inhabiting the stratum below oxygenic phototrophs. A consequence of this is that the wavelengths of light reaching purple sulfur (and non-sulfur) bacteria are limited, due to the absorption of the blue and red regions in the solar spectrum by the chlorophyll-containing

oxygenic phototrophs (Hacking *et al.*, 2015). The most essential pigments in PSB are capable of absorbing NIR and green light and use it for anoxygenic photosynthesis. PSB are key participants in the anoxic cycling of carbon, mostly as primary producers fixing CO_2 and occasionally as light-stimulated consumers of reduced organic compounds (Takahashi *et al.*, 1968; Overmann *et al.* 1994, 1996, 1999). The most critical roles of PSB in ecosystems, however, lies in their capability of reoxidizing hydrogen sulfide produced by sulfate-reducers (Madigan *et al.*, 2009). Hydrogen sulfide is a highly poisonous substance for most biota. The reoxidation of sulfide by PSB yields nontoxic forms of sulfur, such as elemental sulfur (S^0) and sulfate (SO_4^{2-}), thereby detoxifying the associated environments and importantly, closing the essential sulfur oxidation-reduction cycle.

Photosynthetic pathways in phototrophic purple bacteria (including PSB) have been studied for decades (Drews *et al.*, 1985; Parke-Loach *et al.* 1990; Sturgis *et al.*, 1996; Scheer *et al.* 2002; Hashimoto *et al.* 2006; Turro *et al.* 2008; Hunter *et al.* 2009; Ostroumov *et al.* 2013). However, the model organisms for these previous studies were mostly purple non-sulfur bacteria. The light reactions of photosynthesis in phototrophic purple bacteria involve the harvesting of light energy by the bacterial pigments to generate ATP and NADH, and the dark reactions use the ATP and NADH to fix and reduce simple organic molecules into sugar. In light reactions, incident photons are absorbed by an array of light-harvesting (LH) complexes within the intracytoplasmic membrane of purple bacteria. These complexes consist of proteins that contain bacteriochlorophyll (BChl) and carotenoid pigments, which absorb light energy through transforming their bonding and electronic states and funnel it down an energy gradient to a central reaction center (RC) where charge separation occurs across the membrane. The charge separation in the RC drives a series of redox reactions involving other protein complexes such as quinone/quinol, cytochrome *b/c*, and cytochrome *c* complexes bound within the membrane, along which proton motive force (PMF) is formed and powers ATP synthase complexes. Previous book volumes (e.g., Williams *et al.*, 2009;

Wraight *et al.*, 2009; Axelrod *et al.* 2009; Parson *et al.*, 2009; Kramer *et al.* 2009; van Grondelle *et al.*, 2009; Lavergne *et al.* 2009) have provided excellent reviews on the constituents and structures of pigments, LH complexes and RC as well as the mechanisms involved in each step of the light reactions, including pigment excitation, energy transfer from LH complexes to RC, and subsequent electron transfer. The majority of the genetic information needed to build photosynthetic apparatus in purple bacteria is clustered in large groups of genes known as the photosynthesis gene cluster (PGC). While all the structural genes for the photosystem and latter stages of BChl and carotenoid biosynthesis are organized into one or a few large clusters in purple bacteria, the precise gene organization within the cluster is highly variable for different species (Nagashima *et al.*, 2013). Weissgerber *et al.* (2011) sequenced and annotated the full genome of *A. vinosum*, identifying three subunits of the photosynthetic reaction center, *pufC*, *pufM* and *pufL*, which are clustered and co-transcribed with three sets of *pufA* and *pufB* genes encoding light-harvesting complex (LH1) apoproteins (Nagashima *et al.* 2002). In the same study, six potential *puc* gene pairs were identified that encode α- and β- apoproteins for several LH2 complex types and probably provide basis for heterogeneous structures of LH2 (Niedzwiedzki *et al.* 2012). *A. vinosum* was previously shown to produce different absorption spectra when grown under varied nutritional and environmental conditions (Vredenberg *et al.*, 1966; Mechler *et al.* 1978; Hayashi and Morita 1980; Malik 1983) and such changes were confirmed to correlate with the changes in LH2 complexes produced (Niedzwiedzki *et al.* 2012). However, it remains unclear what external factors may regulate the changes in LH2. It was also reported that *A. vinosum* produces one type of bacteriochlorophyll, namely BChl*a*, and carotenoids of the spirilloxanthin series, including lycopene, anhydrorhodovibrin, spirilloxanthin, and rhodopsin. The genes necessary for conversion of the heme biosynthesis intermediate protoporphyrin IX into Bchl*a* were partly identified and

those necessary for spirilloxanthin biosynthesis starting from the C-5 compounds dimethylallyl-PP and isopentyl-PP were also located (Weissgerber *et al.* 2011).

A central feature of PSB is their capability to oxidize reduced sulfur compounds during photo-lithoautotrophic growth, where light energy is used to transfer electrons from reduced sulfur compounds to more reducing electron carriers $NAD(P)^+$ and ferredoxin for carbon dioxide fixation (T. Weissgerber *et al.* 2013). The known substrates used by PSB include primarily sulfide, polysulfides, and elemental sulfur (Frigaard *et al.*,2009). *A. vinosum* can utilize thiosulfate and sulfite as well. Most of our current knowledge of dissimilatory sulfur metabolism in PSB comes from enzyme assays and sequence analysis of specific gene clusters in the model strain *A. vinosum* DSM180. In terms of sulfide oxidation, *A. vinosum* has the genetic capacity to form several different enzymes, including the periplasmic flavocytochrome *c* (Fcc) and membrane-bound sulfide:quinone-oxidoreductases (Sqr), which are predicted to be oriented toward the periplasm (Reinartz *et al.* 1998; Gregersen *et al.* 2011; Weissgerber *et al.* 2011). One of the two Sqr proteins, SqrD, was pointed out to be only present in PSB that produce intracellular sulfur globules (Dahl *et al.*, 2017). Through genomic manipulation and protein analyses, the oxidation of thiosulfate to tetrathionate was shown to involve the diheme cytochrome *c* thiosulfate dehydrogenase and become more dominant under slightly acidic conditions, whereas the oxidation of thiosulfate to sulfate involves *Sox* proteins (i.e., SoxYZ, SoxB, SoxXAK, and SoxL) and is preferred under circumneutral pH (Hensen *et al.* 2006; Welte *et al.* 2009). For further oxidation of sulfur globules, dissimilatory sulfite reductases (the *Dsr* system) were proposed to play essential roles as several *dsr*-deleted mutants of *A. vinosum* were found to be unable to degrade these globules (Pott *et al.*, 1998; Dahl *et al.* 2005; Sander *et al.* 2006; Lübbe *et al.* 2006). *A. vinosum* was also shown to contain the genetic information for rhodaneses, sulfur relay proteins, and polysulfide reductase-like proteins with unknown functions. Further, it was recently revealed that persulfide shuttling

might be an important part of sulfur oxidation pathways in PSB (Liu *et al.* 2014; *Stockdreher et al.* 2014; Dahl 2015; Koch *et al.*, 2018). Compared to sulfide, the sulfane sulfur can be handled more specifically in sulfur oxidation and biosynthesis of iron-sulfur clusters and molybdopterin cofactors, and the involvement of sulfur relay systems may allow the cells to deliver these active sulfurs specifically to their target sites (Kessler *et al.*, 2006; Mueller *et al.*, 2006; Dahl *et al.*, 2015).

Many PSB including *A. vinosum* are able to oxidize externally supplied, virtually insoluble elemental sulfur (reviewed in Dahl 2017). Elemental sulfur is of zero valency and consists of S_8 rings and polymeric sulfur, with traces of S7 rings that are responsible for the yellow color. It remains unclear how PSB are able to bind, activate, and take up solid-phase sulfur. In principle, bacterial cells may interact with their insoluble substrate through direct physical contact via outer membrane proteins or through excreting extracellular substances that solubilize the substrate. For *A. vinosum*, evidence for the formation of soluble intermediates like sulfide or polysulfides during uptake of elemental sulfur was not obtained (Frank *et al.* 2009), rendering direct cell-sulfur contact as a likely option for the cells' interaction with the solid substrate (Franz *et al.* 2007). It was also shown that *A. vinosum* strongly prefers the polymeric sulfur fraction (i.e., sulfur chains) of the elemental sulfur and is likely unable to utilize the S_8 rings (Franz *et al.* 2007). Other than PSB, some purple non-sulfur bacteria (PNSB) were suggested to be able to utilize elemental sulfur as electron donors but the cell-sulfur interaction mechanisms are unknown.

It remains unknown if *A. vinosum* or other PSB are capable of utilizing other solid-phase substrates besides elemental sulfur. In the various habitats of PSB through geological time, there were, and still are, high chances of metal sulfide formation, which may divert free sulfide out of the sulfur cycle and complicate the associated metal-sulfur geochemistry (**Fig. 2-1**). PSB-metal sulfide interaction therefore has its evolutionary basis, especially considering the prevalence and transformations of sulfide-dominated environments on early Earth. Here, we present the first

evidence for *A. vinosum*'s capability of utilizing solid-phase metal sulfide, i.e., pyrite (FeS_2), and provide thorough transcriptomic profiling and substrate characterization data. We confirmed robust but slower growth of the pyrite cell cultures ("py"), with an estimated doubling time of around ~30 h, in comparison to their positive controls (containing $Na_2S{\cdot}H_2O$), with ~12 h doubling time. Concentrations of dissolved sulfide, sulfate, and iron species also showed different patterns for the "py" versus control systems. Comparative analysis of transcriptomic sequencing data revealed extensive upregulation in genes related to various types of cytochromes in "py". Many of these relevant cytochromes are membrane-bound and some may contain multiple hemes based on Blast search and analysis. By contrast, almost all genes encoding light-harvesting complex subunits (i.e., *puf* and *puc* clusters) and bacteriochlorophylls were significantly downregulated. In terms of sulfur metabolism, genes encoding the periplasmic Fcc and membrane-bound Sqr are dramatically upregulated. Expression of most genes in the *sox* cluster were also slightly upregulated, whereas those related to cytoplasmic proteins (i.e., *dsr* and *apr* clusters) are extensively suppressed. We have further compared our differential gene expression profiles with those previously obtained for *A. vinosum* grown on elemental sulfur, thiosulfate, or sulfite versus sulfide (Weissgerber *et al.* 2013), and identified major differences and similarities, which are discussed in depth in the current contribution.

2.3 Materials and Methods

2.3.1 Growth tracking

Growth was monitored over time by carefully taking aliquot samples without disrupting sedimented nanoparticles, thereby preventing an overestimation of cellular density. The samples were processed through a 1:10 dilution in water and subsequently placed in a UV-VIS spectrophotometer for optical density measurements at 600nm.

2.3.2 Strain, medium and culture conditions

The strain of *A. vinosum DSM 180* was obtained from DSMZ, Germany. Culture media for *A. vinosum* was prepared following Pfenning's medium recipe with modifications that removed compounds allowing for potential heterotrophic growth. Several types of media were prepared for the experiments: one for the sulfur-free control, another for the positive controls, and the last for the pyrite-amended cell cultures. Other than the sulfur source, these media are identical in their compositions. Specifically, the positive control medium is amended with $Na_2S{\cdot}9H_2O$, overall consisting of 1.7 mM of $CaCl_2{\cdot}2H_2O$, 250 mg/L of yeast, 6.5 mM of NH_4Cl, 4.6 mM of KCl, 1 mM of $MgCl_2{\cdot}6H_2O$, 20 mM of HEPES, 35 mM of $NaHCO_3$, 5.1 mM of KH_2PO_4 and 5 mM of $Na_2S{\cdot}9H_2O$. The "py" medium did not contain $Na_2S{\cdot}9H_2O$ but 750 mg/L of pyrite. The sulfur-free control contained neither $Na_2S{\cdot}9H_2O$ nor pyrite. In preparation of the full media, we made two types of solutions (A and B) separately. Solution A was prepared through boiling Milli-Q water (18.2 MΩ·cm), degassed with ultrapure N_2 gas during cooling down. All salts except for the carbon and sulfur sources (i.e., $NaHCO_3$ and $Na_2S{\cdot}9H_2O$/pyrite) and KH_2PO_4 were added to the degassed solution, which was further degassed using N_2 for ~45 min. A mineral mix (composition provided in Appendix Table 1) was added to the cooled solution A as a ratio of 10 µL/mL, following which trace amounts of concentrated 6N HCl was added (at a ratio of 1 µL/mL before bottling in serum bottles sealed by rubber septa and aluminum rings. The purpose of adding trace amounts of HCl is two-fold: facilitating the dissolution of all the salts and resulting in a final medium (through mixing A and B) pH in the range of 7.1-7.3. As a separate solution (B), boiled and N_2-degassed/cooled Milli-Q water was sterilized using 0.2-µm syringe filters and stored in a sterile serum bottle, further bubbled using ultrapure N_2 at room temperature for ~15 min. Immediately prior to sealing the bottles with rubber septa, $NaHCO_3$ and $Na_2S{\cdot}9H_2O$ were added. The fast sealing can prevent loss of sulfide and CO_2, keeping the medium composition close to the designated one.

Full media was made by mixing 90% of solution A into 10% of solution B by volume and adding 10 µL of ATCC Vitamin mix per mL of full media. Inoculations of *A. vinosum* were carried by adding 2% (v/v) of the stock cell culture medium (at late exponential growth phase). Two types negative controls were created: non-inoculated culture of pyrite-amended medium, and inoculated culture of the sulfur-free medium. All "py" cell cultures and positive and negative controls were kept in a shaker incubator at 37 ̊C, under an incandescent lamp with tungsten filament.

2.3.3 Nucleic acids extraction and analysis

DNA and RNA samples were recovered from the cell cultures using the GenElute Bacterial Genomic DNA kit (Sigma Aldrich) and the RNeasy Mini kit (Qiagen), respectively. In sampling, 1 mL aliquots of the cell culture medium were removed using N_2-purged syringes. In the case of sampling for RNA extraction, RNAProtect® was immediately added to the aliquots and incubated for 5 min. The sampled aliquots (with/without RNAProtect®) were then centrifuged at 5,000 g for 10 min, following which the supernatant was discarded. The cell pellets were maintained at -80 ̊C until the DNA/RNA extraction was done. For the DNA extraction, the cell pellets were extracted using the Gram-positive quick protocol (which was found to be more efficient than the Gram-negative protocol for *A. vinosum*) from the GenElute Bacteria Genomic DNA kit manual. For the RNA extraction, the cell pellets were first lysed following a protocol recommended by the RNEasy kit. The lysis solution was prepared by mixing 10 µL of proteinase K (20 mg/mL) and 100 µL of lysozyme (15 mg/mL) in the TE buffer solution (10 mM of TrisHCl, 1 mM of EDTA, and pH 8). Enzymatic digestion was carried out at room temperature for 10 min in a rotary shaker. The RNeasy extraction was subsequently done using the lysate following the RNeasy Mini kit instructions. Quantification of DNA and RNA was done using Nanodrop® One spectrophotometer and Qubit fluorometer, while quality control was done through 260/280 and 260/230 ratios and through DIN and RIN analysis using Tapestation 2200.

2.3.4 Transcriptomic sequencing and bioinformatics

The Illumina platform technology was used to sequence both "py" samples and positive controls cDNA libraries, which were derived from total RNA cultures in the logarithmic phase. The sequencing was performed using a 400M read flow cell NextSeq 2000 cartridge with a 150 bp-end read length. To ensure the quality of the samples, FastQC was utilized to confirm their integrity. Trimmomatic software (Bolger *et al.* 2014) was employed to trim reads of adapters, low-quality bases, and fragments smaller than 60 bp from raw data. The resulting high-quality trimmed reads were then aligned to the reference genome of *A. vinosum* (Genbank: CP001896.1) using Bowtie2 software (Langmead and Salzberg 2012), which can generate an indexed version of the reads. For transcript quantification, the paired-end indexed data of both positive control and pyrite samples were used with RSEM software. Furthermore, the DESeq2 package (Love *et al.* 2014) of the R was used for data normalization and differential gene expression analysis of the statistical processing of the data.

2.3.5 Dissolved species characterization

Growth of bacteria in the positive controls and “py” samples was tracked indirectly by measuring the concentrations of dissolved iron, sulfide, and sulfate in the medium solution over time. Collected samples for sulfide measurements were processed immediately to minimize sulfide escape from solution over time. A 100 µL aliquot of each sample was reacted with 40 µL of excess zinc(II) chloride solution (~ 100-fold of the molar amount of sulfide) to form metastable ZnS. The stabilized mixture was then reacted with 250 µL of HACH1 and 250 µL of HACH2 solutions and diluted with 400µl MQ water to generate a ~1:10 dilution. The mixture was placed in a rotary shaker for a period of 10 min. Sulfide measurements were done using the HACH sulfide reagent set (HACH method 8131) which react with any sulfide present including the precipitated ZnS to yield equimolar amount of methylene blue. The concentrations of the generated methylene blue

were measured by tracking the absorption at 665nm using a MultiSkan UV-Vis spectrophotometer. In the case of sulfate measurement, a nitrogen purged syringe was used to collected aliquots of samples that were diluted 1:10 with Milli-Q water and subsequently filtered. Sulfate measurements were performed using a Dionex ICS-2100 ion chromatography system and QC was performed by jointly running a standard curve made with sodium sulfate. Concentrations of major elements in the control and sample solutions were measured using inductively coupled plasma (ICP)-optical emission spectroscopy (OES) or mass spectrometry (MS) depending on the concentration levels. The aliquots of the medium solution for the ICP runs were diluted 100 fold using 2% HNO3 solution and filtered (0.2 μM cutoff) into 15ml conical centrifuge tubes. Samples were analyzed by ICP-OES (iCAP 6500, Thermo Fisher Scientific, Waltham, MA) and ICP-MS (7700 Series, Agilent, Santa Clara, CA) to determine macro- (Ca, K, Mg, Na, P, S) and micro-nutrients (Zn, Fe, Ni, Mo, Cu) levels. To validate measurements, a blank and standard reference materials (NIST-SRF 1570a and 1547, Metuchen, NJ) were prepared and analyzed. Spikes at different concentrations were used to obtain the standard working curve. The recovery rate of all the tested elements was above 99%. Yttrium (Y) was used as an internal standard and a continuing calibration verification (CCV) sample was analyzed every 15 samples.

2.3.6 Solid-phase characterization

Solid phases in the negative control and "py" samples were analyzed using X-ray diffractometry (XRD), transmission electron microscopy (TEM), and X-ray photoelectron spectroscopy (XPS). The solid pellets recovered through centrifugation and supernatant removal were processed using 0.1% TritonX 100 solution containing 10 μg/mL of lysozyme and 10 μg/mL of proteinase K to remove the bacterial cells and biomolecular debris. The pellets were sonicated in the processing solution for 45 min at room temperature. The solid particles were then separated by centrifuging the digestion mixture at 10,000 × g for 5 min at room temperature and removing

the supernatant. The separate solid particles were washed twice with 0.01% Triton-X. All operations were carried out in an anaerobic chamber in sealed containers prepared to prevent sample oxidation. The biomass-digested solid particles were fractioned for XRD, XPS and TEM analyses. The sample preparation for the XPS specimen involved drying the separated particles on top of a glass slide under anaerobic conditions. The XRD specimen were prepared similarly but the final slides were finished by a layer of grease on top of the dried particle sample to protect the samples from oxidation. In the case of TEM sample preparation, 5 μL of anaerobic water was added to the gold grid with ultrathin carbon film and then 10 μL of particle suspension was added. The XPS spectra were collected using a PHI Quantera SXM (ULVAC-PHI, Japan) with a hemispherical energy analyzer and a monoenergetic X-ray source (Al Kα: 1486.6 eV). The survey spectra were collected at 25 W/15 kV with a spot size of 100 μm, 45° take-off angle, and 280 eV pass energy. A 69-eV pass energy with 0.125 eV scan step was chosen for high resolution spectrum acquisition. The high-resolution XPS spectra were fitted using Multipak software, with the charge correction based on adventitious C 1s at 284.8 eV. The XRD samples were analyzed using a Rigaku MiniFlex II Desktop X-ray Diffractometer which operates uses Cu-tube Ka radiation at 30kV and 15mA at a scan rate of 1.5 degrees/minute. The TEM data were gathered using a JEOL JEM 2100 S/TEM at the Nanoscale Characterization and Fabrication Laboratory located in Virginia Polytechnic Institute and State University. The instrument was operated at 200 kV, and TEM bright field images were taken using a Gatan Ultrascan 1000XP CCD camera. The collection of selected area electron diffraction patterns was performed utilizing a Gatan Orius 833 slow scan CCD camera. Furthermore, scanning TEM (STEM) mode was used to obtain Energy dispersive X-ray spectroscopy (EDS) data using a JEOL genuine 60 mm2 Silicon Drift Detector.

2.4 Results

2.4.1 Growth profiles

In positive controls, it takes ~120 h for the cell culture to reach the end of logarithmic phase, yielding a cell density of ~ 9.4×10^6 cells/mL, and the stable phase spans from 140 h to 400 h with comparable optical density at 600 nm (OD_{600}) and pigmentation intensity throughout the period (**Error! Reference source not found.**). The cell density was estimated through correlating the OD_{600} and cell counting results. The "py" cell culture has a lag phase of ~87 h and then rose to a cell density of ~2.5×10^6 cells/mL, about one quarter of that of positive controls, at ~240 h. We have identified further (slower) growth for "py" cell cultures after the OD reached a local maximum (at ~ 240 h), and such growth lasted till ~550 h. The cell growth in "py" was also quantified using the samples' DNA yields, showing a maximum of ~ 4 ng/μL at ~ 550 h, consistent with the OD data. Depletion of sulfide was recorded at ~120 h for positive controls and the production of sulfate through sulfur oxidation reached a maximum of 0.7 mM (**Error! Reference source not found.**). For "py", sulfide concentrations remained below the detection limit while sulfate reached up to ~20 μM within the monitored period of up to 1000 h. The iron concentrations in "py" showed a spike at ~ 550h. The timing of the spike resonates strongly with that of maximum OD and DNA yield. It is noted that the maximum level of iron concentrations in "py" is still rather low, ~ 600 ppb, compared to that (~ 200-300 ppb) in the controls.

2.4.2 Transcriptomic sequencing and differential gene expression analysis

The genome for *A. vinosum* has been reported to be 3.8 Mb encoding ~3,300 proteins and a similar number of genes (Weissgerber *et al.* 2011). The transcriptomic sequencing analysis of the "py" and positive control samples identified a total of 3302 genes, in line with the previous report. Through differential gene expression analysis of "py" vs. positive controls, and using $\log_2FC > 2$ or $\log_2FC < -2$ as well as $P < 0.05$ as the cutoff, we have identified a total of 80

upregulated and 180 downregulated genes (**Error! Reference source not found.** and **Error! Reference source not found.**). Among these differentially regulated genes, ~15% of the total upregulated and 7% of the total downregulated are associated with redox-active proteins such as cytochromes, hydrogenases, reductases, and others with Fe-S motifs. Sulfur metabolic genes accounted for 2% of the total upregulated and 6% of the total downregulated. Genes associated with signal transduction and transcription regulation accounted for 8% of the upregulated and 3% of the downregulated. Photosynthetic RC-related genes were exclusively downregulated (except for those associated with carotenoid biosynthesis), accounting for 9% of the total downregulated sequences. Interestingly, 3% of the upregulated genes are associated with metal efflux controls, and 4% (also of the upregulated) are concerned with cellular appendages sequences, including flagella, fimbriae and pilin genes.

Among the most differentially regulated genes, we identified a collection of cytochrome-related genes, whose fold change for the upregulated ones are quite dramatic. For example, Alvin_1092 and Alvin_1093, which encode flavocytochrome *a* and *b*, involved in hydrogen sulfide-dependent cytochrome *c* reduction, are upregulated by up to 175-fold; and Alvin_0020 and Alvin_0023, which encode a diheme cytochrome *c*, are upregulated by ~ 47-fold. Others in the upregulated list include Alvin_0021, encoding a cytochrome B561 (although it is in the region dominantly encoding *c*-type cytochromes, Alvin_2307, encoding a Ni/Fe hydrogenase *b*-type cytochrome subunit, Alvin_2452-2454, encoding three formate dehydrogenase subunits, and Alvin_2989, encoding quinone, are also upregulated. The downregulated genes, excluding those tabulated in Tables 1-3 (which will be discussed in the following paragraphs), include several genes related to dehydrogenases found in carbon metabolism cycles, such as Alvin_0315, Alvin_0804-805, and Alvin_2427-2428. The former three encode glyceraldehyde-3-phosphate dehydrogenase, pyruvate dehydrogenase complex dihydrolipoamide, and 2-oxoacid

dehydrogenase E1 subunit, respectively, whereas the latter two encode NADH dehydrogenase subunits.

The genes encoding metal ion transporters, Na^+/H^+ antiporter, and flagella, fimbriae, and pili components, are also in the most differentially regulated list. For metal ion transporters, Alvin_0013-0015 likely represent components of efflux transporters of the RND and CzcA families, and Alvin_0019 and Alvin_1521 are respectively associated with FieF Iron efflux pump and a periplasmic efflux protein. The upregulated flagella-associated genes include Alvin_1952-1954, encoding FlaG, a flagellar hook-associated protein, and FliS, respectively. Alvin_3016 is associated with fimbriae biogenesis (i.e., FimT) and Alvin_1186 with a pilin protein PilT.

The expression of genes associated with light harvesting and dissimilatory sulfur metabolism pathways showed consistently distinct patterns for "py" versus positive controls (**Error! Reference source not found.**, **Error! Reference source not found.**, **Error! Reference source not found.** and **Error! Reference source not found.**)and). In the case of light harvesting, genes relevant to biosynthesis of LH1, LH2 and reaction center components were exclusively downregulated. Specifically, the gene clusters, *pufC*, *pufM*, and *pufL*, which are co-transcribed with three sets of *pufA* and *pufB* genes, encoding LH1 apoproteins, were suppressed by various levels, up to 10-fold (Alvin_2547-2555). The upstream *pufH* along with adjacent genes, encoding photosynthetic complex assembly proteins and a hypothetical protein, was also slightly suppressed (Alvin_2634-2637). The genes associated with LH2 apoproteins were suppressed the most, by up to 115-fold (Alvin_0703-0706, and 0708-0709). By comparison, genes related to biosynthesis of Bchl*a* and carotenoids were either moderately suppressed or enhanced in expression (Alvin_1182-1183, 2556, 2561-2563, 2638-2643, and 2564-2570). In the case of dissimilatory sulfur metabolism, *dsr* genes are exclusively downregulated except for *dsrC*. Specifically, *dsr*A/Alvin_1251 and *dsr*B/Alvin_1252, which form a *dsrAB* complex, show a ~22-fold

expression suppression. The other complex within the *dsr* loci is *dsrEFH*, from which *dsrE*/Alvin_1253 decreases by 11-fold and *dsrF*/Alvin_1254 by 7-fold. The genes coding membrane-bound *Dsr* proteins were also downregulated, by ~ 4-fold for *dsrJ*/Alvin_1260, 4-fold for *dsrO*/Alvin_1261, and 3-fold for *dsrP*/Alvin_1262. The only gene that remained relatively unchanged in its expression level is *dsrC*/Alvin_1256. Besides *dsrC*, there are four more genes annotated as TusE/DsrC/DsvC family sulfur relay proteins, namely Alvin_0028, Alvin_0345, Alvin_0732 and Alvin_1508 (Weissgerber *et al.*, 2011), which are respectively upregulated by ~ 2-, ~ 2-, and ~ 4-fold, and downregulated by ~ 7-fold. In the *sox* loci, genes encoding SoxYZ complex were upregulated by 5-fold, while the rest of the *sox* genes seemed unaffected in terms of expression levels. We also evaluated the expression of three genes related to Sgp proteins and found upregulation of Alvin-1095 (representing SgpA) by ~ 42-fold in the differential analysis of "py" vs. positive controls. The other two genes, Alvin_0358 and Alvin_1325, were either slightly downregulated or unchanged.

It is important to highlight that a considerable portion of the total genes, ~30% of the upregulated and ~23% of the downregulated genes, were considered hypothetical proteins or domains of unknown function (DUF) (Appendix Table 0-8 and **Error! Reference source not found.**). A taxonomy analysis was carried out to determine how conserved the sequences of these genes were by running protein blast searches. The taxonomy analysis was used to determine the percentage of hits from γ-Proteobacteria sequences from the total hits. These values can be found as pBlast% in Table 0-8 (Appendix), where 14 out of 18 upregulated genes show 90% or higher blast results, indicating that these sequences originated in γ-Proteobacteria. The same analysis also shows that 16 out of 25 downregulated hypothetical sequences were originally from γ-Proteobacteria organisms.

2.4.3 Pyrite substrate analysis

The pyrite recovered from the cell culture medium showed irregularly shaped particles with wide-ranging dimensions of ~100 nm to several microns (μm) (**Error! Reference source not found.**). In these biological pyrite samples, we observed apparent amorphous domains, with no electron diffraction patterns and rich in iron and/or sulfur, and highly crystalline domains. Based on d-spacing obtained using the electron diffraction micrographs, the solids in the *A. vinosum* culture likely consist of pyrite, pyrrhotite, and elemental sulfur. Although different interpretations may be made based on the electron diffraction patterns alone, the corresponding XPS analyses provide extra constraints on the Fe and sulfur valence states as well as information on existing bonds (**Error! Reference source not found.**). The XPS analyses yielded valuable information regarding iron and sulfur valences in the solid substrate, as well as the sulfur-to-iron composition ratios, based on negative controls and "py" cell cultures. The results showed that only Fe(II) was present in both abiotic and biotic pyrite samples. An asymmetric fit was performed on the iron region of the spectra to calculate the relative abundance of the species identified. The abiotic control (pyrite) showed a main 2p3/2 peak at 706.72 eV, matching the binding energy for Fe(II) valence electrons in pyrite, along with a satellite peak at 707.95 eV, likely resulting from surface defects. The "py" sample (biotic sample) had a peak at 706.37 eV in the iron region, with a satellite peak at 707.58 eV, indicative of the presence of a surface oxide layer on the pyrite. Both samples displayed the same oxidation state - Fe(II), with no evidence of Fe(III) and its satellite peak. The surface composition of both materials was extremely similar, with a small increase in the dominance of the Fe(II) peak, from 65% in the control to 67% in the biotic sample. The fit of the sulfur region of the spectra required doublet peaks, with the area of the 2p3/2 peak set to be twice that of the p1/2 and the distance between them set at 1.18 eV. The abiotic control showed four different sulfur species, including S^{2-} at 161.14 eV for p3/2, with an orbital split p1/2 peak at

162.32 eV, polysulfide at 164.1 eV for p3/2, with a p1/2 peak at 165.28 eV, disulfide at 162.1 eV for p3/2, with a p1/2 peak at 163.28 eV, and a fourth unidentified peak at 162.34 eV and matching orbital split at 163.52 eV. The fourth peak fell 0.14 eV away from the main disulfide peak, but its corresponding species is unknown. The biotic sample showed three sulfur species, including S^{2-} at 161.3 eV and 162.48 eV, disulfide at 161.82 eV and 163 eV, and polysulfide at 163.7 eV and 164.88 eV. Both the control and biotic pyrite samples showed the presence of monosulfide, disulfide, and polysulfide. However, the unidentified peak close to the main disulfide peak in the control disappeared in the biotic sample. Upon closer comparison, the biotic sample showed an increase in the abundance of polysulfides from 9% in the control to 15%, an increase in the monosulfide peaks from 5% in the control to 15% in the biotic sample, and an increase in the disulfide peaks from 47% in the control to 70% in the biotic sample. Nevertheless, considering that apical, bridging, and terminal ligands cause a significant peak position shift, and including the unknown 0.14 eV peak as a variation of disulfide, the biotic sample disulfide decreased from 85% in the control to 70%. Based on both TEM and XPS analyses, we have identified the presence of pyrite, pyhrrotite, and likely polymeric sulfur. The relative abundances of each iron/sulfur species were estimated based on the XPS analysis, and interestingly, the overall sulfur-to-iron ratio increased greatly for the "py" samples (which have been exposed to and interacted with *A. vinosum* cells), reaching ~12.6, compared with that for the negative control samples, ~3.9.

2.5 Discussion

The cell growth profiles and transcriptomic analysis results revealed significant changes in the cells' major metabolic pathways, including electron transport, RC and LH complex biosynthesis, and sulfur oxidation. We have specifically discussed these changes in the following section. Combining these molecular biological analyses with the pyrite substrate analyses, we have

also proposed mechanisms of interaction between *A. vinosum* and pyrite that enabled the bacterial cells' autotrophic growth.

2.5.1 Roles of cytochromes in A. vinosum-pyrite electron transfer

The genome of *A. vinosum* encodes a wide range of cytochromes that are known to play key roles as diffusible electron carriers, dissimilatory sulfur metabolism enzymes, and hydrogenases, etc. In the current study, dramatic upregulation was identified for a number of genes related to *c*-type and, to a lesser extent, *b*-type cytochromes. Further analyses revealed that some of the upregulated genes are associated with soluble or membrane-bound *c*-type cytochromes or flavocytochromes (Alvin_1093, 0020, and 0023), previously classified as diffusible electron carriers. It is noted that Alvin_1093 is one of the top upregulated genes (expression increased by ~ 175-fold) in the "py" cells. Alvin_1093 and Alvin_1092 (upregulated by ~ 75-fold) encode a heterodimer consisting of a 21 kDa diheme cytochrome *c* subunit (FccA) and a 46 kDa flavin-binding subunit (FccB) in *A. vinosum* (Brune *et al.*, 1995). Although soluble *c*-type cytochromes were shown to catalyze the oxidation of sulfide to sulfur or polysulfides *in vitro* electron acceptors (Reinartz *et al.* 1998), the roles of FccA and FccB in *A. vinosum* remain unresolved. As pointed out in Weissgerber *et al.* (2011), mutants in which the genes *fccAB* are inactivated by a kanamycin cassette still oxidize sulfide with rates similar to the wild type (Reinartz *et al.* 1998). Some sulfide-utilizing green sulfur bacteria, e.g. *Chlorobium luteolum*, and purple sulfur bacteria, e.g. *Thiocapsa roseopersicina*, *Thiococcus pfennigii*, and *Allochromatium warmingii*, do not produce flavocytochrome *c*, which is an additional hint that flavocytochrome *c* is not essential for sulfide oxidation (Brune *et al.*, 1995). Interestingly, Alvin_1093 along with Alvin_1092, 0020, and 0022-0023 showed distinctive regulation patterns for the pyrite-supported cells (as shown in the differential gene expression analysis of this study) than the elemental sulfur (S^0)-supported cells (also of *A.vinosum DSM180*), as shown in the differential gene

expression analysis of Weissgerber *et al.* (2013) (Supplementary data at https://datarepo.bioinformatics.utep.edu/getdata?acc=G9T1VZNRYJPIC0C). Specifically, Alvin_0020, 0022, and 0023 were significantly suppressed in the S^0-supported cells versus their positive controls using soluble sulfide, whereas Alvin_1093 was upregulated by ~ 5-fold. Such evident variations strongly indicate that Alvin_0020, 0022-0023, and 1092-1093 have played particularly important roles in *A. vinosum*-pyrite interactions in the current study (further discussion of Fcc is available in a following section on "dissimilatory sulfur metabolism"). We also observed dramatic upregulation of Alvin_1095 (by ~ 45-folds), associated with a 4-heme c-type cytochrome, whose function and pathway have not been resolved.

We then evaluated whether cytochromes in *A. vinosum* may play a role in the cell-pyrite electron transfer, linking intracellular energy reactions to the oxidation of solid pyrite external to the cells. The phenomenon of extracellular electron transfer has been demonstrated in over ~ 100 microbes to date, perhaps most notably in *Geobacter sulfurreducens* and *Shewanella oneidensis*, where a network of multiheme *c*-type cytochromes on the inner membrane, periplasm, and outer membrane couple intracellular energy reactions with the use of external solid electron donors or acceptors (Shi *et al.* 2016; Breuer *et al.* 2015; Chong *et al.* 2018; Costa *et al.* 2018). Multiheme cytochromes (MHCs) in particular are key players in extracellular electron transfer (Chong *et al.* 2018), as the proximity and arrangement of hemes can allow efficient intraprotein electron transfer (Gray *et al.*, 2004). We identified 43 putative *c*-type cytochromes in *A. vinosum* based on the presence of CXXCH heme *c* binding motifs, and of these 18 were putative MHCs (containing multiple CXXCH motifs): specifically, 11 × diheme, 1 × 3-heme, 3 × 4-heme, 1 × 7-heme, and 2 × 8-heme cytochromes (Supplementary Table S3). Some of the larger ones (e.g. 7 or 8-heme) in particular, and various others, have no annotated functions; the expression of these larger MHCs was exclusively enhanced in the "py" cells (Supplementary Table S3). The remaining 25 are

putative monoheme *c*-type cytochromes (Supplementary Table S3). We also probed these genes for the presence of LXXC lipid binding motifs and/or signal peptide, as both periplasmic and membrane-associated cytochromes are required for extracellular electron transfer. LXXC is a lipoprotein consensus sequence for signal peptidase II found in key outer membrane cytochromes in *S. oneidensis* (Myers *et al.*, 2004). SignalP (Teufel *et al.* 2022) can detect 5 types of signal peptides, i.e., a protein can enter the cell's secretory pathway, where it may be localized to the inner membrane, exported to periplasm, or localized to the outer membrane. In total, 19 out of 43 putative cytochromes contained LXXC lipid motif, and 21 were detected by SignalP; 8 were detected for both. The fact that multiple cytochromes are potentially associated with the inner or outer membrane (with others not identified here possibly being soluble electron carriers) is promising towards identifying a potential cytochrome network for extracellular electron transfer in *A. vinosum*. Experimental evidence will be required to confirm the cellular localization of cytochromes in *A. vinosum*, and whether they contribute to extracellular electron transfer. As a disclaimer, other cytochromes of interest may exist, e.g. those without heme *c* motif (CXXCH), or those not detected by the LXXC lipid motif or by SignalP. In total, 10 putative *c*-type cytochromes (including an 8-heme, 2 diheme and 7 monoheme) were upregulated exclusively in the "py" cells (Supplementary Table S3) and may be of particular interest towards investigating the coupling of photosynthesis on the inner membrane to the oxidation of pyrite outside the cell.

2.5.2 Suppressed expression genes encoding LH and RC complex components

A major change identified in the "py" cells is the exclusive downregulation of photosynthetic genes related to the biosynthesis and assembly of LH and RC components (**Error! Reference source not found.** and **Error! Reference source not found.**) and). As a recap, the expression of *puc* clusters encoding LH2 apoproteins were most dramatically suppressed, by up to ~70 fold; the *puf* clusters and genes related to biosynthesis of Bchl *a* were also downregulated, by

~ 8-10-fold for the former and by ~ 2-fold for the latter. The only genes not affected or enhanced in expression within the photosynthetic category are those representing carotenoids biosynthesis (Alvin_2564-2570). It is still premature to conclude what has caused the extensive downregulation of the photosynthetic LH- and RC-related genes in the "py" cells. A likely reason might be that the growth rate of the "py" cells was limited by other factors (e.g., electron supply to the carbon fixation pathway) than the light harvesting rate, and thus, the demand for LH and RC complexes was no longer existent. The relationships among RC, sulfur-oxidation, and carbon fixation remain to be fully resolved. We further evaluated the expression of genes related to ribulose 1,5-biphosphate carboxylase/oxygenase (RuBisCO) in the "py" and positive control cells as both types grew autotrophically with dissolved carbonate as the sole carbon source. *A. vinosum* possesses two complete sets of genes encoding for RuBisCO subunits (Weissgerber *et al.*, 2011): the large subunit RbcA/RbcB is represented by Alvin_1365-1366 and the small one RbcS/RbcL is represented by Alvin_2749-2750 (Viale *et al.* 1989). Opposite trends have been observed for the two sets of RuBisCO genes in the "py" cells, with Alvin_1365-1366 dramatically downregulated by at least 10-fold and Alvin_2749-2750 moderately upregulated by ~ 2-fold. According to the gene arrangement, the *rbcAB* gene belong to IAq-form RuBisCO genes, typically associated with *cbbQ* encoding proteins affecting RuBisCO activity (Hayashi *et al.* 1999), whereas the *rbcSL* genes are IAc-form RuBisCO genes, which were found to be associated with α-carboxysome gene clusters in other anoxygenic photosynthetic bacteria (Badger *et al.*, 2008). The co-occurrence of RuBisCO RbcSL with carboxysomes might allow *A. vinosum* to grow at very low CO_2 concentration. However, carboxysomes have never been reported for *A. vinosum*, and the carbonate levels in "py" versus positive controls are comparably sufficient. Besides the RuBisCO genes, *A. vinosum* harbors a gene encoding an IV-type RuBisCO-like protein (RLP) (Alvin_2545), the expression of which decreased just slightly in the "py" cells. It remains unclear what roles such

RLPs play in *A. vinosum* metabolism, but likely not involved in RuBis-dependent CO_2 fixation (Hanson *et al.*, 2001; Hanson and Tabita 2003).

An alternative reason for the LH and RC "shutdown" might be that the cells have established a different pathway to obtain energy. Regarding what other pathways may be available for *A. vinosum* cells to capture light energy, here we present a bold hypothesis, which assumes that nanoparticulate pyrite may be able to serve as alternative RCs in the *A. vinosum* cells (**Fig. 6**). There are obvious energy and nutrient appeals for *A.vinosum* to enable such cell-pyrite interactions; however, further research is needed to test this hypothesis.

2.5.3 Expression of genes involved dissimilatory sulfur-oxidation metabolism

For genes encoding major enzymes (likely) involved in dissimilatory sulfur metabolism, we have observed opposite trends in their differential expressions (in "py" vs. positive control), primarily divided by associated pathways of the relevant enzymes (**Error! Reference source not found.** and Figure *2-1*)). We will first discuss the genes representing Fcc and Sqr, respectively, although their roles in dissimilatory sulfur-oxidation have not been fully resolved. It has been pointed out in our former discussion on cytochromes that FccA and FccB are likely key electron carriers enabling the *A. vinosum*-pyrite electron transfer. Chen *et al.* (1994) provided a detailed illustration of Fcc structures, which consist of a glutathione reductase-like flavin-binding subunit and a diheme cytochrome subunit. Specifically, the diheme cytochrome folds as two domains, each resembling mitochondrial cytochrome *c*, and has an unusual interpropionic acid linkage joining the two heme groups in the interior of the subunit; the active site of the flavoprotein subunit contains a catalytically important disulfide bridge located above the pyrimidine portion of the flavin ring; further, a tryptophan, threonine, or tyrosine side chain may provide a partial conduit for electron transfer to one of the heme groups located 10 angstroms from the flavin. This specific structure renders Fcc a good candidate for bridging *A. vinosum* cells and pyrite chemically and

energetically. Meanwhile, *A. vinosum* contains two membrane bound Sqr enzymes belonging to types IV (Alvin_2145) and VI (Alvin_1195) (Weissgerber *et al.* 2013). Sqr belong to a family of FAD-dependent oxidoreductases utilizing an active site Cys-S-S-Cys as the key redox element (Walsh 2020). Sqr have been previously identified to reduce the quinone pool present in the photosynthetic or plasma membranes of purple bacterial cells and proposed as candidate proteins for oxidizing sulfide (Reinartz *et al.* 1998; Griesbeck *et al.* 2002). In the case of *Rhodobacter capsulatus*, polysulfides were identified as main reaction products *in vitro*. In our current study, opposite trends were observed in the differential gene expressions ("py" versus positive control) for Alvin_2145, encoding type IV SqrD (upregulated by ~ 4.5 fold) and for Alvin_1195, encoding type IV SqrF (downregulated slightly). In former studies, a correlation between the occurrence of SqrD and the production of intracellular sulfur globules has been indicated (Gregersen *et al.* 2011) through observations that *sqrD* genes are present in members of Chromatiaceae but absent in species of Ectothiorhodospiraceae that exclusively produce extracellular sulfur globules. The observed upregulation of Alvin_2145 in the current study suggests that SqrD has played a significant role in sulfide oxidation and sulfur storage for the *A. vinosum* cells grown on pyrite. By comparison, the downregulation of Alvin_1195 is consistent with previous understanding that SqrF is involved in optimizing cell growth at high sulfide concentrations (Gregersen *et al.* 2011), which was not the case for the pyrite-amended medium in this study.

The general trend for the three clusters of *sox* genes are moderately upregulated or relatively unaffected in the "py" cells (compared to positive controls). The most upregulated *sox* genes in the "py" cells in our study, Alvin_2011 and Alvin_2012, are within the first cluster, encoding SoxY and SoxZ, respectively. The second cluster extending between Alvin_2165 and Alvin_2167 and the third from Alvin_2168 to Alvin_2182 remain relatively unchanged in their expressions. It is noted that the *Sox* protein complex is localized in the periplasm.

It is unknown if the cells grown on pyrite in the current study can form sulfur globules in the periplasm for storage of sulfur compounds that may be further oxidized. The genes representing the envelope proteins of such sulfur globules (i.e., SgpA, SgpB and SgpC) showed interesting patterns in the differential gene expression analysis, however. Specifically, SgpA, SgpB and SgpC are encoded by Alvin_1905, Alvin_0358 and Alvin_1325, respectively. SgpC plays an important role in globule expansion, whereas SgpA and SgpB can be replaced by each other to some extent (Pattaragulwanit *et al.* 1998; Prange *et al.* 2004). In our study, Alvin_1905 and Alvin_0358 were slightly downregulated, and Alvin_1325 remained unchanged. We note here that the expression of genes representing Sgp were not apparently suppressed in the "py" cell cultures compared to positive controls, which creates a sharp contrast with the trends previously reported for "S^0-supported" cell (Weissgerber *et al.* 2013).

Although dissimilatory sulfite reductase (Dsr) proteins were implicated as key participants in oxidation of the stored sulfur globules, genes related to *Dsr* are exclusively downregulated in the current study [except that *dsrC* (Alvin_1256) remained relatively unchanged in its expression level]. In fact, a review chapter on dissimilatory sulfur metabolism in purple sulfur bacteria pointed out that purple non-sulfur bacteria, including those able to oxidize elemental sulfur lack *dsr* genes (Dahl 2017) and the *A. vinosum* cells grown upon external sulfur, showed significant downregulation in their *dsr* genes (Weissgerber *et al.* 2013). Combined with the latest results in this study, it is strongly suggested that *Dsr* are not highly involved in metabolism of external solid substrate of sulfur. *Dsr* proteins are largely localized in the cytoplasm, with a transmembrane complex (DsrMKJOP). It is likely that the specific locality and connection to photosynthetic electron transport chains (Grein *et al.* 2010) of *Dsr* proteins make it difficult for most of them to participate in pyrite utilization. It is noted that while the *dsr* genes are transcribed as one single element, *dsrC* has an additional independent promoter site (Grimm *et al.* 2010), pointing at a

special function of DsrC. Further, besides *dsrC*, there are four more genes annotated as TusE/DsrC/DsvC family sulfur relay proteins, namely Alvin_0028, Alvin_0345, Alvin_0732 and Alvin_1508. We observed upregulation by ~ 2-4-fold for Alvin_0028, 0345, and 0732, and downregulation by ~ 8-fold for Alvin_1508.

These results, combined with analyses of the solution sulfate levels (i.e., the IC analysis) and solid substrate compositions/structures (i.e., the TEM and XPS analyses), suggest that *A. vinosum* cells are capable of oxidizing the pyrite-bound sulfur to polysulfide or even elemental sulfur. It is premature to suggest whether the cells can further oxidize the solid substrate to sulfate based on these analyses as the tested systems are sulfate-starved for assimilatory processes. Further comparative kinetic studies are necessary to confirm the sulfur oxidation pathway in pyrite utilization by *A. vinosum*.

2.5.4 Flagellum and pilin

We have singled out the genes associated with the biosynthesis of flagella and pili because the expression of these genes was greatly enhanced in "py". Many species of purple bacteria swim with the assistance of flagella towards carbon/other nutrient sources and light and away from oxygen, using a complex set of chemosensory pathways (Armitage 2009). The flagellum in bacterial cells is an extremely complex structure, requiring the expression of genes encoding flagellar proteins to be tightly regulated and ordered. The upregulation of Alvin_0408, 1188, 1569, and 3021 opens a discussion on whether pili may play a role in establishing physical contact between *A. vinosum* cells and pyrite. Further, while a possible connection of flagellation and substrate exploration and utilization has not been shown in bacterial cells, flagellar proteins were recently speculated to be involved in direct physical contact with insoluble elemental sulfur for oxidation in *Aquifex aeolicus* (Guiral *et al.* 2012)). Overall, the extensive upregulation of flagellum- and pilin-related genes manifests two key messages. First, mobility is crucial for *A.*

vinosum cells grown upon pyrite. High mobility may help the cells to move around easily to either find the most "bioavailable" spots on pyrite or avoid the adverse effects of metabolic products (such as transformed or reprecipitated iron-sulfide and iron-oxyhydroxide species). Secondly, the enhanced expression of appendage genes also indicates that physical contact is essential in cell-pyrite interactions. Further work is needed to reveal the actual roles of flagella and pili in *A. vinosum* during their growth on pyrite.

2.6 Conclusion

In this study, we showed that *A. vinosum* cells are capable of autotrophic growth using pyrite as the source of sulfur and electron donors. The differential gene expression analysis along with growth profile and substrate characterizations provided valuable insight into the molecular mechanisms underlying the bacterial autotrophic growth. Dramatic upregulation of genes encoding for a range of c-type and b-type cytochromes (including multiheme molecules) points to the high relevance of these proteins in scavenging and relaying electrons from pyrite to other key metabolic pathways. Conversely, the exclusive downregulation of LH and RC complex components reveals that the available electron donor source likely has a dominant control over the bacterial cells' phototrophic activity. The possibility that *A. vinosum* may bypass the phototrophic pathway and directly couple the electron scavenging from electron donor substrate to carbon fixation is also indicated. The results of this study have, for the first time, put the interplay of purple sulfur bacteria and transition metal sulfide chemistry under the spotlight, with the potential to advance multiple fields, including metal and sulfur biogeochemistry, bacterial extracellular electron transfer, and artificial photosynthesis.

2.7: Figures and tables

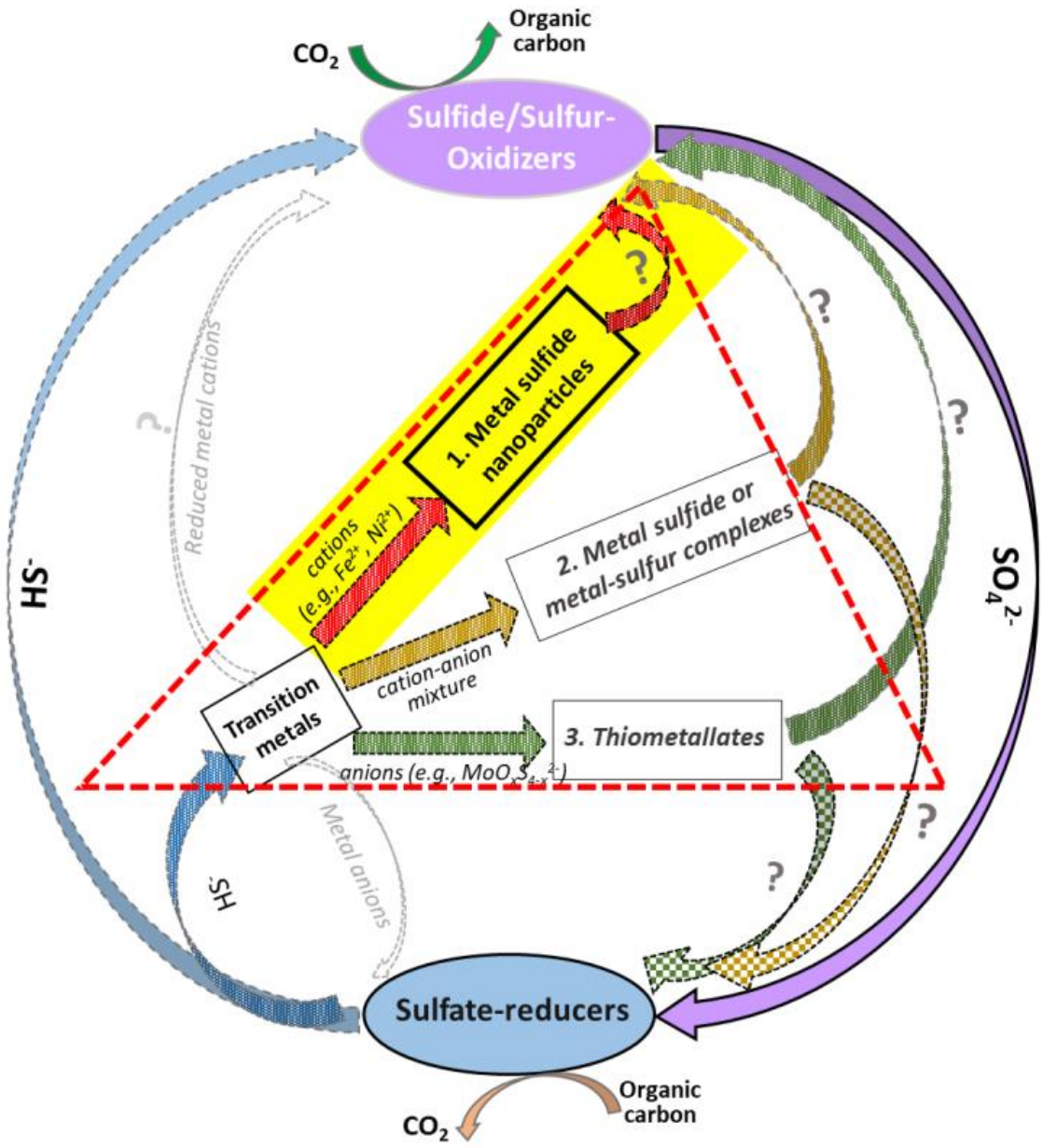

Figure 2-1 Microbial sulfur oxidation-reduction patterns complicated by the presence of transition metal species (TMs) (Courtesy of Dr. Jie Xu). In the absence of TMs, sulfate reducers reduce sulfate to sulfide/elemental sulfur in couple with heterotrophy or mixotrophy, while sulfur-oxidi zers oxidize sulfide/elemental sulfur back to sulfate in couple with autotrophy. In the presence of TMs, TM sulfide nanoparticles or thiometallate clusters may form within the cycle. It is unknown how the formed TM-sulfur nanoparticles or complexes may affect the metabolic activity of associated sulfur-oxidizers that depend on "free" sulfide to support CO_2 fixation.

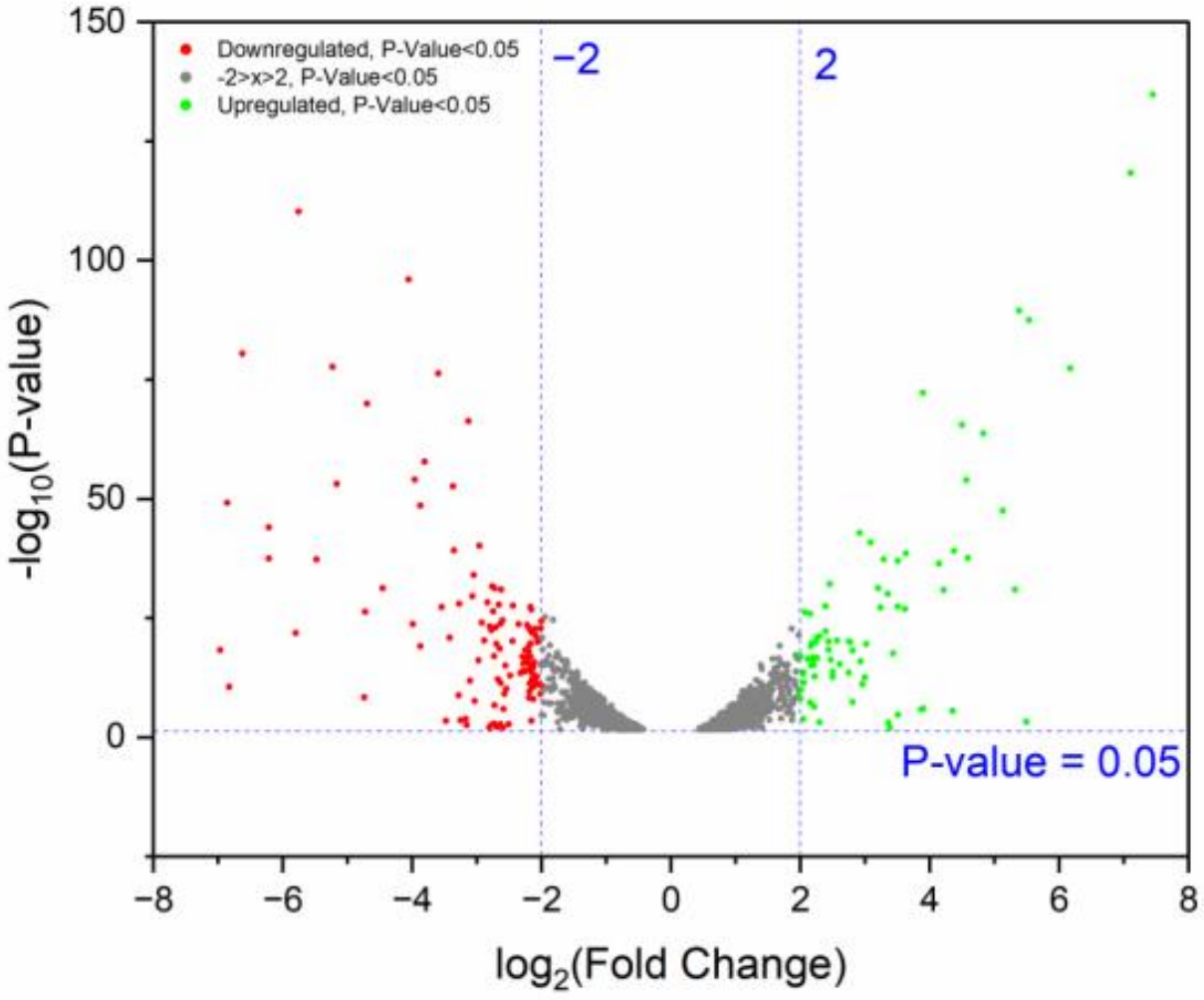

Figure 2-2 The volcano plot showing differential genes expression in *A. vinosum* grown on pyrite versus dissolved sulfide. We used the log2 FC < -2 or log2 FC > 2 as the cutoff; the upregulated genes are displayed as red dots and downregulated genes as green dots.

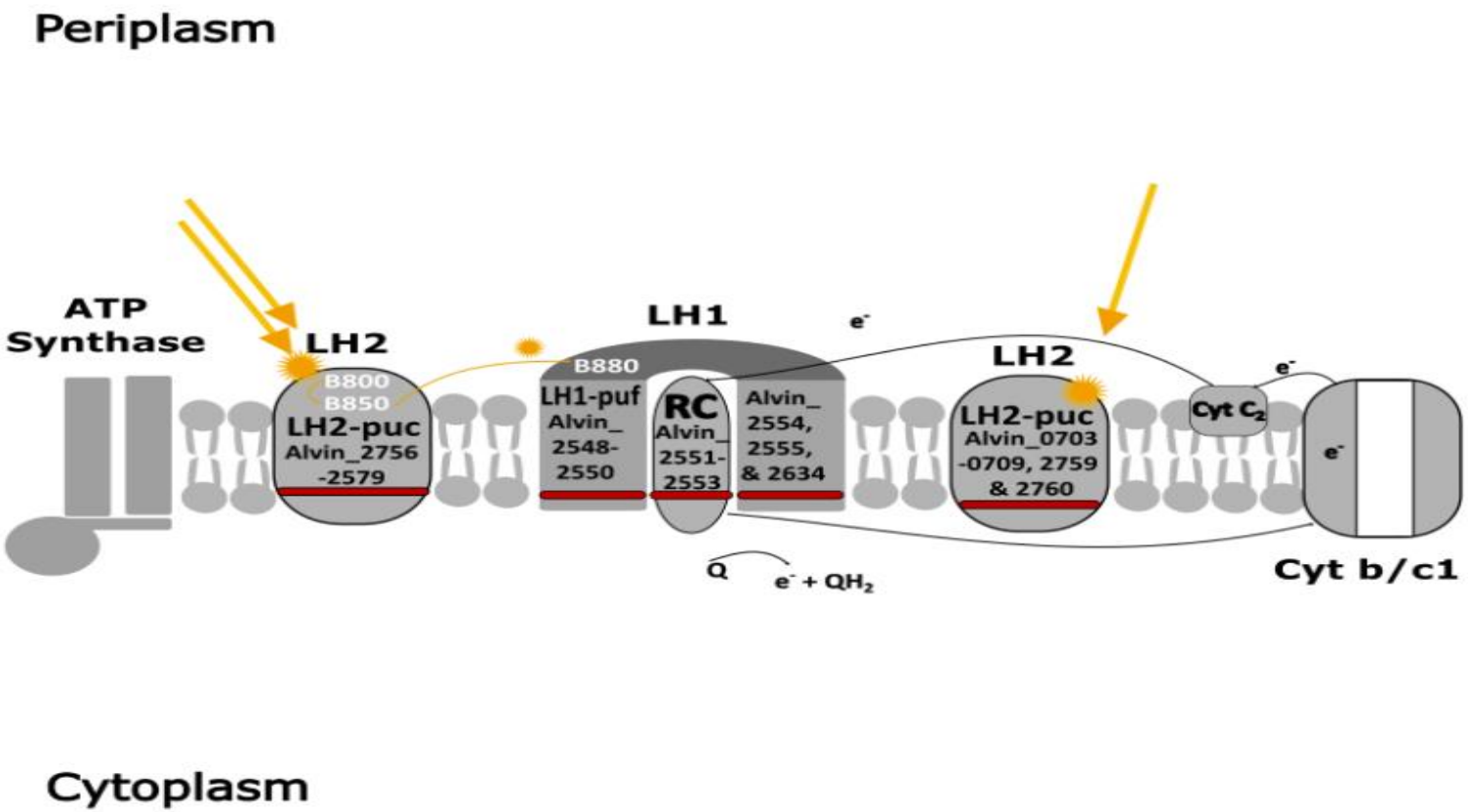

Figure 2-3 Schematic illustrating locations of LH1, LH2, and RC complexes as well as their recognized role in sulfur oxidation. Relevant genes encoding the listed proteins are also indicated. We used green bars to mark the upregulated genes (with a log2FC>2) and red bars for downregulated genes (with a log2FC<-2).

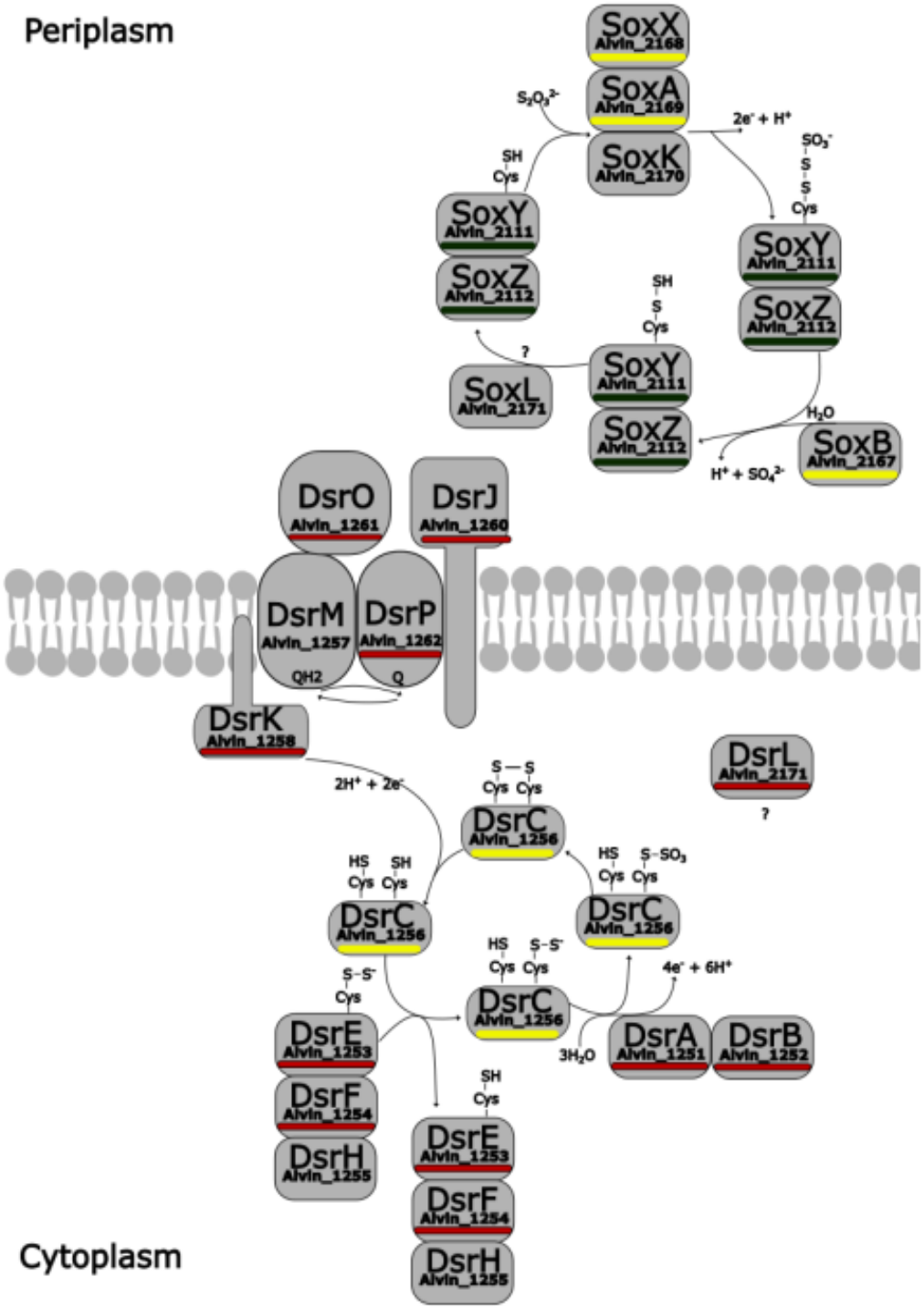

Figure 2-4 Schematic illustrating locations of *sox* and *dsr* proteins and their recognized role in sulfur oxidation. Relevant genes encoding the listed proteins are also indicated. We used green bars to mark the upregulated genes (with a log2FC>2) and red bars to mark the upregulated genes (with a log2FC>2) and red bars to mark downregulated genes (with a log2FC<-2). Yellow bars indicate that the log2FC values for the genes are between -1.5 to 1.5

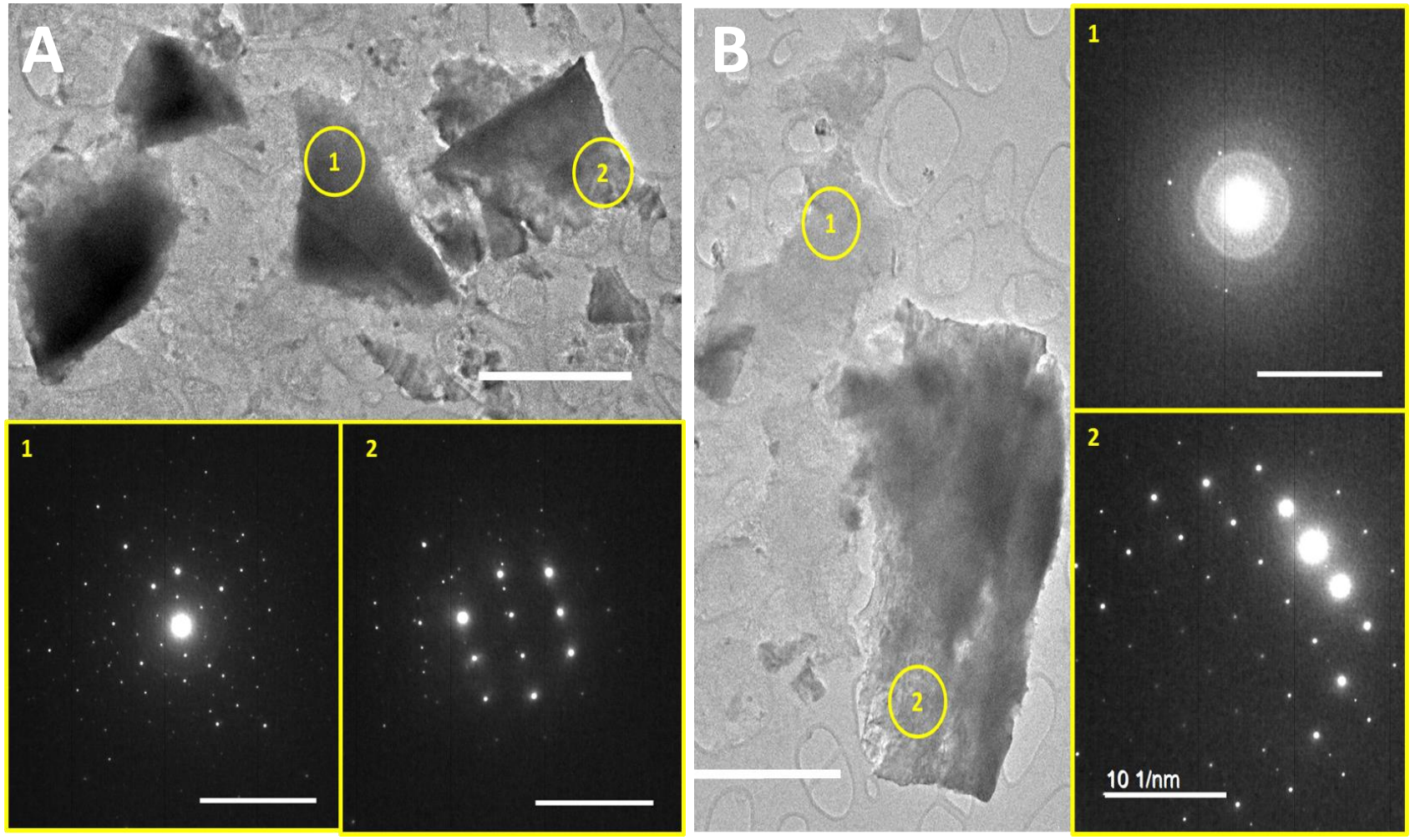

Figure 2-5 High resoluton-transmission electron micrographs displaying plate-like fragments of the solid substrate recovered from *A. vinosum*-pyrite culture medium. The solid materials from the cell culture consist of a significant fraction of amorphous phases, distinctive from the abiotic controls. The biological samples likely contain pyrrhotite and elemental sulfur besides pyrite based on d-spacing measurement/calculation using the obtained electron diffraction micrographs.

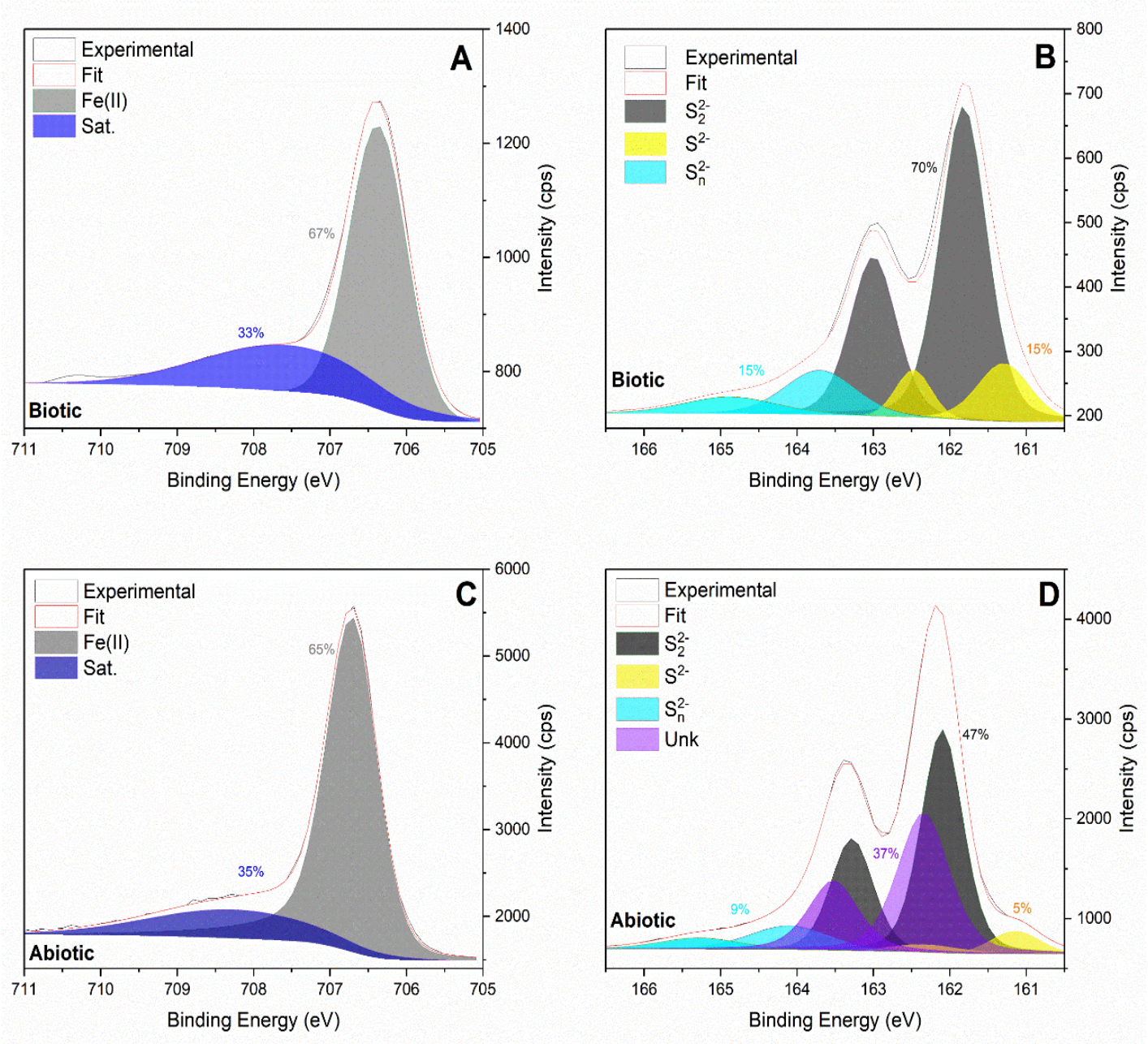

Figure 2-6 X-ray photoelectron spectroscopy (XPS) analysis of solid substrate recovered from *A. vinosum* pyrite cell cultures versus abiotic controls. The plots use different colors to distinguish between different species and also display the relative abundance percentage of each species. (A) and (C) The iron region analysis for the abiotic controls (A) versus biological samples (C); (B) and (D) the sulfur region analysis for the abiotic controls (B) versus biological samples (D).

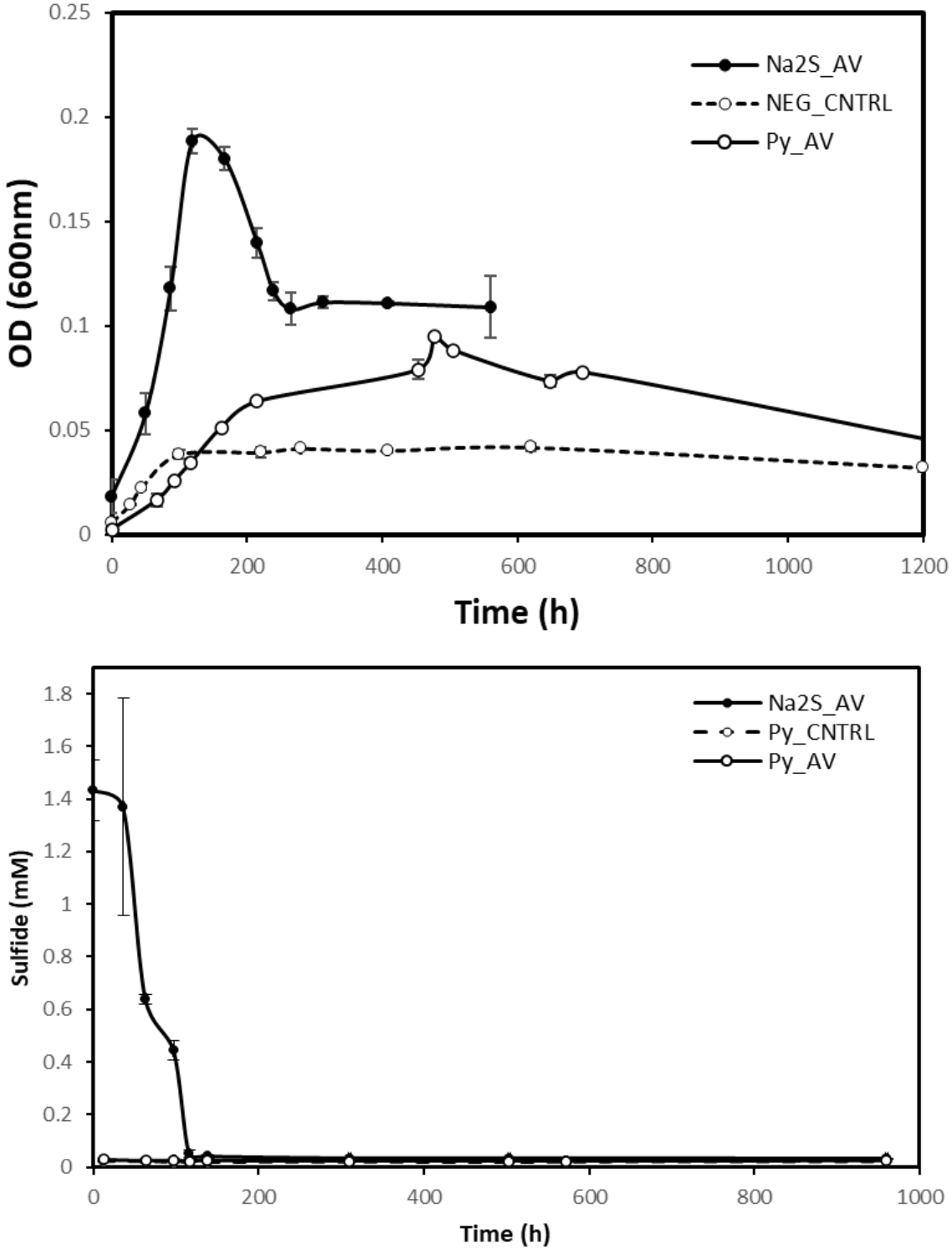

Figure 2-7 Growth profile of pyrite culture showing optical density (600nm) shown above and sulfide depletion curve on the bottom.

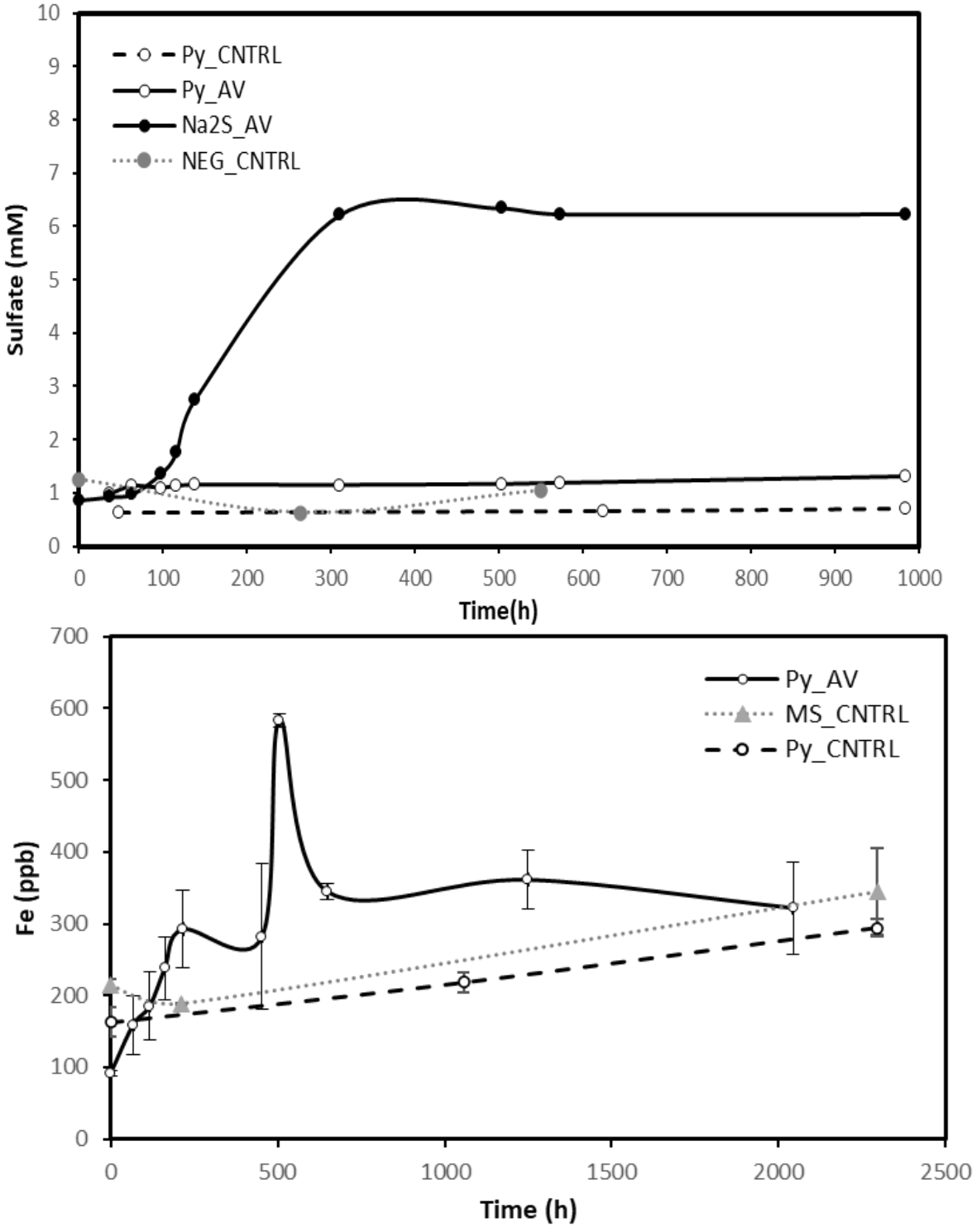

Figure 2-8 Growth profile of Pyrite culture displaying sulfate change plot on the top and ICP-MS on the bottom measuring Iron concentration changes over time.

Table 2-1 Pyrite transcriptome gene table showing genes with log2FC above 2 or below -2

No.	***Gene locus***	***log2FC***	Padj	***KEGG or Strindb annotation***
Upregulated genes				
1	Alvin_1093	7.45	5.6E-132	Diheme cytochrome subunit of sulfide dehydrogenase
2	Alvin_0022	7.10	7.8E-116	Domain of unknown function DUF1924
3	Alvin_1092	6.18	1.7E-75	Flavocytochrome c sulphide dehydrogenase
4	Alvin_0023	5.54	1.8E-85	Diheme cytochrome c
5	Alvin_1379	5.50	1.9E-03	2-isopropylmalate synthase
6	Alvin_1095	5.39	2.1E-87	epoxyqueuosine reductase
7	Alvin_0024	5.32	8.9E-30	membrane protein-like protein
8	Alvin_0021	5.13	4.6E-46	cytochrome B561
9	Alvin_1094	4.83	4.2E-62	uncharacterized protein
10	Alvin_0013	4.59	3.0E-36	outer membrane efflux protein
11	Alvin_2309	4.57	2.1E-52	Hydrogenase (NiFe) small subunit HydA
12	Alvin_2308	4.50	7.3E-64	Hydrogenase (NiFe) small subunit HydA
13	Alvin_0020	4.38	1.0E-37	Diheme cytochrome c
15	Alvin_0014	4.21	1.1E-29	efflux transporter, RND family, MFP subunit
16	Alvin_0025	4.15	3.8E-35	two component transcriptional regulator
18	Alvin_2307	3.90	1.9E-70	Ni/Fe-hydrogenase, b-type cytochrome subunit
21	Alvin_2451	3.63	2.7E-37	molybdopterin oxidoreductase Fe4S4 region
22	Alvin_1527	3.62	7.3E-26	FeoA family protein (Fe2+ transport)
23	Alvin_0019	3.51	2.4E-26	ferrous-iron efflux pump FieF
26	Alvin_1848	3.51	1.1E-35	isocitrate lyase
27	Alvin_2446	3.44	7.5E-17	nitrite and sulphite reductase 4Fe-4S region
29	Alvin_1878	3.36	2.6E-03	nitrogen fixation protein FixT
30	Alvin_0017	3.36	5.6E-29	XRE family transcriptional regulator

31	Alvin_2306	3.29	4.8E-36	hydrogenase expression/formation protein, HoxM
32	Alvin_0018	3.24	4.1E-26	Di-heme cytochrome c peroxidase
33	Alvin_3291	3.20	4.8E-30	hypothetical protein
34	Alvin_1145	3.09	1.9E-39	periplasmic protein CpxP/Spy
35	Alvin_0015	3.02	9.0E-19	heavy metal efflux pump, CzcA family
36	Alvin_2447	3.00	4.2E-12	adenylylsulfate reductase
37	Alvin_2093	2.96	9.6E-11	hydrogenase (NiFe) small subunit HydA
38	Alvin_0016	2.93	3.2E-15	conserved hypothetical protein
39	Alvin_2111	2.92	1.9E-41	Sulfur-oxidizing protein soxy; SoxY
40	Alvin_3196	2.81	3.3E-07	hypothetical protein
41	Alvin_0431	2.81	1.9E-17	hypothetical protein
42	Alvin_1034	2.77	3.5E-19	Phosphoketolase
43	Alvin_3016	2.75	2.7E-19	type IV fimbrial biogenesis protein FimT
44	Alvin_0929	2.75	4.8E-13	hypothetical protein
45	Alvin_0926	2.61	9.7E-15	PRC-barrel domain protein
46	Alvin_2452	2.57	2.1E-19	formate dehydrogenase, alpha subunit
47	Alvin_2092	2.50	3.3E-13	conserved hypothetical protein
48	Alvin_2110	2.50	3.3E-12	peptidase M48 Ste24p
49	Alvin_1143	2.47	1.4E-15	twin-arginine translocation pathway signal
50	Alvin_1556	2.46	5.9E-31	hypothetical protein
51	Alvin_3275	2.44	2.9E-19	phage recombination protein Bet
52	Alvin_1525	2.43	1.1E-17	ferrous iron transport protein B
53	Alvin_2112	2.40	2.4E-21	SoxZ; PFAM: Sulphur oxidation protein SoxZ
54	Alvin_1420	2.39	1.9E-26	iron-sulfur cluster assembly transcription factor IscR
55	Alvin_1524	2.30	2.3E-03	Protein of unknown function DUF1920

56	Alvin_0483	2.29	2.8E-20	catalase/peroxidase HPI
57	Alvin_1152	2.26	3.8E-20	uncharacterized conserved protein UCP029693
58	Alvin_2311	2.26	5.9E-16	transaldolase
59	Alvin_1146	2.24	4.4E-19	hypothetical protein
60	Alvin_1446	2.22	2.7E-12	antitoxin HigA-1
61	Alvin_2710	2.22	2.6E-06	hypothetical protein
62	Alvin_1954	2.21	1.2E-14	flagellar protein FliS
63	Alvin_1856	2.20	5.6E-16	Fe(ii) trafficking protein yggx;
64	Alvin_1521	2.19	2.3E-15	Cu(i)/ag(i) efflux system periplasmic protein cusf;
65	Alvin_0492	2.18	6.2E-19	conserved hypothetical protein
66	Alvin_2145	2.18	6.9E-16	sulfide:quinone oxidoreductase
67	Alvin_0026	2.18	1.5E-14	Integral membrane signal transduction histidine kinase
68	Alvin_0900	2.17	2.1E-14	hypothetical protein
69	Alvin_2989	2.17	2.8E-18	NAD(P)H dehydrogenase (quinone)
70	Alvin_1144	2.15	3.9E-07	CsbD family protein
71	Alvin_1953	2.15	6.9E-25	flagellar hook-associated 2 domain protein
72	Alvin_1150	2.12	9.5E-16	conserved hypothetical protein
73	Alvin_1952	2.07	3.6E-25	flagellar protein FlaG
74	Alvin_2454	2.06	5.3E-11	formate dehydrogenase subunit gamma
75	Alvin_1877	2.05	5.3E-04	4Fe-4S ferredoxin iron-sulfur binding domain protein
76	Alvin_0107	2.05	3.9E-13	conserved hypothetical protein
77	Alvin_2704	2.04	1.1E-12	conserved hypothetical protein
78	Alvin_2312	2.01	1.2E-09	Integral membrane protein TerC (tellurite resistance)
79	Alvin_0098	2.01	2.8E-16	transcriptional regulator, GntR family
80	Alvin_1154	2.00	7.4E-08	conserved hypothetical protein
Downregulated genes				

81	Alvin_0704	-6.85	1.2E-47	Antenna complex alpha/beta subunit
82	Alvin_0703	-6.83	3.3E-10	hypothetical protein
83	Alvin_0705	-6.62	1.5E-78	hypothetical protein
84	Alvin_1741	-6.22	3.7E-36	hypothetical protein
85	Alvin_0706	-6.21	1.4E-42	antenna complex alpha/beta subunit
86	Alvin_0709	-5.80	6.1E-21	Light-harvesting complex 1 beta chain
87	Alvin_0962	-5.75	6.5E-108	uncharacterized protein
88	Alvin_1740	-5.48	4.9E-36	Dinitrogenase iron-molybdenum cofactor biosynthesis protein
89	Alvin_2136	-5.23	9.4E-76	hypothetical protein
90	Alvin_1739	-5.16	1.2E-51	Cobyrinic acid ac-diamide synthase
91	Alvin_1365	-4.74	4.0E-08	Ribulose-bisphosphate carboxylase
92	Alvin_1251	-4.72	2.5E-25	Dissimilatory sulfite reductase alpha subunit
93	Alvin_3072	-4.69	3.2E-68	conserved hypothetical protein
94	Alvin_1252	-4.45	4.8E-30	dissimilatory sulfite reductase beta subunit
95	Alvin_2515	-4.06	9.3E-94	hypothetical protein
96	Alvin_2248	-3.99	8.1E-23	Outer membrane receptor for ferrienterochelin and colicins;
97	Alvin_2497	-3.96	1.7E-52	conserved hypothetical protein
98	Alvin_0747	-3.87	2.6E-18	peptidase C39 bacteriocin processing
99	Alvin_1006	-3.87	3.6E-47	Peroxiredoxin
100	Alvin_2498	-3.59	1.6E-74	nitrogen fixation-related protein
101	Alvin_1253	-3.54	3.2E-26	DsrE
102	Alvin_1367	-3.48	1.3E-03	CbbQ/NirQ/NorQ domain protein
103	Alvin_0707	-3.41	5.2E-20	regulatory protein LuxR
104	Alvin_2767	-3.37	4.1E-51	DEAD/DEAH box helicase domain protein
105	Alvin_1738	-3.35	7.8E-38	Cobyrinic acid ac-diamide synthase

106	Alvin_1711	-3.28	1.8E-08	hypothetical protein
107	Alvin_0500	-3.27	6.8E-27	protein of unknown function DUF150
108	Alvin_1366	-3.25	1.0E-03	Ribulose-bisphosphate carboxylase
109	Alvin_0749	-3.17	5.2E-04	hypothetical protein
110	Alvin_2759	-3.15	8.0E-03	hypothetical protein
111	Alvin_1841	-3.13	1.3E-64	Protein of unknown function
112	Alvin_2550	-3.10	2.2E-11	antenna complex alpha/beta subunit
113	Alvin_2572	-3.07	2.0E-28	RNA polymerase, sigma 32 subunit, RpoH
114	Alvin_3032	-3.04	8.0E-33	conserved hypothetical protein
115	Alvin_0708	-3.03	2.3E-07	hypothetical protein
116	Alvin_1737	-2.98	1.9E-15	Dinitrogenase iron-molybdenum cofactor biosynthesis protein
117	Alvin_2429	-2.95	8.1E-39	NADH-quinone oxidoreductase, B subunit
118	Alvin_1508	-2.92	4.9E-23	sulfur relay protein, TusE/DsrC/DsvC family
119	Alvin_1254	-2.88	1.9E-19	DsrF
120	Alvin_2576	-2.80	1.9E-02	antenna complex alpha/beta subunit
121	Alvin_0501	-2.79	2.6E-22	NusA antitermination factor
122	Alvin_2250	-2.78	1.5E-21	Biopolymer transport protein ExbD/TolR
123	Alvin_2577	-2.78	7.9E-03	antenna complex alpha/beta subunit
124	Alvin_2428	-2.76	1.8E-30	NADH (or F420H2) dehydrogenase, subunit C
125	Alvin_2768	-2.74	2.1E-25	RNP-1 like RNA-binding protein
126	Alvin_1122	-2.73	2.5E-16	conserved hypothetical protein
127	Alvin_2554	-2.73	4.3E-03	antenna complex alpha/beta subunit
128	Alvin_1688	-2.73	1.5E-06	Antibiotic biosynthesis monooxygenase
129	Alvin_2430	-2.73	4.4E-30	NADH-ubiquinone/plastoquinone oxidoreductase chain 3
130	Alvin_3073	-2.70	4.2E-22	C4-dicarboxylate transporter/malic acid transport protein

131	Alvin_0834	-2.69	9.0E-19	NAD(P)(+) transhydrogenase (AB-specific)
132	Alvin_2549	-2.68	1.8E-02	antenna complex alpha/beta subunit
133	Alvin_2249	-2.66	1.1E-26	MotA/TolQ/ExbB proton channel
134	Alvin_2251	-2.65	8.3E-18	Biopolymer transport protein ExbD/TolR
135	Alvin_2551	-2.64	5.0E-03	photosynthetic reaction centre cytochrome c subunit
136	Alvin_2600	-2.63	7.8E-23	SirA family protein
137	Alvin_0744	-2.63	6.5E-11	sigma54 specific transcriptional regulator, Fis family
138	Alvin_2432	-2.62	8.7E-30	triosephosphate isomerase
139	Alvin_0805	-2.60	1.4E-23	2-oxo-acid dehydrogenase E1 subunit, homodimeric type
140	Alvin_2579	-2.59	1.9E-02	antenna complex alpha/beta subunit
141	Alvin_1687	-2.58	6.6E-06	ATP dependent RNA helicase
142	Alvin_2760	-2.57	9.1E-09	antenna complex alpha/beta subunit
143	Alvin_2254	-2.56	2.2E-14	conserved hypothetical protein
144	Alvin_2548	-2.54	7.5E-10	antenna complex alpha/beta subunit
145	Alvin_2552	-2.51	5.5E-03	photosynthetic reaction center, M subunit
146	Alvin_1712	-2.48	2.1E-12	conserved hypothetical protein
147	Alvin_0316	-2.45	2.2E-19	transketolase
148	Alvin_2280	-2.44	1.7E-26	translation initiation factor IF-1
149	Alvin_2599	-2.35	8.7E-23	Rhodanese domain protein
150	Alvin_1690	-2.32	6.1E-13	transport system permease protein
151	Alvin_1754	-2.29	2.9E-13	translation elongation factor P
152	Alvin_1689	-2.28	9.4E-15	periplasmic binding protein
153	Alvin_2484	-2.25	1.5E-17	16S rRNA processing protein RimM
154	Alvin_1483	-2.24	2.9E-13	hydrolase, TatD family
155	Alvin_1890	-2.23	2.1E-15	acyl carrier protein

156	Alvin_0040	-2.20	3.1E-17	ATP synthase F0, A subunit
157	Alvin_2427	-2.20	2.7E-16	NADH dehydrogenase I, D subunit
158	Alvin_1691	-2.19	4.8E-08	ABC transporter related protein
159	Alvin_0499	-2.19	1.2E-14	hypothetical protein
160	Alvin_1259	-2.19	1.7E-18	DsrL
161	Alvin_1753	-2.18	8.6E-22	tRNA synthetase class II
162	Alvin_1893	-2.18	3.3E-09	3-oxoacyl-(acyl-carrier-protein) synthase III
163	Alvin_1258	-2.17	2.9E-26	dsrK
164	Alvin_1896	-2.17	7.0E-19	protein of unknown function DUF177
165	Alvin_3195	-2.16	1.2E-03	hypothetical protein
166	Alvin_0039	-2.16	3.3E-21	ATP synthase I chain
167	Alvin_0804	-2.15	9.7E-26	pyruvate dehydrogenase complex dihydrolipoamide
168	Alvin_0746	-2.15	4.3E-10	hypothetical protein
169	Alvin_0315	-2.14	6.4E-13	glyceraldehyde-3-phosphate dehydrogenase, type I
170	Alvin_1734	-2.12	9.5E-08	Protein of unknown function DUF2269, transmembrane
171	Alvin_1260	-2.11	4.5E-15	dsrJ
172	Alvin_2426	-2.11	2.6E-10	NADH-quinone oxidoreductase, E subunit
173	Alvin_2758	-2.10	7.8E-22	poly(A) polymerase
174	Alvin_2601	-2.09	2.0E-20	conserved hypothetical protein
175	Alvin_2156	-2.08	6.6E-11	GTP-binding protein Obg/CgtA
176	Alvin_2252	-2.07	3.1E-12	TonB family protein
177	Alvin_2491	-2.06	3.8E-19	molybdopterin oxidoreductase
178	Alvin_2602	-2.03	1.6E-19	acetolactate synthase, large subunit
179	Alvin_2415	-2.01	8.4E-09	conserved hypothetical protein
180	Alvin_1644	-2.01	1.4E-14	integration host factor, beta subunit

181	Alvin_1079	-2.01	2.0E-10	cytochrome B561
182	Alvin_2386	-2.00	2.2E-23	peptide chain release factor 1

Table 2-2 Pyrite Sulfur oxidation gene expression for *sox* and *dsr* genes

Gene	Protein	log_2FC	Padj
***dsr* genes**			
Alvin_1251	DsrA	-4.723	2.54E-25
Alvin_1252	DsrB	-4.454	4.76E-30
Alvin_1253	DsrE	-3.541	3.15E-26
Alvin_1254	DsrF	-2.883	1.89E-19
Alvin_1259	DsrL	-2.187	1.70E-18
Alvin_1258	DsrK	-2.168	2.94E-26
Alvin_1260	DsrJ	-2.113	4.47E-15
Alvin_1261	DsrO	-1.987	5.20E-20
Alvin_1262	DsrP	-1.678	1.86E-15
Alvin_1256	DsrC	-1.247	1.07E-07
***sox* genes**			
Alvin_2111	SoxY	2.919	1.91E-41
Alvin_2112	SoxZ	2.40	2.39E-21
Alvin_2167	SoxB	1.22	2.19E-07
Alvin_2169	SoxA	1.175	0.00714587
Alvin_2168	SoxX	1.074	0.00178113

Table 2-3 Pyrite photosynthetic gene expression of *puc* and *puf* genes

Gene	Protein	log_2FC	Padj
***puf* genes (LH1)**			
Alvin_2550	puf/LH1	-3.105	2.23E-11
Alvin_2554	puf/LH1	-2.729	0.0042904
Alvin_2549	puf/LH1	-2.685	0.0180326
Alvin_2551	pufC	-2.637	0.0050426
Alvin_2548	puf/LH1	-2.543	7.53E-10
Alvin_2552	pufM	-2.506	0.0054761
Alvin_2555	puf/LH1	-1.963	9.55E-05
Alvin_2553	pufL	-1.657	1.18E-06
Alvin_2634	puf/LH1	-1.571	1.35E-11
***puc* genes (LH2)**			
Alvin_0704	pucB6	-6.853	1.15E-47
Alvin_0703	pucA6	-6.829	3.27E-10
Alvin_0705	pucA5	-6.622	1.51E-78
Alvin_0706	pucB5	-6.214	1.40E-42
Alvin_0709	pucB4	-5.797	6.10E-21
Alvin_2759	pucA3	-3.155	7.98E-03
Alvin_0708	pucA4	-3.027	2.25E-07
Alvin_2576	pucA2	-2.803	1.89E-02

Alvin_2577	pucB2	-2.775	0.0079294
Alvin_2579	pucB1	-2.594	1.93E-02
Alvin_2760	pucB3	-2.570	9.14E-09
Alvin_2578	pucA1	-1.997	0.000097

Table 2-4 Most upregulated and downregulated hypotheitcal genes on pyrite transcriptome

Gene locus	log2FC	Padj	KEGG or Strindb annotation	pBlast %	AA length	Sequence protein domains	Protein motifs	TM domains	Hydropathicity
Alvin_0022	7.1041489	7.80E-116	Domain of unknown function DUF1924	81.76	118	DUF-1924	signal peptide (1-23)	TM (5-25)	-0.403
Alvin_1094	4.8284897	4.22E-62	uncharacterized protein	97.62	320	Ankyrin repeats	signal peptide (1-27)	none	0.05
Alvin_0703	-6.828682	3.27E-10	hypothetical protein	99.15	53	LHC	none	TM (8-25)	0.692
Alvin_0705	-6.622227	1.51E-78	hypothetical protein	98.51	69	LHC	none	TM (24-46)	0.648
Alvin_1741	-6.216786	3.70E-36	hypothetical protein	100	78	none	coiled-coil (51-71)	none	-0.735
Alvin_2136	-5.228499	9.42E-76	hypothetical protein	99.4	138	none	signal peptide (1-24)	TM (7-24)	-0.107
Alvin_0962	-5.75253	6.48E-108	uncharacterized protein	98.41	176	Ankyrin repeats	signal peptide (1-22)	TM (1-20)	-0.067

Table 2-5 Pyrite Identification of motifs CXXCH and LXXC and Signal Peptides

Gene	Position	Description	Number of CXXCH motif	LXXC motif	NCBI Protein ID	SignalP	Upregulated in cells on pyrite?	upregulated in cells on elemental sulfur?
Alvin_0018	76..80	Di-heme cytochrome c peroxidase	2		ADC60990		Yes (9.4)	Yes (2.2)
	258..262							
Alvin_0020	56..60	Diheme cytochrome c	2	Yes	ADC60992	Yes	Yes (20.8)	No (0.8)
	165..169							
Alvin_0022	48..52	Domain of unknown function DUF1924	1		ADC60994	Yes	Yes (137.6)	No (0.08)
Alvin_0023	54..58	Diheme cytochrome c	2		ADC60995	Yes	Yes (46.5)	No (0.7)
	155..159							
Alvin_0070	50..54	cytochrome c1	1		ADC61042	Yes	Yes (1.5)	No (0.2)
Alvin_0071	9..13	Glutathione S-transferase domain protein	1	Yes	ADC61043		Yes (1.2)	No (0.3)
Alvin_0091	76..80	Thiosulfate dehydrogenase	2		ADC61061	Yes	Yes (2.6)	Yes (1.7)
	187..191							
Alvin_0350	159..163	nicotinate-nucleotide pyrophosphorylase	1		ADC61311		Yes (1.1)	N/A
Alvin_0439	43..47	transmembrane region and signal peptide prediction	1	Yes	ADC61398	Yes	No (0.8)	No (0.1)
Alvin_0679	76..80	Cytochrome-c peroxidase	2	Yes	ADC61628	Yes	No (0.9)	No (0.6)
	222..226							
Alvin_0782	105..109	cytochrome c oxidase, cbb3-type, subunit II	1		ADC61729		Yes (2.2)	Yes (6.2)
Alvin_0784	120..124	cytochrome c class I	2		ADC61731		Yes (1.8)	Yes (6.2)
	206..210							
Alvin_1073	877..881	FAD linked oxidase domain protein	1	Yes	ADC62012		No (0.9)	No (0.4)
Alvin_1093	36..40	cytochrome c class I	2		ADC62032	Yes	Yes (175.0)	Yes (4.5)
	126..130							
Alvin_1095	44..48	NapC/NirT cytochrome c domain protein	4	Yes	ADC62034		Yes (41.8)	Yes (9.6)
	73..77							
	133..137							
	165..169							
Alvin_1259	633..637	DsrL	1		ADC62198		No (0.2)	No (0.2)
Alvin_1260	83..87	DsrJ	3	Yes	ADC62199	Yes	No (0.2)	No (0.1)

	106..110							
	119..123							
Alvin_1395	72..76	cytochrome c family protein	8	Yes	ADC62330	Yes	No (0.5)	No (0.01)
	122..126							
	146..150							
	195..199							
	237..241							
	275..279							
	303..307							
	489..493							
Alvin_1402	172..176	Fe-S cluster assembly protein NifU	1	Yes	ADC62337		No (1.0)	Yes (1.3)
Alvin_1452	46..50	conserved hypothetical protein	7		ADC62387	Yes	Yes (1.7)	Yes (1.1)
	85..89							
	109..113							
	151..155							
	180..184							
	210..214							
	238..242							
Alvin_1454	130..134	hypothetical protein	8		ADC62389		Yes (2.6)	No (1.0)
	230..234							
	262..266							
	306..310							
	360..364							
	392..396							
	419..423							
	681..685							
Alvin_1467	37..41	Alcohol dehydrogenase GroES domain protein	2	Yes	ADC62401		Yes (2.4)	Yes (5.5)
	96..100							
Alvin_1573	150..154	methyl-accepting chemotaxis sensory transducer	1		ADC62506		Yes (1.6)	No (0.8)
Alvin_1694	24..28	cytochrome c class I	1		ADC62626	Yes	No (0.5)	Yes (3.0)
Alvin_1837	50..54	putative lipoprotein	2	Yes	ADC62762	Yes	Yes (1.6)	Yes (1.1)
	389..393							
Alvin_1846	57..61	cytochrome c class I	2		ADC62771	Yes	Yes (1.8)	Yes (1.5)
	151..155							

Alvin_1867	17..21	NADH ubiquinone oxidoreductase 20 kDa subunit	1	Yes	ADC62792		Yes (2.2)	N/A
Alvin_1971	87..91	Coproporphyrinogen dehydrogenase	1	Yes	ADC62895		Yes (2.6)	Yes (5.5)
Alvin_2064	61..65	protein of unknown function DUF255	1	Yes	ADC62986		Yes (1.7)	Yes (4.4)
Alvin_2168	56..60	SoxX	1	Yes	ADC63089	Yes	Yes (2.1)	Yes (5.7)
Alvin_2169	195..199	SoxA	1		ADC63090	Yes	Yes (2.3)	Yes (5.4)
Alvin_2172	89..93	HNH endonuclease	1		ADC63093		No (0.5)	Yes (1.1)
Alvin_2201	150..154	conserved hypothetical protein	1		ADC63122	Yes	No (0.6)	No (0.7)
Alvin_2458	41..45	NapC/NirT cytochrome c domain protein	4		ADC63370		Yes (1.9)	Yes (1.7)
	71..75							
	125..129							
	161..165							
Alvin_2459	46..50	hypothetical protein	1		ADC63371	Yes	Yes (1.8)	No (0.9)
Alvin_2490	13..17	4Fe-4S ferredoxin iron-sulfur binding domain protein	1	Yes	ADC63402		No (0.3)	No (0.2)
Alvin_2551	107..111	photosynthetic reaction center cytochrome c subunit	4	Yes	ADC63461	Yes	No (0.2)	No (0.005)
	152..156							
	247..251							
	307..311							
Alvin_2765	144..148	cytochrome c prime	1		ADC63674	Yes	Yes (2.4)	Yes (2.6)
Alvin_2879	42..46	cytochrome c class I	2		ADC63784	Yes	No (1.0)	No (0.4)
	138..142							
Alvin_3050	37..41	ribosomal protein L31	1		ADC63950		No (0.4)	No (0.7)
Alvin_3069	41..45	Thioredoxin domain protein	1		ADC63969		Yes (1.2)	Yes (6.6)
Alvin_3120	550..554	type II secretion system protein E	1	Yes	ADC64019		No (0.8)	No (0.7)
Alvin_3135	93..97	Radical SAM domain protein	1	Yes	ADC64033		Yes (1.6)	N/A

Chapter 3 Utilization of Iron Sulfide (FeS) by *Allochromatium Vinosum* - Transcriptomic Insight into the Bacteria-Solid Substrate Interaction Mechanisms

3.1 Abstract

Purple sulfur bacteria (PSB), a group of phototrophic sulfur bacteria that thrive in illuminated anoxic environments, have long been acknowledged as vital players in the intricate web of the sulfur cycle. Their role becomes even more pronounced in environments where oxygen is scarce. Within this group, *Allochromatium vinosum* stands out for its unique metabolic capabilities. In this study, we delved deeper into the growth potential of *A. vinosum*, particularly focusing on its ability to utilize solid-phase FeS nanoparticles. These nanoparticles serve a dual purpose, acting as both a sulfur source and an electron-donor, a feature that could have significant implications for biotechnological applications. Our observations revealed some intriguing patterns. When *A. vinosum* was cultured with FeS nanoparticles, its growth rate was curtailed by approximately 20% in comparison to the negative control. This disparity in growth rates led us to postulate that *A. vinosum* might be tapping into metabolic pathways similar to those that bolster the negative control. Nonetheless, growth profiles findings did show evidence of sulfur oxidation activity. A marked change in the expression of sulfur oxidation genes, especially the *sox* expression, was observed. Another significant observation was the increased polysulfide content in XPS. When coupled with a notable 400uM rise in sulfate, as detected by Ion Chromatography (IC), it became evident that a robust sulfur oxidation pathway was at play within the FeS system. Such a pathway would be improbable in a sulfur-depleted environment, highlighting the unique metabolic adaptability of *A. vinosum*.

Our ICP-MS analyses further enriched our understanding. A discernible dissolution effect on abiotic FeS was identified, suggesting that the growth of *A. vinosum* might be augmented by the inherent dissociation properties of FeS. Delving into the transcriptomic data, we found that a significant portion of the transcriptomes from both the FeS system and the negative control were dedicated to encoding redox-active proteins. Two proteins, in particular, flavocytochrome 1093 and the NapC/NirT cytochrome c domain protein Alvin_1095, displayed heightened expression levels in both systems. Their elevated presence hints at a potential central role in redox pathways, possibly forming the core of an electron transport metabolic pathway that efficiently harvests electrons from a variety of substrates. Transcriptomic findings also displayed the upregulation of transporter, hypothetical, hydrogenases and sulfate assimilation genes shown in this study. While our findings provide a comprehensive overview of *A. vinosum*'s growth dynamics in the FeS system, they also underscore the need for further research. The exact influence of *A. vinosum* on FeS utilization in the media remains elusive, as does the full impact of dissolution and other supporting pathways on the overall growth of the culture system.

In conclusion, this research serves as a foundational step towards understanding the intricate relationship between *A. vinosum* and the FeS system. The insights gleaned from our study, from the activation of specific sulfur oxidation genes to the potential roles of electron transport proteins, pave the way for future investigations. A more in-depth exploration is paramount to fully unravel the complexities of *A. vinosum*'s interaction with FeS and its broader implications for the field of microbial ecology and biotechnology.

3.2 Introduction

Purple sulfur bacteria (PSB) are a group of photosynthetic gram-negative bacteria that thrive in aquatic environments and are known for their ability to perform anoxygenic photosynthesis. They belong to the *Proteobacteria* phylum. Aside from *Proteobacteria*'s major contributions to sulfur and carbon cycles are capable of nitrogen fixation (Dincturk, *et al.*, 2011). Purple sulfur bacteria exhibit remarkable adaptability and can utilize various electron donors, including sulfur compounds, organic acids, and hydrogen, making them significant contributors to nutrient cycling and energy exchange in aquatic ecosystems (Ehrenreich *et al.*, 1994; Daldal *et al.*, 2008).

One distinctive characteristic of PSB is their ability to form sulfur globules, which are subsequently oxidized to sulfate as part of their metabolic process. These bacteria deposit solid-phase sulfur globules either outside the cell membrane or inside the periplasmic space, depending on their belonging to the *Ectothiorhodospiracea* or *Chromaticeae* families (Daldal *et al.*, 2008). The sulfur globules formed in purple or green sulfur bacteria have been previously examined and shown to contain organic coating which maintains the gobules' amorphous nature (Prange *et al.*, 1999; Marnocha *et al.*, 2019). Pathways of sulfur globule utilization have also been proposed (Dahl *et al.*, 2020); however, major gaps exist in our understanding of how PSB oxidize the intracellular or extracellular sulfur globules. The capability of PSB in storing sulfur and utilizing both soluble and insoluble forms of sulfur may have enabled them to thrive in diverse environments under anoxic conditions, especially within photic zones (Seitz *et al.*, 1991; Magian *et al.*, 1984; Hunter *et al.*, 2009).

Phylogenetically diverse lineages of bacteria have been found capable of utilizing solid-phase substrate for their energy needs. As reviewed by Doyle *et al.* (2015), many of the identified species are classified as electrochemically active bacteria (EAB). Although the term of EAB has

its roots in the study of microbial electron exchange with electrodes (Lovley *et al.*, 2012), electroactive microorganisms flourish in many electrode- free 'electromicrobiomes' of ecological significance (El-Naggar *et al.*, 2010; Garbini *et al.*, 2023; Temirbekova *et al., 2023;* Lovley *et al.*, 2022)). These microorganisms electrically interact with other microbial species, minerals or soluble extracellular electron acceptors and donors that cannot enter the cell.

The phenomenon of extracellular electron transfer has been demonstrated in over ~ 100 microbes to date, perhaps most notably in *Geobacter sulfurreducens* and *Shewanella oneidensis*, where a network of multiheme c-type cytochromes on the inner membrane, periplasm, and outer membrane couple intracellular energy reactions with the use of external solid electron donors or acceptors (Shi *et al.* 2016; Breuer *et al.* 2015; Chong *et al.* 2018; Costa *et al.* 2018). Multiheme cytochromes (MHCs) in particular are key players in extracellular electron transfer (Chong *et al.* 2018), as the proximity and arrangement of hemes can allow efficient intra-protein electron transfer (Gray *et al.*, 2004).

Within the collection of microbes that utilize solid-phases either through oxidation or reduction, a few different bacterial classes have been described in the literature. Electrochemically active bacteria (EAB) harness energy from solid-phase substrates through various mechanisms. Direct interspecies electron transfer (DIET) involves direct electron exchange between microorganisms, facilitated by conductive pili and membrane-bound cytochromes, with materials like carbon and magnetite acting as electron conduits (Wang W et al., 2021). Mineral respiration, another EAB mechanism, involves microbial reduction of solid minerals, with electron transfer mediated by outer membrane cytochromes like MtrC and OmcA (Mitchell et al., 2012). Extracellular Electron Transfer (EET) is a process where EAB transfer electrons externally, involving the Mtr pathway in Shewanella odeinensis and flavin molecules for electron shuttling (Light SH et al., 2018; Shi et al., 2016). Specific bacterial pathways, such as in

Rhodopseudomonas palustris (Miranda-Brito et al., 2023) and Sideroxydans lithotrophicus (Zhou N et al., 2022), highlight diverse mechanisms for iron and metal oxidation.

The utilization of external solid-phase substrates by anoxygenic photosynthetic bacteria (i.e., PSB) remains an intriguing area of investigation. Although Franz *et al.* demonstrated that a PSB strain *Allochromatium vinosum* was able to grow on commercially available elemental sulfur as the electron donor (Franz *et al.*, 1997 and 1999), cavears remain in our understanding of which part of the elemental sulfur is bioavailable and what pathway the bacteria follow to metabolize the substrate. The purpose of our study was to investigate the utilization of FeS by *A. vinosum* as both an electron source and sulfur source. Previous research has demonstrated that other bacteria, such as Acidothiobacillus ferrooxidans, can also utilize FeS in mining settings (Zhan *et al.*, 2019). The utilization of FeS by *A. vinosum* could potentially lead to a re-evaluation of the role of phototrophic sulfur bacteria (PSB) in nutrient cycles within their environments. Additionally, this study aims to shed light on the potential use of *A. vinosum* in microbial fuel cells. Following confirming that *A. vinosum* can grow autotrophically using pyrite as the sole electron donor, we continue to test the possibility of *A. vinosum* using iron monosulfide formed from organic ligand-free precipitation synthesis. We found that FeS system displayed evidence of sulfur oxidation but at least to a an extent due to the dissolution effect of FeS as shown in the abiotic control ICP-MS measurements. Furthermore, having FeS sustaining only a portion of the cells that the negative control can support suggests that *A. vinosum* didn't influence release of electrons from FeS or sulfur. The collection of redox active proteins upregulated in the transcriptome analysis may grant for a deeper look into this system. In our study we found that flavocytochrome Alvin_1093 and NapC/NirT cytochrome c domain protein Alvin_1095 exhibited significant upregulated in the transcriptome. Other redox-active genes, including Alvin_0020, Alvin_0022, Alvin_0021, and Alvin_1402, were identified to contain lipid and heme binding motifs. Transcriptome analysis showed considerable upregulation

of genes associated directly or indirectly with cytochromes, flavin molecules, proteins found widespread in the literature to be involved in electron transfer reaction in EAB.

In summary, our study provides insights into the potential utilization of solid-phase FeS nanoparticles by *A. vinosum* and highlights the distinct transcriptomic responses and metabolic shifts associated with growth on FeS. The findings need to be studied further and assess the dilution contribution and find an explanation for the reduced growth compared to negative control.

3.3 Materials and Methods

3.3.1 Growth tracking

Growth was monitored over time by carefully taking aliquot samples without disrupting sedimented nanoparticles, thereby preventing an overestimation of cellular density. The samples were processed through a 1:10 dilution in water and subsequently placed in a UV-VIS spectrophotometer for optical density measurements at 600nm.

3.3.2 Strain, medium and culture conditions

A. vinosum DSM 180 was obtained from DSMZ, Germany. Media were prepared following Pfenning's recipe with modifications that removed compounds allowing for heterotrophic growth. Three types of media were prepared: sulfur-free control, positive control, and FeS-amended cell cultures (see appendix table 1 for media ingredients). The positive control medium was amended with $Na_2S{\cdot}9H_2O$, while the FeS medium contained 750 mg/L of FeS. The sulfur-free control contained neither $Na_2S{\cdot}9H_2O$ nor FeS. To prepare the media, two solutions (A and B) were made separately. Solution A was prepared by boiling Milli-Q water and degassing it with N_2 gas. All salts except for the carbon and sulfur sources were added to the degassed solution and further degassed with N2 for 45 min. A mineral mix, 10 µL/mL. was added to the cooled solution A, followed by trace amounts of concentrated 6N HCl to a pH of 7.1-7.3. Solution B was prepared by boiling and N2-degassed/cooled Milli-Q water and then sterilized using 0.2-µm syringe filters.

$NaHCO_3$ and $Na_2S \cdot 9H_2O$/FeS were added to solution B immediately prior to sealing the bottles. Full media was made by mixing 90% of solution A and 10% of solution B by volume. Then, *A. vinosum* was inoculated into the media by adding 2% (v/v) of the stock cell culture medium. Two types of negative controls were created: non-inoculated culture of FeS-amended medium, and inoculated culture of the sulfur-free medium. All cultures were incubated at 37°C under a tungsten lamp. To assess the potential growth of bacteria in the presence of various components of the culture media, a negative control was prepared. The negative control system was formulated with the same composition as all other MS and positive control systems, except for the exclusion of a sulfur source. The negative control system was then inoculated with *A. vinosum* at a concentration of 2% by volume.

3.3.3 DNA/RNA extraction and QC

Both DNA and RNA were extracted from the cell cultures utilizing a combination of chemical and enzymatic techniques. To begin the extraction process, 1 mL aliquots of the cell culture medium were carefully withdrawn and treated with RNAProtect® to preserve RNA integrity. Subsequently, the samples underwent centrifugation at 5000g for 10 minutes, after which the supernatant was removed, and the remaining samples were promptly frozen at -80°C for storage. The cell pellets obtained from the centrifugation were then subjected to specific extraction protocols: the GenElute Bacterial Genomic DNA kit from Sigma Aldrich was employed for DNA extraction, while the RNeasy Mini kit from Qiagen was utilized for RNA extraction. For RNA extraction, the cell pellets were subjected to a 10-minute treatment with a solution containing proteinase K (10 µL of 20 mg/mL) and lysozyme (100 µL of 15 mg/mL) that had been diluted in TE buffer with a pH of 8. This enzymatic treatment facilitated the digestion of the cell walls, resulting in the release of DNA. Following the extraction procedures, the quality and quantity of the extracted DNA and RNA were evaluated using the Nanodrop® One spectrophotometer and

Qubit fluorometer. To ensure quality control, measurements of the 260/280 and 260/230 ratios were taken, and additional assessment was performed through DIN and RIN analysis using the Tapestation 2200.

3.3.4 Transcriptome and Bioinformatic pipeline

3.3.4.1 RNAseq

To conduct RNA sequencing, cDNA libraries were prepared from total RNA cultures in the logarithmic phase for both NiS samples and the positive control. Next generation sequencing Illumina technology was employed to perform RNAseq analysis. Library preparation kit *Illumina Stranded total RNA prep with ribo-zero plus* (catalog 20040525) was used and run using a *NextSeq 1000/2000 P2 Reagents (300 Cycles) v3* cartridge (catalog 20046813), generating paired-end reads with a read length of 100 bp.

3.3.4.2 Bioinformatics Analysis

The quality of the sample reads was assessed using FastQC (Andrew S, 2010). Raw data underwent processing with Trimmomatic software, which removes adapter regions, eliminats low-quality bases, and discards reads smaller than 60 bp (Anthony M *et al.*, 2014). The resulting high-quality trimmed reads were then aligned to the reference genome of *A. vinosum* (Genbank: CP001896.1) using Bowtie2 software, enabling the generation of indexed reads (Langmead *et al.*, 2012). RSEM software was employed for transcript quantification, utilizing the paired-end indexed data from both the positive control and NiS samples (Li B *et al.*, 2011). Data normalization and statistical analysis to identify differentially expressed transcripts were performed using the DESeq2 package within the R console (Love M *et al.*, 2014). Genes were considered significantly expressed if they had a log2FC change great than 2 or less than -2 with an adjusted p-value below 0.05.

In the analysis of *A. vinosum* transcriptome, STRINGdb was used to construct interactive protein maps to enable visualization of the relationships among the proteins. STRINGdb provides confidence scores for each interaction, contributing to the assessment of their reliability. Leveraging the interactive protein maps and the extensive information available on STRINGdb (Scklarczyk D *et al.*, 2023), I enhanced my analysis by proposing novel connections, evaluating potential interactions, and expanding my comprehension of the biological significance underlying the observed gene expression changes.

The transcriptome was further analyzed based on gene categories associated with sulfur metabolism, redox reactions, CXXCH/LXXC motif-containing genes through the use of SignalP 5.0 (DTU Health Tech, 2023), photosynthesis, hypothetical proteins, and others, as these categories have the potential to contribute to FeS utilization. Additionally, genes that did not fit into these predefined categories were also explored to gain insights into the complete metabolic response of the bacteria under FeS conditions.

3.3.5 Dissolved species characterization

Concentrations of dissolved iron, sulfide, and sulfate in the medium solution were utilized as indirect indicators to track the growth of bacteria in both the positive controls and FeS samples over time. To prevent sulfide loss, collected samples for sulfide measurements were promptly processed. A 100 µL aliquot of each sample was mixed with an excess of zinc(II) chloride solution (approximately 100-fold molar excess of sulfide) to generate metastable ZnS. This stabilized mixture was further reacted with HACH1 and HACH2 solutions, followed by dilution with 400 µL of MQ water to achieve a ~1:10 dilution. The resulting mixture underwent agitation in a rotisserie shaker for 10 minutes. Sulfide measurements were conducted using the HACH sulfide reagent set (HACH method 8131), which reacts with any present sulfide, including the precipitated ZnS, producing an equimolar amount of methylene blue. Absorption at 665 nm was monitored

using a MultiSkan UV-Vis spectrophotometer to quantify the concentrations of generated methylene blue. Sulfate measurements involved collecting aliquots of samples using a nitrogen-purged syringe, followed by a 1:10 dilution with Milli-Q water and subsequent filtration. Dionex ICS-2100 ion chromatography system was employed for sulfate measurements, and quality control was ensured by running a standard curve made with sodium sulfate concurrently. Inductively coupled plasma (ICP)-optical emission spectroscopy (OES) or mass spectrometry (MS) techniques were used to determine the concentrations of major and trace elements in the control and sample solutions, depending on the concentration levels. Aliquots of the medium solution for ICP runs underwent a 100-fold dilution using 2% HNO3 solution and were filtered into 15 mL conical centrifuge tubes (0.2 μm cutoff). Analysis was performed using inductively coupled plasma optical emission spectroscopy (ICP-OES) (iCAP 6500, Thermo Fisher Scientific, Waltham, MA) and inductively coupled plasma mass spectrometry (ICP-MS) (7700 Series, Agilent, Santa Clara, CA) to measure macro- (Ca, K, Mg, Na, P, S) and micro-nutrients (Zn, Fe, Ni, Mo, Cu) levels. Validation of measurements involved preparing and analyzing blank and standard reference materials (NIST-SRF 1570a and 1547, Metuchen, NJ). Standard working curves were generated using spikes at different concentrations, and the recovery rate of all tested elements exceeded 99%. Yttrium (Y) served as an internal standard, and a continuing calibration verification (CCV) sample was analyzed every 15 samples to ensure accuracy.

3.3.6 Solid-phase characterization

Solid phases for biotic and abiotic FeS nanoparticle samples were analyzed using transmission electron microscopy (TEM) and X-ray photoelectron spectroscopy (XPS). The solid pellets obtained through centrifugation and supernatant removal were processed with a 0.1% Triton X-100 solution containing 10 μg/mL of lysozyme and 10 μg/mL of proteinase K to remove bacterial cells and biomolecular debris. Sonication of the pellets in the processing solution was

performed for 45 minutes at room temperature. Subsequently, the solid particles were separated by centrifuging the digestion mixture at 10,000g for 5 minutes at room temperature, followed by removal of the supernatant. The separated solid particles underwent two washes with 0.01% Triton X. All procedures were conducted within the anaerobic chamber using sealed containers to prevent sample oxidation.

For TEM and XPS analyses of the biomass-digested solid particles, specific sample preparation methods were employed. For XPS specimen preparation, the separated particles were dried on a glass slide under anaerobic conditions. Regarding TEM sample preparation, a gold grid with an ultrathin carbon film was utilized. First, 5 μL of anaerobic water was added to the grid, followed by the addition of 10 μL of particle suspension.

XPS spectra were collected using a PHI Quantera SXM instrument (ULVAC-PHI, Japan) with a hemispherical energy analyzer and a monochromatic aluminum target. Survey spectra were obtained at 25 W/15 kV with a spot size of 100 μm, a 45° take-off angle, and a 280 eV pass energy. High-resolution spectrum acquisition employed a 69 eV pass energy with a 0.125 eV scan step. The high-resolution XPS spectra were fitted using Multipak software, with charge correction based on the C 1s species at 284.8 eV.

TEM data were gathered using a JEOL JEM 2100 S/TEM at the Nanoscale Characterization and Fabrication Laboratory located in Virginia Polytechnic Institute and State University. The instrument operated at 200 kV, and TEM bright field images were captured using a Gatan Ultrascan 1000XP CCD camera. Selected area electron diffraction patterns were collected utilizing a Gatan Orius 833 slow scan CCD camera. Furthermore, scanning TEM (STEM) mode was used to obtain Energy Dispersive X-ray Spectroscopy (EDS) data, employing a JEOL genuine 60 mm2 Silicon Drift Detector.

3.4 Results

3.4.1 Growth profiles

The growth characteristics and cell densities of the positive control, negative control, and FeS cell cultures were investigated. In the positive control, the cell culture reached the end of the logarithmic phase after approximately ~400 hours, resulting in a cell density of approximately 9.5 × 10^6 cells/mL. The stable phase extended from 400 to 1200 hours, with consistent pigmentation observed throughout the growth cycle. *A. vinosum* exhibited growth in the negative control, requiring around 100 hours to reach the logarithmic phase with a cell density of 1.92 × 10^6 cells/mL. The stationary phase persisted for approximately 600 hours before a gradual decline in cell density was observed. The FeS cell culture exhibited a significantly extended lag phase of approximately 650 hours before entering the logarithmic phase, which occurred around 1400 hours. At the peak of the logarithmic phase, the cell density reached 1.5 × 10^5 cells/mL. Subsequently, from around 1600 hours, the culture experienced a progressive decrease in cell numbers until tracking was discontinued at 2000 hours. Notably, the FeS system achieved only one-sixth of the cell density observed in the positive control and grew approximately one-fifth less than the negative control culture (Figure 3-1 Growth profile measured in OD (600nm) on the top and sulfide utilization plot on the bottom)

Sulfide concentrations changes were measured for FeS cultures, positive and negative control. In the case of FeS and negative control the sulfide concentration remained unchanged remaining at baseline with no detection of solution sulfide. On the other hand, the positive control depleted from ~2.4mM sulfide concentration to no detection in about 150 hours. Sulfate concentrations started to increase at ~100 to ~400 h to reach maximum sulfate of ~6 mM in the positive control, while the FeS control sulfate concentration remained constant. Nonetheless, the biotic FeS sample did show an increase of ~400uM compared to controls (Figure 3-2).

The iron concentrations in FeS showed a very irregular pattern below 500 h, sodium concentrations were used to assess dilution issues if any and none was found. Thus, the irregulat patterns of iron concentrations was reflective of the bacterial interaction with the FeS nanoparticles and their dissolution products. The cell-free FeS control, which does not contain *A. vinosum* but only the cell culture media showed an increase in iron concentrations up to ~ 600 ppb over the cultivation time of ~ 2300 h, very similar to the level observed in the biological samples (~ 700 ppb). Overall, the ICP data showed that the FeS nanoparticles in the control and samples did release soluble iron through dissolution, which creates a contrast to my previous work on *A. vinosum*-pytire culture. Concentrations of other major solution components are reported in appendix (Appendix - Table S1)

3.4.2 Solid-phase characterization

3.4.2.1 High Resolution Transmission Electron Microscopy

High resolution transmission electron microscopy analysis showed notable differences between the FeS biotic and FeS control samples, revealing variations in particle morphology, aggregation state, and crystallinity. In the FeS control, irregularly shaped particles were observed, some of which formed aggregates, with amorphous morphology and showing poor crystallinity. The biotic FeS sample contained particles size was smaller than ~ 20 nm and the secondary aggregate size was smaller than 100 nm (Appendix Table 0-12 and Figure 3-5 HR-TEM displaying amorphous particles in the abiotic FeS control and more globular particles with increased crystallinity in the biotic FeS sample (d-spacing values can be found in Table 0-12 in the appendix section).). While most of the aggregate were amorphous, a few regions exhibited electron diffraction patterns reflective of the material's crystallinity. Electron diffraction patterns detected in some areas displayed d-spacing values associated with mackinawite (FeS) . By comparison, the cell-reacted FeS was of globular particles that were uniformly scattered within irregular

aggregates, similar to the control sample in morphology. However, electron diffraction analysis revealed that bio-FeS samples contained higher percentage of crystalline materials. The measured d-spacing values also correspond to mackinawite as in the abiotic control but possessing other d-spacing values from an unidentified crystal phase. The complete list of d-spacings can be found in the appendix section (Figure 3-5 and Appendix Table 0-10).

3.4.2.2 X-ray Photoelectron Spectroscopy

In the XPS analysis of the FeS control, several distinct species were observed in the sulfur region, characterized by multiple peaks (Figure 3-3). The experimental curve of sulfide was fitted with six peaks, revealing three sets of peaks at different binding energies. The first set, located at 160.8 eV (2p 3/2) and 162 eV (2p 1/2), corresponds to surface monosulfide previously identified in mackinawite (Han, D.S, 2013). The second set, with higher binding energies at 161.6 eV (2p 3/2) and 162.7 eV (2p 1/2), is associated with disulfide due to covalent bonding (Han D *et al.*, 2013). The third set of peaks, centered at 163.7 eV (2p 3/2) and 164.9 eV (2p 1/2), falls within the range of polysulfides (Fantauzzi M *et al.*, 2015).

Moving to the iron region of the abiotic FeS, six peaks were required for an appropriate fit of the experimental spectra, which were associated to different Iron species and surface effects. The first peak observed at 706.3 eV falls within the elemental iron range (Thermo, 2023). The peak at 706.9 eV, with the highest area, is associated with iron (II) in mackinawite (Han *et al.*, 2013). A satellite peak is observed at 708.1 eV, while the peak at 709 eV corresponds to Fe(II)S from the bulk material (Han *et al.*, 2013). The first of the last two peaks at 710.1 eV is in the range of Fe(III)S and Fe(II)O and cannot be easily differentiated (Liang *et al.*, 2023). The second peak at 711.2 eV is likely attributed to Fe(III)O (Liang *et al.*, 2023).

The XPS analysis of the FeS biotic sample revealed the presence of distinct species in the sulfur region, as evidenced by the presence of multiple peaks. The experimental curve of sulfide

was fitted with six peaks, revealing three sets of peaks at different binding energies. The first set located corresponding to surface monosulfide was found at 160.6 eV (2p 3/2) and 161.8 eV (2p 1/2). The second set associated with disulfide, was found at at 161.4 eV (2p 3/2) and 162.6 eV (2p 1/2). The third polysulfide set of peaks was at 163.2 eV (2p 3/2) and 164.4 eV (2p 1/2).

In the case of the iron region of the spectrum, six peaks were required for an appropriate fit of the experimental spectra. The first peak observed at 706.1 eV falls in the elemental iron range (Thermo, 2023), but it also appears in the control, while the second peak at 706.8 eV is associated with iron (II)S. The third satellite peak is observed at 708.1 eV, while the fourth 709.1eV corresponds to Fe(II)S from the bulk material. The fifth peaks at 710.2 eV is Fe(III)S or Fe(II)O, while the sixth peak at 711.3 eV is likely attributed to Fe(III)O.

3.4.3 Transcriptomic sequencing and differential gene expression analysis

Significant differences in gene expression included 48 upregulated and 154 genes downregulated genes in the FeS culture compared to the positive control. While the negative control identified 36 upregulated and 119 downregulated significantly differentially expressed genes comperd to the positive control (Figure 3-4 and Table 3-5) . Full transcriptome raw files can be found at https://datarepo.bioinformatics.utep.edu/getdata?acc=G9T1VZNRYJPIC0C.

3.4.3.1 Genes encoding CXXCH/LXXC motif containing cytochromes

The objective of analyzing proteins with heme-binding and lipid-binding motifs is to explore the role of cytochromes in facilitating electron transfer between cells and external solid-phase FeS, connecting intracellular energy processes to electron transfer-mediated utilization of FeS. Several genes with heme and lipid binding motifs showed significant upregulation (Refer: Table 3-1).

In the transcriptomic analysis of *A. vinosum*, several genes exhibited significant differential expression, providing insights into the metabolic adjustments the organism undergoes. The gene

Alvin_0021, encoding for Cytochrome B561—a b-type cytochrome with two-heme sites—showed a pronounced upregulation of 10-fold, with a corresponding NEG value of 4-fold. Similarly, Alvin_2447, which encodes the adenylysulfate reductase involved in the sulfate assimilation pathway, was upregulated 5-fold with a NEG value of 4-fold. Notably, the genes Alvin_2452 and Alvin_2453, encoding the alpha and beta subunits of formate dehydrogenase associated with the Wood-Ljungdahl pathway, displayed upregulation of 4-fold and 5-fold, respectively, with corresponding NEG values of 4-fold and 8-fold. A cluster of genes, Alvin_2306 through Alvin_2309, related to Ni/Fe hydrogenases and involved in reversible redox reactions using hydrogen gas or H+ ions, exhibited upregulation ranging from 6-fold to 10-fold. Furthermore, Alvin_1093, encoding the cytochrome c class I, FccA—a flavocytochrome-containing subunit—was notably upregulated by 32-fold with a NEG value of 25-fold. Lastly, Alvin_1095, which encodes the NapC/NirT cytochrome c domain protein, a tetra-heme c-type cytochrome, also exhibited a substantial upregulation of 32-fold, with a corresponding NEG value of 38-fold.

In the transcriptomic analysis of *A. vinosum*, a total of 43 putative c-type cytochromes were identified based on the presence of CXXCH heme c binding motifs. Within this group, 18 were classified as MHCs, which contain multiple CXXCH motifs. A detailed breakdown of these MHCs revealed 11 diheme cytochromes, one 3-heme, three 4-heme, one 7-heme, and two 8-heme cytochromes, as detailed in Table 3-1. It's noteworthy to mention that some of the larger cytochromes, particularly those with 7 or 8 hemes, along with a few others, currently lack annotated functions.

3.4.3.2 Anoxygenic photosynthesis associated genes

In the transcriptome analysis of the FeS sample, we concentrated on the expression of genes related to photosynthesis, specifically those within the *puf*, *puc*, carotenoid, and *RubisCo* gene groups. These groups correspond to the LH1, LH2 complexes, photosynthetic pigments, and

carbon dioxide fixation genes, all of which are vital for anoxygenic photosynthesis (Table 3-3 and Table 0-10).

In our analysis, we observed distinct expression patterns for several genes associated with photosynthesis and other cellular processes.

For the *puf* genes, which are integral to the LH1 complex, the majority exhibited either slight downregulation or remained unchanged in their expression. Specifically, genes Alvin_2634 through Alvin_2637 had expression values ranging from 0.3-fold to 1-fold, with corresponding NEG values between 0.3-fold and 1-fold. Alvin_2547 demonstrated an expression of 0.26-fold with a NEG value of 0.5-fold. However, a subset of *puf* genes, specifically those from Alvin_2548 to Alvin_2555, displayed significant downregulation, with log2FC values falling between -2.79 and -3.63.

Turning our attention to the *puc* genes, which are associated with the LH2 complex, we found consistent downregulation in genes Alvin_2576 to Alvin_2579. Their expression values spanned from -0.0625-fold to -0.04-fold, and their corresponding NEG values ranged between 0.4-fold and 0.7-fold. Interestingly, Alvin_2580's expression remained relatively unchanged, hovering close to zero with a NEG value of 0.9-fold.

In the realm of carotenoid genes, the majority displayed relatively stable expression levels, with values between 0.42-fold to 0.91-fold and corresponding NEG values from 0.64-fold to 1-fold. However, two genes, Alvin_2567 and Alvin_2566, stood out with upregulated expressions of 1.5-fold/NEG(1.5-fold) and 2.8-fold/NEG(1.8-fold), respectively.

Lastly, for the RuBisCO genes, the large subunit genes RbcA/RbcB, specifically Alvin_1365 and Alvin_1366, showed expressions of 0.104-fold/NEG(0.123-fold) and 0.213-fold/NEG(0.176-fold), respectively. On the other hand, the small subunit genes RbcS/RbcL,

namely Alvin_2749 and Alvin_2750, exhibited increased expression levels of 1.34-fold/NEG(0.54-fold) and 1.13-fold/NEG(1.36-fold), respectively.

3.4.3.3 dsr and sox sulfur oxidation genes

We analyzed the differential expression of genes involved in sulfur oxidation in *A. vinosum* to asses if bacteria were activating sulfur oxidation pathways, as measured by expression values compared against the positive control. The results are detailed in Table 3-4 and Table 0-6.

For the *dsr* genes, which are integral to the *dsr* pathway, a significant downregulation was evident. Specifically, genes DsrA, DsrB, DsrE, DsrF, DsrH, DsrC, DsrK, DsrL, DsrJ, DsrM, DsrO, DsrP, and DsrN exhibited expression values that ranged from 0.03-fold to 0.29-fold/ NEG 0.01-fold to 0.6-fold.

Turning to the *Sox* gene family, which is associated with sulfur oxidation, most genes exhibited relatively stable expression levels. Specifically, SoxY, SoxZ, SoxB, SoxX, SoxA, and SoxK had expression values that ranged between 0.59-fold and 0.62-fold/ NEG value of 1-fold across all these genes. However, the SoxL gene stood out with a slight downregulation, showing an expression of 0.36-fold and a corresponding NEG value of 1-fold.

Sulfur oxidation *dsr* genes were significantly downregulated, though not as markedly as in the negative control. In contrast, the expression of *sox* genes remained largely consistent with the positive control. However, the *Sox* genes in the FeS sample were slightly more downregulated than in the negative control. It's important to note that most of the *Sox* genes did not meet the Padj value threshold, as illustrated in Table 3-4.

While most sulfur genes were significantly differentially expressed (Padj < 0.05), SoxA (Padj $= 0.63$), SoxK (Padj $= 0.17$), Soxk (Padj $= 0.16$), SoxX (Padj $= 0.22$), SoxY (Padj $= 0.25$) and SoxB (Padj $= 0.50$) exceeded the significance threshold.

3.4.3.4 Transporters

The transcriptome analysis revealed a significant upregulation of various transporters; to understand the reasons for their increased expression, a more in-depth analysis was conducted, and the results of the gene expressions are presented herein.

In our findings, several transporter genes in *A. vinosum* displayed notable differential expression. The cation diffusion facilitator family transporters, Alvin_0019 and Alvin_1529, showed upregulations of 10.3-fold / NEG(3-fold) and 12.3-fold / NEG(1-fold), respectively. The efflux transporter from the RND family, MFP subunit, Alvin_0014, exhibited a 28.8-fold increase / NEG(4-fold). The heavy metal efflux pump, CzcA family, Alvin_0015, was upregulated by 15.6-fold / NEG(2-fold). The tripartite ATP-independent periplasmic transporters, DctQ component (Alvin_1062) and TRAP dicarboxylate transporter, DctP subunit (Alvin_1063), showed upregulations of 4.6-fold / NEG(2-fold) and 5.6-fold / NEG(2-fold), respectively. Lastly, the outer membrane efflux protein, Alvin_0013, displayed a 19.5-fold increase / NEG(2-fold).

Several transporter gene classes exhibited upregulation, with a notable majority associated with metal or ion efflux. This includes the Cation Diffusion Facilitator Family Transporters, which specialize in cation efflux. In a similar vein, the Efflux Transporter from the RND Family's MFP Subunit is implicated in cation efflux. The Heavy Metal Efflux Pump from the CzcA Family plays a role in metal efflux. Furthermore, the Outer Membrane Efflux Protein, potentially involved in both cation and metal efflux, was also observed to have increased expression.

3.4.3.5 Hypothetical genes

Analyzing the differential expression of hypothetical protein genes in the FeS sample compared to the positive control can help predict functions of proteins with no annotations and spotlight them as potential targets for further research.

In our transcriptomic analysis of *A. vinosum*, several genes stood out for their high expression levels. Specifically, Alvin_0016 and Alvin_0017 exhibited upregulations of 12.1-fold / NEG(3-fold) and 12.5-fold / NEG(3-fold), respectively. A series of genes, ranging from Alvin_1190 to Alvin_1528, showed expression levels between 8.5 to 9.2-fold, with corresponding NEG values from 0.8-fold to 2-fold. Additionally, some putative genes displayed significant expression. The putative transposase, Alvin_1448, was upregulated by 5.6-fold / NEG(1-fold), and a protein with the domain of unknown function DUF1924, Alvin_0022, showed a 7.2-fold increase / NEG(5-fold).

3.5 Discussion

3.5.1 Growth kinetics of FeS cell culture vs. positive and neagive controls

The cell density revealed by optical density (600 nm) measurements was lower for the FeS culture samples than the negative control. There may be multiple scenarios explaining for this observation. Scenario 1: the cell growth in the FeS was supported in similar ways as that is the negative ctrl; scenario 2: the OD measurement for the cells in the FeS-amended culture was an estimation for the actual cell density in the FeS sample due to cell attachment to substrate nanoparticles and separation difficulty; and scenario 3: the FeS cell growth underwent a different growth pathway, but reached similar cell density levels but at different time as the negative control. The relatively long lag phase (~ 650 h) for the FeS cells created a contrast to those in the negative control, which quickly reached the log phase under 100 h. Assuming that the FeS cells grew through similar pathways as those in the negative control, the difference in growth kinetics could be explained by the adverse effect of the FeS substrate. The ICP-MS data did show that soluble iron concentrations increased along with time in the FeS culture samples and cell-free FeS control. Specifically, the iron concentrations reached up to 700 ppb. Although significant, the iron concentration in the FeS cell culture samples is only ~ 2-3 fold of that in the positive control

samples, and not close to the cytotoxic levels (Bird *etal.*, 2013). The specific growth path of the *A. vinosum* cells in the FeS cell culture are further discussed later in the transcriptomic section.

Interestingly, significant increase in sulfate concentrations were also observed in the FeS sample, which stronly indicated that *A. vinosum* cells were capable of utilizing the sulfur in FeS. This also indicates that the bacteria grown on FeS follows a different pathway than those grown on pyrite, for which increase in sulfate concentrations was not observed. When compared to the positive control, the FeS samples have a sulfate concentration ~ 16 times lower. The production of sulfate may be via multiple mechanisms, which needs to discussed along with the transcriptomic data. It is likely that the the cells in FeS samples could use the sulfide liberated through FeS nanoparticle dissolution, and followed similar path as the positive control but at much slower rates. However, the transcriptomic data did not quite support this explanation with major differences in the gene expression related to redox active proteins and sulfur metabolism enzymes. Alternatively, the enhanced iron concentrations could be a result of the bacterial scavenge of FeS for sulfur, which concomitantly released iron from the substrate. In the case of sulfide, concentrations remained at baseline with no detection, while positive control depleted in sulfide in about 150hrs. This makes sense, as any potential sulfide release from FeS would likely be immediately be absorbed by cells, as shown in the sulfide depletion curve in that the available sulfide quickly is exhausted. It is important to point out that positive control was prepared with 6.1mM concentration of Na_2S. The much lower concentrations of sulfide detected reflected the potential loss of sulfide through sampling and preparation procedures. But as the procedures are consistent for all sample, the effect was considered minimal.

3.5.2 Modification of the FeS substrate revealed by HRTEM and XPS analysis

The presence of *A. vinosum* bacteria significantly enhanced the crystallinity of the FeS nanoparticles, which is in line with the findings of biomineralization experiments (Picard *et al.*,

2018; Mansor *et al.*, 2020) although sulfate-reducer were used in these former studies. The explanation for the enhanced iron sulfide crystallinity in the presence of bacterial cells is that the cell surface may provide nucleation sites for initial crystal nuclei to form and the extracellular metabolites may aid in organizing and aligning the formed nuclei, promoting the formation of more crystalline structures. Additionally, the microenvironmental conditions created by the bacteria, such as favorable pH or redox conditions, potentially facilitated accelerated seed crystal formation and subsequent crystallization. These bacterial-mediated processes collectively resulted in an overall increase in crystallinity, as confirmed by HRTEM images of the nanoparticles exposed to *A. vinosum*. FeS control showed few regions with electron diffraction patterns that pointed to the formation of mackinawite and chalcopyrite, while in the biotic FeS sample, cubanite ($CuFe_2S_3$) mineral phases aside from chalcopyrite and mackinawite. It's important to highlight that the media is supplemented with mineral mixture explaining the potential formation of cubanite and chalcopyrite mineral phases although this needs further evaluation.

The abiotic control (FeS) iron region showed two peaks (706.9 eV and 709 eV) related to surface and bulk material of Fe(II)S. Bulk iron atoms are surrounded by more chemical groups leading to more electron interactions and thus higher binding energy when compared to surface iron less groups around it. The two peaks related to Fe(II)S at 706.9 and 709 eV retained their relative proportions in both cell-reacted and control samples. There is a peak at 706.3eV related to elemental iron, which appears in both control and cell-reacted FeS samples and in very similar proportions, and thus, this peak does not relate to any changes in the systems. This could be due to either chemical contamination from reactants used to make FeS, or potentially the peak rises from surface defects of the material whose binding energy falls within the native iron range. There were two peaks of Fe(III) species, one at 710.1 eV for Fe(III)S and another at 711.2 eV for Fe(III)O. The Fe(III)S is intrinsic part of poorly crystalline mackinawite (ref) and the occurrence

of Fe(III)O is resulting from speciation of the Fe(III)S at the solid-water interface. As such, both species exist in the cell-free control and it does not mean that the FeS samples were oxidized. The relative abundance of the Fe(III) showed a slight increase of 3% in cell-reacted FeS on both peaks when compared to the control, indicating that the presence of *A. vinosum* enhanced the oxidation of FeS. This observation also highlights the possibility of an iron oxidation pathway for the growth of *A. vinosum* on FeS. If *A. vinosum* belongs to electrochemical active bacteria and could enable EET, they might be able to utilize cytochromes for electron transfers. Although such mechanisms were only reported for iron-reducing bacteria (Shi *et al.*, 2016), bidirectional electron transfer through similar cellular apparatus is possible (Figure 3-3).

In the case of the sulfur region, the same three species prevail across both samples. The most abundant disulfide peak seems to decrease from 73% in the control to 51% in the biotic sample, while the monosulfide peaks go from 12% to 31%. As *A. vinosum* is a sulfur oxidizer, a trend where disulfide and monosulfide decrease would make sense. The appearance of Iron (III) is interesting and suggest a bacterial facilitated electron movement across FeS material. In the case of the polysulfide fraction, there is a 3% abundance increase in biotic sample which is an intermediate in the oxidation of sulfur (Findlay *et al.*, 2016). Thus, this could be used as an indicator that bacteria are oxidizing the sulfide in the FeS substrate. Still, is important to keep in mind that the differences in polysulfide content between the two samples is close. Finally, when considering the overall abundance of iron and sulfur, it was found that the control had a S/Fe ration of 1.26, while the biotic sample had it reduced to 0.97. Thus, this would support that the notion that sulfur is being taken from the FeS material. In summary, the XPS of the biotic samples seem to show evidence that sulfide in FeS is being utilized for metabolic purposes by *A. vinosum* as shown by increase in polysulfide peak abundance. Furthermore, the appearance of Fe (III) iron peaks points to potential redox reactions facilitated by *A. vinosum* which could be providing an

electron transport system. More evidence is needed to verify the potential of *A. vinosum* on FeS verification, however.

3.5.3 Transcriptomic sequencing and differential gene expression analysis

3.5.3.1 CXXCH/LXXC motif containing genes

In the transcriptomic analysis of the FeS dataset, we observed differential expression of several cytochrome genes with diverse motifs, providing insights into their potential functions. Alvin_1093 exhibited a remarkable 44-fold upregulation compared to the positive control / NEG(25-fold), encoding a flavocytochrome subunit of sulfide dehydrogenase, which is part of the pathway to oxidize sulfide into elemental sulfur. Flavocytochromes, capable of reversible redox reactions through heme moieties and flavin groups, are versatile molecules for electron transfer in both directions. Interestingly, this gene was also upregulated 24-fold in the negative control (24-times) (Alvin_1093 in negative control). Furthermore, this protein contains a signal peptide, indicating its involvement in secretory pathway and its potential localization on the cell surface or extracellular milieu. Similarly, Alvin_1095 showed significant upregulation of 31-fold / NEG(38-fold), compared to the positive control, encoding a putative tetra-heme c-type cytochrome with a predicted signal peptide (by SignalP 3.0 HMM). This suggests that the protein may be located outside of the cell. Furthermore, this protein contains an LXXC lipid binding motif, strengthening the possibility of its association with the cell membrane. Annotated as NapC/NirT cytochrome c domain protein, it is speculated to be involved in nitrite oxidation. Interestingly, according to STRINGdb, it is associated with ccmA, which has been linked to conductive nanowires (Costa 2018) (Alvin_1095 in STRINGdb). Interestingly, Alvin_2174 did not display significant overexpression (log2FC change = -0.9, Padj = 0.0536), this gene was also upregulated 37-fold in the negative control (37-times).

Other proteins described as cytochrome *c* diheme binding proteins, likely co-expressed according to STRINGdb, were upregulated in FeS-exposed bacteria. Alvin_0020 showed a 10-fold upregulation/ NEG(3-fold), while Alvin_0023 displayed a 7-fold/ NEG(4-fold) upregulation. Compared to lower expression in the negative control 3-fold and 4-fold, respectively. Interestingly, only Alvin_0020 possesses a lipid binding motif, indicating its potential association with the membrane, whereas Alvin_0023 is associated with Alvin_0020 but found in the cytoplasm, periplasm, or extracellular environment (Alvin_0023 associated with Alvin_0020). Despite its proximity to Alvin_0020, Alvin_0018 may represent another non-related dihaem cytochrome c protein. This cytochrome protein appears to possess peroxidase activity, facilitating the transfer of electrons from substrates to hydrogen peroxide, resulting in the production of water. It is noteworthy that these proteins have a high potential haem of +320mV, enabling the transfer of electrons from donating proteins to low potential heme (-330mM) (Bick 2000). Alvin_0022, a protein with both heme and lipid binding motifs, exhibited a 7-fold upregulation / NEG(5-fold). However, it does not appear to be related to Alvin_0020 according to STRINGdb. Instead, it seems to be associated with dsrP (-2.7log2FC) and petB (-1.6log2FC) genes involved in sulfur oxidation and the respiratory chain through a ubiquinol-cytochrome c reductase complex. Furthermore, the protein contains motif DUF1924, which contains a signal peptide predicted by SignalP, suggesting its potential for secretion or surface localization facilitating electron transfer reactions.

These findings reveal the expression of cytochrome genes with specific motifs, such as the CXXCH heme binding motif, LXXC lipid binding motif, and signal peptides, providing insights into which cytochrome proteins could be associated with the membrane of the cell or be excreted out to facilitate electron transfer between the cell and its environment.

3.5.3.2 Redox active proteins

Other proteins involved in redox reactions, with no found motifs, that showed significant upregulation in the gene expression analysis are listed in this section. Cytochrome B561 (Alvin_0021) was upregulated 10-fold/ NEG(4-fold) in FeS cultures. This *b*-type cytochrome containing protein has transmembrane domains, two-haem sites and are reduced by ascorbate (vitamin C). These proteins have been proposed to shuttle electrons across membranes from ascorbate substrate (Verelst 2003). It's important to notice that these proteins have low homology across species and thus there is still the potential that in *A. vinosum* another substrate or more than one substrate can act as an electron donor to shuttle into the cell. This cytochrome was found to be upregulated 4-fold showing lower expression than in FeS system. Furthermore, it's interesting to notice that this gene would be associated through gene neighborhood to cycA which is another suspect of electron transport in solid respiration (Costa 2018). Although, cycA is not upregulated in the transcriptome with a log2FC of -1.8.

The protein adenylysulfate reductase (Alvin_2447) exhibited an upregulation of 5-fold / NEG(4-fold) in the study. This protein plays a crucial role in the sulfate assimilation pathway, which involves the uptake of sulfate into the cell for the synthesis of cystine and other organosulfur compounds. Adenylysulfate reductase is redox active and functions by catalyzing the reduction of adenylylsulfate (APS) protein to sulfite. It's interesting to see the negative control possessing a similar expression value. It is unclear if this pathway is being activated by bacteria in both systems to harvest energy from sulfite, or if this is a way for the cells to make sulfur-containing amino acids.

Alvin_2452 was upregulated 4-times/ NEG(4-fold) and Alvin_2453 5-times/ NEG(8-fold) in the transcriptome of FeS exposed *A. vinosum* compared to positive control. Alvin_2452 gene is responsible for the translation of the alpha subunit of the formate dehydrogenase protein, while

Alvin_2453 makes the beta subunit. This enzyme is part of an energy metabolism pathway called Wood-Ljungdahl pathway. This pathway allows utilization of hydrogen as an electron donor and carbon dioxide as acceptor to generate organic matter and energy (Ragsdale 2008 and James 1990). Is worthwhile to mention that genes associated with this enzyme are also upregulated in the negative control. The comparable expression between FeS and negative control could mean that at least a portion of the growth displayed by *A. vinosum* in the negative control could be attributed to the carbonate found in the media. It's noted that formate has been recognized as an accessory reductant for more complex molecules, which could mean that despite the expression of these genes in both systems they might follow different pathways, where one system uses the formed formate for its oxidation while in the other system could use formate only as an intermediate for a secondary redox reaction (James 1990). Still, this is only potential explanation but more work needs to be conducted to assess the contribution of formate dehydrogenase in FeS system.

In the FeS transcriptome, four genes related to Ni/Fe hydrogenases showed significant upregulation. Alvin_2306 exhibited a 6-fold increase / NEG(9-fold), followed by Alvin_2307 with a 7-fold increase / NEG(11-fold), Alvin_2308 with a 10-fold increase / NEG(7-fold), and Alvin_2309 with a 10-fold increase in expression / NEG(9-fold). It is worth noting that some hydrogenases show greater upregulation than in FeS system. These genes encode proteins involved in reversible redox reactions, utilizing hydrogen gas as electron donors or H+ ions as electron acceptors. Alvin_2309 encodes the Ni/Fe hydrogenase small subunit Hyd A, Alvin_2308 encodes the Ni-dependent hydrogenase and Alvin_2307 encodes the Ni/Fe hydrogenase cytochrome *b* subunit. Co-expression and gene-fusion analyses, by STRINGdb, suggest a functional relationship between these Ni/Fe hydrogenase genes. Notably, [NiFe]-hydrogenases are believed to have played a crucial role in the metabolism of the Last Universal Common Ancestor (LUCA). Intriguingly, the closest evolutionary relatives of [NiFe]-hydrogenases are proteins involved in

respiratory complex I/NADH dehydrogenase (Yu H, 2021). This suggests a potential link between [NiFe]-hydrogenases and the ancestors of modern respiratory complex I, which are responsible for NADH oxidation, ubiquinone reduction, and proton pumping. It is difficult to assess the role of these redox proteins in either FeS or the negative control, as there is no hydrogen in the culture systems. The reversible reaction of making hydrogen gas would need a source of electrons, which could come from sulfide, but no apparent link of sulfur oxidation and hydrogenases in PSB. Thus, suggesting an alternative pathway where electron transfer is likely facilitated by hydrogenase from an undetermined substrate is a possibility.

3.5.3.3 Photosynthetic genes

Photosynthetic *puc* and *puf* genes were significantly downregulated compared to both negative and positive controls (Table 3-3 and Table 0-5). The depressed expression of photosynthetic genes ranged from 6.4E-4 fold to 1.6E-1 fold for FeS expression, while in the negative control downregulation was not as great with 2.2E-2 fold to 1.6E-1 fold. It's also important to highlight that *puc* genes were downregulated more in both systems than *puf* genes. The more pronounced downregulation of photosynthetic genes in FeS suggests that there is likely a greater reliance of the negative control on the photosynthetic system compared to the FeS system. This could be due to light being refracted by nanoparticles or absorbed by the black nanoparticles, resulting in less light reaching the photosynthetic complex. It is important to explain that carotenoid related genes expression remained largely unchanged compared to the positive control (Alvin_1182-1183, 2556, 2561-2563, 2638-2643, and 2564-2570), while the negative control display a very similar pattern. Potentially, revealing a greater role in the active energy pathway supporting both cultures, or playing the protective role that carotenoids are known for, although again there isn't a big difference in expression profile of carotenoid genes. Lastly, RubisCo genes associated with carbon dioxide fixation were also analyzed revealing 0.1-fold downregulation of

the large subunit on both systems, while the small subunit showed comparable expression to the positive control on both systems as well. Expression profile of small RubisCo remains unclear as it is usually associated with carboxysomes, but these are not found in PSB (Table 0-11).

3.5.3.4 *dsr* and *sox* sulfur oxidation genes

The expression of sulfur oxidation *dsr* genes exhibited downregulation, particularly evident in the negative control. This finding is consistent with expectations, considering that the negative control grows in sulfur-free media, thus no possible sulfur oxidation. Conversely, the expression of *sox* genes remained relatively stable or slightly downregulated compared to the positive control, and their expression levels in the negative control were comparable. These results suggest that *sox* genes may play a significant role in sulfur oxidation metabolism compared to downregulated expression profile in *dsr* genes.

Notably, *sox* genes are known to be involved in the oxidation of polysulfides to sulfate, which provides a plausible explanation for the higher polysulfide fraction observed in the FeS XPS sulfur spectra, with 17% compared to the 14.3% in the control. The expression values strongly support the notion that the cultured bacteria utilize sulfide from the FeS solid as a sulfur source. The marginal change in polysulfide content in the biotic XPS sample is also coherent with a culture that reached a low cell density. In summary, *dsr* and *sox* transcription profiles of FeS coupled with XPS and IC, showing 400uM increase in sulfate, show that *A. vionsum* cells are using FeS as a source of electrons and sulfur. Still, ICP-MS findings of the abiotic FeS system do show increased Fe(II) ions over time, suggesting a solubility effect that may lead to *A. vinsoum* following sulfur oxidation driven mainly by dissolution effect. Still, this needs further evaluation.

3.5.3.5 Transporters

For the FeS sample, upregulation of genes coding for heavy metal efflux proteins was identified. These genes include Alvin_0013 (20-fold) / NEG(2-fold), Alvin_0014 (8.2-fold) /

NEG(4-fold), Alvin_0015 (8-fold) / NEG(2-fold) and Alvin_0019 (10-fold) / NEG(3-fold). These genes have been annotated in various databases, including KEGG, STRINGdb, InterPro, and UniProt, as efflux proteins associated with metal resistance. Specifically, the Alvin_0014 gene encodes for a membrane fusion protein (MFP) subunit belonging to the RND family (Resistance, Nodulation, and Cell division). The Alvin_0015 gene encodes for a heavy metal efflux pump, which, based on the Interpro protein family descriptions, is classified as a member of the Cus protein family. Proteins in this family are known to be involved in the efflux of heavy metal ions and contribute to metal resistance in the cell (Outten FE, 2001). Two efflux genes, Alvin_0019, coding for ferrous-iron efflux pump FieF protein involved in expulsion of Fe2+ ions outside of the cell (Pi H, 2017) were also upregulated. Alvin_0013 was annotated as outer membrane protein in heavy metal efflux system. The upregulation of these efflux genes was likely a response to the soluble iron released from the substrate through the culturing experiment, potentially a response of ions entering the cell. The activation of these genes could also relate to uptake purely from these proteins acting as transporters and potentially they are intaking an important substrate. Still, as some of these genes are annotated as relating to metal efflux proteins, the possibility of a flux of ions between cell and surroundings becomes a possibility that needs to be explored further. These findings shed light on the altered expression patterns of transporter genes and provide insight into how *A. vinosum* may utilize FeS.

Other transporter related genes Alvin_1062 (4.6-fold) / NEG(2-fold) and Alvin_1063 (5.6-fold) / NEG(2-fold) are TRAP (tripartite ATP independent periplasmic) transporters. These transporters work through substrate binding and regulate transit to and from periplasm. These transporters have shown to interact with a wide range of substrates including organic acids, vitamins sugars, polypeptides, amino acids, and metal–chelate complexes (Mulligan C, 2011). The

upregulation of these genes expressed in the negative control as well, to a lesser extent, might point to transit of key molecules into the periplasmic space.

In general, transporter genes play crucial roles in cellular processes, including ion transport, metal detoxification, and nutrient uptake. The differential expression of these genes suggests their active involvement in the transport molecules between the cell and its environment.

3.5.3.6 Hypothetical genes

In the FeS group, two conserved hypothetical genes were identified. Alvin_0893 showed to contain an HTH_17 motif, which is known as a DNA binding motif (Mattis AN, 2008). Another gene, Alvin_0016, contained the DUF3240 motif along with a transmembrane (TM) domain. The third gene, Alvin_0017, was shown to contain a signal peptide sequence, indicating the potential protein export of coding protein outside of the cell. Furthermore, a transmembrane domain. Lastly, Alvin_0017 contained the DUF3340 motif, as well as the DUF2992 motif. DUF3340 is known to be present in the C-terminus of tail-specific proteases.

Homology analysis of hypothetical genes in the FeS transcriptome analysis show that 50% of the genes were conserved in g-proteobacteria, with homology results of 95% or higher. The motif analysis of the most upregulated hypothetical genes revealed that Alvin_0017 and Alvin_0016 are likely coding for membrane associated proteins or excreted proteins. In the context of our study, the significant upregulation of hypothetical protein gene expression holds critical importance as it provides valuable insights into the metabolic adaptation and potential mechanisms utilized by *A. vinosum* bacteria in utilizing solids as electron sources. Hypothetical proteins, although lacking well-defined functional annotations, play pivotal roles in various cellular processes and are often involved in response to specific environmental cues. The substantial upregulation of these genes suggests that they may be crucial players in the process of utilizing solid-phase electron donors, such as FeS, and could potentially be associated with electron transfer

pathways or other key metabolic functions. By shedding light on the genetic response of *A. vinosum* to solid-phase substrates, these genes may hint at previously unknown metabolic pathways or energy-harnessing mechanisms. Investigating these genes could provide insights into the bacterium's adaptive strategies, so highlighting them could become important for future studies.

3.5.3.7 Other genes

The transcriptome analysis also revealed several proteins with diverse functions. The membrane protein-like protein (Alvin_0024) exhibited a moderate 4.9-fold/ NEG(3-fold). upregulation. Although its specific function remains unclear, it is predicted to have a role in membrane-associated processes. Further investigation is required to elucidate its precise function and cellular significance.

The molybdopterin converting factor, subunit 1 (Alvin_1928), displayed a 4.1-fold/ NEG(1-fold). upregulation. This protein is involved in the biosynthesis and maturation of molybdenum cofactor, which is essential for the activity of various enzymes involved in redox reactions. Its upregulation suggests an increased demand for molybdenum cofactor biosynthesis and utilization within the cell.

The peptidase M61 domain protein (Alvin_0284) showed a 5.4-fold/ NEG(4-fold). upregulation. This protein belongs to the M61 peptidase family, which is involved in the degradation of extracellular proteins. It plays a role in protein turnover and remodeling processes, potentially contributing to cellular homeostasis and adaptation.

The Ankyrin protein (Alvin_1094) exhibited a significant upregulation of 28-fold/ NEG(35-fold). Ankyrins are versatile proteins that participate in diverse cellular functions, including cytoskeleton organization, ion channel regulation, and signal transduction. The

upregulation of this protein suggests its involvement in dynamic cellular processes and molecular interactions.

The 2-isopropylmalate synthase (Alvin_1379) displayed a 7.9-fold/ NEG(2-fold). upregulation. This enzyme is involved in the biosynthesis of leucine and is essential for the production of this amino acid. Its upregulation indicates an increased demand for leucine biosynthesis, likely due to cellular growth and metabolic requirements.

These proteins represent a range of cellular functions, including membrane-associated processes, cofactor biosynthesis, proteolytic activity, cellular organization, and amino acid metabolism. The differential expression of these proteins provides insights into their potential roles in cellular processes and highlights their importance in maintaining cellular function and adaptation.

3.6 Conclusion

One of the study's captivating findings is the optical density growth profile, indicating more growth on the negative control than on FeS. This suggests that the mechanisms supporting FeS growth might not extend beyond those in place for the negative control, implying no FeS utilization. Nevertheless, evidence of sulfur oxidation emerged, evident in increased sulfate levels in ion chromatography and elevated polysulfides detected through XPS analysis in biotic FeS. However, this is likely attributed to FeS nanoparticle dissolution, as demonstrated by higher iron levels in abiotic FeS through ICP-MS. This suggests that despite the reduced growth observed in the FeS culture, some of its growth can be attributed to sulfur oxidation. This raises the question of how negative control-related pathways might influence FeS growth.

The transcriptomic analysis of *A. vinosum* in the presence of FeS revealed significant upregulation of several key genes, shedding light on potential mechanisms involved in its interaction with solid-phase substrates. Notably, proteins like flavocytochrome 1093 and

NapC/NirT cytochrome c domain protein Alvin_1095 exhibited high expression in both the negative control and FeS conditions, indicating a pathway in which bacteria is using electrons to harvest energy from surrounding molecules. An intriguing observation was the upregulation of formate dehydrogenase in both the FeS and negative control, despite no apparent electron source for formate formation, leaving its role ambiguous. Additionally, other heme-containing proteins Alvin_0020, Alvin_0022, Alvin_0021 and Alvin_1402, which are associated with lipid binding domain, showed upregulation. Upregulation of redox active proteins with high probability of being associated with the membrane it is interesting as it might involve an electron transport pathway between extracellular environment to cell.

Following sulfur oxidation evidence found suggesting a separate energy producing pathway to negative control, at least partially, the greater observed downregulation of *puf* and *puc* genes in FeS system may suggest a greater influence of photosynthetic system in energy producing pathway of FeS. This idea needs to be tested to determine the extent of its validity. RubisCo gene expression also do not reveal evidence of carbon dioxide fixation, in spite of small subunit revealing comparable expression to positive control.

The upregulation of transcriptome transporter genes, such as Alvin_0014, Alvin_0019, and Alvin_1062, suggests potential ion exchange between the cell and its surroundings. However, the increased expression of TRAP indicates the uptake of an unspecified substrate into the periplasmic space. Notably, these proteins are known to interact with a diverse array of substrates, including metal-chelate complexes (Mulligan C, 2011).

The upregulation of redox-active genes is intriguing, hinting at a potential electron transport pathway. However, the dissolution of abiotic FeS and reduced growth compared to the negative control constrain the conclusions. Further research is required to understand *A. vinosum's*

use of FeS nanoparticles, the role of photosynthesis, and the mechanism behind the release of FeS into the solution

3.7: Figures and tables

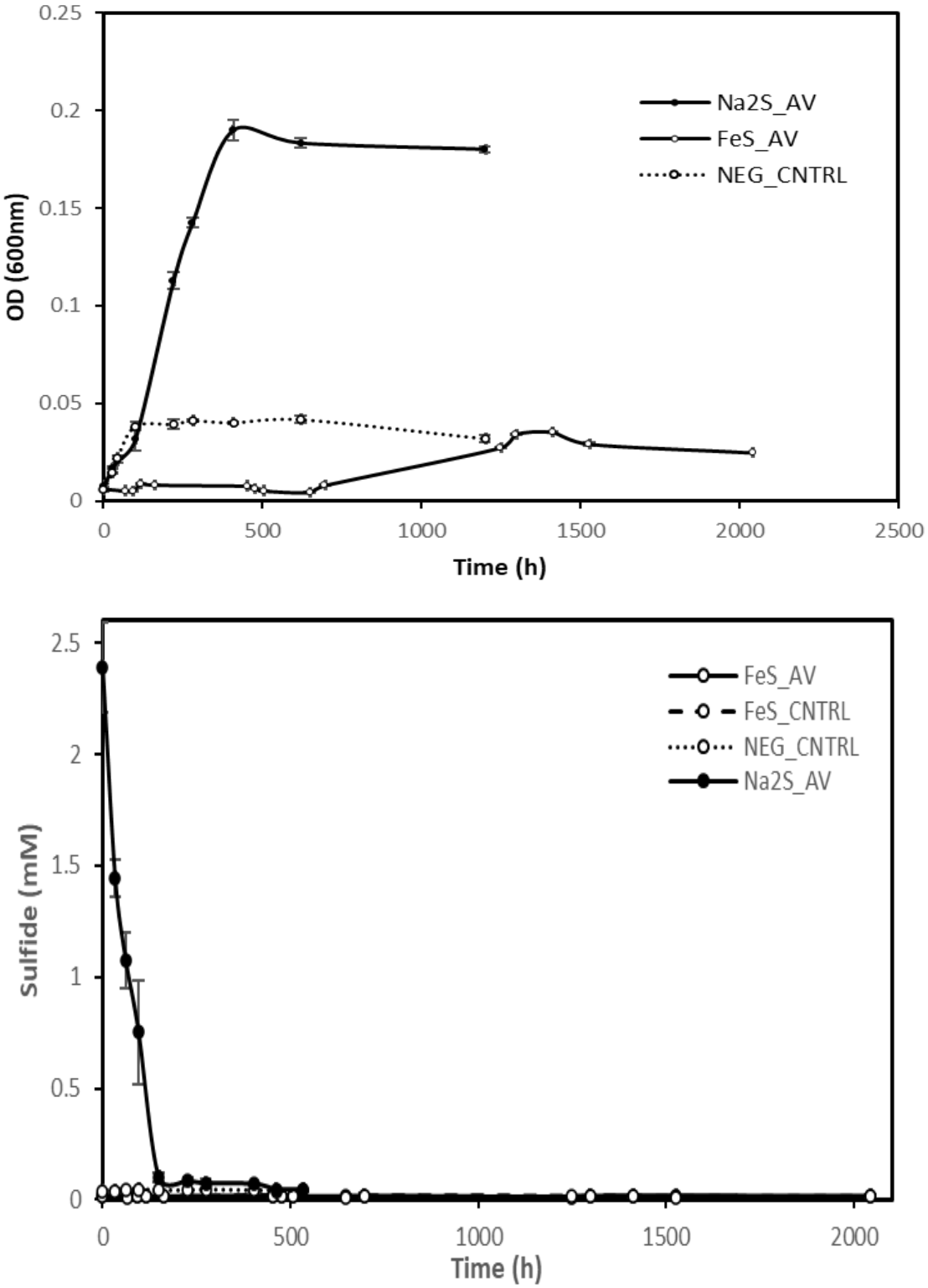

Figure 3-1 Growth profile measured in OD (600nm) on the top and sulfide utilization plot on the bottom.

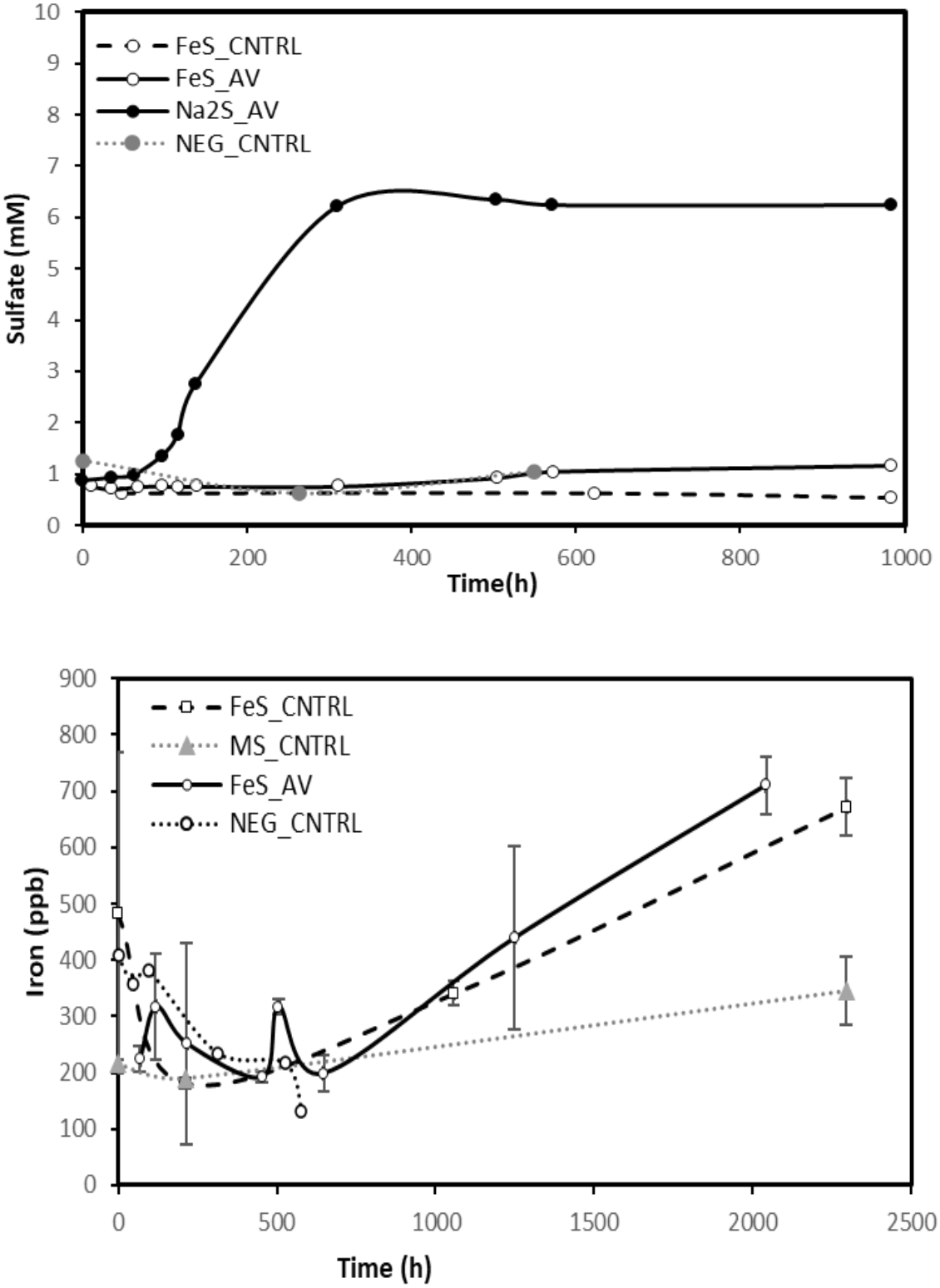

Figure 3-2 Growth profile of pyrite culture showing sulfate concentration changes over time in culture media on the top and Iron concentration changes on the bottom

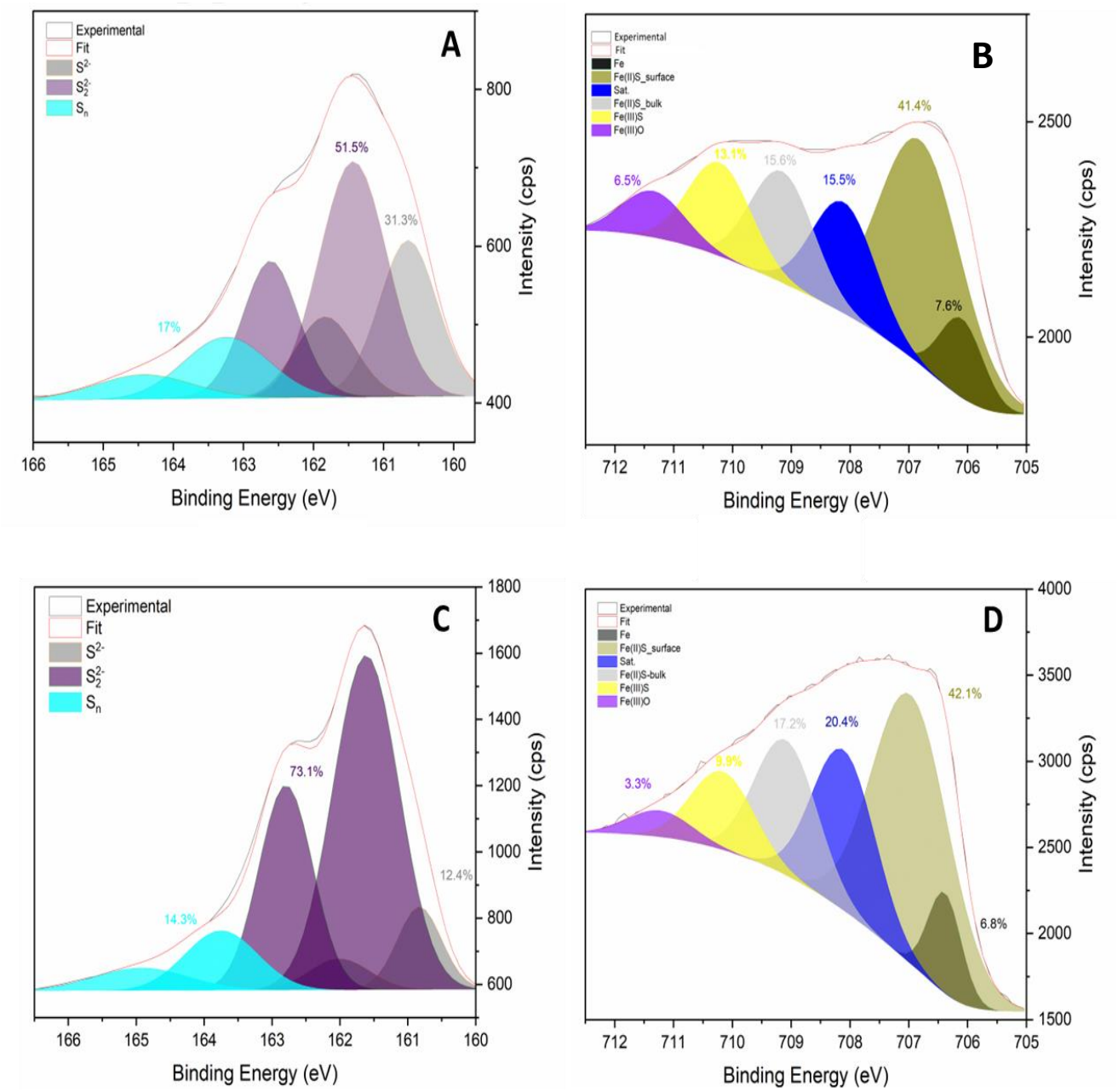

Figure 3-3 Solid-phase characterization through X-ray photoelectron spectroscopy or FeS. Both A and B show characterization of biotic FeS with A showing iron XPS region and B the sulfur region, while C and D show abiotic Fes control spectra with C displaying Iron region and D the sulfur region

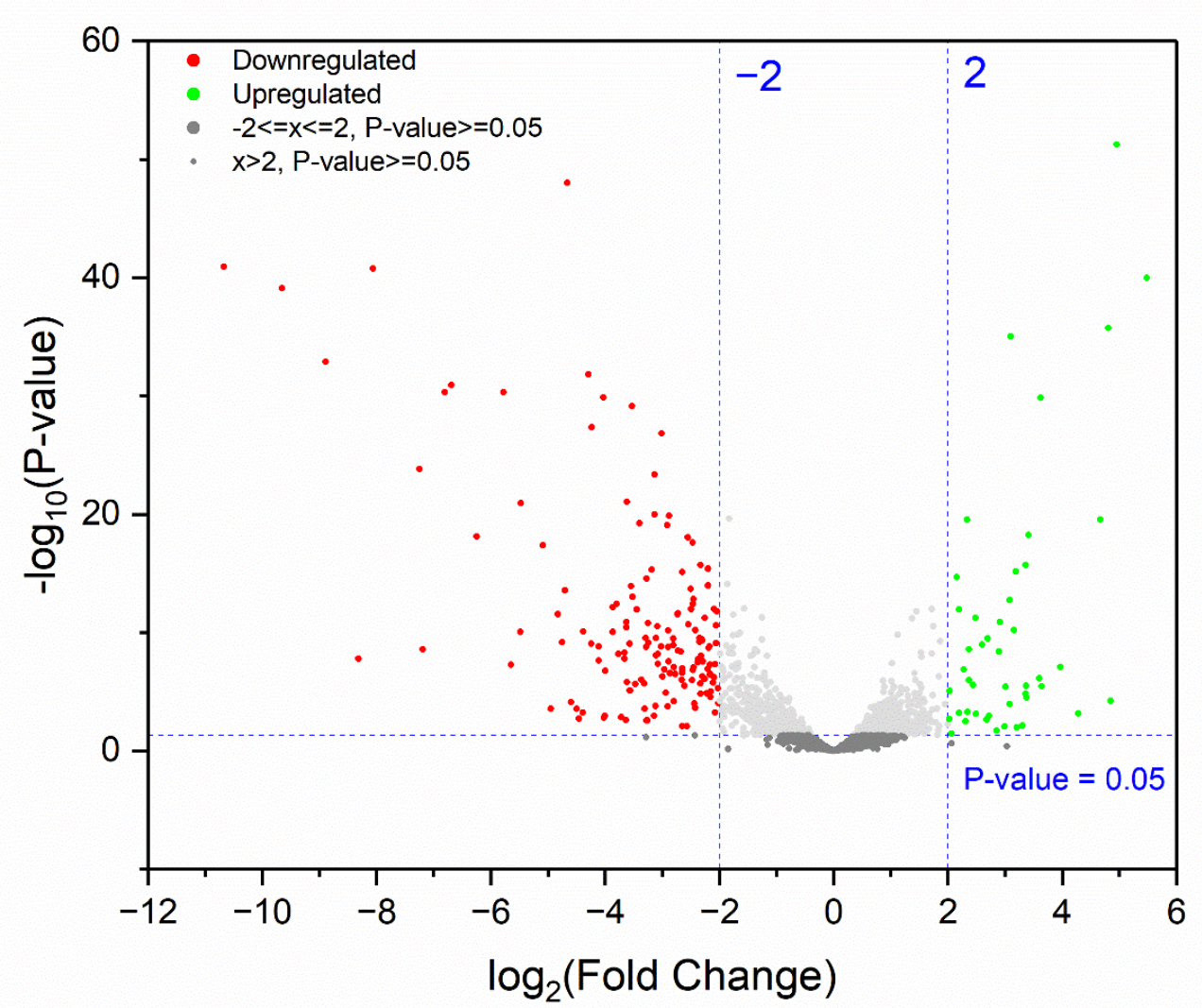

Figure 3-4 Volcano plot of FeS transcriptome

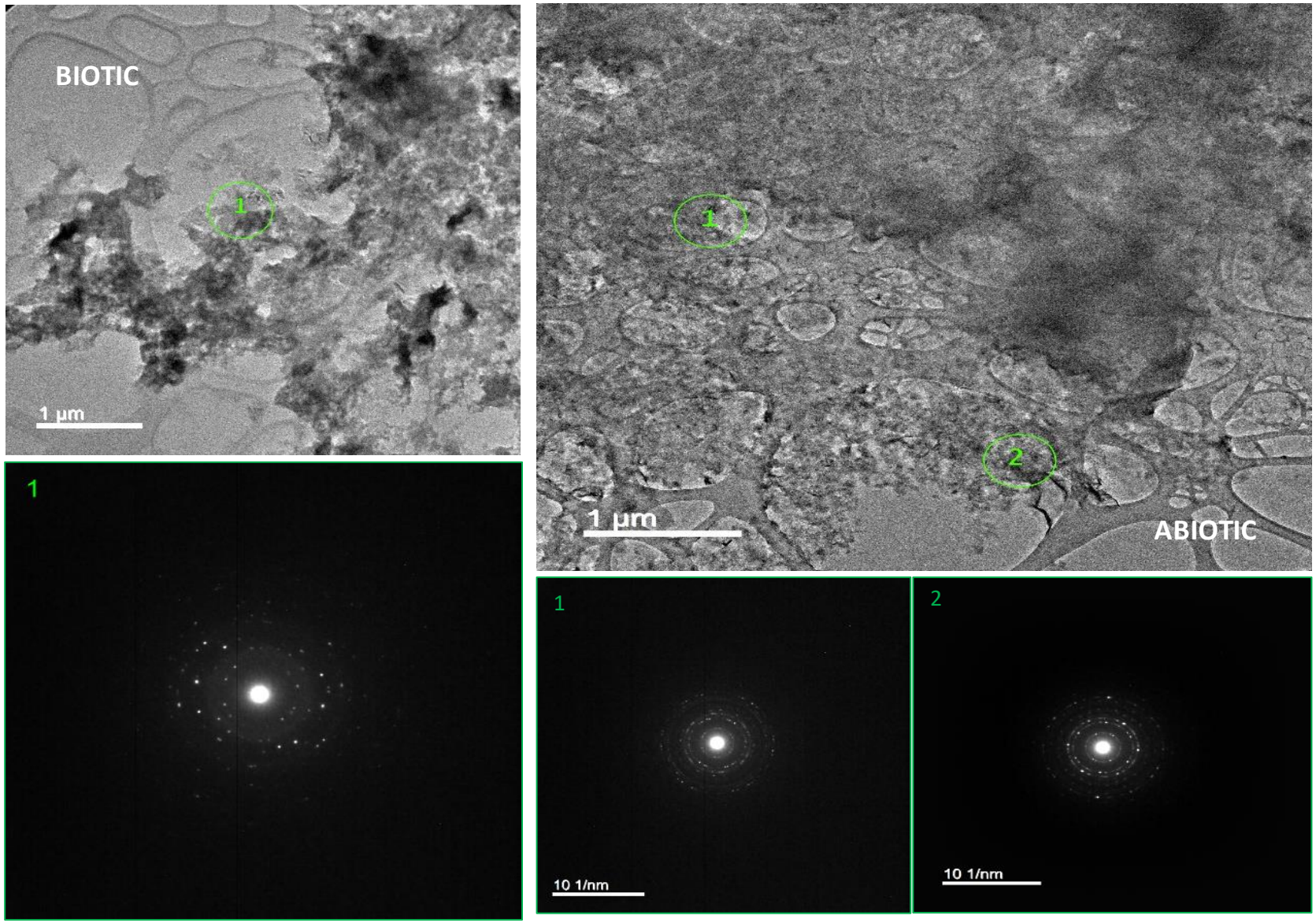

Figure 3-5 HR-TEM displaying amorphous particles in the abiotic FeS control and more globular particles with increased crystallinity in the biotic FeS sample (d-spacing values can be found in Table 0-12 in the appendix section).

Table 3-1 FeS Identification of motifs CXXCH and LXXC and Signal Peptides

Gene	Position	Description	Number of CXXCH motif	LXXC motif	NCBI Protein ID	SignalP	Upregulated in cells on FeS	Upregulated in cells on elemental sulfur	Upregulated in Negative Control
Alvin_0018	76..80	Di-heme cytochrome c peroxidase	2		ADC60990		Yes (8)	Yes (2.2)	Yes (2.4)
	258..262								
Alvin_0020	56..60	Diheme cytochrome c	2	Yes	ADC60992	Yes	Yes (10.4)	No (0.8)	Yes (3.3)
	165..169								
Alvin_0022	48..52	Domain of unknown function DUF1924	1		ADC60994	Yes	Yes (7.2)	No (0.08)	Yes (4.9)
Alvin_0023	54..58	Diheme cytochrome c	2		ADC60995	Yes	Yes (6.6)	No (0.7)	Yes (3.9)
	155..159								
Alvin_0070	50..54	cytochrome c1	1		ADC61042	Yes	No (0.4)	No (0.2)	No (0.5)
Alvin_0071	9..13	Glutathione S-transferase domain protein	1	Yes	ADC61043		No (0.8)	No (0.3)	No (0.6)
Alvin_0091	76..80	Thiosulfate dehydrogenase	2		ADC61061	Yes	Yes (1.7)	Yes (1.7)	Yes (1.3)
	187..191								
Alvin_0350	159..163	nicotinate-nucleotide pyrophosphorylase	1		ADC61311		Yes (1.3)	N/A	Yes (1.3)
Alvin_0439	43..47	transmembrane region and signal peptide prediction	1	Yes	ADC61398	Yes	No (0.3)	No (0.1)	No (0.6)
Alvin_0679	76..80	Cytochrome-c peroxidase	2	Yes	ADC61628	Yes	No (0.6)	No (0.6)	No (0.9)
	222..226								
Alvin_0782	105..109	cytochrome c oxidase, cbb3-type, subunit II	1		ADC61729		No (0.7)	Yes (6.2)	Yes (1.7)
Alvin_0784	120..124	cytochrome c class I	2		ADC61731		No (0.8)	Yes (6.2)	Yes (1.7)
	206..210								

Alvin_1073	877..881	FAD linked oxidase domain protein	1	Yes	ADC62012		No (1)	No (0.4)	No (0.7)
Alvin_1093	36..40	cytochrome c class I	2		ADC62032	Yes	Yes (44.6)	Yes (4.5)	Yes (24.6)
	126..130								
Alvin_1095	44..48	NapC/NirT cytochrome c domain protein	4	Yes	ADC62034		Yes (31.1)	Yes (9.6)	Yes (37.8)
	73..77								
	133..137								
	165..169								
Alvin_1259	633..637	DsrL	1		ADC62198		No (0.1)	No (0.2)	No (0.1)
Alvin_1260	83..87	DsrJ	3	Yes	ADC62199	Yes	No (0.1)	No (0.1)	No (0.1)
	106..110								
	119..123								
Alvin_1395	72..76	cytochrome c family protein	8	Yes	ADC62330	Yes	No (0.3)	No (0.01)	No (0.2)
	122..126								
	146..150								
	195..199								
	237..241								
	275..279								
	303..307								
	489..493								
Alvin_1402	172..176	Fe-S cluster assembly protein NifU	1	Yes	ADC62337		Yes (2.2)	Yes (1.3)	Yes (2.2)
Alvin_1452	46..50	conserved hypothetical protein	7		ADC62387	Yes	Yes (1.5)	Yes (1.1)	Yes (1.1)
	85..89								
	109..113								
	151..155								
	180..184								
	210..214								
	238..242								
Alvin_1454	130..134	hypothetical protein	8		ADC62389		No (1)	No (1.0)	No (0.7)
	230..234								
	262..266								
	306..310								
	360..364								
	392..396								

	419..423								
	681..685								
Alvin_1467	37..41	Alcohol dehydrogenase GroES domain protein	2	Yes	ADC62401		No (0.2)	Yes (5.5)	No (0.3)
	96..100								
Alvin_1573	150..154	methyl-accepting chemotaxis sensory transducer	1		ADC62506		No (0.9)	No (0.8)	No (1)
Alvin_1694	24..28	cytochrome c class I	1		ADC62626	Yes	Yes (1.8)	Yes (3.0)	Yes (1.5)
Alvin_1837	50..54	putative lipoprotein	2	Yes	ADC62762	Yes	Yes (1.3)	Yes (1.1)	Yes (2)
	389..393								
Alvin_1846	57..61	cytochrome c class I	2		ADC62771	Yes	Yes (1.5)	Yes (1.5)	Yes (1.6)
	151..155								
Alvin_1867	17..21	NADH ubiquinone oxidoreductase 20 kDa subunit	1	Yes	ADC62792		No (0.9)	N/A	Yes (1.1)
Alvin_1971	87..91	Coproporphyrinogen dehydrogenase	1	Yes	ADC62895		No (0.8)	Yes (5.5)	No (0.9)
Alvin_2064	61..65	protein of unknown function DUF255	1	Yes	ADC62986		No (0.2)	Yes (4.4)	No (0.3)
Alvin_2168	56..60	SoxX	1	Yes	ADC63089	Yes	Yes (1.3)	Yes (5.7)	Yes (1.1)
Alvin_2169	195..199	SoxA	1		ADC63090	Yes	Yes (1.1)	Yes (5.4)	No (0.9)
Alvin_2172	89..93	HNH endonuclease	1		ADC63093		No (0.9)	Yes (1.1)	No (0.8)
Alvin_2201	150..154	conserved hypothetical protein	1		ADC63122	Yes	No (0.4)	No (0.7)	No (0.4)
Alvin_2458	41..45	NapC/NirT cytochrome c domain protein	4		ADC63370		Yes (1.8)	Yes (1.7)	Yes (1.6)
	71..75								
	125..129								
	161..165								
Alvin_2459	46..50	hypothetical protein	1		ADC63371	Yes	Yes (2)	No (0.9)	Yes (1.9)
Alvin_2490	13..17	4Fe-4S ferredoxin iron-sulfur binding domain protein	1	Yes	ADC63402		No (0.3)	No (0.2)	No (0.3)
Alvin_2551	107..111	photosynthetic reaction center cytochrome c subunit	4	Yes	ADC63461	Yes	No (0.1)	No (0.005)	No (0.3)
	152..156								
	247..251								

	307..311								
Alvin_2765	144..148	cytochrome c prime	1		ADC63674	Yes	No (0.3)	Yes (2.6)	No (0.6)
Alvin_2879	42..46	cytochrome c class I	2		ADC63784	Yes	No (1)	No (0.4)	No (0.7)
	138..142								
Alvin_3050	37..41	ribosomal protein L31	1		ADC63950		No (0.6)	No (0.7)	No (0.5)
Alvin_3069	41..45	Thioredoxin domain protein	1		ADC63969		No (0.2)	Yes (6.6)	No (0.3)
Alvin_3120	550..554	type II secretion system protein E	1	Yes	ADC64019		Yes (1.3)	No (0.7)	Yes (1.1)
Alvin_3135	93..97	Radical SAM domain protein	1	Yes	ADC64033		Yes (2.6)	N/A	Yes (2.5)

Table 3-2 Most upregulated and downregulated hypothetical genes for FeS transcriptome

Gene locus	log2FC (FeS)	Padj (FeS)	log2FC (NEG)	Padj (NEG)	Kegg or Strindb annotation	pBlast %	AA length	Sequence protein domains	Protein motifs (AA locus)	Transmembrane domains (AA locus)	Hydropathicity
Upregulated genes											
Alvin_0017	3.6407	0.00005	1.4520	0.1715	hypothetical protein Alvin_0017	95	133	none	signal peptide (26-27)	TM (5-23)	-0.149
Alvin_0016	3.5982	0.00001	1.7825	0.0597	hypothetical protein Alvin_0016	83	101	DUF3240	none	TM (59-78)	0.17
Alvin_0034	3.3657	0.00020	1.1561	0.2903	hypothetical protein Alvin_0034	32	112	none	none	none	-0.571
Alvin_0893	3.2060	0.04316	4.2432	0.0044	hypothetical protein Alvin_0893	59	86	HTH_17	none	none	-0.459
Alvin_1191	3.1585	0.00000	1.1371	0.0705	hypothetical protein Alvin_1191	97	163	DUF3340, DUF2992	none	none	-1.082
Downregulated genes											
Alvin_0703	-10.6741	0.00000	-5.3825	0.0000	hypothetical protein	99	53	LHC	none	TM (23-51)	0.692

					Alvin_0703						
Alvin_0705	-8.0640	0.00000	-5.2530	0.0000	hypothetical protein Alvin_0705	98	69	DUF5989, LHC	none	TM (24-46)	0.648
Alvin_3072	-7.2490	0.00000	-6.5204	0.0000	hypothetical protein Alvin_3072	63	61	DUF2892, Pox_P21	none	TM (11-27 & 30-52)	0.793
Alvin_1741	-6.8081	0.00000	-5.4702	0.0000	hypothetical protein Alvin_1741	29	78	DUF5320, FoP_duplication	none	none	-0.735
Alvin_2515	-5.7798	0.00000	-5.6970	0.0000	hypothetical protein Alvin_2515	99	202	Mod_r, GBP_C	signal peptide (22-23)	TM (06-25)	-0.902

Table 3-3 FeS photosynthetic gene expression of *puf* and *puc* genes

No.	Gene locus	log2FC (FeS)	Padj (FeS)	log2FC (NEG)	Padj (NEG)	Annotation
***puf* genes (LH1)**						
1	Alvin_2554	-3.634066	0.015142	-1.294482	0.471556	puf/LH1
2	Alvin_2548	-3.615404	0.000025	-0.792069	0.480608	puf/LH1
3	Alvin_2549	-3.567375	0.000109	-0.890936	0.451954	puf/LH1
4	Alvin_2550	-3.560588	0.000115	-1.498040	0.162794	puf/LH1
5	Alvin_2552	-3.272447	0.015665	-2.649278	0.061690	puf/LH1
6	Alvin_2553	-3.259926	0.015490	-2.611817	0.064066	puf/LH1
7	Alvin_2555	-3.120657	0.001619	-1.325815	0.246577	puf/LH1
8	Alvin_2551	-2.796485	0.000712	-1.976107	0.025298	puf/LH1
9	Alvin_2547	-1.918547	0.081518	-1.016969	0.409853	puf/LH1
10	Alvin_2637	-1.582827	0.085038	-1.316279	0.171470	puf/LH1
11	Alvin_2636	-0.598188	0.451644	-1.726529	0.010760	puf/LH1
12	Alvin_2635	-0.559236	0.425852	-1.106660	0.080923	puf/LH1
13	Alvin_2634	-0.047346	0.954552	-0.109868	0.883949	puf/LH1
***puc* genes (LH2)**						
14	Alvin_0703	-10.674125	0.000000	-5.382470	0.000000	pucA6
15	Alvin_0704	-9.650563	0.000000	-5.528480	0.000000	pucB6
16	Alvin_0706	-8.891176	0.000000	-4.948448	0.000000	pucB5
17	Alvin_0709	-8.314175	0.000000	-3.864599	0.013577	pucB4
18	Alvin_0705	-8.063998	0.000000	-5.253038	0.000000	pucA5
19	Alvin_2759	-4.947318	0.002552	0.297924	0.900823	pucA3
20	Alvin_0708	-4.699489	0.000000	-3.003893	0.000002	pucA4
21	Alvin_2576	-4.597203	0.000837	-0.575461	0.767512	Lux/LH2
22	Alvin_2760	-4.455893	0.011969	-0.017335	0.995574	pucB3
23	Alvin_2577	-4.388163	0.004599	-0.762006	0.712280	Lux/LH2
24	Alvin_2578	-4.022919	0.009897	-1.044325	0.595913	Lux/LH2
25	Alvin_2579	-4.004724	0.007686	-1.236322	0.503230	Lux/LH2
26	Alvin_2580	-0.141035	0.760208	-0.130225	0.790827	Lux/LH2

Table 3-4 Sulfur oxidation gene expression for *sox* and *dsr* genes

Gene	Protein	log2FC (FeS)	Padj (FeS)	log2FC (NEG)	Padj (NEG)
***dsr* genes**					
Alvin_1252	DsrB	-5.6489639	0.0000011	-6.8973136	0.0000000
Alvin_1251	DsrA	-5.4785498	0.0000000	-6.1322032	0.0000000
Alvin_1253	DsrE	-4.7533377	0.0000000	-6.2967142	0.0000000
Alvin_1254	DsrF	-4.1128256	0.0000005	-5.1124280	0.0000000
Alvin_1258	DsrK	-3.7962670	0.0000000	-4.4047500	0.0000000
Alvin_1259	DsrL	-3.5434234	0.0000000	-4.2673562	0.0000000
Alvin_1260	DsrJ	-3.2740779	0.0000000	-3.8993626	0.0000000
Alvin_1256	DsrC	-3.2456456	0.0000000	-2.9251296	0.0000000
Alvin_1257	DsrM	-2.9378550	0.0001730	-3.4362076	0.0000089
Alvin_1261	DsrO	-2.8960953	0.0000000	-3.5743868	0.0000000
Alvin_1262	DsrP	-2.7346725	0.0000000	-3.0316707	0.0000000
Alvin_1255	DsrH	-2.4543136	0.0000020	-2.0042812	0.0002028
Alvin_1263	DsrN	-1.3872185	0.0000018	-1.2323723	0.0000379
Alvin_1264	DsrR	-1.0179640	0.0203186	-0.6178828	0.1963651
Alvin_1265	DsrS	-1.0061974	0.0013562	-0.7334078	0.0276782
***sox g*enes**					
Upregulated Genes					
Alvin_2111	SoxY	0.6218670	0.1375203	0.4992858	0.2576249
Alvin_2112	SoxZ	0.5305224	0.1192602	0.2637139	0.5008392
Alvin_2167	SoxB	0.4993742	0.4970123	0.0197858	0.9839592
Alvin_2168	SoxX	0.4264933	0.2245081	0.1117592	0.7997775
Alvin_2169	SoxA	0.1817818	0.6269973	-0.0926740	0.8268918
Downregulated Genes					
Alvin_2171	SoxL	-1.4273945	0.0000633	-0.0204548	0.9700032
Alvin_2170	SoxK	-0.6998984	0.1664526	0.1621101	0.7899313

Table 3-5 FeS transcriptome gene table showing genes with log2FC above 2 or below -2

No.	Gene locus	log2FC (FeS)	Padj (FeS)	log2FC (NEG)	Padj (NEG)	Annotation
Upregulated Genes						
1	Alvin_1093	5.4800000	0.0000000	4.6233592	0.0000000	cytochrome c class I, FccA
2	Alvin_1095	4.9570000	0.0000000	5.2415821	0.0000000	NapC/NirT cytochrome c domain protein
3	Alvin_0014	4.8500000	0.0006700	1.8222738	0.2802455	efflux transporter, RND family, MFP subunit
4	Alvin_1094	4.8070000	0.0000000	5.1117525	0.0000000	Ankyrin
5	Alvin_1092	4.6640000	0.0000000	4.1939124	0.0000000	Flavocytochrome c sulphide dehydrogenase flavin-binding protein, FccB
6	Alvin_0013	4.2830000	0.0054000	0.6657844	0.7523724	outer membrane efflux protein
7	Alvin_0015	3.9660000	0.0000018	1.0922448	0.2918687	heavy metal efflux pump, CzcA family
8	Alvin_0017	3.6410000	0.0000530	1.4520158	0.1715025	hypothetical protein Alvin_0017
9	Alvin_1529	3.6260000	0.0000000	-0.0338206	0.9557078	cation diffusion facilitator family transporter
10	Alvin_0016	3.5980000	0.0000130	1.7824510	0.0597347	hypothetical protein Alvin_0016
11	Alvin_2308	3.4130000	0.0000000	2.8744723	0.0000000	nickel-dependent hydrogenase large subunit
12	Alvin_0020	3.3780000	0.0003600	1.7393082	0.1031132	Diheme cytochrome c
13	Alvin_0019	3.3710000	0.0000510	1.4551948	0.1329511	cation diffusion facilitator family transporter
14	Alvin_0034	3.3660000	0.0002000	1.1561422	0.2903281	hypothetical protein Alvin_0034
15	Alvin_2309	3.3630000	0.0000000	3.2115191	0.0000000	hydrogenase (NiFe) small subunit HydA
16	Alvin_0021	3.3080000	0.0320000	1.9126671	0.2635259	cytochrome B561
17	Alvin_0893	3.2060000	0.0430000	4.2431836	0.0043830	hypothetical protein Alvin_0893
18	Alvin_2446	3.1870000	0.0000000	2.1624349	0.0000014	nitrite and sulphite reductase 4Fe-4S region
19	Alvin_1191	3.1580000	0.0000000	1.1371041	0.0704973	hypothetical protein Alvin_1191

20	Alvin_2451	3.1000000	0.0000000	3.0341472	0.0000000	molybdopterin oxidoreductase Fe4S4 region
21	Alvin_1528	3.0820000	0.0000000	-0.3818499	0.5711215	protein of unknown function DUF156
22	Alvin_1447	3.0810000	0.0012000	0.4863944	0.7069938	hypothetical protein Alvin_1447
23	Alvin_1708	3.0360000	0.5900000	2.4400137	0.6817633	hypothetical protein Alvin_1708
24	Alvin_0018	3.0080000	0.0000570	1.2634505	0.1486855	Di-heme cytochrome c peroxidase
25	Alvin_1379	2.9900000	0.0380000	1.0747368	0.5340113	2-isopropylmalate synthase
26	Alvin_2307	2.9070000	0.0000000	3.4640354	0.0000000	Ni/Fe-hydrogenase, b-type cytochrome subunit
27	Alvin_1190	2.8970000	0.0000001	0.7565301	0.2731574	hypothetical protein Alvin_1190
28	Alvin_0022	2.8510000	0.0700000	2.2839001	0.1667924	Domain of unknown function DUF1924
29	Alvin_0023	2.7190000	0.0076000	1.9719568	0.0684427	Diheme cytochrome c
30	Alvin_1189	2.6970000	0.0000000	0.5472497	0.3734252	hypothetical protein Alvin_1189
31	Alvin_3202	2.6790000	0.0130000	2.7270889	0.0111084	hypothetical protein Alvin_3202
32	Alvin_2306	2.6000000	0.0000000	3.1777616	0.0000000	hydrogenase expression/formation protein
33	Alvin_1448	2.4900000	0.0055000	0.1735818	0.8913823	putative transposase
34	Alvin_1063	2.4820000	0.0000000	1.3009845	0.0030975	TRAP dicarboxylate transporter, DctP subunit
35	Alvin_0284	2.4400000	0.0000420	2.1292585	0.0005858	peptidase M61 domain protein
36	Alvin_2447	2.3710000	0.0000001	1.8479614	0.0000673	adenylylsulfate reductase, thioredoxin dependent
37	Alvin_0026	2.3700000	0.0000180	1.1589011	0.0667381	integral membrane sensor signal transduction histidine kinase
38	Alvin_0025	2.3470000	0.0043000	1.0881098	0.2468944	two component transcriptional regulator, winged helix family
39	Alvin_2453	2.3400000	0.0000000	3.0303434	0.0000000	formate dehydrogenase, beta subunit
40	Alvin_0024	2.3080000	0.0180000	1.3796589	0.1969108	membrane protein-like protein

41	Alvin_0060	2.2770000	0.0000028	0.2716808	0.6981900	hypothetical protein Alvin_0060
42	Alvin_1062	2.1980000	0.0000000	0.7614830	0.0579929	Tripartite ATP-independent periplasmic transporter DctQ component
43	Alvin_0283	2.1970000	0.0049000	1.6924440	0.0402079	RNP-1 like RNA-binding protein
44	Alvin_2452	2.1570000	0.0000000	1.9372901	0.0000000	formate dehydrogenase, alpha subunit
45	Alvin_1686	2.0620000	0.4100000	2.1311171	0.3734252	hypothetical protein Alvin_1686
46	Alvin_3205	2.0610000	0.1100000	1.7788150	0.1725462	hypothetical protein Alvin_3205
47	Alvin_1928	2.0320000	0.0001200	0.2205595	0.7758212	molybdopterin converting factor, subunit 1
48	Alvin_0937	2.0200000	0.0130000	1.0961006	0.2224819	hypothetical protein Alvin_0937
Downregulated Genes						
49	Alvin_0703	-10.6740000	0.0000000	-5.3824698	0.0000000	hypothetical protein Alvin_0703
50	Alvin_0704	-9.6510000	0.0000000	-5.5284800	0.0000000	antenna complex alpha/beta subunit
51	Alvin_0706	-8.8910000	0.0000000	-4.9484483	0.0000000	antenna complex alpha/beta subunit
52	Alvin_0709	-8.3140000	0.0000004	-3.8645991	0.0135774	antenna complex alpha/beta subunit
53	Alvin_0705	-8.0640000	0.0000000	-5.2530380	0.0000000	hypothetical protein Alvin_0705
54	Alvin_3072	-7.2490000	0.0000000	-6.5203648	0.0000000	hypothetical protein Alvin_3072
55	Alvin_1006	-7.1930000	0.0000001	-7.0169062	0.0000002	Peroxiredoxin
56	Alvin_1741	-6.8080000	0.0000000	-5.4702111	0.0000000	hypothetical protein Alvin_1741
57	Alvin_1740	-6.6930000	0.0000000	-5.3021788	0.0000000	Dinitrogenase iron-molybdenum cofactor biosynthesis protein
58	Alvin_3073	-6.2430000	0.0000000	-5.6986961	0.0000000	C4-dicarboxylate transporter/malic acid transport protein
59	Alvin_2515	-5.7800000	0.0000000	-5.6970305	0.0000000	hypothetical protein Alvin_2515
60	Alvin_1252	-5.6490000	0.0000011	-6.8973136	0.0000000	DsrB

61	Alvin_1251	-5.4790000	0.0000000	-6.1322032	0.0000000	DsrA
62	Alvin_1739	-5.4720000	0.0000000	-4.9003460	0.0000000	Cobyrinic acid ac-diamide synthase
63	Alvin_1738	-5.0880000	0.0000000	-3.7836766	0.0000000	Cobyrinic acid ac-diamide synthase
64	Alvin_2759	-4.9470000	0.0026000	0.2979242	0.9008234	hypothetical protein Alvin_2759
65	Alvin_1324	-4.8230000	0.0000000	-2.9777020	0.0002441	Redoxin domain protein
66	Alvin_1253	-4.7530000	0.0000000	-6.2967142	0.0000000	DsrE
67	Alvin_0708	-4.6990000	0.0000000	-3.0038926	0.0000019	hypothetical protein Alvin_0708
68	Alvin_2136	-4.6590000	0.0000000	-5.2392623	0.0000000	hypothetical protein Alvin_2136
69	Alvin_2576	-4.5970000	0.0008400	-0.5754608	0.7675116	antenna complex alpha/beta subunit
70	Alvin_1434	-4.4970000	0.0024000	-3.0798773	0.0535113	Protein of unknown function DUF2061, membrane
71	Alvin_2760	-4.4560000	0.0120000	-0.0173347	0.9955743	antenna complex alpha/beta subunit
72	Alvin_2577	-4.3880000	0.0046000	-0.7620062	0.7122796	antenna complex alpha/beta subunit
73	Alvin_1737	-4.3830000	0.0000000	-3.1990383	0.0000358	Dinitrogenase iron-molybdenum cofactor biosynthesis protein
74	Alvin_0962	-4.2880000	0.0000000	-4.6720255	0.0000000	Ankyrin
75	Alvin_0440	-4.2430000	0.0000000	-4.6107064	0.0000000	Chaperonin Cpn10
76	Alvin_1508	-4.2340000	0.0000000	-4.1473569	0.0000000	sulfur relay protein, TusE/DsrC/DsvC family
77	Alvin_1254	-4.1130000	0.0000006	-5.1124280	0.0000000	DsrF
78	Alvin_2572	-4.1090000	0.0000000	-2.2373314	0.0075534	RNA polymerase, sigma 32 subunit, RpoH
79	Alvin_2107	-4.0290000	0.0000000	-4.0075908	0.0000000	hypothetical protein Alvin_2107
80	Alvin_2578	-4.0230000	0.0099000	-1.0443251	0.5959125	antenna complex, alpha/beta subunit
81	Alvin_2579	-4.0050000	0.0077000	-1.2363220	0.5032305	antenna complex alpha/beta subunit
82	Alvin_1435	-3.9920000	0.0000035	-2.8099801	0.0024353	Ferritin Dps family protein

83	Alvin_0707	-3.8680000	0.0000000	-2.9177028	0.0000014	regulatory protein LuxR
84	Alvin_0854	-3.8630000	0.0000000	-3.3020719	0.0000009	Chaperonin Cpn10
85	Alvin_1258	-3.7960000	0.0000000	-4.4047500	0.0000000	DsrK
86	Alvin_0853	-3.7630000	0.0000002	-3.6858548	0.0000005	chaperonin GroEL
87	Alvin_1197	-3.7180000	0.0096000	-3.7266296	0.0058672	hypothetical protein Alvin_1197
88	Alvin_1853	-3.6600000	0.0000004	-3.3099806	0.0000089	efflux transporter, RND family, MFP subunit
89	Alvin_0358	-3.6550000	0.0000001	-2.8803268	0.0000781	Sulfur globule protein SgpB
90	Alvin_2554	-3.6340000	0.0150000	-1.2944821	0.4715559	antenna complex alpha/beta subunit
91	Alvin_1250	-3.6250000	0.0000000	-2.8999261	0.0000027	hypothetical protein Alvin_1250
92	Alvin_0345	-3.6240000	0.0000000	-2.7268448	0.0000089	sulfur relay protein, TusE/DsrC/DsvC family
93	Alvin_2548	-3.6150000	0.0000250	-0.7920694	0.4806077	antenna complex alpha/beta subunit
94	Alvin_2497	-3.6140000	0.0000000	-3.9596021	0.0000000	hypothetical protein Alvin_2497
95	Alvin_0441	-3.5700000	0.0000000	-4.3052942	0.0000000	chaperonin GroEL
96	Alvin_2549	-3.5670000	0.0001100	-0.8909360	0.4519543	antenna complex alpha/beta subunit
97	Alvin_2550	-3.5610000	0.0001100	-1.4980398	0.1627942	antenna complex alpha/beta subunit
98	Alvin_1259	-3.5430000	0.0000000	-4.2673562	0.0000000	DsrL
99	Alvin_2498	-3.5260000	0.0000000	-3.7395737	0.0000000	nitrogen fixation-related protein
100	Alvin_1468	-3.5170000	0.0000000	-2.1987663	0.0000622	YceI family protein
101	Alvin_1742	-3.4660000	0.0000340	-1.1536392	0.1579171	protein of unknown function DUF134
102	Alvin_2661	-3.4480000	0.0000000	-2.8628045	0.0000001	protein of unknown function DUF323
103	Alvin_0312	-3.3940000	0.0000000	-2.4703655	0.0000000	fructose-bisphosphate aldolase, class II, Calvin cycle subtype
104	Alvin_2063	-3.3600000	0.0000170	-3.1361610	0.0000901	hypothetical protein Alvin_2063

105	Alvin_0009	-3.3120000	0.0000330	-3.4184250	0.0000236	heat shock protein Hsp20
106	Alvin_1524	-3.3040000	0.0025000	-1.3986550	0.2460073	Protein of unknown function DUF1920
107	Alvin_1905	-3.2880000	0.0000000	-0.0934715	0.9214111	sulfur globule protein SgpA
108	Alvin_3199	-3.2790000	0.1800000	0.7672562	0.7045733	hypothetical protein Alvin_3199
109	Alvin_1323	-3.2780000	0.0000000	-3.0818422	0.0000005	glutathione-disulfide reductase
110	Alvin_1260	-3.2740000	0.0000000	-3.8993626	0.0000000	DsrJ
111	Alvin_2552	-3.2720000	0.0160000	-2.6492775	0.0616899	photosynthetic reaction center, M subunit
112	Alvin_2553	-3.2600000	0.0150000	-2.6118172	0.0640655	photosynthetic reaction center L subunit
113	Alvin_1256	-3.2460000	0.0000000	-2.9251296	0.0000000	DsrC
114	Alvin_1249	-3.2390000	0.0000000	-2.6953260	0.0000082	hypothetical protein Alvin_1249
115	Alvin_2600	-3.1850000	0.0000000	-2.1806892	0.0000005	SirA family protein
116	Alvin_1196	-3.1420000	0.0076000	-3.0799370	0.0060205	hypothetical protein Alvin_1196
117	Alvin_0316	-3.1340000	0.0000000	-3.6277239	0.0000000	transketolase
118	Alvin_1365	-3.1340000	0.0000000	-3.6182577	0.0000000	Ribulose-bisphosphate carboxylase
119	Alvin_2555	-3.1210000	0.0016000	-1.3258147	0.2465773	antenna complex alpha/beta subunit
120	Alvin_1920	-3.1110000	0.0000000	-1.4475008	0.0195161	Superoxide dismutase
121	Alvin_2965	-3.1080000	0.0000002	-1.2248273	0.0684427	TPR repeat-containing protein
122	Alvin_0739	-3.0840000	0.0000000	-2.3365390	0.0000121	FeS assembly protein SufB
123	Alvin_3241	-3.0780000	0.0000010	-2.2137249	0.0010171	protein of unknown function DUF302
124	Alvin_1385	-3.0760000	0.0000002	-2.8426786	0.0000023	GrpE protein
125	Alvin_1384	-3.0140000	0.0000000	-2.4253753	0.0000264	heat-inducible transcription repressor HrcA
126	Alvin_3032	-3.0080000	0.0000000	-1.8284716	0.0000000	hypothetical protein Alvin_3032

127	Alvin_2667	-2.9940000	0.0000098	-1.9643453	0.0075642	iron-sulfur cluster assembly accessory protein
128	Alvin_1849	-2.9590000	0.0000026	-1.8028353	0.0091222	pyridoxamine 5'-phosphate oxidase
129	Alvin_1257	-2.9380000	0.0001700	-3.4362076	0.0000089	DsrM
130	Alvin_0315	-2.9130000	0.0000000	-2.6153536	0.0000000	glyceraldehyde-3-phosphate dehydrogenase, type I
131	Alvin_1862	-2.9040000	0.0017000	-1.0509724	0.3400269	protein of unknown function Spy-related protein
132	Alvin_1261	-2.8960000	0.0000000	-3.5743868	0.0000000	DsrO
133	Alvin_1202	-2.8920000	0.0000000	-2.6356151	0.0000001	ATPase-like, ParA/MinD
134	Alvin_0258	-2.8860000	0.0000006	-2.3440254	0.0001091	Rhodanese domain protein
135	Alvin_1366	-2.8800000	0.0000000	-2.4285075	0.0000000	Ribulose-bisphosphate carboxylase
136	Alvin_2980	-2.8640000	0.0000052	-1.8482258	0.0068726	hypothetical protein Alvin_2980
137	Alvin_2660	-2.8070000	0.0000000	-2.3646597	0.0000078	methyltransferase
138	Alvin_1359	-2.8030000	0.0000000	-2.6877664	0.0000001	ATP-dependent chaperone ClpB
139	Alvin_2551	-2.7960000	0.0007100	-1.9761065	0.0252980	photosynthetic reaction centre cytochrome c subunit
140	Alvin_1733	-2.7930000	0.0000018	-2.0304441	0.0004965	peptidase M15D vanX D-ala-D-ala dipeptidase
141	Alvin_1386	-2.7730000	0.0000063	-3.0461331	0.0000007	chaperone protein DnaK
142	Alvin_1262	-2.7350000	0.0000000	-3.0316707	0.0000000	DsrP
143	Alvin_2274	-2.7260000	0.0000000	-1.0317289	0.0379289	High potential iron-sulfur protein
144	Alvin_1248	-2.7200000	0.0000001	-2.1113375	0.0000789	CRISPR-associated protein, Cas6-related protein
145	Alvin_0804	-2.6710000	0.0000001	-2.7382692	0.0000001	pyruvate dehydrogenase complex dihydrolipoamide acetyltransferase

146	Alvin_1735	-2.6530000	0.0000170	-2.1192048	0.0010173	transcriptional coactivator/pterin dehydratase
147	Alvin_1036	-2.6530000	0.0370000	-0.4238403	0.7326594	hypothetical protein Alvin_1036
148	Alvin_1918	-2.6510000	0.0000049	-1.8828920	0.0025519	glutaredoxin-like protein
149	Alvin_2033	-2.6490000	0.0000023	-1.7869070	0.0032446	oxidoreductase FAD/NAD(P)-binding domain protein
150	Alvin_0740	-2.6460000	0.0000000	-2.2286238	0.0000000	FeS assembly ATPase SufC
151	Alvin_0766	-2.6460000	0.0000045	-2.3990116	0.0000554	protein of unknown function DUF198
152	Alvin_2032	-2.6090000	0.0000500	-1.7234103	0.0135774	Peroxiredoxin
153	Alvin_1526	-2.5630000	0.0370000	-1.9955307	0.1071322	FeoA family protein
154	Alvin_2601	-2.5530000	0.0000000	-1.5400289	0.0000023	hypothetical protein Alvin_2601
155	Alvin_0742	-2.5400000	0.0000000	-1.7046545	0.0001069	FeS assembly SUF system protein
156	Alvin_2037	-2.4970000	0.0000000	-3.1541978	0.0000000	protein of unknown function DUF224 cysteine-rich region domain protein
157	Alvin_1121	-2.4960000	0.0000000	-2.9456647	0.0000000	AprA
158	Alvin_1734	-2.4770000	0.0000190	-2.9796387	0.0000001	Protein of unknown function DUF2269, transmembrane
159	Alvin_0313	-2.4690000	0.0000000	-2.4714424	0.0000000	pyruvate kinase
160	Alvin_1119	-2.4580000	0.0000000	-2.6240614	0.0000000	AprM
161	Alvin_2043	-2.4570000	0.0000030	-2.4987453	0.0000027	methionine aminopeptidase, type I
162	Alvin_1255	-2.4540000	0.0000020	-2.0042812	0.0002028	DsrH
163	Alvin_0741	-2.4480000	0.0000000	-2.2630947	0.0000000	FeS assembly protein SufD
164	Alvin_0631	-2.4340000	0.0010000	-1.9479869	0.0123718	hypothetical protein Alvin_0631
165	Alvin_1525	-2.4290000	0.1400000	-1.5679388	0.3835748	ferrous iron transport protein B

166	Alvin_1467	-2.4160000	0.0000000	-1.7451957	0.0000468	Alcohol dehydrogenase GroES domain protein
167	Alvin_1420	-2.4150000	0.0021000	-1.2411833	0.1586592	transcriptional regulator, BadM/Rrf2 family
168	Alvin_2426	-2.3810000	0.0000007	-1.2865346	0.0166133	NADH-quinone oxidoreductase, E subunit
169	Alvin_0805	-2.3700000	0.0000004	-2.6773815	0.0000000	2-oxo-acid dehydrogenase E1 subunit, homodimeric type
170	Alvin_1120	-2.3450000	0.0000000	-2.8268268	0.0000000	AprB
171	Alvin_2427	-2.3410000	0.0000000	-1.3047711	0.0048499	NADH dehydrogenase I, D subunit
172	Alvin_2668	-2.3330000	0.0002000	-1.6916883	0.0115813	Fe-S metabolism associated SufE
173	Alvin_1118	-2.3320000	0.0000000	-2.2653624	0.0000000	sulfate adenylyltransferase
174	Alvin_2039	-2.3300000	0.0000310	-2.9900061	0.0000000	hydrogenase (NiFe) small subunit HydA
175	Alvin_0320	-2.3210000	0.0000002	-1.9542722	0.0000315	adenosylhomocysteinase
176	Alvin_2422	-2.3020000	0.0000000	-1.0922311	0.0160923	NADH-quinone oxidoreductase, chain I
177	Alvin_0314	-2.2950000	0.0000000	-2.4016542	0.0000000	Phosphoglycerate kinase
178	Alvin_1852	-2.2940000	0.0000006	-2.3053381	0.0000007	acriflavin resistance protein
179	Alvin_1994	-2.2940000	0.0000091	-1.5059854	0.0072400	ubiquinone biosynthesis O-methyltransferase
180	Alvin_0259	-2.2880000	0.0000007	-1.9698954	0.0000379	Peptidylprolyl isomerase
181	Alvin_2038	-2.2570000	0.0000130	-3.0448822	0.0000000	hypothetical protein Alvin_2038
182	Alvin_0321	-2.2550000	0.0000000	-1.4467334	0.0001328	5,10-methylenetetrahydrofolate reductase
183	Alvin_3233	-2.2260000	0.0001900	-1.6291627	0.0100430	putative thiol-disulphide oxidoreductase DCC
184	Alvin_1322	-2.2060000	0.0000024	-1.6645512	0.0007789	2,3-bisphosphoglycerate-independent phosphoglycerate mutase
185	Alvin_2423	-2.2000000	0.0000000	-1.0510987	0.0021790	NADH dehydrogenase (quinone)
186	Alvin_1079	-2.1950000	0.0000000	-2.2293398	0.0000000	cytochrome B561

187	Alvin_2001	-2.1930000	0.0000001	-2.1276434	0.0000002	putative transcriptional regulator, Crp/Fnr family
188	Alvin_3000	-2.1730000	0.0000000	-2.3888471	0.0000000	glutamine synthetase, type I
189	Alvin_1318	-2.1660000	0.0000064	-2.5391306	0.0000001	4Fe-4S ferredoxin iron-sulfur binding domain protein
190	Alvin_1861	-2.1640000	0.0000011	-1.0378474	0.0410512	membrane-flanked domain protein
191	Alvin_0779	-2.1600000	0.0003600	-1.2175339	0.0700581	Peptidase M23
192	Alvin_2425	-2.1550000	0.0000064	-1.1327431	0.0359035	NADH-quinone oxidoreductase, F subunit
193	Alvin_2064	-2.1510000	0.0001400	-1.7937334	0.0023565	protein of unknown function DUF255
194	Alvin_0834	-2.1030000	0.0000280	-1.9797338	0.0001100	NAD(P)(+) transhydrogenase (AB-specific)
195	Alvin_0680	-2.0880000	0.0000120	-0.6099044	0.2983663	protein of unknown function DUF1271
196	Alvin_0499	-2.0880000	0.0000000	-1.8604683	0.0000000	hypothetical protein Alvin_0499
197	Alvin_0803	-2.0740000	0.0000011	-2.1761616	0.0000004	dihydrolipoamide dehydrogenase
198	Alvin_0559	-2.0700000	0.0044000	-1.5953734	0.0363904	transcriptional regulator, TetR family
199	Alvin_2421	-2.0580000	0.0000000	-0.8292709	0.0538470	NADH-ubiquinone/plastoquinone oxidoreductase chain 6
200	Alvin_2419	-2.0560000	0.0000000	-1.1317048	0.0024200	proton-translocating NADH-quinone oxidoreductase, chain L
201	Alvin_2424	-2.0430000	0.0000000	-1.2102685	0.0004010	NADH-quinone oxidoreductase, chain G
202	Alvin_3069	-2.0220000	0.0000750	-1.8275089	0.0005003	Thioredoxin domain protein
203	Alvin_2295	-2.0170000	0.0009900	-0.9668023	0.1317583	hypothetical protein Alvin_2295

Chapter 4 Transcriptomic Evidence for the Use of Nickel Sulfide as the Electron Donor by Allochromatium vinosum for Autotrophic Growth

4.1 Abstract

Purple sulfur bacteria (PSB) are photosynthetic microorganisms known for their vital role in geochemical cycles, particularly the sulfur cycle, within anoxic environments. They contribute significantly to the oxidation of reduced sulfur species. This study focuses on the successful autotrophic growth of *Allochromatium vinosum*, a model PSB strain, utilizing solid-phase nickel sulfide NiS nanoparticles as both sulfur and electron donors. In contrast to the positive control that utilized conventional sodium sulfide as the sulfur and electron donor source, the NiS cell culture displayed a longer growth duration, peaking at 700 hours. This resulted in approximately 2.5 times the cellular growth compared to the negative control, whereas the positive control reached its peak at 400 hours. Despite this, neither the ion chromatography nor the sulfide depletion plot provided indications of sulfur oxidation, possibly due to incomplete sulfide oxidation to elemental sulfur.

Both XPS and TEM analyses showcased NiS transformations, with XPS revealing a peak within the elemental nickel region. The transcriptome revealed an abundant array of proteins linked to electron transport, although many were also upregulated in the negative control. This similarity might stem from the utilization of electron transport proteins to harness energy from various substrates, although the absence of carbon metabolism genes underscores their distinct metabolic paths.

The transcriptome analysis revealed intriguing differential gene expression among key sulfur oxidation, photosynthetic, transporter, and electron transport proteins. Notably, redox-active proteins like Fe/Ni hydrogenases and formate dehydrogenase, including hydrogenase proteins,

exhibited upregulation in both NiS and the negative control pathways. This suggests potential activation of the Wood-Ljungdahl pathway, albeit without an identified electron donor. Sulfur oxidation genes, with upregulated *sox* and downregulated dsr, hint at a preference for thiosulfate oxidation. Upregulation of transporter genes like K+-ATPases and metal efflux genes was unique to the NiS sample, possibly reflecting responses to ion homeostasis and detoxification, strongly suggesting ion accumulation and NiS releasing ions for utilization. Furthermore, cytochromes Alvin_1093 and Alvin_1095 displayed expression in both samples, more pronounced in NiS. These cytochromes may play a role in facilitating electron transport processes to or from NiS nanoparticles.

Overall, these findings shed light on the modified pathways of photosynthesis and sulfur metabolism in the NiS-nanoparticle supported PSB cultures, thereby enhancing our understanding of their metabolic capabilities and extracellular electron transfer mechanisms. Moreover, these results hold implications for comprehending the coevolution of early Earth's biology and geology, as well as fuel and energy generation applications.

4.2 Introduction

Purple sulfur bacteria (PSB) are a group of photosynthetic bacteria that exhibit remarkable adaptability and play important roles in aquatic ecosystems. PSB are known for their ability to perform anoxygenic photosynthesis, utilizing a variety of electron donors including sulfur compounds (Ehrenreich *et al.*, 1994; Daldal *et al.*, 2008). They thrive in environments where anaerobic conditions, light, and sulfide concentrations intersect, such as stratified water bodies and microbial mats (Seitz *et al.*, 1991; Magian *et al.*, 1984; Hunter *et al.*, 2009). PSB are key participants in the cycling of carbon and sulfur, acting as primary producers and reoxidizing hydrogen sulfide produced by sulfate-reducers (Madigan *et al.*, 2009). The reoxidation of sulfide by PSB yields nontoxic forms of sulfur, i.e., elemental sulfur (S^0) and sulfate (SO_4^{2-}), detoxifying

the environment and closing the essential sulfur oxidation-reduction cycle (Madigan *et al.*, 2009). The formation and utilization of elemental sulfur globules are distinctive features of PSB, which also occurs in chemolithotrophic sulfur bacteria. PSB possess the unique ability to utilize solid-phase elemental sulfur globules as part of their metabolic process. Such sulfur globules are deposited either outside the cell membrane or inside the periplasmic space, depending on their belonging to the *Ectothiorhodospiraceae* or *Chromatiaceae* families (Daldal *et al.*, 2008). Through their metabolic activities, PSB contribute significantly to nutrient cycling, energy exchange, and maintaining the ecological balance in aquatic habitats (Dincturk *et al.*, 2011; Daldal *et al.*, 2008)

The utilization of solid-phase substrates, such as elemental sulfur, by photosynthetic bacteria like *A. vinosum* remains an area with limited understanding. However, if this phenomenon is verified, the presence of extracellular electron transfer processes in *A. vinosum* could yield substantial benefits. These advantages encompass heightened microbial cooperation and diversified community-level metabolic processes. Furthermore, these processes could impact the alteration of available organic materials and influence nutrient availability, potentially accelerating the release of metals from solid surfaces. These mechanisms bear profound implications for bacterial physiology, ecological interactions, and even industrial applications. Additionally, the interplay between PSB and metal sulfides holds evolutionary significance, especially considering the prevalence and transformations of sulfide-rich environments during early Earth's history.

Electrochemically active bacteria (EAB) are microorganisms that harness energy from inorganic materials through electron transfer (Lovley, 1987; Hallbeck, 1990; Deng, 2021). A key pathway in EAB bacteria is extracellular electron transfer (EET), where electrons move from cytosol to the environment. EET Mtr pathway in bacteria like Shewanella odeinensis involves proteins like MtrA, MtrB, and MtrC, allowing electrons to be transferred from the cytoplasmic

membrane to the bacterial surface. Flavin-based EET involves transferring electrons from cytosolic NADH to quinone molecules, which then shuttle electrons to external acceptors. Outer membrane cytochromes like OmcA also assist in transferring electrons (Mitchell *et al.*, 2012). Flavocytochromes play a significant role in EET. Listeria monocytogenes has a unique flavin-based mechanism where NADH dehydrogenase catalyzes electron exchange to a quinone derivative, which then shuttles electrons using secreted flavins (You *et al.*, 2018).

A metagenomic study of several bacterial species from Betaproteobacteria and Gammaproteobacteria classes including but not limited to Ectothiorhodospira, thiorhodospira and thiocapsa genuses, as well as Allochromatium vinosum, were study for sulfur oxidation genes activated because of sulfur oxidation. The primary sulfur oxidation pathway identified in the genomes called the Sox-Dsr-Soe pathway. In this pathway the sulfane sulfur generated from thiosulfate through the SoxXYZAB components, is likely carried into cells as persulides, as seen in phototropic sulfur oxidizers. Persulfide can add to DsrC facilitated by Rhd, TusA and DsrEFH. Persulfated Dsr then can be used by DsrAB protein compelx. This seroheme containing protein can carry the revesible reduction of sulfite to sulfide, as seen in sulfate-reducing micoorganisms. This process leads to formation of sulfite and disulfide bonds within DsrC, which are reduced by free thiols and DsrMKJOP membrane complex facilitating restart of sulfur relay system. Following sulfite generation, it can undergo further conversion to sulfate facilitated by the SoeABC complex. This process involves the creation of sulfite and disulfide bonds within DsrC. Subsequently, these bonds are reduced to free thiols by the transmembrane DsrMKJOP complex, thereby aiding the restart of the sulfur relay system. Moreover, the produced sulfite undergoes transformation into sulfate via the activity of the cytoplasmic enzyme complex SoeABC. It's noteworthy that the production of sulfite in the cytoplasm results from the reverse action of the dissimilatory sulfite reductase DsrAB. In parallel, SoeABC is associated with sulfite oxidation. Intriguingly, certain

purple sulfur bacteria can harness externally available sulfite as a source of photosynthetic electron donation. However, the precise mechanisms governing sulfite oxidation in these organisms continue to remain largely elusive.

"Sox-Hdr-Soe" pathway, with SoxXYZAB, HdrCBAHypHdrCB, and SoeABC involvement in sulfur oxidation. At the core of the pathway SoxXYZAB, genes were observed in the sulfur oxidizing bacteria that followed this pathway (Watanabe *et al.*, 2019). SoxAX facilitates the conversion of thiosulfate to cystine residue on SoxY in the SoxYZ complex and subsequently the sulfonate group is removed by hydrolysis by SoxB with resulting generation of sulfate and SozYZ with the sulfane sulfur. Although mechanisms of sulfite oxidation are largely unknown, evidence has been found in the literature about the role of SoxAX, SoxYZ and SoxB in sulfite oxidation (Dahl *et al.*, 2013). The role heterodisulfide reductases (Hdr proteins) in sulfur oxidation was observed in studied in Hyphomicrobium denitrificans, (Koch *et al.*, 2018). Silencing of hdr genes led to the ability of the bacteria to metabolize dimethylsulfide and a lower rate of sulfate formation from thiosulfate compared to the wild type under chemoorganoheterotrophic conditions. The pathway involved HdrCBAHypHdrCB but has not been understood yet. In thiosulfate metabolism, HdrCBAHypHdrCB might functionally substitute for Dsr system.

In the context of sulfur oxidation across various species, an important protein identified through metagenomic analysis is Fccab, which is membrane-bound and commonly active across species studied, including *A. vinosum* (Watanabe el al., 2019). Notably, other investigations have highlighted intriguing alternatives to thiosulfate oxidation. For instance, Sulfuriferula multivorans possesses the doxDA gene encoding a membrane-bound thiosulfate:quinone oxidoreductase, coupling thiosulfate oxidation with quinone reduction (Müller *et al.*, 2004). Additionally, it's noteworthy that an alternate pathway for sulfite oxidation has been observed, involving its indirect

oxidation via the APS enzyme. This process is catalyzed by APS reductase and ATP sulfurylase, as outlined by Dahl *et al.*, (2013).

In the context of various alternative sulfur oxidation pathways, several pertinent proteins were identified within *A. vinosum*'s transcriptome. The sulfite oxidation enzyme complex (SoeABC) involves Alvin_2491 (soeA), Alvin_2490 (soeB), and Alvin_2489 (soeC) genes. Alvin_2491 displayed comparable expression to the positive control and a minor downregulation of -1.5 in the negative control, whereas Alvin_2490 was slightly downregulated by -1.4, with similar expression in the negative control. Alvin_2489 showed comparable expression to the positive control and a slight downregulation in the negative control. Notably, Alvin_1092 and Alvin_1093, associated with flavocytochrome (fccab) protein, exhibited significant upregulation in the negative control and higher upregulation across all MS systems. The APS genes, Alvin_1119 to Alvin_1121, demonstrated varying expression levels. Alvin_1119 was downregulated by 0.1-fold compared to the negative control's 0.3-fold, while Alvin_1120 and Alvin_1121 exhibited no substantial change. In terms of dsrAB and dsrEFH, their downregulation was more pronounced in the negative control. Conversely, dsrC exhibited comparable expression levels in both conditions. Likewise, the transmembrane-associated dsrMKJOP genes displayed comparable downregulation across the NiS sample and negative control. Furthermore, genes *sox* AX, *sox* YZ, and SoxB exhibited comparable expression levels across all MS and negative control systems. Specifically, soxB's expression remained unchanged relative to the positive control, while experiencing slight downregulation in the negative control.

As demonstrated in Koch's research, heterodisulfide reductases have been identified as potential alternatives to the Dsr system, potentially replacing it in certain sulfur-oxidizing bacteria. While these proteins are not present in *A. vinosum*, their existence highlights the potential for alternative sulfur oxidation pathways. The findings of this study present a transcriptomic analysis

showcasing the presence of various components, such as cytochromes, hydrogenases (including Ni/Fe hydrogenases), transporter proteins, and pili genes. These components may potentially play a role in uncharacterized sulfur oxidation pathways related to NiS utilization. This pioneering study presents compelling evidence that highlights *A. vinosum*'s proficiency in harnessing solid-phase metal sulfides, with a specific focus on NiS nanoparticles. Furthermore, through extensive transcriptomic profiling and substrate characterization, we unveil novel insights into the intricate molecular mechanisms that underpin this distinctive metabolic capacity.

4.3 Materials and Methods

4.3.1 Growth tracking

Growth was monitored over time by carefully taking aliquot samples without disrupting sedimented nanoparticles, thereby preventing an overestimation of cellular density. The samples were processed through a 1:10 dilution in water and subsequently placed in a UV-VIS spectrophotometer for optical density measurements at 600nm.

4.3.2 Strain, medium and culture conditions

The study employed the *A. vinosum* DSM 180 strain obtained from DSMZ in Germany. Cultivation of *A. vinosum* involved a modified version of Pfenning's medium, which excluded certain compounds necessary for heterotrophic growth. Various media formulations were prepared, including a sulfur-free control (negative), positive controls, and cultures supplemented with NiS. The positive control medium consisted of $Na_2S{\cdot}9H_2O$ along with several other components, as detailed in table 1 of the appendix. The NiS-amended medium had the same components but replaced $Na_2S{\cdot}9H_2O$ with solid NiS. The sulfur-free control lacked either $Na_2S{\cdot}9H_2O$ or NiS.

To prepare the complete media, two separate solutions, A and B, were created. Solution A involved boiled Milli-Q water, which was degassed with ultrapure N_2 gas during the cooling

process. Salts, except for carbon and sulfur sources ($NaHCO_3$ and $Na_2S \cdot 9H_2O$/NiS), and KH_2PO_4 were added to the degassed solution. Solution A was further degassed with N_2 for approximately 45 minutes. A mineral mix specified in Appendix Table 1 was introduced to solution A at a ratio of 10 µL/mL. A small amount of concentrated 6N HCl was added to aid salt dissolution and achieve a final medium pH between 7.1 and 7.3. Solution A was bottled in serum bottles sealed with rubber septa and aluminum rings.

Solution B, prepared separately, involved sterilizing boiled and degassed Milli-Q water using 0.2-µm syringe filters. The filtered solution was stored in a sterile serum bottle and bubbled with ultrapure N_2 at room temperature for approximately 15 minutes. $NaHCO_3$ and $Na_2S \cdot 9H_2O$/NiS were added to solution B before sealing the bottles with rubber septa. Quick sealing minimized the loss of sulfide and CO_2, ensuring the intended medium composition was maintained. The complete media was obtained by mixing 90% of solution A with 10% of solution B by volume, and ATCC Vitamin mix was added at a ratio of 10 µL per mL of the complete media.

To assess the potential growth of bacteria in the presence of various components of the culture media, a negative control was prepared. The negative control system shared the same composition as all other MS and positive control systems, except for the omission of a sulfur source. This experimental setup aimed to evaluate whether bacteria could thrive in the absence of a sulfur source, specifically examining the contribution of NiS to bacterial growth. Inoculations of both controls and NiS bottles of *A. vinosum* were performed by adding 2% (v/v) of the stock cell culture medium during the late exponential growth phase. All NiS cell cultures, positive controls, and negative controls were incubated in a shaker incubator at 37°C under a tungsten lamp

4.3.3 Nucleic acids extraction and analysis

The recovery of DNA and RNA samples from the cell cultures was achieved using the GenElute Bacterial Genomic DNA kit from Sigma Aldrich and the RNeasy Mini kit from Qiagen,

respectively. To collect the samples, 1 mL aliquots of the cell culture medium were drawn using syringes purged with N2 gas. In the case of RNA extraction, RNAProtect® was promptly added to the aliquots, followed by a 5-minute incubation. The sampled aliquots, with or without RNAProtect®, were then subjected to centrifugation at 5,000 g for 10 minutes, and the supernatant was discarded. The resulting cell pellets were stored at -80°C until further DNA/RNA extraction procedures. For DNA extraction, the cell pellets were processed using the Gram-positive quick protocol, as it was determined to be more effective for *A. vinosum* compared to the Gram-negative protocol provided in the GenElute Bacterial Genomic DNA kit manual. On the other hand, for RNA extraction, the cell pellets underwent lysis following a recommended protocol utilizing a lysis solution composed of proteinase K, lysozyme, and a TE buffer solution. The enzymatic digestion was carried out at room temperature for 10 minutes on a rotary shaker. The subsequent RNA extraction was performed using the lysate in accordance with the instructions provided by the RNeasy Mini kit. Quantification of the extracted DNA and RNA samples was conducted using a Nanodrop® One spectrophotometer and a Qubit fluorometer, while quality control assessments were performed based on the 260/280 and 260/230 ratios. Additionally, DIN and RIN analysis was carried out using the Tapestation 2200 system.

4.3.4 Transcriptomic sequencing and bioinformatics

4.3.4.1 RNAseq

To conduct RNA sequencing, cDNA libraries were prepared from total RNA cultures in the logarithmic phase for both NiS samples and the positive control. Next generation sequencing Illumina technology was employed to perform RNAseq analysis. Library preparation kit Illumina Stranded total RNA prep with ribo-zero plus (catalog 20040525) was used and run using a NextSeq 1000/2000 P2 Reagents (300 Cycles) v3 cartridge (catalog 20046813), generating paired-end reads with a read length of 100 bp.

4.3.4.2 Bioinformatics Analysis

The quality of the sample reads was assessed using FastQC (Andrew S *et al.*, 2010). Raw data underwent processing with Trimmomatic software, which removes adapter regions, eliminats low-quality bases, and discards reads smaller than 60 bp (Anthony M *et al.*, 2014). The resulting high-quality trimmed reads were then aligned to the reference genome of *A. vinosum* (Genbank: CP001896.1) using Bowtie2 software, enabling the generation of indexed reads (Langmead *et al.*, 2012). RSEM software was employed for transcript quantification, utilizing the paired-end indexed data from both the positive control and NiS samples (Li B *et al.*, 2011). Data normalization and statistical analysis to identify differentially expressed transcripts were performed using the DESeq2 package within R (Love M *et al.*, 2014). Genes were considered significantly expressed if they had a log2FC change great than 2 or less than -2 with an adjusted p-value below 0.05. Please note that the log_2FC values provided indicate the fold change in gene expression relative to control conditions, with negative values representing downregulation.

In the analysis of *A. vinosum* transcriptome, STRINGdb was used to construct interactive protein maps to enable visualization of the relationships among the proteins. STRINGdb provides confidence scores for each interaction, contributing to the assessment of their reliability. Leveraging the interactive protein maps and the extensive information available on STRINGdb (Scklarczyk D *et al.*, 2023), I enhanced my analysis by proposing novel connections, evaluating potential interactions, and expanding my comprehension of the biological significance underlying the observed gene expression changes.

The transcriptome was further analyzed based on gene categories associated with sulfur metabolism, redox reactions, CXXCH/LXXC motif-containing genes, photosynthesis, hypothetical proteins, and others, as these categories have the potential to contribute to NiS

utilization. Additionally, genes that did not fit into these predefined categories were also explored to gain insights into the complete metabolic response of the bacteria under NiS conditions.

4.4.5 Dissolved species characterization

Growth of bacteria in the positive controls and NiS samples was monitored indirectly by measuring the concentrations of dissolved nickel, sulfide, and sulfate in the medium solution over time. To minimize sulfide escape, collected samples for sulfide measurements were promptly processed. Each sample (100 μL) was mixed with excess zinc(II) chloride solution (approximately 100-fold molar excess of sulfide) to generate metastable ZnS. The stabilized mixture was subsequently reacted with HACH1 and HACH2 solutions, diluted with 400 μL of MQ water to achieve a ~1:10 dilution, and agitated in a rotisserie shaker for 10 minutes. Sulfide measurements were performed using the HACH sulfide reagent set (HACH method 8131), which reacts with all sulfide present, including the precipitated ZnS, resulting in equimolar methylene blue formation. The concentrations of methylene blue were determined by tracking absorption at 665 nm using a MultiSkan UV-Vis spectrophotometer. For sulfate measurements, aliquots of the samples were collected using a nitrogen-purged syringe, diluted 1:10 with Milli-Q water, and subsequently filtered. Sulfate concentrations were determined using a Dionex ICS-2100 ion chromatography system, and quality control was performed by concurrently running a standard curve prepared with sodium sulfate. Concentrations of major and trace elements in the control and sample solutions were measured using inductively coupled plasma-optical emission spectroscopy (ICP-OES) or inductively coupled plasma-mass spectrometry (ICP-MS), depending on the concentration levels. Aliquots of the medium solution were diluted 100-fold using 2% HNO_3 solution and filtered into 15 ml conical centrifuge tubes (0.2 μm cutoff). Macro- (Ca, K, Mg, Na, P, S) and micro-nutrients (Zn, Ni, Mo, Cu) were analyzed using ICP-OES (iCAP 6500, Thermo Fisher Scientific, Waltham, MA) and ICP-MS (7700 Series, Agilent, Santa Clara, CA). To validate the measurements, blank

and standard reference materials (NIST-SRF 1570a and 1547, Metuchen, NJ) were prepared and analyzed. Standard working curves were generated using spikes at different concentrations, and all tested elements showed a recovery rate above 99%. Nickel (Ni) was quantified using ICP techniques, whereas iron (Fe) was not analyzed in this study. To ensure accuracy, an internal standard (Yttrium, Y) and a continuing calibration verification (CCV) sample were included in the analysis.

4.3.6 Solid-phase characterization

Solid phases in the negative control and NiS nanoparticles were analyzed using transmission electron microscopy (TEM) and X-ray photoelectron spectroscopy (XPS). The solid pellets obtained through centrifugation and supernatant removal were processed with a 0.1% Triton X-100 solution containing 10 μg/mL of lysozyme and 10 μg/mL of proteinase K to remove bacterial cells and biomolecular debris. Sonication of the pellets in the processing solution was performed for 45 minutes at room temperature. Subsequently, the solid particles were separated by centrifuging the digestion mixture at 10,000g for 5 minutes at room temperature, followed by removal of the supernatant. The separated solid particles underwent two washes with 0.01% Triton X. All procedures were conducted within the anaerobic chamber using sealed containers to prevent sample oxidation. For TEM and XPS analyses of the biomass-digested solid particles, specific sample preparation methods were employed. For XPS specimen preparation, the separated particles were dried on a glass slide under anaerobic conditions. Regarding TEM sample preparation, a gold grid with an ultrathin carbon film was utilized. First, 5 μL of anaerobic water was added to the grid, followed by the addition of 10 μL of particle suspension. XPS spectra were collected using a PHI Quantera SXM instrument (ULVAC-PHI, Japan) with a hemispherical energy analyzer and a monochromatic aluminum target. Survey spectra were obtained at 25 W/15 kV with a spot size of 100 μm, a 45° take-off angle, and a 280 eV pass energy. High-resolution

spectrum acquisition employed a 69 eV pass energy with a 0.125 eV scan step. The high-resolution XPS spectra were fitted using Multipak software, with charge correction based on the C 1s species at 284.8 eV. TEM data were gathered using a JEOL JEM 2100 S/TEM at the Nanoscale Characterization and Fabrication Laboratory located in Virginia Polytechnic Institute and State University. The instrument operated at 200 kV, and TEM bright field images were captured using a Gatan Ultrascan 1000XP CCD camera. Selected area electron diffraction patterns were collected utilizing a Gatan Orius 833 slow scan CCD camera. Furthermore, scanning TEM (STEM) mode was used to obtain Energy Dispersive X-ray Spectroscopy (EDS) data, employing a JEOL genuine 60 mm2 Silicon Drift Detector.

4.4 Results

4.4.1 Growth profiles, solid-phase characterization, and analyte analysis

In positive controls, it takes ~400 h for the cell culture to reach the end of logarithmic phase, yielding a cell density of ~ 9.5×10^6 cells/mL, and the stable phase spans from 400 h to 1200 h with consistent pigmentation throughout growth cycle. By comparison, *A. vinosum* also displayed growth in the negative control taking about 100h to reach logarithmic, at a cell density of 1.92×10^6 cells/ml, once in stationary it lasted to about 600 h before cell density started to decrease. In the case of the NiS cell culture, the culture took ~700 h before reaching the top of the log-phase at a cell density of 5.2×10^6 cells/ml. Once the top of the log phase was reached, the cell density started to consistently decrease until ~1200 h where the culture was not tracked anymore. One can see that the NiS system grew to ~1/2 of the cell density achieved by the positive control and it grew to a cell density 2.7 times greater than that of the negative control culture (Figure 4-1).

In the case of sulfide concentration, NiS and negative control remained at baseline with no detection of it being release in solution, while positive control depleted from 2.4 mM sulfide concentrations in 150hr. On the other hand, sulfate concentration measured in millimolar remained

constant for NiS and NiS control throughout the growth cycle of the bacteria. The positive control on the other hand, shows sulfate starting to increase at 100hr, while taking ~400hr for it to reach maximum sulfate from positive control at 6 mM change.

Nickel concentrations in the NiS cell culture showed a very irregular patter below 160 h, Na-ICP plots were used to assess a dilution issue but none was found confirming the nickel ion flux. Concentration changes fluctuated twice between 0.5-2.5ppm, after which nickel gradually stabilized to 0.5ppm. The NiS control which did not contain *A. vinosum*, but just the culture media along with NiS substrate showed a very high initial nickel concentration, which declined gradually to levels comparable to NiS-free media control. The high initial nickel concentration was most likely a carryover of that from the stock suspension containing the synthesized NiS nanoparticles. The gradual decline of the nickel concentration in the NiS control showed that the medium components behaved as sinks for the soluble nickel (Figure 4-2). Concentrations of other major solution components were reported in the supplemental information.

4.4.2 Solid-phase characterization

4.4.2.1 HRTEM

HRTEM analysis revealed significant differences between the NiS biotic and NiS control samples, elucidating variations in particle morphology, aggregation, and crystallinity. In the NiS control sample, irregularly shaped particles were observed, forming amorphous plate-like clusters with well-defined edges and varying densities throughout the field. These particles were smaller than 100nm in size, and no distinct electron patterns were identified, indicating poor crystallinity. However, faint ring d-spacing calculations suggested the possible presence of millerite (Appendix Table 0-10). In contrast, the biotic NiS sample exhibited clear rectangular structures with sharp edges, partially concealed by amorphous clusters. The biotic sample displayed a higher degree of crystallinity compared to the control, with several regions showing well-defined electron

diffraction patterns. While these patterns revealed only a few spots for analysis, some of them indicated d-spacing values associated with millerite and vaesite (Figure 4-3 and Appendix Table 0-10).

4.4.2.2 XPS

The XPS analysis of the NiS biotic sample provided valuable insights into the sulfur region, revealing the presence of distinct species as indicated by the presence of multiple peaks. The experimental curve of sulfide was meticulously fitted with eight peaks, unveiling four sets of peaks characterized by different binding energies. The first set, corresponding to peaks at 159.6 eV (2p 3/2) and 160.86 eV (2p 1/2), potentially arises from surface effects. Moving on, the second set associated with monosulfide was observed at 160.84 eV (2p 3/2) and 162 eV (2p 1/2). The third set of peaks, attributed to disulfide, was found at 161.9 eV (2p 3/2) and 163.1 eV (2p 1/2). Finally, the fourth set representing polysulfide displayed peaks at 163.6 eV (2p 3/2) and 164.8 eV (2p 1/2). In the nickel region of the spectrum, an appropriate fitting of the experimental spectra necessitated five peaks. The first peak observed at 851.1 eV could not be unambiguously identified and might potentially arise from surface effects. The second peak at 852.1 eV falls within the elemental nickel range. Moving forward, the third peak at 853.4 eV is associated with Ni(II)S, while the fourth peak at 855.5 eV corresponds to Ni(II)O. Finally, the fifth peak at 859.6 eV represents a satellite peak.

The XPS of the abiotic sample sulfur region curve was fitted instead with six peaks relating to only three different sulfur species. The first set, associated with monosulfide was observed at 160.99 eV (2p 3/2) and 162.15 eV (2p 1/2). The second set of peaks, attributed to disulfide, was found at 162.17 eV (2p 3/2) and 163.14 eV (2p 1/2). Finally, the third set representing polysulfide displayed peaks at 163.33 eV (2p 3/2) and 164.32 eV (2p 1/2). In the case of the Nickel region for abiotic FeS, the first peak observed at 852.45 eV was found to associate with Ni(II)S species. The

second peak at 854.33 eV falls was found for $Ni(II)(OH)_2$ species. To conclude, the third peak at 858.98 eV associated with satellite peak rising from surface effects.

4.4.3 Transcriptomic sequencing and differential gene expression analysis

In the NiS culture compared to the positive control, we observed significant differences in gene expression, with 91 genes upregulated and 170 genes downregulated. On the other hand, the negative control showed 36 upregulated and 119 downregulated significantly differentially expressed genes compared to the positive control (Figure 4-5 and Table 4-5). Full transcriptome raw files can be found at https://datarepo.bioinformatics.utep.edu/getdata?acc=G9T1VZNRYJPIC0C.

4.4.3.1 CXXCH/LXXC motif containing genes

By analyzing proteins with heme-binding and lipid-binding motifs, we aim to understand the pivotal role of cytochromes in mediating electron transfer between cells and solid-phase NiS. This bridges intracellular energy dynamics with the utilization of NiS, underscoring the potential of interfacial interactions

Our analysis revealed differential expression in several genes. Alvin_1093, encoding a flavocytochrome-containing subunit, showed an upregulation of 32-fold (positive control) and 25-fold (negative control). Alvin_1095, encoding a tetra-heme c-type cytochrome, was upregulated by 32-fold and 38-fold in the positive and negative controls, respectively. Alvin_1402, encoding the Fe-S cluster assembly protein NifU, exhibited a 4-fold upregulation, with a 2-fold increase in the negative control. The Radical SAM domain protein gene, Alvin_3135, was upregulated 6-fold and 2-fold in positive and negative controls, respectively.

Alvin_2447, linked to sulfate assimilation, displayed an 8-fold and 4-fold upregulation in positive and negative controls. Genes Alvin_0903 and Alvin_1402, related to nitrogen fixation, both showed a 2-fold upregulation. Hydrogenase-related genes, Alvin_2306 to Alvin_2309,

exhibited upregulations ranging from 5-fold to 9-fold, with corresponding values in the negative control. Lastly, Alvin_2451, involved in glyoxylate and dicarboxylate metabolism, showed an 8-fold upregulation in both controls.

We observed an upregulation of various cytochromes, hydrogenases, and nitrogen fixation-related proteins that contain redox-active heme binding motifs.

4.4.3.2 Genes associated with Anoxygenic photosynthesis

In our transcriptome analysis of the FeS sample, we focused on genes tied to photosynthesis, especially those in the puf, puc, carotenoid, and RubisCo categories. These gene groups are associated with the LH1 and LH2 complexes, photosynthetic pigments, and carbon dioxide fixation — all essential components of anoxygenic photosynthesis (refer to Tables 4-3 and 0-11)

For the *puc* genes**,** most exhibited expression values ranging from 0.0012-fold to 0.18-fold, with corresponding NEG values between 0.023-fold and 0.54-fold. Notably, Alvin_2580 displayed an expression close to 0.99-fold and 0.87-fold in the positive and negative controls, respectively.

The *puf* genes showed varied expression. Genes from Alvin_2547 to Alvin_2550 had expression values between 0.24-fold and 0.54-fold, with corresponding NEG values ranging from 0.35-fold to 0.51-fold. Alvin_2634 exhibited an expression of 1.02-fold and 0.90-fold in the positive and negative controls, respectively.

Regarding the carotenoid genes, a group including Alvin_1182-Alvin_1183, Alvin_2561-Alvin_2563, and Alvin_2638-Alvin_2640 showed expression values between 0.46-fold and 0.86-fold, with NEG values from 0.5454-fold to 0.89-fold. Alvin_2556 stood out with a 2.7578-fold upregulation in the positive control and 1.6598-fold in the negative control. Another set, comprising Alvin_2641 to Alvin_2643, Alvin_2564-Alvin_2565, and Alvin_2566 - Alvin_2568,

displayed expression values between 1-fold and 1.5-fold, with corresponding NEG values from 1-fold to 2.28-fold.

Lastly, for the RubisCo genes**,** the large subunit genes showed expression values between 0.1-fold and 0.13-fold, with NEG values from 0.09-fold to 0.21-fold. The small subunit genes exhibited a broader range, with expression values from 0.53-fold to 1.48-fold and corresponding NEG values between 1.34-fold and 1.13-fold.

In summary, most *puc* genes exhibited significant downregulation, with the notable exception of Alvin_2580, which had an expression comparable to the positive control. In contrast, *puf* genes displayed milder downregulation. While some carotenoid genes showed slight downregulation, others had expressions akin to the positive control. Notably, Alvin_2556 demonstrated upregulation. *RubisCo* genes, which are associated with carbon fixation, revealed downregulation in the large subunit, whereas the small subunit, represented by Alvin_2570, maintained an expression comparable to the positive control.

Several genes did not meet the significance threshold with Padj *values greater than 0.05. These include Alvin_2552 (*Padj *= 0.27), Alvin_2553 (*Padj *= 0.23), Alvin_2576 (*Padj *= 0.15), Alvin_2577 (*Padj *= 0.28), Alvin_2578 (*Padj *= 0.38), Alvin_2579 (*Padj *= 0.30), Alvin_2580 (*Padj *= 0.98), Alvin_2634 (*Padj *= 0.98), Alvin_2635 (*Padj *= 0.16), Alvin_2636 (*Padj *= 0.19), Alvin_2637 (*Padj *= 0.05), Alvin_2759 (*Padj *= 0.37), and Alvin_2760 (*Padj *= 0.46). The elevated* Padj *values for these genes suggest that their expression changes might not be statistically significant in the context of our analysis.*

4.5.3.3 dsr and sox sulfur oxidation genes

We analyzed the differential expression of genes involved in sulfur oxidation in *A. vinosum* to asses if bacteria were activating sulfur oxidation pathways, as measured by expression values compared against the positive control. The results are detailed in Table 4-2 and Table 0-6.

In the *dsr* genes, Alvin_1251 to Alvin_1262 showed expressions of 0.01 to 0.04 with NEG values of 0.01-fold to 0.05-fold. Meanwhile, Alvin_1263 to Alvin_1265 had expressions of 0.29 to 0.44 and NEG values of 0.35-fold to 0.54-fold.

For the *sox* genes, Alvin_2111 to Alvin_2112 had expressions between 0.83 and 0.87 with NEG values of 1.20-fold to 1.41-fold. Alvin_2167 (SoxB) showed 1.99-fold/NEG(1.01-fold). Alvin_2168 to Alvin_2170 ranged from 0.67 to 0.87/NEG(0.92-fold to 1.11-fold), and Alvin_2171 (SoxL) was at 0.25-fold/NEG(0.98-fold).

We observed that *dsr* genes were predominantly downregulated, with the exception of Alvin_1263 and Alvin_1265, which were only moderately downregulated. On the other hand, most *Sox* genes exhibited expression levels comparable to the positive control. However, Alvin_2171 showed mild downregulation, while Alvin_2167 displayed a slight upregulation.

4.4.3.4 ATP activated proteins

In the NiS transcriptome analysis, we observed differential expression of several ATP-related genes, which are presented herein. In our findings, K+-transporting ATPases showed significant upregulation. Alvin_1159, encoding the B subunit, had a 4.3-fold increase (NEG 2-fold). Alvin_1157, encoding the F subunit, exhibited a 5.4-fold increase (NEG 1-fold). Alvin_1158, responsible for active potassium ion transport as the A subunit, surged by 6-fold (NEG 2-fold). Additionally, the AAA ATPase central domain protein, Alvin_1450, was upregulated by 4.2-fold (NEG 0.7-fold). We observed upregulation of K^+ transporting ATPases and other annotated gene as AAA ATPase central domain. The observed differential expression patterns of ATP-related genes in the NiS sample provide insights into their potential roles in ATP-related activities and their response to environmental conditions.

4.4.3.5 Transporters

In the transcriptomic study, we identified a marked increase in the expression of several transporters. To delve deeper into the causes of this upregulation, we undertook a comprehensive analysis, the findings of which are detailed in this section.

In our findings, several transporters displayed significant upregulation. The Cation Diffusion Facilitator Family Transporter, Alvin_1529, surged by 8.6-fold (NEG 1-fold). The Efflux Transporter, RND Family, MFP Subunit, Alvin_0014, increased by 8.1-fold (NEG 4-fold). Alvin_0015, from the Heavy Metal Efflux Pump, CzcA Family, showed a 7.99-fold upregulation (NEG 2-fold). Lastly, the Potassium-Transporting ATPase A Subunit, Alvin_1158, exhibited around a 6-fold increase (NEG 2-fold).

Many transporter gene groups showed increased expression, predominantly linked to metal or ion efflux. Among these are the Cation Diffusion Facilitator Family Transporters, known for their role in cation efflux. Similarly, the Efflux Transporter of the RND Family's MFP Subunit has a role in cation efflux. Additionally, the CzcA Family's Heavy Metal Efflux Pump is associated with metal efflux.

Other sulfur related genes that stood out are highlighted. In our findings, genes related to sulfate transport and metabolism displayed significant upregulation. The Sulfate ABC Transporter's inner membrane subunits, CysT (Alvin_2443) and CysW (Alvin_2442), exhibited upregulation of 4.47-fold (NEG 2-fold) and approximately 4.23-fold (NEG 2-fold), respectively. The gene encoding the Sulfate Adenylyltransferase small subunit, Alvin_2448, showed around a 4.1-fold increase (NEG 3-fold). Additionally, the Sulfate Transporter, Alvin_2752, also demonstrated a similar upregulation of approximately 4.1-fold (NEG 2-fold).

4.4.3.6 Hypothetical genes

By assessing the variations in expression of hypothetical protein genes in the NiS sample against the positive control, we can potentially decipher the roles of proteins that currently lack annotations. This analysis not only deepens our understanding but also pinpoints these proteins as promising candidates for in-depth future studies.

In our analysis, several genes with unknown functions exhibited significant upregulation (Table *0-3* and Table *4-1*. Specifically, Alvin_1191 showed an 11.2-fold increase (NEG 2-fold), while Alvin_1447 was upregulated by a remarkable 42.7-fold (NEG 1-fold). Alvin_0034 displayed a substantial 52-fold upregulation (NEG 2-fold), and Alvin_1448 had a 22-fold increase in expression (NEG 1-fold).

4.4.3.7 Other

Other genes with significant upregulation but no apparent contribution to NiS utilization by *A. vinosum* are shown here. In our transcriptomic analysis, several genes displayed significant upregulation. The gene Alvin_0772, encoding the integral membrane protein MviN, exhibited a 5.17-fold increase in expression compared to the positive control, with a NEG value of 1-fold. The ankyrin protein-encoding gene, Alvin_1094, showed a pronounced upregulation of approximately 28-fold, with a NEG value of 35-fold. Additionally, Alvin_1379, which encodes the 2-isopropylmalate synthase involved in leucine biosynthesis, demonstrated a substantial upregulation of about 15-fold, with a NEG value of 2-fold.

4.5 Discussion

4.5.1 Growth profiles

The lack of apparent change in the concentration of sulfate in the NiS cell culture solution over time would suggest that the cells could not oxidize sulfur obtained from the NiS system completely to sulfate. Nonetheless, NiS culture showed significantly higher growth than the

negative control (as shown by the OD data), confirming the utilization of NiS nanoparticles by cells. Specifically, differences in the cell density are significant between the NiS cell culture and the negative control, with NiS-supported cells growing to 1/2 of the cell density of the positive control and ~2-3 times higher than that in the negative control. Nonetheless, IC does not show change in sulfate concentration increase for the biotic sample potentially signaling incomplete sulfur oxidation, although no evidence of elemental sulfur was found either.

In the context of sulfide, concentrations remained at baseline levels that were largely below the detection limit of the method, whereas the positive control exhibited a depletion of sulfide within approximately 150 hours. This observation aligns with the expectation that any released sulfide from NiS would be rapidly absorbed by cells, as evidenced by the swift exhaustion of available sulfide in the depletion curve. It is crucial to emphasize that the positive control was prepared with a 6.1 mM concentration of Na_2S, contrasting with the 2.4 mM level shown in the plot, possibly indicating a loss of sulfide through aqueous speciation during sampling events. On the other hand, the ICP-MS data displays fluctuating nickel concentrations during the growth of NiS cell culture, indicating of convoluted processes concerning Ni sequestration and release. Specifically, the concentrations of nickel fluctuated significantly from 0.5-3ppm implying nickel ion flux between the cell and the solution. Eventually, nickel stabilized at similar levels to the metal sulfide-free medium control. Based on these data, nickel was not actively released from the substrate in the later stages of the cell growth into solution, which is in line with sulfate concentration analysis and strongly suggests that the primary growth of *A. vinosum* cells in the NiS sample was not due to NiS dissolution effect. The fact that the NiS cultures are supporting such a high cell density compared to negative control implies that the NiS substrate was used as electron donors for energy metabolism.

HR-TEM showed the presence of vaesite (NiS_2) and millerite (NiS) in biotic FeS. The biotic samples compared to NiS control revealed higher crystallinity as seen by greater number of fields of views with discrete electron diffraction patterns. The presence of vaesite could be the result of bacterial mediated oxidation of monosulfide. Related to this, is the observed nickel ion fluctuation before 200hrs in biotic FeS, seems to suggest a bidirectional flux of nickel ions between cell and NiS, which eventually reached equilibrium after 600hr potentially underling an exchange of ions between the cell and NiS surface/bulk. It worth noting that XPS did not show any nickel (III) peaks largely eliminating metal oxidation as a pathway *A. vinsoum* cells may use for energy metabolism. However, the existence of a cryptic nickel cycle driving sulfur oxidation cannot be ruled out although we have not confirmed the sulfur oxidation product. There is evidence of a peak at ~ 852 eV which falls, which has been previously interpreted as the elemental nickel range. This is interesting as it might point to another pathway for nickel sequestration in the biotic system as this peak was not observed in the control, but the same conumdrum exists in term of electron balance and flows. In the XPS analyses, unknown peaks are present in the nickel and sulfur regions in both biotic and control samples. For example, the peak at ~ 854 eV could be interpreted as adventious carbon from extracellular matrix material covering the surface of NiS instead of nickel species (Miller *et al.*, 2002). Alternatively, this unknown peak could also represent surface modification of NiS by ions like sodium, potassium of other transition metals filling up vacancies. Its important to highlight that XPS is an analysis of the outermost layers of materials, while HRTEM relies on scattered fields that have begun displaying lattice fringes for mineral identification, which means limitations exist in both methods especially for materials of amorphous nature.

Since the negative control showed significant growth potential on a system lacking sulfur and most likely polymeric carbon in the form of yeast extract. If electrons generated from this

unidentified pathway were expelled from cell it could lead to nickel reduction keeping nickel ion levels constant in solution and potentially releasing some sulfide for its oxidation. This hypothesis would result in *A. vinsoum* not being able to contribute in natural systems in the release of nickel into the water column, at least not in considerable amounts, but still supporting its growth with NiS minerals and accelerating surface modfications on them.

4.5.2 Solid-phase potential evidence of NiS reduction and sulfur oxidation

The TEM analysis showed that exposure of the NiS substrate nanoparticles to *A. vinosum* increased crystallinity in the material as observed in other biogenic MS systems (Mansor M *et al.*, 2020). Bacteria may have this effect by acting as nucleation sites, through extracellular matrix formation or microenvironmental conditions generating ideal microniche pH or redox conditions to accelerate seed formation and crystallization. The NiS control did not show clear electron diffraction patterns but the diffused ring patterns indicated the presence of millerite (NiS). Upon bacterial exposure, some electron diffraction patterns showed the appearance of not only millerite but also vaesite (NiS_2). Formation of vaesite would require sulfide oxidation in a culture system with no oxygen or other strong oxidizing agents in the media. There is still a possibility that sulfate in medium could in theory provide a chemical pathway for oxidation of free sulfide in NiS cultures, but is also true that ultimately this would reflect an electron transfer pathway in NiS surface material to the bacterial cell, through the use of sulfide or elemental sulfur.

While electron diffraction patterns can be interpreted in various ways, XPS analyses offer additional information and constraints regarding the valence states of iron and sulfur, as well as insights into the existing chemical bonds (Figure 4-4). The XPS analyses provided valuable insights into the valence states of iron and sulfur in the solid substrate.

When analyzing the nickel region for both samples it stands out that both contain the same three peaks at 852, 854 and 859eV showing no major changes. Nonetheless, the biotic sample showed

a peak at elemental nickel range, in gray, which does not appear in the control (Figure 4-4). This is interesting, as in the culture there are no strong reducing agents in the preparation of the media. There is an expectation for the formation of extracellular matrix material for purple sulfur bacteria, which could give rise to new peaks from surface interaction with carbon. Nonetheless, if this were to be in fact elemental nickel, it would mean that it had to form due to the interaction of NiS with *A. vinosum*. This would require electrons to flow into Ni(II), which could happen only if an electron exchange system was established between the substrate material and the cell. There are caveats in this explanation, however: the bacterial cells were probably in desperate demand for electrons to enable autotrophy, and how can it leak out electrons to reduce Ni(II)? If the bacteria grow autotrophically, one possible reason was that the electron transfer from the NiS substrate to the bacterial cells was not inefficient. The other peak at 852.1 eV is likely a peak rising from the surface of NiS interaction with adventitious carbon from extracellular matrix material, or there is a possibility as well of it being a contamination peak from cobalt which would have a peak 2p 3/2 peak close.

For the sulfur region, there is considerable change in the surface of the biotic NiS sample. Most apparent is the marked increase in polysulfides which is an intermediate in the oxidation of sulfur (Findlay *et al.*, 2016). Thus, this could be used as an indicator that bacteria are oxidizing the sulfide in the NiS substrate, as in the only source of sulfur in the culture. Another interesting observation is the how the disulfide peaks increase in abundance. This is counterintuitive as disulfide would be expected to decrea se, the same way that monosulfide abundance is shown to decrease. Still, this is not the case. This conversion would require the oxidation of sulfur and potentially the formation of disulfide mineral phases. The peaks at 159/160 eV are of unknown origin but fall outside the range for elemental sulfur or any other common sulfur species. Thus,

these peaks most likely rise from surface defects like a contamination peak or adventitious carbon contamination.

In summary, the XPS of the biotic samples showed evidence that the sulfide in NiS was utilized for metabolic purposes by *A. vinosum* as shown by increase in polysulfide peak abundance. Furthermore, elemental Nickel peak points to potential redox reactions facilitated by *A. vinosum* with the substrate material.

4.5.3 Transcriptomic sequencing and differential gene expression analysis

4.5.3.1 Redox active proteins

The protein adenylysulfate reductase (Alvin_2447) was upregulated 8-fold/ NEG(4-fold). This protein is involved in sulfate assimilation pathway, thus intaking of sulfate into the cell for cystine synthesis and other organosulfur compounds (Kopriva S *et al.*, 2003). It is redox active catalyzing the reduction of APS protein to sulfite. Two nitrogen metabolism gene, Alvin_0903 and Alvin_1402, were upregulated by ~ 4-5-fold/ NEG(2-fold) each in their expressions. Alvin_1402 encodes for a Nif family protein, which is involved in nitrogen fixation in other microorganisms thus facilitating conversion of nitrogen gas to reduced forms like ammonia (Poza-Carrión *et al.*, 2014). Nonetheless, nitrogen fixation is an energy expensive process and therefore bacterial cultures would not prefer them as the primary way for nitrogen nutrient requisition unless of no other choice. There was plenty of ammonium in the culture medium and thus, it is unclear as to why the bacterial cells activated these energy expensive pathways. Possibilities of using this pathway for other metabolisms exist.

In the transcriptome of NiS cell cultures, four hydrogenase-related genes were upregulated, namely Alvin_2306, Alvin_2307, Alvin_2308, and Alvin_2309, showing significant fold increases of 5-fold / NEG(9-fold), 6-fold / NEG(11-fold), 9-fold / NEG(7-fold), and 9-fold / NEG(9-fold), respectively. These genes encode proteins involved in reversible redox reactions

using hydrogen gas or H^+ ions. Specifically, they include a hydrogenase maturation protease (Alvin_1306), Ni/Fe hydrogenase small subunit HydA (Alvin_2309), Ni-dependent hydrogenase (Alvin_2308), and Ni/Fe hydrogenase cytochrome b subunit (Alvin_2307). These Ni/Fe hydrogenase genes are co-expressed and gene-fused, as indicated by STRINGdb. [NiFe]-hydrogenases, to which these genes belong, are believed to have played a crucial role in energy metabolism of the Last Universal Common Ancestor (LUCA). Notably, the proteins related to the respiratory complex I/NADH dehydrogenase are the closest evolutionary relatives of [NiFe]-hydrogenases. This suggests a connection between ion pumping membrane [NiFe]-hydrogenases and the ancestors of modern respiratory complex I, which are involved in the coupling of NADH oxidation, ubiquinone reduction, and proton pumping.

The protein molybdopterin oxidoreductase with Fe4S4 cluster (Alvin_2451/8-fold/ NEG(8-fold)) is involved in various energy production pathways. One such pathway is glyoxylate and dicarboxylate metabolism, where substrates undergo the glyoxylate cycle using acetyl-coA to initiate a series of reactions that ultimately result in the production of succinate and malate, along with two molecules of ATP. This pathway provides the cell with energy not only in the form of ATP but also through succinate and malate, which can be utilized by *A. vinosum* in the citric acid cycle to extract additional energy. Glyoxylate and dicarboxylate molecules can be derived from the breakdown of lipids and other organic compounds, making them integral to the cell's overall metabolism.

4.5.3.2 CXXCH/LXXC and signal peptide motif containing genes

In this analysis, heme binding proteins that were upregulated and downregulated were investigated, as they have been implicated in facilitating electron transport in bacterial solid respiration according to existing literature. Considering the insoluble nature of the MS substrates used in this experiment, it is reasonable to explore membrane-bound molecules that are capable of

electron transfer. The CXXCH motif, which represents a conserved sequence of amino acids, is known to be associated with heme binding sites. Heme proteins, such as cytochromes, exhibit reversible redox reactions, making them suitable candidates for electron transfer reactions, as previously observed in the literature (Costa *et al.*, 2018). On the other hand, LXXC motifs are conserved lipid binding sites that can be used, along with the presence of a signal peptide, to predict which proteins are located on the cell surface and likely to interact with extracellular MS substrates. This approach is valuable for identifying proteins with significant expression values with redox capabilities that are either membrane bound or exported, even if their functions are currently unknown. One of the most relevant heme-containing molecules that could be involved in electron transfer are cytochrome molecules due to their reversible redox capabilities. Specifically, Cytochrome molecules along with flavins have been found to be involved in EET and reductive dissolution by different groups (You L *et al.*, 2018).

Several *CXXCH/LXXC* motif containing genes exhibited significant upregulation, providing insights into their potential roles in NiS metabolism. Alvin_1093 showed a remarkable 32-fold NEG(25-fold) upregulation compared to the positive control. This gene encodes a flavocytochrome-containing subunit of the enzyme sulfide dehydrogenase, involved in the oxidation of sulfide to elemental sulfur. Flavocytochromes are versatile molecules capable of reversible redox reactions through heme moieties and flavin groups, facilitating electron transfer in both directions. Furthermore, the amino acid sequence analysis revealed the presence of a signal peptide, suggesting its involvement in electron transfer reactions and potential localization on the cell surface or extracellular milieu. Interestingly, Alvin_1093 was also upregulated 25-fold in the negative control.

Alvin_1095 displayed a 32-fold/ NEG(38-fold). upregulation against the positive control. This gene encodes a putative tetra-heme c-type cytochrome a lipid binding motif, suggesting

potential membrane association. Annotated as NapC/NirT cytochrome c domain protein, it may be involved in nitrite oxidation, (Reyes F *et al.*, 1996), still media only contain ammonia as a nitrogen source prohibiting this nitrite oxidation in culture and potentially revealing its involvement in a new electron transport pathway. Interestingly, according to STRINGdb, it is associated with ccmA, which has been linked to conductive nanowires (Costa *et al.*, 2018) (Alvin_1095 in STRINGdb).

Another gene of interest Alvin_1402, which demonstrated a 4-fold/ NEG(2-fold). upregulation. This gene encodes a protein annotated as the Fe-S cluster assembly protein Nifu. In *Azotobacter vinelandii,* this protein is characterized as a subunit of nitrogenase involved in nitrogen fixation and Fe-S cluster formation. However, its function in *A. vinosum* remains to be determined. Notably, Alvin_1402 contains both CXXCH and LXXC heme and lipid binding motifs.

Furthermore, Alvin_3135 exhibited a 6-fold/ NEG(2-fold). upregulation compared to the positive control. Annotated as a Radical SAM protein, this gene encodes a protein superfamily known for containing S-adenosylmethionine (SAM) groups, which undergo reductive cleavage by a Fe-S center. SAM proteins have been associated with various reactions, including isomerization, sulfur insertion, anaerobic oxidation, and protein radical formation in other organisms. Interestingly, Alvin_3135 also possesses an LXXC lipid binding motif, suggesting a potential association with the cell membrane.

4.5.3.3 Photosynthetic genes

The expression of photosynthetic genes was found to be significantly downregulated in comparison to both the negative and positive controls. Statistically validated genes exhibited a range of log2FC values from -10.6 to -2.8, indicating a notable decrease in their expression. In contrast, the negative control showed expression levels ranging from a log2FC of -5.5 to -2.6, with

fewer statistically validated genes. These findings suggest that the negative control relies more on photosynthetic proteins than the NiS culture. Notably, the expression of carotenoid-related genes remained largely unchanged when compared to the positive control. This includes genes such as Alvin_1182-1183, 2556, 2561-2563, 2638-2643, and 2564-2570.

4.5.3.4 dsr and sox sulfur oxidation genes

The expression of sulfur oxidation *dsr* genes was found to be downregulated, with a more significant suppression observed in the negative control. This observation aligns with expectations, as the negative control grows in sulfur-free media, lacking the ability for sulfur oxidation. In contrast, the expression of *sox* genes remained relatively unchanged or slightly downregulated compared to the positive control, and their expression rates in the negative control were comparable as well. These findings suggest that *sox* activity may play a more prominent role in supporting sulfur oxidation compared to dsr. Given that *sox* genes have been associated with the oxidation of polysulfides to sulfate, this may provide an explanation for the increased polysulfide fraction observed in the NiS XPS sulfur spectra, which showed 10.8% compared to the 1.8% in the control. The expression values strongly support the notion that the cultured bacteria are utilizing sulfide from the NiS solid as a sulfur source.

4.5.3.5 ATP activated proteins

In the NiS experimental sample, several ATP requiring protein related genes were found to be differentially expressed compared to the control. K^+-transporting ATPase protein subunits Alvin_1159 (4.3-fold/ NEG(2-fold)), B subunit, Alvin_1158 (6-fold/ NEG(2-fold)), A subunit and Alvin_1157 (5.4-fold/ NEG(1-fold)), F subunit form part of K+-transporting ATPase protein involved in the transport of potassium across the membrane. These proteins have been found to be activated through signal transduction pathways activated by changes in turgor pressure (Epstein *et al.*, 1990). They have been observed to overexpress under low K^+ concentrations in R. sphaeroides

(Abee, T, 1992). This plasma membrane protein uses to transport K^+ into the cytoplasm using ATP as the driving force of regulated transport. Furthermore, in a study by Arguello, it was found that P1b-type ATPases that expel transition metals from cells have structural similarities to K^+ ATPase (Arguello *et al.*, 2011). Since the culture media is not deficient in potassium (4.6mM), it is possible that the expression of this gene was incited by differences in osmolarity across the membrane and could have led to Nickel transport across the cell membrane. This could be a way for free ions in extracellular fluid from NiS to be let into the cell, or a way for the cell to expel high intracellular Nickel concentration. It's important to know that this physiological protein could influence membrane polarization, which could hide an alternative mechanism to allow other molecules to transit across the membrane.

The genes corresponding to a AAA ATPase central domain protein (Alvin_1450) and a AAA_5 family protein (Alvin_3277) were upregulated by 4.2 / NEG(0.7-fold) and 5.5 fold / NEG(3-fold), respectively, compared to positive control. These proteins are usually involved in cell cycle regulation, DNA unwinding and protein degradation (Miller, JM, 2016). These are ATP dependent proteins that perform mechanical work in the cell. There is no evident reason for the activation of this protein upon exposure to NiS, although its upregulation is only moderate. The culture did show consistent growth for days reaching a maximum density about ~1/3 of what is achieved with positive control, since these genes are more activated when compared to the control it wouldn't make sense for this activation to be related to cell cycle regulation. Thus, it's possible that the activation is a response to stress inside of the cell in aiding in molecular recycling inside of the cell. Still, there is not enough information to comfortably make this claim.

4.5.3.6 Transporters

In the NiS experimental sample, several transporter genes displayed significant differential expression compared to the control. The cation diffusion facilitator family transporter

(Alvin_1529) exhibited a high level of expression (~ 8.7-fold / NEG(1-fold)), suggesting its involvement in facilitating the diffusion of cations across the cell membrane for NiS exposed *A. vinosum* (Xiong A *et al.*, 1998). This protein hasn't been studied sufficiently but through homology it has been characterized as a transporter protein. Through gene interaction map using STRINGdb, it was found a co-expression and gene neighborhood, association with gene Alvin_1816 was found. This gene encodes for a heavy metal translocating P-type ATPase protein family, which are involved in different divalent transition metal transport and efflux across membrane (Axelsen *et al.*, 1998). It's important to highlight that this association does not prove that Alvin_1529 is involved in Nickel transmembrane transport.

Similarly, a set of genes Alvin_0014 (8.2-fold / NEG(4-fold)) and Alvin_0015 (8-fold / NEG(2-fold)) coding for heavy metal efflux protein subunits were found in the transcriptome of NiS. Alvin_0014 gene codes for a MFP (membrane fusion protein) subunit belonging to the RND family (Resistance, Nodulation, and Cell division). Alvin_0015 gene codes for the heavy metal efflux pump, According to Interpro protein family descriptions, this protein is part of the Cus protein family which are involved in the efflux of heavy metal ions and promoting metal resistance in the cell (Outten *et al.*, 2001 and Kunito T *et al.*, 1996). Both genes are annotated in Kegg, Strindb, Interpro and Uniprot databases as being efflux proteins related to metal resistance.

In part, this is certainly a toxicity adaptation by the cell. Still, the presence of these efflux genes strongly seems to confirm that Nickel is accumulating in the cell. At the same time, it reveals a flux of ions from the NiS material to the cell and vice versa. Thus, this strongly suggests that sulfide can also dissociate, and therefore, the culture is at least partially sustained by sulfide as electron donor. Still, this does not contribute in elucidated the mechanisms through which NiS dissociates and enters the cell. These findings highlight the altered expression patterns of transporter genes and provide insights into their potential roles in the NiS assimilation.

4.5.3.7 Sulfur assimilation

The upregulation of these four genes reveal the need of sulfate by *A. vinosum* from the medium and it also reveals the oxidation of sulfide as the culture did not contain sulfate salts and NiS is the only other source of sulfur in these cultures. *A. vionsum* is likely undergoing assimilatory sulfate reduction to make up for sulfate lack in the media. This would result in the assimilation of sulfur into sulfur containing aminos acids like cystine. Furthermore, the upregulation of these gene would result in a reduction in the amount of sulfate in the media leading to an inaccurate assessment of the rate of oxidation of NiS through the ion chromatography measurements.

4.5.3.8 Pili

In the transcriptome analysis, it was identified that gene Alvin_3265, which encodes a protein containing the PilT protein domain. The PilT protein domain is commonly associated with the type IV pilus (T4P) system and had a moderately upregulated (5.25-fold / NEG(1-fold)). This is interesting as pili have been deemed to be conductive in S. odeidensis and deemed as nanowires (Gorby Y *et al.*, 2006). Thus, the upregulation of a pilli gene could reflect the relevance of motility of bacteria when cultured with NiS. This could be an indicator that there is a need for direct contact with bacteria and NiS surface for electron shuttling from material to the cell to occur. When accounting for the many cytochrome containing proteins and redox proteins upregulated in the transcriptome this becomes an appealing explanation. Nonetheless, this could also be interpreted as the bacteria attempting to relocate to other places in the culture bottle. As it was seen in the transporter genes, the cells can be seen to be experiencing stress and are dealing with it through efflux pumps. There is not enough information to determine what is happening but it grants for a closer structural analysis or redox studies of the pilli of *A. vinosum* to elucidate its potential to act as an electron carrier as in S. odedensis.

4.5.3.9 Hypothetical genes

In our transcriptome analysis, we discovered a group of highly expressed genes with unknown functions in bacteria exposed to insoluble metal sulfides. One of these genes, Alvin_1447, contained a Gly-zipper_YMGG motif and a transmembrane (TM) domain spanning amino acids 370-400 and 430-475, indicating a potential association with the cellular membrane. Another highly expressed gene, Alvin_0034, featured two motifs, namely DUF4351 and DUF2630. DUF4351 is a proteobacteria conserved protein motif, while DUF2630 represents a domain of unknown function. Furthermore, Alvin_0034 contained a TM domain from amino acids 70-90, suggesting its potential involvement in membrane-related processes. The third gene, Alvin_3266 contained the SWI2_SNF2 motif, known for its role in DNA binding and ATPase activity, as well as the HSDR_N motif. Upregulated hypothetical genes found in NiS transcriptome are not restricted to the ones shown in this section, collectively, hypothetical genes display a homology with 50% conserved sequences from g-proteobacteria, with homology results of 98% or higher (Table *0-3*). The most upregulated Alvin_1447 and Alvin_0034 show transmembrane domains, this contain higher likelihood to be involved in interfacial electron transfer processes.

These highly expressed hypothetical genes present intriguing targets for further investigation, as unraveling their functions could provide insights into novel mechanisms and pathways associated with bacterial responses to insoluble metal sulfides. These genes, despite their undefined functions, play essential roles in cellular processes and are likely associated with electron transfer pathways or key metabolic functions. This insight advances our understanding of *A. vinosum's* adaptability to solid-phase substrates, contributing to the study of electron transfer processes in photosynthetic bacteria. Future studies are warranted to decipher the precise roles of these genes and explore their potential implications in sulfide metabolism, redox reactions, and cellular adaptations to challenging environments.

4.5.3.10 Other

In the differential gene expression analysis, we identified upregulation of gene Alvin_0772, which codes for the integral membrane protein MviN. Integral membrane proteins play critical roles in various cellular processes, including transport, signal transduction, and membrane integrity. The upregulation of Alvin_0772 expression was significant (5.17-fold / NEG(1-fold)), indicating its active participation in specific cellular functions. The exact function of MviN in *A. vinosum* is not fully characterized, but in other organisms, MviN has been implied playing a role in cell wall synthesis and cell membrane remodeling. It is plausible that the Alvin_0772-relevant protein may contribute to similar processes in *A. vinosum* cell cultures supported by NiS. Further investigations are warranted to elucidate the precise role of Alvin_0772 in cellular physiology and its potential implications for membrane-related functions.

Related to the energy production of the NiS-supported cell cultures, we identified several genes that may play important roles in sulfide metabolism, redox reactions, and cellular adaptation. Among the highest upregulated genes, we observed a strong transcriptional response in several key genes. The ankyrin protein encoded by Alvin_1094 exhibited the highest expression level (approximately 28-fold / NEG(35-fold)), suggesting its involvement in diverse cellular processes such as protein-protein interactions and signal transduction. The expression of Alvin_1379, encoding 2-isopropylmalate synthase involved in leucine biosynthesis, was also substantially elevated, indicating an increased demand for amino acid synthesis. Furthermore, Alvin_3135 encoding a Radical SAM domain protein, known to participate in sulfur and iron-sulfur cluster biogenesis, showed notable upregulation, potentially indicating its role in redox processes. Additionally, Alvin_0386 encoding ribonuclease H, involved in RNA degradation, exhibited increased expression levels. Although the direct connection of these genes to sulfide metabolism

and redox reactions is not fully elucidated, their elevated expression suggests their importance in cellular responses to insoluble metal sulfides.

4.5.3.11 Top downregulated proteins

In this study, we identified a cluster of downregulated genes related to the antenna complex in purple sulfur bacteria exposed to insoluble metal sulfides. These genes include Alvin_0704, Alvin_0706, and Alvin_0709, encoding putative antenna complex alpha/beta subunits. The log2FC expression values for these genes were -9.68 / NEG(0-fold), -8.83 / NEG(0-fold), and -7.28 / NEG(0.1-fold), respectively. The downregulation of these genes suggests a diminished capacity for light harvesting and energy transfer in response to the presence of insoluble metal sulfides.

Furthermore, we observed the downregulation of several hypothetical genes with unknown functions, which may have specific roles in purple sulfur bacteria or their adaptation to insoluble metal sulfides. Among them, Alvin_0703 and Alvin_0705 showed log_2FC values of of -9.67 / NEG(0-fold) and -8.45 / NEG(0-fold), respectively. These findings highlight the potential impact of insoluble metal sulfides on the photosynthetic apparatus and the potential existence of unknown molecular processes in purple sulfur bacteria that are capable of enabling autotrophic carbon fixation. The downregulation of these genes suggests a reconfiguration of cellular pathways to cope with the challenges imposed by insoluble metal sulfides, potentially influencing energy utilization, redox reactions, and other metabolic activities. Further investigations are required to elucidate the precise functions of these genes and their involvement in the response to sulfide metabolism and redox reactions in purple sulfur bacteria.

4.6 Conclusion

One of the most compelling pieces of evidence supporting *A. vinosum*'s utilization of NiS as a solid-state substrate for autotrophic growth is the optical density results, which indicated over

twice the growth on NiS compared to the negative control. Despite the negative control's growth demonstrating the bacteria's ability to utilize other media components for growth, it's crucial to note that the media composition was identical for both the negative control and NiS cultures. This underscores a robust argument: the NiS cultures must be engaging an alternative metabolic pathway, distinct from the one supporting growth in the negative control.

The transcriptome analysis revealed a diverse set of upregulated genes, including hydrogenases, cytochromes, and other redox-active proteins. This intriguing discovery points towards these genes' potential roles in electron transfer reactions within the growing cell. Notably, the downregulation of the Rubisco large subunit and the unchanged expression of the small subunit suggest ongoing carbon fixation, albeit at lower levels compared to the positive control. The absence of a sulfur source implies that an unknown electron donor is likely fueling the cell's growth.

The notable increase in expression of Fe/Ni hydrogenases (Alvin_2306, Alvin_2307, Alvin_2308, and Alvin_2309) and formate dehydrogenase (Alvin_2452) suggests potential formate formation, serving as an energy source for the bacteria. These genes are similarly upregulated in the negative control, albeit less than the NiS system, while hydrogenases were more pronounced in the negative control. This hints at formate generation through carbonate reduction with an unspecified electron source, as hydrogen is scarce in the culture. This hints at an electron transport process driving formate production by formate hydrogenase, partially in the negative control and NiS system, or involving an unidentified secondary pathway.

The observation of a peak within the XPS elemental nickel range in biotic NiS, unlike in abiotic NiS, is intriguing. This might be attributed to electron export from the cell. Similarly, as discussed earlier, hydrogenases raise questions. Given the hydrogen shortage in the medium, other enzymes could potentially utilize alternate substrates for electron generation. It's worth noting that

the elemental nickel peak might potentially stem from incorrect curve fitting in the biotic sample, necessitating further exploration to validate this possibility.

Among the highly upregulated cytochrome proteins, Alvin_1093 stood out with a remarkable 32-fold increase. This protein is a subunit of sulfide dehydrogenase and contains a flavocytochrome domain, its significance enhanced by the presence of a signal peptide. Additionally, the upregulation of Alvin_1095, a gene encoding a tetra-heme c-type cytochrome with an anticipated signal peptide and lipid binding motif, indicates its potential association with the cell membrane.

Gene expression profiles of both photosynthetic and sulfur oxidation genes offer valuable insights into the mechanisms underlying the growth of NiS cultures. The suppression of photosynthetic *puc* and *puf* genes indicated reduced reliance on photosynthesis for energy, while carotenoid gene expression remained comparable to positive control, implying greater significance of these pigments in energy production in NiS cultures. Sulfur oxidation genes, *sox* and dsr, strongly indicates NiS utilization as a sulfur source by *A. vinosum*. Comparable *sox* gene expression to the positive control, along with polysulfide detection in biotic NiS samples via XPS analysis, validates active sulfur oxidation. Dsr's less inhibited expression compared to the negative control further reinforces its role in sulfur oxidation, albeit less than sox. Moreover, Alvin_2447 upregulation, related to sulfate assimilation, implies possible underestimation of sulfur oxidation extent, suggesting comprehensive sulfur metabolism in NiS presence.

The transcriptomic analysis unveiled significant upregulation of various transporter genes in *A. vinosum* in response to NiS, suggesting their potential roles in ion homeostasis and cellular detoxification mechanisms. Increased expression of K+-transporting ATPase protein subunits, AAA ATPase central domain protein, and metal efflux genes indicates their involvement in maintaining cellular metal homeostasis and expelling metal ions, including nickel. This

upregulation suggests an ion flux between the cell and NiS, supported by the ICP-MS plot revealing significant nickel concentration changes, particularly at the growth cycle's onset. As growth continued, nickel concentration decreased, signifying nickel ion efflux from the cell to the environment. This decline is reinforced by a metallic peak in the XPS analysis of biotic NiS samples, indicating metallic nickel's presence. These findings underscore *A. vinosum*'s intricate response to NiS, revealing vital transporters that enable efficient substrate utilization.

The moderate upregulation of gene Alvin_3265, encoding the PilT protein domain associated with the type IV pilus (T4P) system, with a fold change of 5.25, raises intriguing possibilities for its role in *A. vinosum*'s interaction with NiS. The significance of this expression could be linked to various factors, such as stress response, mobility for efficient electron harvesting from NiS, or the pilus' function as a conductive appendage in facilitating electron transfer into the cell. Further investigations are warranted to elucidate the precise contribution of pili in *A. vinosum*'s utilization of NiS as a sulfur and electron source, as well as its potential role in electron transfer mechanisms.

The substantial upregulation of hypothetical genes in the transcriptome of NiS-treated *A. vinosum* suggests their potential involvement in the electron transport pathway. Genes like Alvin_1447, featuring transmembrane domains and showing a remarkable 34-fold upregulation, along with Alvin_0034, displaying a significant 46.0-fold increase and containing DUF4351 and DUF2630 motifs, and a TM domain, indicate their likely role in facilitating electron transfer across the cell membrane. Similarly, the 16.0-fold upregulation of Alvin_3266 raises intriguing possibilities for its contribution to electron transport pathways. These findings highlight novel proteins that may play crucial roles in the utilization of NiS as a sulfur and electron source by *A. vinosum*, warranting further exploration and functional characterization to fully comprehend their significance in the electrochemical activity of the bacterium.

In conclusion, our transcriptomic analysis has not only revealed the remarkable adaptability of *A. vinosum* to utilize NiS nanoparticles as both a sulfur and electron source but has also shed light on specific proteins that are potentially involved in this process. The significant upregulation of redox active proteins such as Fe/Ni hydrogenases, formate dehydrogenase, flavocytochrome 1093, and tetra-heme c-type cytochrome Alvin_1095, indicates their crucial roles in utilizing NiS for energy production and electron transfer. These findings provide valuable insights into the molecular mechanisms underlying *A. vinosum*'s unique ability to interact with solid-phase substrates, furthering our understanding of its metabolic adaptability and potential applications in various environmental and industrial contexts.

4.7: Tables and Figures

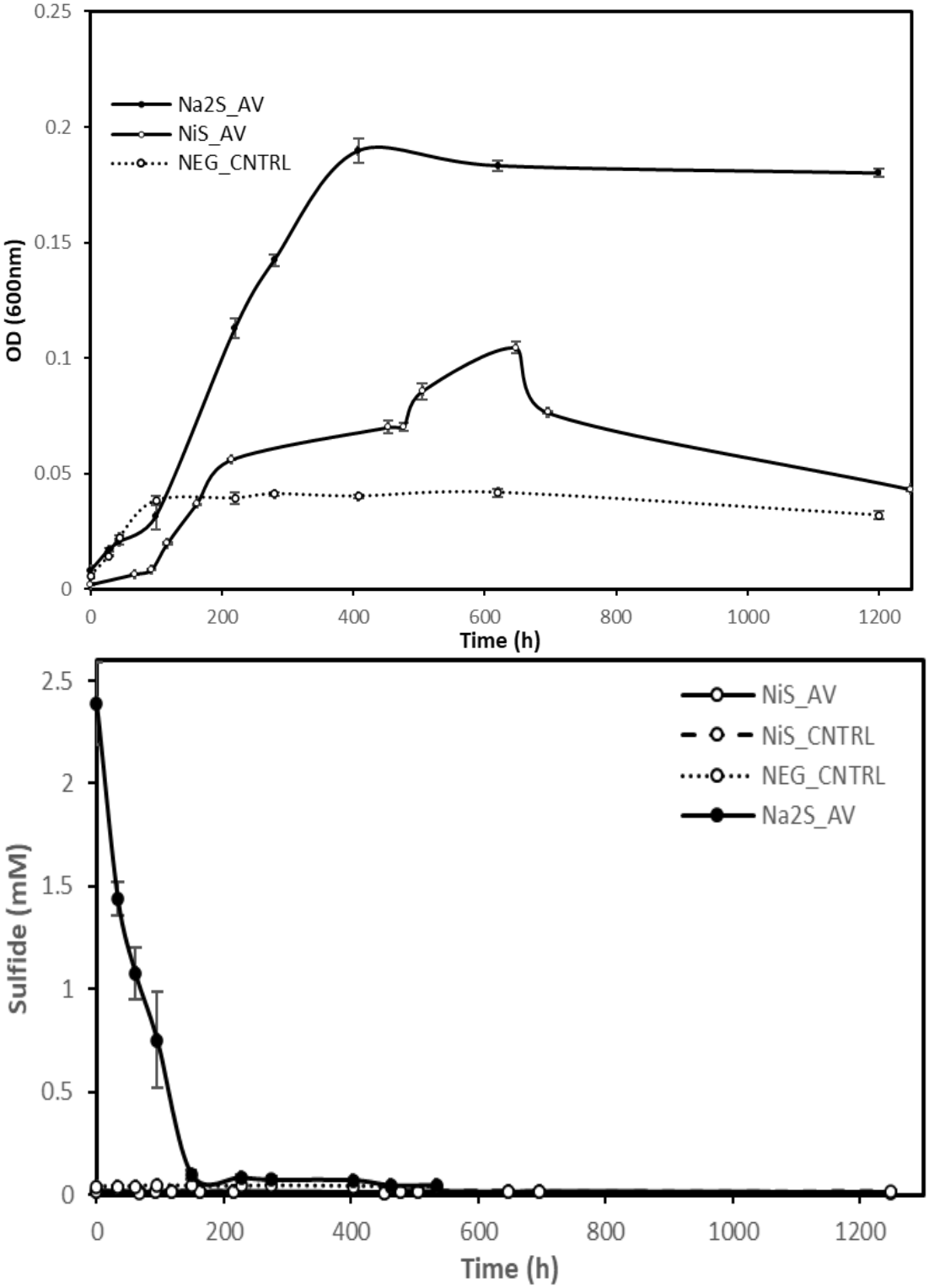

Figure 4-1 Growth profiles OD (600nm) on top and sulfide depletion on the bottom

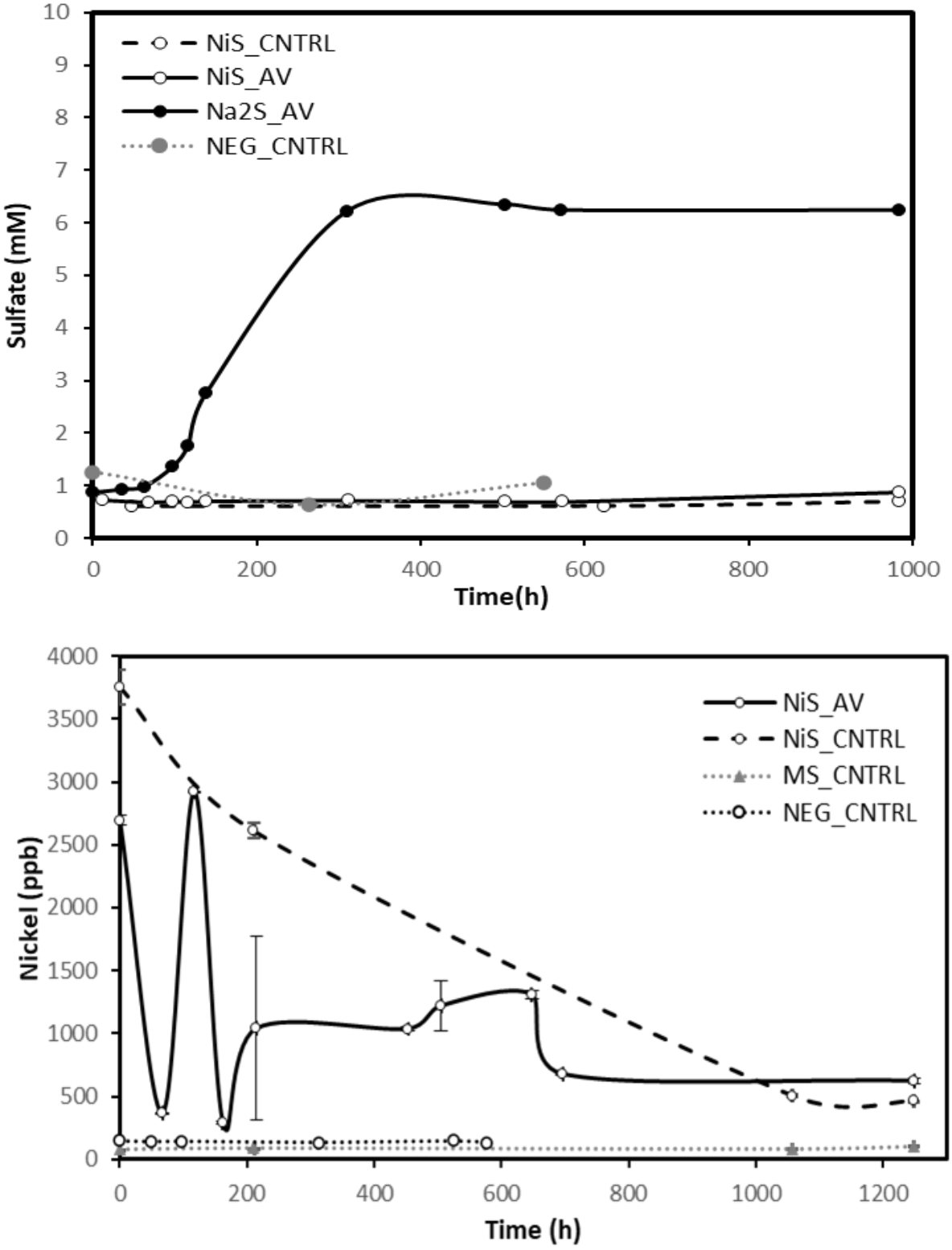

Figure 4-2 Growth profile showing sulfate concentration changes in the media on top and nickel concentration changes in the bottom

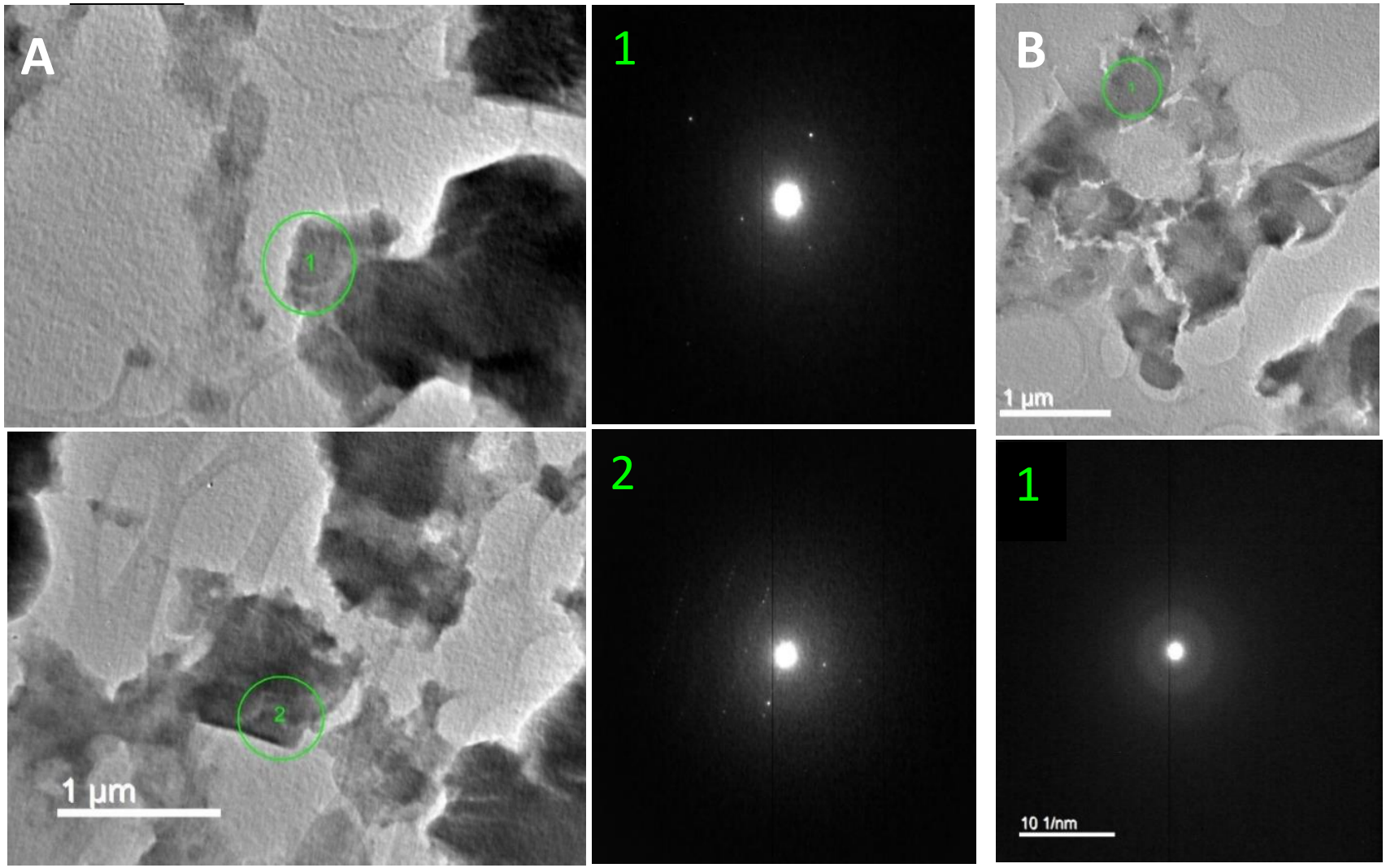

Figure 4-3 Images of NiS using HR-TEM displaying electron diffraction patterns identifying different mineral phases. The biotic sample shown in the left quadrant as A and the abiotic sample as B in the right quadrant.

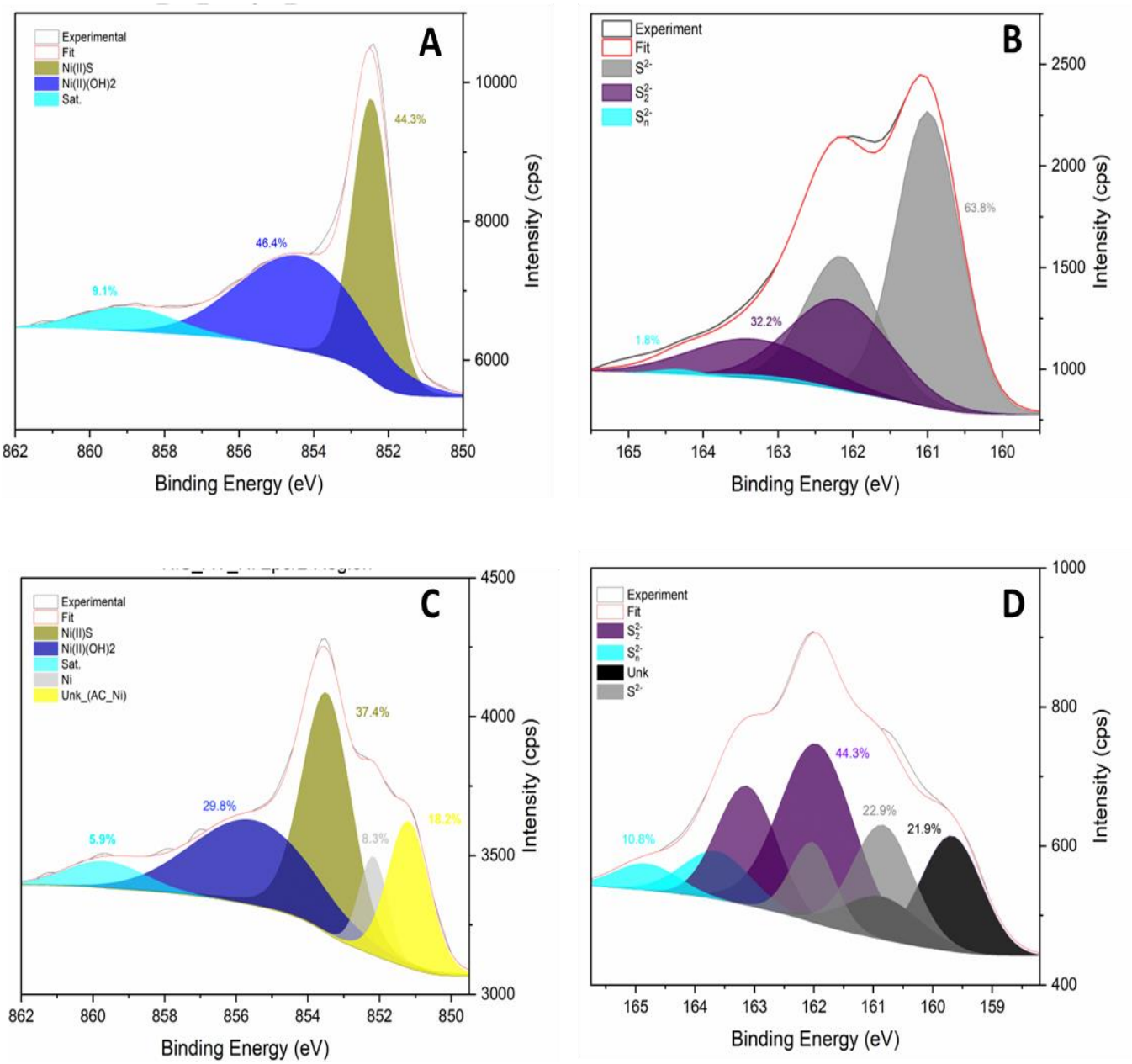

Figure 4-4 Solid-phase characterization through X-ray photoelectron spectroscopy of NiS. Both A and B show characterization of abiotic NiS with A displaying nickel region and B. the sulfur region of the spectra. While C and D show biotic NiS control with C showing Iron region and D the sulfur region

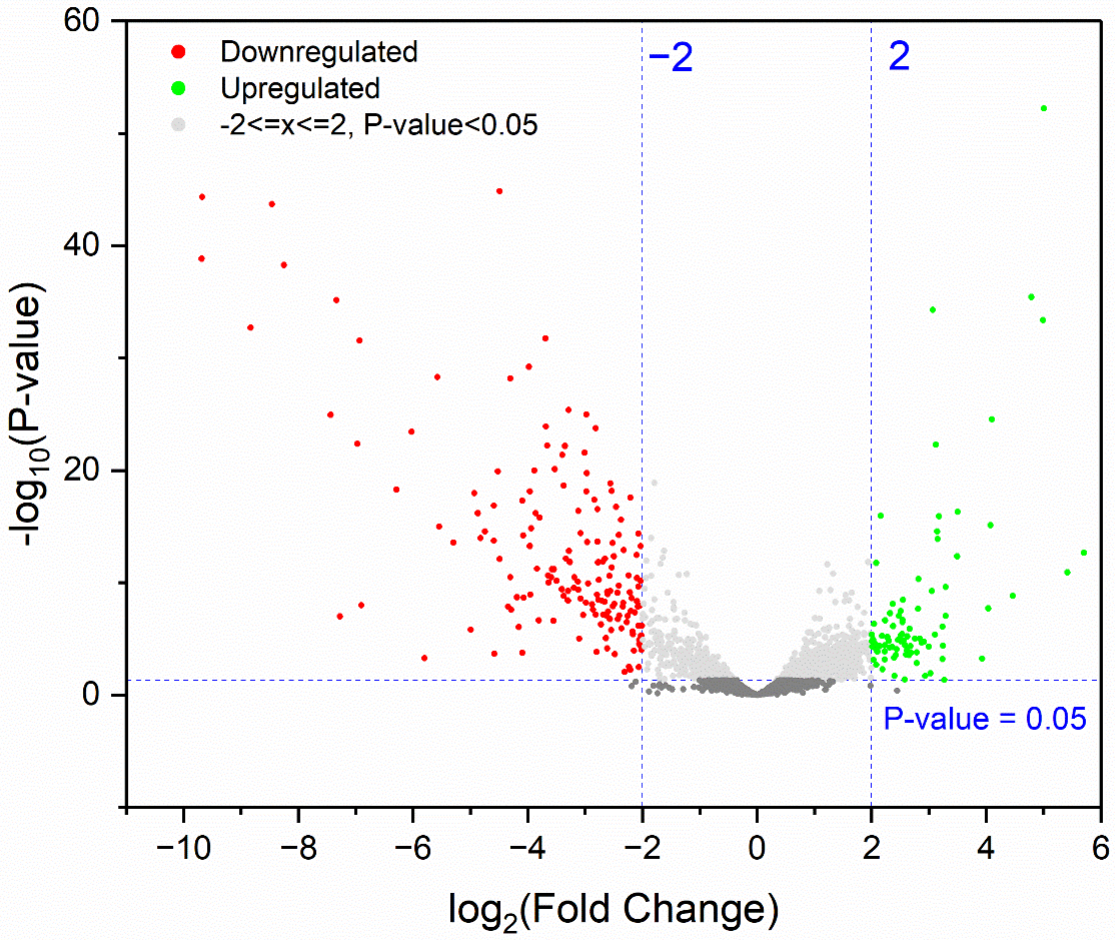

Figure 4-5 Volcano plot of NiS transcriptome

Table 4-1 Most upregulated and downregulated hypothetical genes for NiS transcriptome

Gene locus	log2FC (NiS)	Padj (NiS)	log2FC (NEG)	Padj (NEG)	Kegg or Strindb annotation	pBlast %	AA length	Sequence protein domains	Protein motifs (AA locus)	Transmembrane domains (AA locus)	Hydropathicity
Upregulated genes											
Alvin_0034	5.700200	0.000000	1.156142	0.290328	hypothetical protein Alvin_0034	32	112	none	none	none	-0.571
Alvin_1447	5.417300	0.000000	0.486394	0.706994	hypothetical protein Alvin_1447	95	529	Gly-zipper_YMGG	none	TM (370-400 & 430-475)	-0.185
Alvin_1448	4.459200	0.000000	0.173582	0.891382	putative transposase	39	341	DUF4351, DUF2630	none	TM (70-90)	-0.246
Alvin_3266	4.035300	0.000000	0.728559	0.502104	protein of unknown function DUF450	87	1043	SWI2_SNF2, HSDR_N	none	none	-0.326
Downregulated genes											
Alvin_0703	-9.673000	0.000000	-5.382470	0.000000	hypothetical protein Alvin_0703	99	53	LHC	none	TM (23-51)	0.692
Alvin_0705	-8.454600	0.000000	-5.253038	0.000000	hypothetical protein Alvin_0705	98	69	DUF5989, LHC	none	TM (24-46)	0.648

Alvin_1741	-8.246400	0.000000	-5.470211	0.000000	hypothetical protein Alvin_1741	29	78	DUF5320, FoP_duplication	none	none	-0.735
Alvin_3072	-7.430600	0.000000	-6.520365	0.000000	hypothetical protein Alvin_3072	63	61	DUF2892, Pox_P21	none	TM (11-27 & 30-52)	0.793
Alvin_1197	-5.800200	0.003139	-3.726630	0.005867	hypothetical protein Alvin_1197	100	32	none	none	TM (13-30)	0.341
Alvin_2515	-5.572000	0.000000	-5.697031	0.000000	hypothetical protein Alvin_2515	99	202	Mod_r, GBP_C	signal peptide (22-23)	TM (06-25)	-0.902

Table 4-2 NiS Sulfur oxidation gene expression for *sox* and *dsr* genes in the transcriptome of NiS

Gene	Protein	log2FC (NiS)	Padj (NiS)	log2FC (NEG)	Padj (NEG)
***dsr* genes**					
Alvin_1252	DsrB	-4.992609	0.000021	-6.897314	0.000000
Alvin_1253	DsrE	-4.286253	0.000000	-6.296714	0.000000
Alvin_1251	DsrA	-4.153981	0.000013	-6.132203	0.000000
Alvin_1258	DsrK	-4.072434	0.000000	-4.404750	0.000000
Alvin_1260	DsrJ	-3.882064	0.000000	-3.899363	0.000000
Alvin_1254	DsrF	-3.805981	0.000004	-5.112428	0.000000
Alvin_1259	DsrL	-3.787829	0.000000	-4.267356	0.000000
Alvin_1261	DsrO	-3.187302	0.000000	-3.574387	0.000000
Alvin_1256	DsrC	-3.122150	0.000000	-2.925130	0.000000
Alvin_1262	DsrP	-2.769079	0.000000	-3.031671	0.000000
Alvin_1255	DsrH	-2.703600	0.000000	-2.004281	0.000203
Alvin_1257	DsrM	-2.478966	0.001623	-3.436208	0.000009
Alvin_1263	DsrN	-1.444152	0.000000	-1.232372	0.000038
Alvin_1264	DsrR	-1.273148	0.002052	-0.617883	0.196365
Alvin_1265	DsrS	-1.043797	0.000643	-0.733408	0.027678
***sox g*enes**					
Upregulated Genes					
Alvin_2167	SoxB	0.9927007	0.1120449	0.0197858	0.9839592
Downregulated Genes					
Alvin_2171	SoxL	-2.030399	0.000000	-0.020455	0.970003
Alvin_2170	SoxK	-0.715283	0.130330	0.162110	0.789931
Alvin_2169	SoxA	-0.467047	0.129520	-0.092674	0.826892
Alvin_2112	SoxZ	-0.293136	0.418069	0.263714	0.500839
Alvin_2168	SoxX	-0.139120	0.731614	0.111759	0.799777
Alvin_2111	SoxY	-0.134399	0.791465	0.499286	0.257625

Table 4-3 NiS Photosynthetic gene expression of *puf* and *puc* genes

No.	Gene locus	log2FC (NiS)	Padj (NiS)	log2FC (NEG)	Padj (NEG)	Annotation
***puf* genes (LH1)**						
1	Alvin_2548	-2.234004	0.012904	-0.792069	0.480608	puf/LH1
2	Alvin_2550	-2.220393	0.020835	-1.498040	0.162794	puf/LH1
3	Alvin_2549	-2.204825	0.021985	-0.890936	0.451954	puf/LH1
4	Alvin_2637	-1.711802	0.049775	-1.316279	0.171470	puf/LH1
5	Alvin_2554	-1.704810	0.286093	-1.294482	0.471556	puf/LH1
6	Alvin_2553	-1.695495	0.229783	-2.611817	0.064066	puf/LH1
7	Alvin_2551	-1.692740	0.048076	-1.976107	0.025298	puf/LH1
8	Alvin_2555	-1.686991	0.101606	-1.325815	0.246577	puf/LH1
9	Alvin_2552	-1.596881	0.267117	-2.649278	0.061690	puf/LH1
10	Alvin_2547	-1.097282	0.340962	-1.016969	0.409853	puf/LH1
11	Alvin_2636	-0.914467	0.189671	-1.726529	0.010760	puf/LH1
12	Alvin_2635	-0.868359	0.155273	-1.106660	0.080923	puf/LH1
13	Alvin_2634	0.025128	0.976816	-0.109868	0.883949	puf/LH1
***puc* genes (LH2)**						
14	Alvin_0704	-9.681058	0.000000	-5.528480	0.000000	pucB6
15	Alvin_0703	-9.673049	0.000000	-5.382470	0.000000	pucA6
16	Alvin_0706	-8.831110	0.000000	-4.948448	0.000000	pucB5
17	Alvin_0705	-8.454626	0.000000	-5.253038	0.000000	pucA5
18	Alvin_0709	-7.275103	0.000002	-3.864599	0.013577	pucB4
19	Alvin_0708	-4.822547	0.000000	-3.003893	0.000002	pucA4
20	Alvin_2576	-2.114347	0.148030	-0.575461	0.767512	Lux/LH2
21	Alvin_2577	-1.801035	0.284542	-0.762006	0.712280	Lux/LH2
22	Alvin_2579	-1.705944	0.295028	-1.236322	0.503230	Lux/LH2
23	Alvin_2759	-1.666101	0.371643	0.297924	0.900823	pucA3
24	Alvin_2578	-1.522145	0.380872	-1.044325	0.595913	Lux/LH2
25	Alvin_2760	-1.480100	0.463482	-0.017335	0.995574	pucB3
26	Alvin_2580	-0.015991	0.977133	-0.130225	0.790827	Lux/LH2

Table 4-4 *NiS identification of motifs CXXCH and LXXC and signal peptides*

Gene	Position	Description	Number of CXXCH motif	LXXC motif	NCBI Protein ID	SignalP	Upregulated in cells on NiS	Upregulated in cells on elemental sulfur	Upregulated in Negative Control
Alvin_0018	76..80	Di-heme cytochrome c peroxidase	2		ADC60990		Yes (3.3)	Yes (2.2)	Yes (2.4)
	258..262								
Alvin_0020	56..60	Diheme cytochrome c	2	Yes	ADC60992	Yes	Yes (3.2)	No (0.8)	Yes (3.3)
	165..169								
Alvin_0022	48..52	Domain of unknown function DUF1924	1		ADC60994	Yes	Yes (2.3)	No (0.08)	Yes (4.9)
Alvin_0023	54..58	Diheme cytochrome c	2		ADC60995	Yes	Yes (2.3)	No (0.7)	Yes (3.9)
	155..159								
Alvin_0070	50..54	cytochrome c1	1		ADC61042	Yes	No (0.3)	No (0.2)	No (0.5)
Alvin_0071	9..13	Glutathione S-transferase domain protein	1	Yes	ADC61043		No (0.6)	No (0.3)	No (0.6)
Alvin_0091	76..80	Thiosulfate dehydrogenase	2		ADC61061	Yes	Yes (1.1)	Yes (1.7)	Yes (1.3)
	187..191								
Alvin_0350	159..163	nicotinate-nucleotide pyrophosphorylase	1		ADC61311		Yes (1.2)	N/A	Yes (1.3)
Alvin_0439	43..47	transmembrane region and signal peptide prediction	1	Yes	ADC61398	Yes	No (0.3)	No (0.1)	No (0.6)
Alvin_0679	76..80	Cytochrome-c peroxidase	2	Yes	ADC61628	Yes	No (0.7)	No (0.6)	No (0.9)
	222..226								
Alvin_0782	105..109	cytochrome c oxidase, cbb3-type, subunit II	1		ADC61729		No (0.6)	Yes (6.2)	Yes (1.7)
Alvin_0784	120..124	cytochrome c class I	2		ADC61731		No (0.6)	Yes (6.2)	Yes (1.7)
	206..210								
Alvin_1073	877..881	FAD linked oxidase domain protein	1	Yes	ADC62012		No (0.7)	No (0.4)	No (0.7)
Alvin_1093	36..40	cytochrome c class I	2		ADC62032	Yes	Yes (31.9)	Yes (4.5)	Yes (24.6)
	126..130								
Alvin_1095	44..48		4	Yes	ADC62034		Yes (32.1)	Yes (9.6)	Yes (37.8)

	73..77	NapC/NirT cytochrome c domain protein							
	133..137								
	165..169								
Alvin_1259	633..637	DsrL	1		ADC62198		No (0.1)	No (0.2)	No (0.1)
Alvin_1260	83..87	DsrJ	3	Yes	ADC62199	Yes	No (0.1)	No (0.1)	No (0.1)
	106..110								
	119..123								
Alvin_1395	72..76	cytochrome c family protein	8	Yes	ADC62330	Yes	No (0.3)	No (0.01)	No (0.2)
	122..126								
	146..150								
	195..199								
	237..241								
	275..279								
	303..307								
	489..493								
Alvin_1402	172..176	Fe-S cluster assembly protein NifU	1	Yes	ADC62337		Yes (4.3)	Yes (1.3)	Yes (2.2)
Alvin_1452	46..50	conserved hypothetical protein	7		ADC62387	Yes	Yes (2.9)	Yes (1.1)	Yes (1.1)
	85..89								
	109..113								
	151..155								
	180..184								
	210..214								
	238..242								
Alvin_1454	130..134	hypothetical protein	8		ADC62389		Yes (1.1)	No (1.0)	No (0.7)
	230..234								
	262..266								
	306..310								
	360..364								
	392..396								
	419..423								
	681..685								
Alvin_1467	37..41	Alcohol dehydrogenase GroES domain protein	2	Yes	ADC62401		No (0.1)	Yes (5.5)	No (0.3)
	96..100								

Alvin_1573	150..154	methyl-accepting chemotaxis sensory transducer	1		ADC62506		No (0.9)	No (0.8)	No (1)
Alvin_1694	24..28	cytochrome c class I	1		ADC62626	Yes	Yes (1.8)	Yes (3.0)	Yes (1.5)
Alvin_1837	50..54	putative lipoprotein	2	Yes	ADC62762	Yes	Yes (1.3)	Yes (1.1)	Yes (2)
	389..393								
Alvin_1846	57..61	cytochrome c class I	2		ADC62771	Yes	Yes (1.3)	Yes (1.5)	Yes (1.6)
	151..155								
Alvin_1867	17..21	NADH ubiquinone oxidoreductase 20 kDa subunit	1	Yes	ADC62792		No (0.9)	N/A	Yes (1.1)
Alvin_1971	87..91	Coproporphyrinogen dehydrogenase	1	Yes	ADC62895		Yes (1.1)	Yes (5.5)	No (0.9)
Alvin_2064	61..65	protein of unknown function DUF255	1	Yes	ADC62986		No (0.2)	Yes (4.4)	No (0.3)
Alvin_2168	56..60	SoxX	1	Yes	ADC63089	Yes	No (0.9)	Yes (5.7)	Yes (1.1)
Alvin_2169	195..199	SoxA	1		ADC63090	Yes	No (0.7)	Yes (5.4)	No (0.9)
Alvin_2172	89..93	HNH endonuclease	1		ADC63093		Yes (1.1)	Yes (1.1)	No (0.8)
Alvin_2201	150..154	conserved hypothetical protein	1		ADC63122	Yes	No (0.4)	No (0.7)	No (0.4)
Alvin_2458	41..45	NapC/NirT cytochrome c domain protein	4		ADC63370		Yes (1.9)	Yes (1.7)	Yes (1.6)
	71..75								
	125..129								
	161..165								
Alvin_2459	46..50	hypothetical protein	1		ADC63371	Yes	Yes (2.5)	No (0.9)	Yes (1.9)
Alvin_2490	13..17	4Fe-4S ferredoxin iron-sulfur binding domain protein	1	Yes	ADC63402		No (0.4)	No (0.2)	No (0.3)
Alvin_2551	107..111	photosynthetic reaction center cytochrome c subunit	4	Yes	ADC63461	Yes	No (0.3)	No (0.005)	No (0.3)
	152..156								
	247..251								
	307..311								
Alvin_2765	144..148	cytochrome c prime	1		ADC63674	Yes	No (0.2)	Yes (2.6)	No (0.6)
Alvin_2879	42..46	cytochrome c class I	2		ADC63784	Yes	Yes (1.7)	No (0.4)	No (0.7)
	138..142								

Alvin_3050	37..41	ribosomal protein L31	1		ADC63950		No (0.8)	No (0.7)	No (0.5)
Alvin_3069	41..45	Thioredoxin domain protein	1		ADC63969		No (0.2)	Yes (6.6)	No (0.3)
Alvin_3120	550..554	type II secretion system protein E	1	Yes	ADC64019		Yes (1.1)	No (0.7)	Yes (1.1)
Alvin_3135	93..97	Radical SAM domain protein	1	Yes	ADC64033		Yes (5.7)	N/A	Yes (2.5)

Table 4-5 NiS transcriptome. Gene table showing only genes with log2FC above 2 or below -2.

No.	Gene locus	log2FC (NiS)	Padj (NiS)	log2FC (NEG)	Padj (NEG)	Annotation
Upregulated Genes						
1	Alvin_0034	5.70000	0.00000	1.15614	0.29033	hypothetical protein Alvin_0034
2	Alvin_1447	5.41700	0.00000	0.48639	0.70699	hypothetical protein Alvin_1447
3	Alvin_1095	5.00200	0.00000	5.24158	0.00000	NapC/NirT cytochrome c domain protein
4	Alvin_1093	4.99300	0.00000	4.62336	0.00000	cytochrome c class I, FccA
5	Alvin_1094	4.78500	0.00000	5.11175	0.00000	Ankyrin
6	Alvin_1448	4.45900	0.00000	0.17358	0.89138	putative transposase
7	Alvin_2446	4.10000	0.00000	2.16243	0.00000	nitrite and sulphite reductase 4Fe-4S region
8	Alvin_1092	4.07200	0.00000	4.19391	0.00000	Flavocytochrome c sulphide dehydrogenase flavin-binding protein, FccB
9	Alvin_3266	4.03500	0.00000	0.72856	0.50210	protein of unknown function DUF450
10	Alvin_1379	3.93100	0.00350	1.07474	0.53401	2-isopropylmalate synthase
11	Alvin_1528	3.50400	0.00000	-0.38185	0.57112	protein of unknown function DUF156
12	Alvin_1191	3.49200	0.00000	1.13710	0.07050	hypothetical protein Alvin_1191
13	Alvin_3179	3.29200	0.00000	1.11052	0.18511	ATP-dependent DNA helicase, RecQ family
14	Alvin_0284	3.29200	0.00000	2.12926	0.00059	peptidase M61 domain protein
15	Alvin_1686	3.26500	0.11000	2.13112	0.37343	hypothetical protein Alvin_1686
16	Alvin_3263	3.24300	0.00037	1.08579	0.33367	hypothetical protein Alvin_3263
17	Alvin_3205	3.24000	0.00380	1.77881	0.17255	hypothetical protein Alvin_3205
18	Alvin_0937	3.23600	0.00001	1.09610	0.22248	hypothetical protein Alvin_0937
19	Alvin_2308	3.17600	0.00000	2.87447	0.00000	nickel-dependent hydrogenase large subunit
20	Alvin_2309	3.15000	0.00000	3.21152	0.00000	hydrogenase (NiFe) small subunit HydA
21	Alvin_2447	3.14000	0.00000	1.84796	0.00007	adenylylsulfate reductase, thioredoxin dependent
22	Alvin_1529	3.11900	0.00000	-0.03382	0.95571	cation diffusion facilitator family transporter
23	Alvin_1449	3.10300	0.00005	-0.30146	0.79428	hypothetical protein Alvin_1449
24	Alvin_2451	3.06500	0.00000	3.03415	0.00000	molybdopterin oxidoreductase Fe4S4 region
25	Alvin_1190	3.05400	0.00000	0.75653	0.27316	hypothetical protein Alvin_1190

26	Alvin_0014	3.02800	0.04000	1.82227	0.28025	efflux transporter, RND family, MFP subunit
27	Alvin_0015	2.99800	0.00045	1.09224	0.29187	heavy metal efflux pump, CzcA family
28	Alvin_0893	2.93500	0.05800	4.24318	0.00438	hypothetical protein Alvin_0893
29	Alvin_3275	2.91200	0.00019	2.31152	0.00564	phage recombination protein Bet
30	Alvin_3264	2.87200	0.00021	0.63854	0.53268	virulence protein, putative
31	Alvin_0283	2.84100	0.00011	1.69244	0.04021	RNP-1 like RNA-binding protein
32	Alvin_1189	2.82100	0.00000	0.54725	0.37343	hypothetical protein Alvin_1189
33	Alvin_3212	2.80800	0.00000	1.66741	0.00693	hypothetical protein Alvin_3212
34	Alvin_3220	2.79000	0.00120	1.00104	0.34797	hypothetical protein Alvin_3220
35	Alvin_3202	2.78900	0.00720	2.72709	0.01111	hypothetical protein Alvin_3202
36	Alvin_3276	2.75900	0.00011	1.49026	0.06639	phage-type endonuclease
37	Alvin_3273	2.68600	0.00130	2.95943	0.00050	hypothetical protein Alvin_3273
38	Alvin_3229	2.67700	0.00042	0.79541	0.40350	hypothetical protein Alvin_3229
39	Alvin_0941	2.66200	0.00002	1.16378	0.11088	hypothetical protein Alvin_0941
40	Alvin_0016	2.65200	0.00190	1.78245	0.05973	hypothetical protein Alvin_0016
41	Alvin_0940	2.62100	0.00008	1.56476	0.03486	Cyclopropane-fatty-acyl-phospholipid synthase
42	Alvin_3278	2.61400	0.00088	1.41370	0.11568	hypothetical protein Alvin_3278
43	Alvin_3274	2.59900	0.00170	2.37941	0.00628	hypothetical protein Alvin_3274
44	Alvin_1158	2.58600	0.00034	1.13227	0.18359	potassium-transporting ATPase, A subunit
45	Alvin_0013	2.57800	0.10000	0.66578	0.75237	outer membrane efflux protein
46	Alvin_3207	2.55800	0.00015	1.08100	0.17841	Gp157 family protein
47	Alvin_2307	2.54300	0.00000	3.46404	0.00000	Ni/Fe-hydrogenase, b-type cytochrome subunit
48	Alvin_1337	2.54000	0.00000	0.85189	0.20410	YCII-related protein
49	Alvin_0281	2.54000	0.00001	-0.01732	0.98601	S-adenosylmethionine/tRNA-ribosyltransferase-isomerase
50	Alvin_0903	2.52800	0.00005	1.26094	0.07839	nitrogenase MoFe cofactor biosynthesis protein NifE
51	Alvin_1702	2.50800	0.00006	0.90025	0.23580	hypothetical protein Alvin_1702
52	Alvin_3135	2.50600	0.00017	1.29737	0.08832	Radical SAM domain protein
53	Alvin_0771	2.50400	0.00000	0.12556	0.87570	transcriptional regulator, XRE family
54	Alvin_0770	2.47300	0.00000	-0.21172	0.79183	hypothetical protein Alvin_0770
55	Alvin_3277	2.46500	0.00013	1.48254	0.04039	ATPase associated with various cellular activities AAA_5
56	Alvin_1157	2.44400	0.58000	0.33805	0.95571	K+-transporting ATPase, F subunit
57	Alvin_0386	2.44100	0.00072	0.35053	0.73254	ribonuclease H
58	Alvin_0895	2.42400	0.00190	1.11202	0.22320	hypothetical protein Alvin_0895

59	Alvin_1700	2.39700	0.05900	0.71892	0.68048	phage transcriptional regulator, AlpA
60	Alvin_3265	2.39300	0.00300	0.37124	0.74394	PilT protein domain protein
61	Alvin_0285	2.37900	0.00001	1.68366	0.00425	biotin/acetyl-CoA-carboxylase ligase
62	Alvin_0772	2.37100	0.00000	0.14079	0.84450	integral membrane protein MviN
63	Alvin_2240	2.35800	0.00046	0.05935	0.95673	transcription-repair coupling factor
64	Alvin_2306	2.31900	0.00000	3.17776	0.00000	hydrogenase expression/formation protein
65	Alvin_0387	2.31600	0.00053	0.27549	0.77788	DNA polymerase III, epsilon subunit
66	Alvin_2967	2.30100	0.00016	0.40573	0.62848	small GTP-binding protein
67	Alvin_0936	2.28400	0.00010	0.74118	0.30430	Molecular chaperone-like protein
68	Alvin_3279	2.27600	0.00008	0.97984	0.15019	hypothetical protein Alvin_3279
69	Alvin_0402	2.27300	0.00008	0.86453	0.20909	TrkA-N domain protein
70	Alvin_0060	2.23600	0.00000	0.27168	0.69819	hypothetical protein Alvin_0060
71	Alvin_0116	2.23000	0.00400	2.75229	0.00040	putative hemolysin
72	Alvin_0896	2.22800	0.00100	1.49273	0.04659	hypothetical protein Alvin_0896
73	Alvin_2311	2.22500	0.00037	1.08742	0.13243	transaldolase
74	Alvin_0017	2.18900	0.02100	1.45202	0.17150	hypothetical protein Alvin_0017
75	Alvin_1155	2.18000	0.00007	1.08159	0.08474	glycosyltransferase 36
76	Alvin_2443	2.16000	0.00000	1.25713	0.00003	sulfate ABC transporter, inner membrane subunit CysT
77	Alvin_1378	2.14000	0.00042	1.14980	0.09685	transcriptional regulator, AsnC family
78	Alvin_1726	2.10700	0.00110	1.34140	0.06169	RNA polymerase, sigma-24 subunit, ECF subfamily
79	Alvin_1159	2.09700	0.00110	1.19622	0.09896	K+-transporting ATPase, B subunit
80	Alvin_1402	2.09000	0.00038	1.14706	0.08582	Fe-S cluster assembly protein NifU
81	Alvin_2442	2.08100	0.00000	0.86605	0.02024	sulfate ABC transporter, inner membrane subunit CysW
82	Alvin_3262	2.07900	0.01000	0.78688	0.42815	restriction modification system DNA specificity domain protein
83	Alvin_1450	2.06900	0.00045	-0.44781	0.56792	AAA ATPase central domain protein
84	Alvin_3208	2.05800	0.00058	0.81593	0.25664	single-strand binding protein
85	Alvin_2752	2.05500	0.00026	1.21124	0.05613	sulphate transporter
86	Alvin_2448	2.04400	0.00001	1.39943	0.00494	sulfate adenylyltransferase, small subunit
87	Alvin_1146	2.03900	0.00430	2.05201	0.00567	hypothetical protein Alvin_1146
88	Alvin_0640	2.02600	0.00012	0.36281	0.61558	two component transcriptional regulator, LuxR family
89	Alvin_0639	2.01100	0.00043	0.57319	0.42985	multi-sensor signal transduction histidine kinase

90	Alvin_1634	2.00500	0.00006	0.73656	0.21831	DnaA regulatory inactivator Hda
91	Alvin_0275	2.00200	0.00017	0.75211	0.24270	glycosyl transferase family 2
Downregulated Genes						
92	Alvin_0704	-9.68100	0.00000	-5.52848	0.00000	antenna complex alpha/beta subunit
93	Alvin_0703	-9.67300	0.00000	-5.38247	0.00000	hypothetical protein Alvin_0703
94	Alvin_0706	-8.83100	0.00000	-4.94845	0.00000	antenna complex alpha/beta subunit
95	Alvin_0705	-8.45500	0.00000	-5.25304	0.00000	hypothetical protein Alvin_0705
96	Alvin_1741	-8.24600	0.00000	-5.47021	0.00000	hypothetical protein Alvin_1741
97	Alvin_3072	-7.43100	0.00000	-6.52036	0.00000	hypothetical protein Alvin_3072
98	Alvin_1740	-7.33400	0.00000	-5.30218	0.00000	Dinitrogenase iron-molybdenum cofactor biosynthesis protein
99	Alvin_0709	-7.27500	0.00000	-3.86460	0.01358	antenna complex alpha/beta subunit
100	Alvin_3073	-6.97200	0.00000	-5.69870	0.00000	C4-dicarboxylate transporter/malic acid transport protein
101	Alvin_1739	-6.92900	0.00000	-4.90035	0.00000	Cobyrinic acid ac-diamide synthase
102	Alvin_1006	-6.90000	0.00000	-7.01691	0.00000	Peroxiredoxin
103	Alvin_1737	-6.28500	0.00000	-3.19904	0.00004	Dinitrogenase iron-molybdenum cofactor biosynthesis protein
104	Alvin_1738	-6.02000	0.00000	-3.78368	0.00000	Cobyrinic acid ac-diamide synthase
105	Alvin_1197	-5.80000	0.00310	-3.72663	0.00587	hypothetical protein Alvin_1197
106	Alvin_2515	-5.57200	0.00000	-5.69703	0.00000	hypothetical protein Alvin_2515
107	Alvin_1324	-5.54100	0.00000	-2.97770	0.00024	Redoxin domain protein
108	Alvin_0440	-5.29300	0.00000	-4.61071	0.00000	Chaperonin Cpn10
109	Alvin_1252	-4.99300	0.00002	-6.89731	0.00000	DsrB
110	Alvin_1250	-4.92800	0.00000	-2.89993	0.00000	hypothetical protein Alvin_1250
111	Alvin_0441	-4.87000	0.00000	-4.30529	0.00000	chaperonin GroEL
112	Alvin_0708	-4.82300	0.00000	-3.00389	0.00000	hypothetical protein Alvin_0708

113	Alvin_0854	-4.74600	0.00000	-3.30207	0.00000	Chaperonin Cpn10
114	Alvin_2667	-4.58700	0.00000	-1.96435	0.00756	iron-sulfur cluster assembly accessory protein
115	Alvin_0345	-4.58700	0.00000	-2.72684	0.00001	sulfur relay protein, TusE/DsrC/DsvC family
116	Alvin_1434	-4.57700	0.00150	-3.07988	0.05351	Protein of unknown function DUF2061, membrane
117	Alvin_2661	-4.51800	0.00000	-2.86280	0.00000	protein of unknown function DUF323
118	Alvin_2136	-4.48900	0.00000	-5.23926	0.00000	hypothetical protein Alvin_2136
119	Alvin_0358	-4.48400	0.00000	-2.88033	0.00008	Sulfur globule protein SgpB
120	Alvin_1435	-4.33700	0.00000	-2.80998	0.00244	Ferritin Dps family protein
121	Alvin_0853	-4.30100	0.00000	-3.68585	0.00000	chaperonin GroEL
122	Alvin_1508	-4.30000	0.00000	-4.14736	0.00000	sulfur relay protein, TusE/DsrC/DsvC family
123	Alvin_1253	-4.28600	0.00000	-6.29671	0.00000	DsrE
124	Alvin_0009	-4.18800	0.00000	-3.41842	0.00002	heat shock protein Hsp20
125	Alvin_1251	-4.15400	0.00001	-6.13220	0.00000	DsrA
126	Alvin_1196	-4.09200	0.00130	-3.07994	0.00602	hypothetical protein Alvin_1196
127	Alvin_1468	-4.09100	0.00000	-2.19877	0.00006	YceI family protein
128	Alvin_1258	-4.07200	0.00000	-4.40475	0.00000	DsrK
129	Alvin_2572	-4.07200	0.00000	-2.23733	0.00755	RNA polymerase, sigma 32 subunit, RpoH
130	Alvin_2107	-3.97400	0.00000	-4.00759	0.00000	hypothetical protein Alvin_2107
131	Alvin_1249	-3.96400	0.00000	-2.69533	0.00001	hypothetical protein Alvin_1249
132	Alvin_1359	-3.95700	0.00000	-2.68777	0.00000	ATP-dependent chaperone ClpB
133	Alvin_1853	-3.95000	0.00000	-3.30998	0.00001	efflux transporter, RND family, MFP subunit
134	Alvin_1920	-3.94000	0.00000	-1.44750	0.01952	Superoxide dismutase

135	Alvin_1260	-3.88200	0.00000	-3.89936	0.00000	DsrJ
136	Alvin_2660	-3.85600	0.00000	-2.36466	0.00001	methyltransferase
137	Alvin_2965	-3.83500	0.00000	-1.22483	0.06844	TPR repeat-containing protein
138	Alvin_1254	-3.80600	0.00000	-5.11243	0.00000	DsrF
139	Alvin_1259	-3.78800	0.00000	-4.26736	0.00000	DsrL
140	Alvin_2498	-3.69100	0.00000	-3.73957	0.00000	nitrogen fixation-related protein
141	Alvin_0962	-3.68100	0.00000	-4.67203	0.00000	Ankyrin
142	Alvin_0312	-3.65800	0.00000	-2.47037	0.00000	fructose-bisphosphate aldolase, class II, Calvin cycle subtype
143	Alvin_1323	-3.63800	0.00000	-3.08184	0.00000	glutathione-disulfide reductase
144	Alvin_2032	-3.63300	0.00000	-1.72341	0.01358	Peroxiredoxin
145	Alvin_2668	-3.59000	0.00000	-1.69169	0.01158	Fe-S metabolism associated SufE
146	Alvin_0258	-3.57200	0.00000	-2.34403	0.00011	Rhodanese domain protein
147	Alvin_2063	-3.54800	0.00000	-3.13616	0.00009	hypothetical protein Alvin_2063
148	Alvin_1918	-3.54100	0.00000	-1.88289	0.00255	glutaredoxin-like protein
149	Alvin_2497	-3.52600	0.00000	-3.95960	0.00000	hypothetical protein Alvin_2497
150	Alvin_0707	-3.49700	0.00000	-2.91770	0.00000	regulatory protein LuxR
151	Alvin_1386	-3.40500	0.00000	-3.04613	0.00000	chaperone protein DnaK
152	Alvin_1121	-3.39300	0.00000	-2.94566	0.00000	AprA
153	Alvin_2980	-3.37200	0.00000	-1.84823	0.00687	hypothetical protein Alvin_2980
154	Alvin_1120	-3.36700	0.00000	-2.82683	0.00000	AprB
155	Alvin_1119	-3.34600	0.00000	-2.62406	0.00000	AprM
156	Alvin_0739	-3.33000	0.00000	-2.33654	0.00001	FeS assembly protein SufB

157	Alvin_1849	-3.30400	0.00000	-1.80284	0.00912	pyridoxamine 5'-phosphate oxidase
158	Alvin_0008	-3.29500	0.00000	-2.00419	0.00337	ABC transporter related protein
159	Alvin_1385	-3.29500	0.00000	-2.84268	0.00000	GrpE protein
160	Alvin_1366	-3.28600	0.00000	-2.42851	0.00000	Ribulose-bisphosphate carboxylase
161	Alvin_1202	-3.27400	0.00000	-2.63562	0.00000	ATPase-like, ParA/MinD
162	Alvin_1248	-3.26000	0.00000	-2.11134	0.00008	CRISPR-associated protein, Cas6-related protein
163	Alvin_1743	-3.19200	0.00000	-0.27103	0.74298	hypothetical protein Alvin_1743
164	Alvin_1261	-3.18700	0.00000	-3.57439	0.00000	DsrO
165	Alvin_1256	-3.12200	0.00000	-2.92513	0.00000	DsrC
166	Alvin_2033	-3.11800	0.00000	-1.78691	0.00324	oxidoreductase FAD/NAD(P)-binding domain protein
167	Alvin_1467	-3.11100	0.00000	-1.74520	0.00005	Alcohol dehydrogenase GroES domain protein
168	Alvin_1742	-3.09900	0.00011	-1.15364	0.15792	protein of unknown function DUF134
169	Alvin_0779	-3.07900	0.00000	-1.21753	0.07006	Peptidase M23
170	Alvin_2600	-3.07400	0.00000	-2.18069	0.00000	SirA family protein
171	Alvin_3241	-3.02600	0.00000	-2.21372	0.00102	protein of unknown function DUF302
172	Alvin_1365	-3.00600	0.00000	-3.61826	0.00000	Ribulose-bisphosphate carboxylase
173	Alvin_0766	-2.98000	0.00000	-2.39901	0.00006	protein of unknown function DUF198
174	Alvin_1118	-2.97800	0.00000	-2.26536	0.00000	sulfate adenylyltransferase
175	Alvin_0316	-2.97700	0.00000	-3.62772	0.00000	transketolase
176	Alvin_0315	-2.96600	0.00000	-2.61535	0.00000	glyceraldehyde-3-phosphate dehydrogenase, type I
177	Alvin_2274	-2.96300	0.00000	-1.03173	0.03793	High potential iron-sulfur protein
178	Alvin_1994	-2.94000	0.00000	-1.50599	0.00724	ubiquinone biosynthesis O-methyltransferase

179	Alvin_1384	-2.87200	0.00000	-2.42538	0.00003	heat-inducible transcription repressor HrcA
180	Alvin_3233	-2.86200	0.00000	-1.62916	0.01004	putative thiol-disulphide oxidoreductase DCC
181	Alvin_2037	-2.83700	0.00000	-3.15420	0.00000	protein of unknown function DUF224 cysteine-rich region domain protein
182	Alvin_3032	-2.81500	0.00000	-1.82847	0.00000	hypothetical protein Alvin_3032
183	Alvin_1905	-2.81300	0.00000	-0.09347	0.92141	sulfur globule protein SgpA
184	Alvin_3291	-2.80000	0.00120	-1.65722	0.08524	hypothetical protein Alvin_3291
185	Alvin_2038	-2.78900	0.00000	-3.04488	0.00000	hypothetical protein Alvin_2038
186	Alvin_0740	-2.77900	0.00000	-2.22862	0.00000	FeS assembly ATPase SufC
187	Alvin_3201	-2.77900	0.00000	-1.01489	0.02318	hypothetical protein Alvin_3201
188	Alvin_2500	-2.77400	0.00000	-1.87253	0.00004	cytochrome d ubiquinol oxidase, subunit II
189	Alvin_1262	-2.76900	0.00000	-3.03167	0.00000	DsrP
190	Alvin_2043	-2.76800	0.00000	-2.49875	0.00000	methionine aminopeptidase, type I
191	Alvin_0680	-2.75500	0.00000	-0.60990	0.29837	protein of unknown function DUF1271
192	Alvin_1735	-2.72000	0.00001	-2.11920	0.00102	transcriptional coactivator/pterin dehydratase
193	Alvin_1255	-2.70400	0.00000	-2.00428	0.00020	DsrH
194	Alvin_0742	-2.69100	0.00000	-1.70465	0.00011	FeS assembly SUF system protein
195	Alvin_2031	-2.67700	0.00000	-1.54317	0.01211	Protein of unknown function, PGPGW, transmembrane
196	Alvin_0804	-2.65900	0.00000	-2.73827	0.00000	pyruvate dehydrogenase complex dihydrolipoamide acetyltransferase
197	Alvin_2422	-2.64800	0.00000	-1.09223	0.01609	NADH-quinone oxidoreductase, chain I
198	Alvin_1387	-2.63300	0.00010	-2.26139	0.00155	chaperone protein DnaJ
199	Alvin_1744	-2.61600	0.00000	0.06565	0.94296	GTP-binding protein HSR1-related protein
200	Alvin_2425	-2.61100	0.00000	-1.13274	0.03590	NADH-quinone oxidoreductase, F subunit

201	Alvin_1420	-2.60700	0.00060	-1.24118	0.15866	transcriptional regulator, BadM/Rrf2 family
202	Alvin_1318	-2.60600	0.00000	-2.53913	0.00000	4Fe-4S ferredoxin iron-sulfur binding domain protein
203	Alvin_0007	-2.59900	0.00000	-1.64337	0.00438	protein of unknown function DUF214
204	Alvin_2011	-2.57300	0.00000	-1.11443	0.02165	hypothetical protein Alvin_2011
205	Alvin_2039	-2.56300	0.00000	-2.99001	0.00000	hydrogenase (NiFe) small subunit HydA
206	Alvin_0259	-2.55900	0.00000	-1.96990	0.00004	Peptidylprolyl isomerase
207	Alvin_0313	-2.55800	0.00000	-2.47144	0.00000	pyruvate kinase
208	Alvin_3070	-2.53800	0.00002	-1.54475	0.02006	hypothetical protein Alvin_3070
209	Alvin_2423	-2.53400	0.00000	-1.05110	0.00218	NADH dehydrogenase (quinone)
210	Alvin_2418	-2.53300	0.00000	-0.99578	0.03167	proton-translocating NADH-quinone oxidoreductase, chain M
211	Alvin_0741	-2.52100	0.00000	-2.26309	0.00000	FeS assembly protein SufD
212	Alvin_2486	-2.50600	0.00000	-1.02581	0.07162	protein of unknown function DUF399
213	Alvin_2499	-2.49200	0.00000	-2.64854	0.00000	cytochrome bd ubiquinol oxidase subunit I
214	Alvin_2426	-2.49000	0.00000	-1.28653	0.01661	NADH-quinone oxidoreductase, E subunit
215	Alvin_1257	-2.47900	0.00160	-3.43621	0.00001	DsrM
216	Alvin_2601	-2.45200	0.00000	-1.54003	0.00000	hypothetical protein Alvin_2601
217	Alvin_0082	-2.43300	0.00000	-1.34260	0.00571	peptide methionine sulfoxide reductase
218	Alvin_0055	-2.42400	0.00000	-1.29942	0.02667	SOUL heme-binding protein
219	Alvin_2427	-2.41200	0.00000	-1.30477	0.00485	NADH dehydrogenase I, D subunit
220	Alvin_2419	-2.41100	0.00000	-1.13170	0.00242	proton-translocating NADH-quinone oxidoreductase, chain L
221	Alvin_0754	-2.39800	0.00000	-1.45560	0.00836	molybdopterin oxidoreductase
222	Alvin_2424	-2.37200	0.00000	-1.21027	0.00040	NADH-quinone oxidoreductase, chain G

223	Alvin_2064	-2.36300	0.00002	-1.79373	0.00236	protein of unknown function DUF255
224	Alvin_1852	-2.33900	0.00000	-2.30534	0.00000	acriflavin resistance protein
225	Alvin_1426	-2.33100	0.00000	-1.23238	0.01371	ATP-dependent protease La
226	Alvin_2765	-2.32100	0.00000	-0.67183	0.10311	cytochrome c prime
227	Alvin_1524	-2.31000	0.03200	-1.39866	0.24601	Protein of unknown function DUF1920
228	Alvin_3069	-2.26800	0.00001	-1.82751	0.00050	Thioredoxin domain protein
229	Alvin_0805	-2.25000	0.00000	-2.67738	0.00000	2-oxo-acid dehydrogenase E1 subunit, homodimeric type
230	Alvin_2421	-2.23900	0.00000	-0.82927	0.05385	NADH-ubiquinone/plastoquinone oxidoreductase chain 6
231	Alvin_2548	-2.23400	0.01300	-0.79207	0.48061	antenna complex alpha/beta subunit
232	Alvin_2550	-2.22000	0.02100	-1.49804	0.16279	antenna complex alpha/beta subunit
233	Alvin_3000	-2.21300	0.00000	-2.38885	0.00000	glutamine synthetase, type I
234	Alvin_2549	-2.20500	0.02200	-0.89094	0.45195	antenna complex alpha/beta subunit
235	Alvin_2036	-2.20300	0.00000	-2.45086	0.00000	nickel-dependent hydrogenase large subunit
236	Alvin_1861	-2.19800	0.00000	-1.03785	0.04105	membrane-flanked domain protein
237	Alvin_3199	-2.18600	0.30000	0.76726	0.70457	hypothetical protein Alvin_3199
238	Alvin_2221	-2.18300	0.00000	-1.56662	0.00027	ATP-dependent Clp protease, ATP-binding subunit clpA
239	Alvin_2414	-2.17000	0.00003	-0.91874	0.11935	hypothetical protein Alvin_2414
240	Alvin_2042	-2.16200	0.00005	-2.21448	0.00005	UTP-GlnB uridylyltransferase, GlnD
241	Alvin_0106	-2.14900	0.00091	-1.83859	0.00665	Rubredoxin-type Fe(Cys)4 protein
242	Alvin_2979	-2.13200	0.00000	-1.60443	0.00049	20S proteasome A and B subunits
243	Alvin_2576	-2.11400	0.15000	-0.57546	0.76751	antenna complex alpha/beta subunit
244	Alvin_1860	-2.09700	0.00000	-0.87187	0.01272	hypothetical protein Alvin_1860
245	Alvin_2034	-2.09300	0.00000	-0.63169	0.12714	hypothetical protein Alvin_2034

246	Alvin_0912	-2.08700	0.00000	0.48259	0.33664	Redoxin domain protein
247	Alvin_2001	-2.07200	0.00000	-2.12764	0.00000	putative transcriptional regulator, Crp/Fnr family
248	Alvin_3089	-2.07100	0.00000	-1.13468	0.00018	cytochrome B561
249	Alvin_0321	-2.07000	0.00000	-1.44673	0.00013	5,10-methylenetetrahydrofolate reductase
250	Alvin_1322	-2.06400	0.00001	-1.66455	0.00078	2,3-bisphosphoglycerate-independent phosphoglycerate mutase
251	Alvin_1325	-2.06100	0.01400	0.42618	0.70766	sulfur globule protein SgpC
252	Alvin_0157	-2.05400	0.00001	-1.09993	0.03737	FAD linked oxidase domain protein
253	Alvin_2501	-2.05300	0.00027	-1.40364	0.01945	cyd operon protein YbgT
254	Alvin_2662	-2.05200	0.00013	-1.48160	0.01095	peptidase S16 lon domain protein
255	Alvin_1917	-2.04500	0.00000	-1.41077	0.00102	ribonuclease T
256	Alvin_2571	-2.03900	0.00036	-0.72959	0.29184	magnesium chelatase accessory protein
257	Alvin_2171	-2.03000	0.00000	-0.02045	0.97000	sulfur transferase, SoxL
258	Alvin_1079	-2.02700	0.00000	-2.22934	0.00000	cytochrome B561
259	Alvin_1198	-2.02400	0.00006	-1.34525	0.01533	protein-export membrane protein SecF
260	Alvin_2108	-2.01600	0.00078	-1.36676	0.03863	ATPase associated with various cellular activities AAA_5
261	Alvin_3234	-2.01400	0.00006	-1.37086	0.01204	sec-C motif domain protein
262	Alvin_0320	-2.00900	0.00001	-1.95427	0.00003	adenosylhomocysteinase

Chapter 5 Conclusion

5.1 Summary of Major Findings

The present research project has been conducted with the overarching objective of understanding if purple sulfur bacteria, i.e., *A. vinosum* may utilize solid-phase metal sulfide nanoparticles as sulfur and electron donors, and if so, what underlying mechanisms drive the cell-metal sulfide interactions. I also developed specific hypotheses that have served as guiding principles throughout the study.

Firstly, it was hypothesized that *A. vinosum* possesses the ability to utilize synthetic and natural metal sulfide (MS), especially their nanoparticles forms, as the sole electron donor for growth. Three disctinct types of MS were tested, including iron sulfide and nickel sulfide nanoparticles synthesized from simple anoxic aqueous chemistry, and pyrite, which are pulvurized powders of a natural pyrite crystal. The *A. vinosum* cells showed identifiable growth using all three solid phases although the corresponding growth patterns and gene expressions showed major distinctions.

Secondly, it was hypothesized that *A. vinosum* can actively interact with MS (nano)particles through a range of cell-solid interfacial processes beyond the dissolution effect. If the cell growth on MS were results of the utilization of soluble sulfide resulting from MS dissolution, the growth should follow very similar pathways as the positive control using a soluble sulfide source. However, in my experiments of the three cell-MS systems, I identified major and intriguing variations in the cells' gene expressions compared to those in the positive control.

Lastly, it was hypothesized that *A. vinosum* may possess EET capabilities, which enables the autotrophic growth of the cells using MS as sulfur and electron donors. In my experiments,

strong hints were identified for EET mechanisms involved in the bacterial scavenging of the MS substrate. However, further studies are required to fully clarify the EET pathways.

Overall, I have achieved all the major goals through my systematic experiments, data collection, and data analysis of the *A. vinosum*-MS systems.

5.2 Comparison of Growth Profiles among Different Metal Sulfide Systems

5.2.1 NiS growth profiles

Unexpectedly in the case of NiS, IC shows no change in the concentration of sulfate in solution over time. This would correlate with no sulfide oxidation in a NiS system. Nonetheless, NiS culture showed more growth than negative control, meaning that NiS growth must be supported by other pathways beyond those that support negative control. The unchanging concentration of sulfate in solution could be explained by activation of the sulfate assimilation pathway which would lead to utilization of cell-made sulfate for its assimilation into sulfur containing molecules like cystine and thus would maintain constant sulfate levels. This possibility is supported by the upregulation of Alvin_2447 (8-fold), adenylylsulfate reductase, which is involved in sulfate assimilation (Bick *et al.*, 2000). When compared to the other MS systems, this same gene is upregulated 4-fold in FeS and 8-fold in pyrite. Thus, all MS systems would display a lower sulfate concentration in IC as a portion of the sulfate generated by sulfur oxidation would be reabsorbed and integrated into the cell. A group studying sulfate reduction pathway in *Methanothermococcus thermolithotrophicus* found that at least 100uM of Na_2SO_4 was assimilated to support the cell's functions (Jespersen *et al.*, 2023).

A second potential explanation of constant sulfate levels would be that a metal oxidizing pathway is driving part of the energy metabolism in the NiS cultures like the Mto mechanisms found in *Sideroxidans lithotropicus* (Shi *et al.*, 2016). In this case, the ions could be selectively be

removed from the NiS through chelating molecules and oxidized through a membrane bound porin complex that would transfer electrons through quinone into the reaction center of the photosynthetic apparatus (Shi *et al.*, 2016). In this instance, the vacancies generated in solid by leaving nickel ions in the surface of NiS would need to be occupied by other ions, modifying the surface to contains scattered non-nickel cations, or charge imbalance generated by the vacancies could lead to sulfide release in solution that would be used by the cell in anoxygenic photosynthesis. HR-TEM evidence only showed the presence of Vaesite (NiS_2) and Millerite (NiS), so no evidence of crystal phases incorporating other elements. In the case of XPS though, there is an unknown peak at ~854eV which was theorized to rise from adventurous carbon from extracellular matrix material covering the surface of NiS. Nonetheless, this unknown peak could also represent surface modification of NiS by ions like sodium, potassium of other transition metals filling up vacancies. It's important to highlight that XPS is an analysis of the outermost layers of materials, while HRTEM relies on scattered fields that have begun displaying lattice fringes for mineral identification. When looking at data from ICP-MS to track changes of Nickel in solution, an unusual pattern appeared where concentration shifted drastically between 0.5-3ppm during the first 200h and kept of fluctuating mildly with a downwards trend. So, there was no net release of Nickel into the water column, despite upregulation of efflux genes. This could mean that flux of ions between cell and NiS eventually reached equilibrium and that expelled ions are being integrated back into solid NiS surface through vacancies generated by leaving Ni^{2+}. However, XPS did not show any 3+ oxidation peaks eliminating this as a pathway the A. vinsoum may be using energy metabolism when grown with Nickel. Nonetheless, there is evidence of a peak at ~852eV which falls within elemental Nickel range. This is interesting as it shows that *A. vinsoum* as being electrochemically active. The negative control showed significant growth potential on a system

lacking sulfur and most likely polymeric carbon in the form of yeast extract. Thus, if electron generated from this unidentified pathway were expelled from cell it could lead to nickel reduction keeping nickel ion levels constant in solution and potentially releasing some sulfide for its oxidation. This would mean that *A. vinsoum* would not contribute in natural systems in the release of nickel into the water column.

The third potential explanation would be that sulfate is not being produced because only sulfide is being oxidized and cells are accumulating elemental sulfur intracellularly. Nonetheless, this last possibility is unlikely as there were no signs of elemental sulfur on XPS or HRTEM and is likely that in the cell rupture procedure of sample prep for these techniques, remnants of it would have remained. It is also important to keep in mind that concentration changes of sulfate are expected to be low, primarily because changes of MS systems would occur from surface modifications. The interfacial interaction of the cell and MS systems would lead to slower kinetics and lower concentrations of sulfate and ions. In summary, the *dsr* transcriptomic downregulation compared to negative control and other MS systems suggests that sulfur oxidation is taking place at low rates compared to positive control. The constant sulfate concentrations are likely to reductive assimilation pathway but still active as observed by more vigorous cell density compared to negative control. The exact mechanism through which this is happening is difficult to narrow without more information, but the mechanisms seems to lead to dissociation of both sulfide and Nickel ions from NiS substrate.

In terms of sulfide depletion profiles, no change was observed. Regardless, of the mechanism of sulfide oxidation taking place in NiS cultures, the kinetics would be slow being an interfacial process. In other words, the expected sulfide release in NiS is expected to be slow and whenever available surrounding cells can intake it and oxidize it immediately before escaping in

solution. Nonetheless, this does suggest proximity between cells and NiS substrate. Finally, optical density (OD) plots for Nickel displays higher density of cells compared to the negative control. Meaning, that cells at the very least are following a complementary pathway aside from the one that negative control is using to generate energy and lead to the observed growth profile.

5.2.2 Pyrite growth profiles

The IC plot for the pyrite culture shows a significant increase of approximately 6 mM in sulfate concentration in the positive control, while the sulfate concentration remains unchanged for pyrite. Surprisingly, pyrite exhibited the lowest suppression of *dsr* genes (-5 > log2FC > -2.5) among all the MS systems analyzed. These genes are responsible for intracellular oxidation of elemental sulfur into sulfate. Additionally, the negative control showed even greater suppression of *dsr* genes (-6 > log2FC > -3) despite the absence of a sulfur source, confirming the role of the other MS systems (pyrite: -5 > log2FC > -3, NiS: -4 > log2FC > -3, and pyrite: -5 > log2FC > -3) in facilitating sulfur oxidation, albeit at lower levels than the positive control. The upregulation of Alvin_2447 also indicates active sulfate assimilation, likely leading to the suppression of sulfate levels in the media.

The concentration of sulfide remains unchanged over time, indicating its rapid uptake by the bacteria from pyrite. The increase in sulfate concentration in the media, as confirmed by the IC plot, further supports sulfide oxidation. The rapid utilization of sulfide, as seen in the sulfide depletion plot, suggests that any sulfide released from pyrite is quickly consumed by the cells. The optical density plot shows slightly higher cell density in the pyrite culture compared to the negative control. Interestingly, cultures with more finely ground pyrite exhibited similar optical density to NiS in this study. The lag phase for pyrite culture was around 100 hours before growth began, while the negative control took a similar time to reach the top of the log phase. Upregulation of

genes related to formate dehydrogenase (Alvin_2453 and Alvin_2452) may contribute to growth, but genetic profiling indicates increased formate dehydrogenase activity in the negative control as well, suggesting that pyrite may also utilize a secondary pathway involving sulfur oxidation. Regarding XPR analysis for pyrite, only Fe(II) oxidation peaks were observed in both the control and biotic samples, indicating no iron oxidation occurred upon exposure to *A. vinosum*. The absence of changes in oxidation state, combined with evidence supporting active sulfur oxidation, suggests a continuous flux of iron ions between pyrite and the cells or their accumulation inside the cell. However, assessing sulfur content is challenging due to uncertainties in polysulfide and disulfide changes caused by the introduction of peaks labeled as unknown, which affected the shifting area values.

5.2.3 FeS growth profiles

The IC plot for the FeS culture reveals a significant increase of 400uM of sulfate in the solution. However, due to the culture's reducing conditions, it suggests that the oxidation process occurred intracellularly. Surprisingly, among all the MS systems analyzed, FeS exhibited the highest suppression of *dsr* genes (-5 > log2FC > -3), which are responsible for intracellular oxidation of elemental sulfur into sulfate. Furthermore, it is worth noting that the negative control showed even greater suppression of *dsr* genes (-6 > log2FC > -3) despite the absence of a sulfur source. This validates that the other MS systems (FeS: -5 > log2FC > -3, NiS: -4 > log2FC > -3, and pyrite: -5 > log2FC > -3) do indeed facilitate sulfur oxidation, albeit at much lower levels than the positive control. Specifically, their sulfur oxidation activity is approximately 32 to 16 times lower compared to the positive control.

In the case of sulfide is clear that there is no perceivable change in its concentration over time. Just as previously discussed, sulfate increment in media as shown by IC does confirm sulfide

oxidation. The unchanging pattern most likely reflect close association between bacteria and FeS and its immediate uptake into the cell. Furthermore, IC shows 400uM change in sulfate, when compared to positive control that shows capacity to process 6.1mM it makes sense for sulfide that gets released from FeS to be depleted as soon as it becomes available. Surprisingly, optical density plot is very puzzling, revealing a culture supporting less cell density than the negative control. This is very confusing because it would strongly point to FeS cell density to be supported by the same pathway that supports the growth on the negative control. When looking at the OD plot, it took FeS culture ~700hr to leave the lag phase and start to grow. In contrast the negative control took a few days to reach the top of the log curve. This difference in lag periods could be explained if the FeS culture was lagging due to toxicity of the surrounding FeS. Hence, lag difference could not be used to differentiate between distinguish energy metabolic pathways and it is still possible that FeS is growing using negative control unidentified pathway reaching similar cellular density. This is further supported by the comparable FeS upregulation of Alvin_2453 (4-fold) and Alvin_2452 (4-fold) related to formate dehydrogenase, which is similarly upregulated in negative control Alvin_2453 (8-fold) and Alvin_2454 (7-fold). Still, genetic profiling does show an increased formate dehydrogenase activity coming from negative control, which would support that FeS is also using a secondary pathway that involves sulfur oxidation.

Although for this to be true it would mean that sulfide oxidation to sulfate would have to come from abiotic factors. In an anaerobic closed system this is unlikely, specially since the concentration changed considerably to 0.4mM to ~1/16 of what of the sulfate displayed by positive control. If you couple both *dsr* expression with sulfate concentration changes in solution it points to sulfur oxidation pathway most likely without following path that negative control took. This

must be the case if both negative control and FeS OD are the same and changes in sulfate in the medium are so high.

In the case of XPR for FeS, there is a peak at 706eV which falls within the range of metallic iron, just like it did for biotic sample of NiS. This peak could also reflect electron transfer activity come from *A. vinosum*. It's also important to highlight that Fe (III) related peaks also appeared in the XPS spectra. FeS is very sensitive to oxidation and despite careful sample preparation is likely that the oxidation show here comes from abiotic factors and formed at some point during sample preparation and analysis. Nonetheless, since electron transfer is a possibility, is important to highlight that it's been proposed that this process has been proposed as bidirectional giving rise to the possibility of an Iron oxidation pathway (Shi L *et al.,* 2016). Unlike Nickel, Iron requires less energy for oxidation as show by XPS 2p ranges of Nickel (850-862eV) and Iron (705-712eV). Furthermore, some EAB proposed mechanisms point to the involvement of cytochrome based molecules as drivers of redox reactions, which themselves rely on Iron active centers. This heme coordination centers, which use Fe-S motifs, modulate redox potential based on chelated molecules which are used for reversible redox reactions. Since it Ni (II) peaks require more energy to knock bonding electrons compared to Fe(III) peaks it would make sense for Ni(III) peaks to be absent from XPS while Fe(III) are present in Iron region. Thus, the possibility of Iron oxidation cannot be completely ruled out.

5.3 Transcriptome comparison of MS and negative control

A. vinosum transcriptomes of MS and negative control cultures displayed the upregulation of key proteins which suggest that culture growth was sustained through more than one metabolic pathway and provided insights into potential mechanisms of electrochemically active process.

5.3.1 Negative control

5.3.1.1 Negative control analysis

The fact that *A. vinosum* is growing in the absence of a sulfur source is surprising. This microorganism is extremely adaptable and can growth heterotrophically as well, capable of growing in organic acids like formate, acetate, propionate, butyrate, pyruvate, fumarate, succinate, malate and glycolate that act as electron donors. Nonetheless, culture media lacked all of these with the only organic carbon sources being HEPES (N-2-hydroxyethylpiperazine-N'-2-ethanesulfonic acid) and yeast extract. HEPES is a buffering agent with no known instances of its utilization for growth. It's unlikely that this can be used by bacteria for energy as enzymatic pathways that transform sugars and organic acids tend to be very substrate specific and this molecule is not only larger than usual substrates but it also contains varied functional groups. The other carbon source available in the media is yeast extract, which is suspect for fueling photoheterotrophic energy metabolism. Regardless, of the energy metabolic pathway being used by *A. vinosum* in negative control, it's supporting its growth to cell densities comparable to FeS and growing to lower than cell densities supported by both NiS and pyrite.

In terms of genetic profiling the negative control displayed severe downregulation of photosynthetic *puc* and *puf* genes, but not as much as MS transcriptomes. This would suggest that the energy metabolic pathway being used depends on LH1 and LH2 complexes. The sulfur oxidation genes *sox* and *dsr* showed the most downregulation compared to MS transcriptomes, which would be expected for a culture lacking a sulfur source. The negative control was the transcriptome that was the closest to the positive control with very few upregulated genes. Nonetheless, compared to MS transcriptomes there were several genes that followed the same expression pattern. Aside from all transcriptomes showing downregulation on photosynthetic

genes (i.e *puc* and *puf*) and sulfur oxidation genes (i.e *sox* and *dsr*), other relevant redox genes followed the similar expression levels to MS transcriptomes.

5.3.1.2 Formate dehydrogenase negative control

One of the interesting findings in the negative control is the upregulation of Alvin_2453 (8-fold) and Alvin_2454 (7-fold), which code for formate dehydrogenase. This enzyme allows the reduction of carbon dioxide into formate in the presence of an electron donor. In other organisms it has been found that NADH acts as the electron donor for formate generation (Calzadiaz-Ramirez *et al.*, 2022). Since NADH is generated in glycolysis, it would mean that the cells are most likely using carbon from the yeast extract, or potentially they could be utilizing another electron donor to form formate. This substrate has been reported to support the growth of *A. vinosum* (Weissgerber T *et al.*, 2011). It's important to highlight that culture media does contain significant amount of $NaHCO_3$ (i.e 35mM) to fuel the formation of formate. Nonetheless, for formate to form 2 moles of electron are needed per mole of carbon dioxide, thus the limiting factor would be the electron donor.

5.3.1.3 Hydogenases as potential electron generating pathway

It is important to mention that the negative control also upregulated Alvin_2309 hydrogenase (NiFe) small subunit HydA (8-fold), which catalyzes the reversible reaction of converting hydrogen gas to protons and electrons. This would offer an alternative source of electrons to drive metabolic processes including formate generation. Nonetheless, even though hydrogen was introduced in the bottle during sampling, it would still be found in trace amounts, which would question the extend of its contribution in the overall growth of the MS bottles. Other hydrogenase related genes were also upregulated Alvin_2306 (8-fold), Alvin_2307 (11-fold) and Alvin_2308 (7-fold), all of which seem to make different subunits of an Ni/Fe hydrogenase, which

aside from the reversible splitting of hydrogen into electrons and protons it also has been found to be involved in nitrogen fixation.

5.3.1.4 Evaluation of the existence of EET mechanisms

Other interesting genes that were found to be upregulated were Alvin_1094 (34-fold) and Alvin_1143 (4-fold). These genes code for an ankyrin containing protein and the twin-arginine translocation pathway signal, respectively. Ankyrins are membrane associated proteins that are thought to stabilize membrane and are involved in cell signaling pathways. On the other hand, the twin-arginine pathway transports folded proteins across the membrane of which some have been shown to contain redox cofactors (Palmer T *et al.,* 2012). This is very exciting as it opens the possibility of an EET pathway that is supporting growth. The direction of the flow of electrons remains a question, even though the electrons generated from hydrogenases might suggest the release of electrons from the cell, the scarcity of hydrogen remains a factor. Furthermore, if this were to be the case, the loss of electrons would change redox condition in intracellular space ultimately leading to the oxidation of NADH and thus would suggest an alternative electron donor source. Conversely, twin-arginine pathway opens up the possibility of redox active proteins to be expelled from the cell and potentially oxidize yeast components bringing electrons back to fuel formate formation and subsequent oxidation in glycolysis.

Furthermore, the small transcriptome of the negative control also showed upregulation of flavocytochrome genes, Alvin_1092 (17-fold) and Alvin_1093 (25-fold). Flavocytochromes have seen to be involved in EET metal reducing pathway of *S. odinensis* where electrons are taken from quinol to membrane (Shi L *et al.*, 2016). EET mechanisms are believed to be bidirectional allowing release and import of electrons within the same pathway (Shi L *et al.*, 2016).

Because of all of this, it seems reasonable to propose that negative control is not using common carbon metabolic pathways to support its growth. Instead, the evidence seems to point out to a potential bidirectional EET pathway in which electrons are transported across the membrane and fueling the growth of bacteria in the negative control. More importantly, it suggests that *A. vinosum* can potentially use EET to transport electrons across the membrane.

5.3.2 MS Transcriptomes

Upregulation of hydrogenases seem to point to an electron generating pathway from hydrogen gas that is likely at least partially used to generate formate to be used in glycolysis and fuel growth in FeS, pyrite and negative control with no formate dehydrogenase expression found for NiS transcriptome. Nonetheless, contribution of this pathway for culture growth may be limited due not only due to the scarcity of hydrogen in media but by growth profiles of NiS and pyrite supporting a higher cell population density.

Sulfur oxidation genes were less downregulated, in terms of expression values, compared to the MS systems. Downregulation of *dsr* genes compared to the negative control and the unchanged expression of *sox* genes compared to positive control provide evidence for sulfur oxidation pathways to be active in all MS systems. This is further supported by XPS sulfur spectra of both FeS and NiS, which seem to show decreased disulfide peaks. Furthermore, FeS show a higher polysulfide fraction observed in the NiS XPS sulfur spectra (17%) compared to the in the FeS control (14.3%), while NiS XPS sulfur spectra showed 10.8% polysulfide in biotic sample compared to the 1.8% in the NiS control and XPS biotic pyrite which seems to show a reduced sulfide peak, although an appearance of a fourth peak in the biotic sample makes it hard to determine if polysulfide content increased or not. The fewer downregulated *dsr* genes in MS cultures compared to negative control indicate that sulfur oxidation pathway is active. In addition,

the expression of *sox* genes remained relatively stable or slightly downregulated for MS systems compared to the positive control, and their expression levels in the negative control were comparable. These results suggest that *sox* genes may play a more significant role in supporting sulfur oxidation compared to *dsr* genes. Notably, *sox* genes are known to be involved in the oxidation of polysulfides to sulfate, which provides a plausible explanation for the increased levels in biotic FeS and NiS samples. The expression profile of *dsr* and *sox* as well as XPS evidence strongly support the notion that the cultured bacteria utilize sulfide from MS solid. Even the marginal change in polysulfide content in the biotic FeS XPS sample is also coherent with a culture that reached a low cell density, while pyrite OD being slightly higher than the negative control would be explained as well by the reduced surface area of the pyrite chunks compared to nanoparticles and small aggregates of the other MS systems.

Pili have been demonstrated to play a crucial role in establishing a connection between bacterial cells and solid substrate materials by directly contacting the surface of these materials, as observed in various strains of the *Geobacter* genus (Lovley *et al.*, 2019). In our study, the upregulation of flagellar genes Alvin_1952-1954 and pilin gene Alvin_3016 in the presence of pyrite, as well as gene Alvin_326 in FeS, suggests their potential involvement in facilitating movement and direct contact with the MS substrate. These findings align with other observations in our study, further supporting the significance of this interaction. The relatively low optical density (OD) of the pyrite sample, in contrast to NiS, could be attributed to the limited surface area provided by the roughly ground pyrite chunks. In instances where pyrite growth was not analyzed for transcriptomic analysis, we observed OD values comparable to those displayed by NiS in our study. This potential relationship between growth and surface area underscores the importance of direct cell-substrate contact for enhanced substrate utilization. (Lovley *et al.*, 2019).

One thing that stood out within all MS growth conditions was the upregulation of transporter genes. Genes like Alvin_0014 and Alvin_0015 encode efflux transporters which, exhibited the least upregulation in all MS systems with an eight-fold upregulation in the NiS transcriptome compared to the positive control. In the FeS transcriptome, these genes demonstrated three- and two-fold higher expression, respectively, in comparison to the NiS transcriptome. Interestingly, in the presence of pyrite, these genes were upregulated twice as much as in the NiS condition. Additionally, the FeS transcriptome exhibited the expression of other efflux genes, Alvin_0013, which showed a considerable upregulation of 20-fold and Alvin_0019 involved in Fe2+ ion efflux with a 10-fold upregulation. Thus, FeS displayed the most upregulation followed by pyrite and then NiS. These efflux proteins are believed to be involved in metallic ion discharge from within the cell, which would mean that ions are getting inside of the cell in the first place. Thus, confirming a bidirectional flux of metal ions between the cell and its environment. It is important to remember that Pyrite, NiS and FeS are all considered insoluble sulfides, thus dissolution under the anaerobic conditions in the culture bottle is not expected to happen.

On the other hand, the negative control did not display any changes in the expression of transporter genes compared to positive control; this is important. The first scenario for upregulation of transporter genes to be limited to MS systems could reflect the toxicity related to bioaccumulation of Nickel and Iron in the respective MS systems. Despite this being a possibility, this could also be challenged by the upregulation of other transporter genes in the transcriptome that are thought to facilitate intake of metallic ions into the cell. In the case of FeS transcriptome, Alvin_1062 (4.6-fold) and Alvin_1063 (5.6-fold) are TRAP (tripartite ATP independent periplasmic) transporters which Mulligan has deemed as substrate binding channels that intake molecules into the cell, of which e metal-chelate complexes have been shown to be uptaken

(Mulligan *et al.*, 2011). It's important to point out that this study is not specific for *A. vinosum* and does not mean that metal-chelate complexes is what is being take into the cell. Still, it's a reasonable inference when looking at the increasing intracellular ion concentrations. Furthermore, it is important to remember that pyrite, NiS and FeS are all considered insoluble sulfides, thus dissolution under the anaerobic conditions in the culture bottle is not expected to happen. One of the mechanisms in which bacteria uses solid materials is by using chelating agents. Hence, introducing the possibility of that the bacteria sensed the MS substrate in the vicinity and modified gene expression to transport constituents into the cell. Not surprisingly, all MS systems activated signal transduction genes with uncharacterized pathways. In the case of FeS, Alvin_0025 (5-fold) and Alvin_0026 (5-fold) were expressed, while on Nickel Alvin_0639 (4-fold) was stimulated, for pyrite Alvin_0067 (2-fold) was upregulated and no signal transduction gene was upregulated in the negative control. This means that MS presence indeed activated the gene machinery in the cell as expected, although there is not enough information to infer the exact mechanisms through which this happens.

In our study, we investigated the expression of conserved hypothetical genes in four different systems: NiS, pyrite, FeS, and a negative control. The results revealed intriguing findings that support an active electron transfer pathway supporting the growth of *A. vionsum*. In the NiS group, highly expressed genes such as Alvin_1447 exhibited the Gly-zipper_YMGG motif. These genes also contained transmembrane (TM) domains, suggesting their potential association with the cellular membrane. This highlights the potential role of this protein in facilitating electron transfer across the membrane to support other metabolic pathways in the cell. Similarly, in the pyrite group, Alvin_0022 displayed a motif found in Cytochrome c-type proteins, along with a TM domain and a signal peptide sequence. These characteristics suggest a potential role in EAB-

related processes, as the presence of TM domains and signal peptides is often associated with membrane-associated proteins involved in extracellular electron transfer. In the FeS group, Alvin_0016 exhibited a proteobacteria-restricted protein motif (DUF3240) and a TM domain, while Alvin_0017 had a signal peptide and multiple motifs (DUF3340, DUF2992). This suggest the potential secretion of a redox active protein, which can be associated with EET and reductive dissolution EAB pathways. In the pyrite group, Alvin_1094 displayed an ankyrin repeat motif and a signal peptide, indicating its potential involvement in protein-protein interactions and possible export. Additionally, we observed the presence of the OmpA motif in Alvin_3273, which is associated with the porin-cytochrome complex in EET pathway (Shi L *et al.*, 2016).

Overall, the expression patterns and the presence of TM domains, signal peptides, and specific motifs in these conserved hypothetical genes across different systems indicate their potential role in extracellular electron transfer and membrane-associated processes. These findings provide valuable insights into the potential involvement of these genes in EAB mechanisms in metal sulfide environments, shedding light on novel pathways and mechanisms underlying bacterial responses to insoluble metal sulfides. Further investigations are warranted to uncover the precise functions of these genes and their contributions to electron transport processes in different environmental contexts.

Probably the biggest evidence found in this study to support EAB capability by *A. vinsoum* lies in rich transcriptome upregulation of heme binding molecules, some of which thought to be membrane bound or exported. Protein motif were used to associate proteins with excretory pathways (i.e signal peptide), membrane association (i.e LXXC motif) or reversible redox capabilities (i.e CXXCH motif). This was the strategy used in narrowing down the proteins that had the higher probability of being involved in EET and reductive dissolution mechanisms.

Cytochrome molecules along with flavins have been found to be involved in EET and reductive dissolution strategies by different groups (You L *et al.*, 2018 and Dulay H *et al.*, 2020). Likely due to the reversible redox capabilities of these molecules, they are ideal for the transport of electrons. Gene Alvin_1093 a c-type flavocytochrome and Alvin_1095 annotated as NapC/NirT cytochrome c domain protein, with the latter containing a LXXC lipid binding motif, displayed outstanding upregulation in all MS systems and the negative control. Both proteins are considerably upregulated in all systems, highlighting their importance in supporting growth in their respective cultures. NapC/NirT cytochrome c domain protein has been associated before with oxidation of nitrite to nitrate, still all anaerobic cultures only contain ammonia as a nitrogen source prohibiting this pathway in all systems (Reyes F *et al.*, 1996). Interestingly, according to STRINGdb, it is associated with ccmA, which has been linked to conductive nanowires (Costa *et al.*, 2018) (Alvin_1095 in STRINGdb). In addition, this protein contains a lipid binding motif, supporting evidence of its involvement in a novel electron transfer pathway. In the case of Alvin_1093, flavocytochromes have been linked in the past with EET and reductive dissolution pathways (Shi L *et al.*, 2016 and Dulay H *et al.*, 2020).

Other proteins that did not appear in the negative control transcriptome, which also were scanned for signal peptide, LXXC and CXXCH motifs make up proteins that are potentially involved in electron transport processes in the presence of MS. In the case of pyrite, a diheme cytochrome c Alvin_0020 (21-fold), DUF1924 motif containg Alvin_0022 (138-fold) and diheme cytochrome c Alvin_0023 all heme binding proteins were shown to contain signal peptides, while Alvin_0020 also contained a lipid binding motif. For the NiS transcriptome, both Alvin_1402 (4-fold) a Fe-S cluster assembly protein Nifu and Alvin_3135 (6-fold) heme binding proteins contain lipid binding motifs. Finally in the case of FeS, diheme cytochrome c Alvin_0023 (7-fold),

DUF1924 Alvin_0022 (7-fold) and diheme cytochrome c Alvin_0020 (10-fold) all were found to contain signal peptides, while diheme cytochrome c peroxidase Alvin_0018 (8-fold) and aforementioned Alvin_0020 contain lipid binding motifs.

These findings reveal the expression of cytochrome genes with specific motifs, such as the CXXCH heme binding motif, LXXC lipid binding motif, and signal peptides, providing insights into which cytochrome proteins could be associated with the membrane of the cell or be excreted out to facilitate electron transfer between the cell and its environment.

Photosynthetic genes displayed downregulation across all samples compared to the positive control with the most downregulation experienced by the MS systems pyrite>FeS>NiS across both *puf* anc *puc* genes. The negative control showed downregulation as well but considerably less than the MS systems suggesting a bigger reliance of the photosynthetic system for the negative control. The only MS system that grew to a lower cell density than the negative control was FeS. As mentioned previously in this chapter, there is enough evidence to support the idea that negative control may be using an electrochemically active pathway to support its metabolism. If the negative control and MS systems were supporting their growth at least partially due to electron transport related processes., it would explain the similarities in the expression of CXXCH and LXXC motif proteins with all MS systems. Furthermore, FeS expression evidence points to active sulfur oxidation. This is the only MS system that showed evident increase in sulfate in IC. Still, the culture grew less than the negative control growing in the same media constituents and concentrations with the added FeS. A potential vital difference between the FeS and the other systems is that particles are black and remain in suspension much longer compared to NiS which forms aggregates and settles quicker, while pyrite with settles immediately. This likely reduced the amount of light that reaches the photosynthetic apparatus in the cells. If the reaction center,

LH1, LH2, or carotenoids were involved in the electron transfer it would make sense that FeS culture would have the most depressed growth of all the MS systems. Carotenoid related genes expression remained largely unchanged compared to the positive control for all systems. Thus, the reduced OD of FeS compared to negative control may end up the connection needed to highlight the importance of the photosynthetic apparatus in the electron transport processes found in *A. vinosum*.

5.4 Hypothesis re-evaluation

By thoroughly investigating these hypotheses, this study aimed to provide valuable insights into the metabolic capabilities of *A. vinosum* and to unravel the gene expression patterns associated with its utilization and interaction with metal sulfide nanoparticles. The findings derived from this research contribute to a deeper understanding of the mechanisms underlying microbial interactions with nanoparticles, paving the way for potential applications in various fields, including biotechnology and environmental remediation.

1. *A. vinosum* possesses the ability to utilize synthetic metal sulfide (MS) nanoparticles as the sole electron donor for growth?

The study uncovered evidence suggesting that *A. vinosum*, is possibly utilizing hydrogenases, which produced electrons that likely fueled formate production, whose oxidation can generate ATP. Additionally, findings indicated active sulfur oxidation from MS systems, as evidenced by reductive sulfate assimilation and consistent sulfate concentrations for pyrite and NiS, while FeS exhibited an increase in sulfate levels. Furthermore, *dsr* and *sox* expression profile showed evidence of increase polysulfide production in NiS and FeS as shown in XPS. The upregulation of ion transporters and the minimal to no ion concentration changes in MS systems, along with the observed modifications of MS surface observed through metallic peaks for Fe and

Ni on XPS and TEM analyses showing increased crystallization and presence of chalcopyrite for FeS (copper containing mineral), provided further indications of ion flux between the cell and MS systems. In summary, it's unresolved if hydrogen supports solid-phase utilization, if it does at all considering the limiting nature of it, or to what extent. Nonetheless, there is sufficient evidence to suggest that *A. vinosum* is supporting growth using MS as a source of electrons.

2. *A. vinosum* can actively interact with the interface of MS nanoparticles, leading to the release of both metal ions and sulfur into the surrounding environment.

Based on the observations made in this study, it can be concluded that the hypothesis stating that *A. vinosum* can actively interact with the interface of MS nanoparticles, leading to the release of both metal ions and sulfur into the surrounding environment, has not been fully proven.

In the case of NiS, no noticeable changes in the concentration of nickel ions were observed, suggesting that *A. vinosum* does not release nickel ions into the water column from minerals such as millerite (NiS) and potentially vaesite (NiS2) in natural systems. Similarly, minimal to no changes in iron concentration were detected for pyrite using ICP-MS. However, there was an increase in the concentration of iron ions when FeS was subjected to *A. vinosum* compared to the control. This indicates that *A. vinosum* might contribute to the release of iron ions into the water column from FeS, potentially benefiting local microbial ecosystems.

Furthermore, based on ion chromatography (IC) results and transcriptomic expression of *dsr* genes compared to the negative control, cells exposed to MS cultures exhibited sulfur oxidation, albeit at lower rates than the positive control. This suggests that *A. vinosum* can partially oxidize sulfur in the presence of MS nanoparticles. The upregulation of specific flagellar and pilin genes in the presence of pyrite indicates their potential involvement in facilitating movement and direct contact with the MS substrate. The limited surface area provided by roughly ground pyrite

chunks may contribute to the lower optical density (OD) observed compared to NiS. The importance of direct cell-substrate contact for enhanced substrate utilization is further emphasized by the relationship between growth and surface area.

While a flux of ions between cells and MS systems has been identified, leading to surface modifications of MS substrates, the overall evidence suggests that the active interaction of *A. vinosum* with MS nanoparticles in terms of metal ion and sulfur release is not fully supported by the observed results of this study. Further research is needed to explore and confirm the extent of *A. vinosum*'s interaction with MS nanoparticles and the consequent release of metal ions and sulfur to the surrounding water column.

3. Gene expression of *A. vinosum* would exhibit discernible differences when exposed to MS nanoparticles compared to growth under soluble sulfide conditions.

Although gene expression in the MS systems showed similarities to the negative control, there is compelling evidence to suggest that this is due to an uncharacterized electron transfer pathway by electrochemically active *A. vinosum* to harvest energy from surrounding molecules. However, it is noteworthy that MS systems, except for FeS, exhibited a larger and more diverse transcriptome compared to the negative control, pyrite, and NiS. This observation is supported by the presence of a substantial number of upregulated and downregulated genes in all MS systems, indicating significant differences in gene expression patterns compared to the positive control.

5.5 Important findings and potential applications

Some evidence found in this transcriptome analysis support the possibility that *A. vinosum* may be using an extracellular electron transfer (EET) pathway to harvest the electrons from MS substrates. Evidence included but not limited to XPS evidence showing reduction of metal ions and potential oxidation on FeS, while gene expression profiles of *sox* and *dsr* genes along with IC

evidence in MS systems compared to negative control support that MS cultures are successfully using MS as sulfur and electron source. The ability of *A. vinosum* to participate in electron transfer processes enhances its ecological relevance and holds promise for microbial fuel cells, offering sustainable energy production alternative.

The differences in growth profiles between FeS, pyrite and NiS further provide insights into not only the need for direct contact of cells with MS substrates, as observed by reduced culture cell density based on surface area, but also the potential need for photosynthesis molecules potentially carotenoids or RC as part of the possible EET pathway found in this study.

Another relevant finding is the potential association of Alvin_1095, annotated as NapC/NirT cytochrome c domain protein and thought to be involved in nitrite oxidation (Reyes F *et al.*, 1996), with a novel EET pathway. This protein is likely membrane bound as suggested by presence of LXXC motif. In our experimental setup there is no nitrate or nitrite, only ammonia, in the media composition prohibiting this pathway in culture

A formate production pathway was observed in *A. vinosum* which would permit regulation of CO_2 in water systems which has ecological and commercial significance, providing a cost-effective route for valuable formate production. Moreover, its photosynthetic capabilities, metabolic versatility, open doors for bioenergy production, environmental remediation, and pharmaceutical applications. Overall, *A. vinosum's* EET capabilities and unique properties present opportunities for sustainable and innovative solutions in various domains.

5.6 Limitations

It is crucial to acknowledge the limitations associated with transcriptomic studies, despite their valuable insights into gene expression patterns. These limitations include the potential for incomplete coverage due to incomplete reference databases, the disparity between gene expression

and protein abundance (Li Y *et al.*, 2018), and technical variability in sample processing. Furthermore, the dynamic nature of gene expression may not be captured in a single time point along with the challenges in functional interpretation with limiting annotation data. In this study tracking of sulfate, sulfide, growth rate and metal ion concentrations were measured over time to complement transcriptomic findings. Nonetheless, understanding these limitations allows for a more cautious interpretation of transcriptomic findings and emphasizes the importance of integrating multiple approaches to validate and gain a more comprehensive understanding of gene expression results.

5.7 Future work

Regardless of the evidence found in this study, suggesting that *A. vinosum* is using a series of cytochrome molecules to harvest electrons from MS systems, it is essential to further confirm this by monitoring this electron transfer using electrodes. Conducting electrochemical experiments that directly couple these bacteria with metallic surfaces would provide valuable insights into the electron transport processes between the solid-phase and the bacterial cells. Additionally, complementing these experiments with proteomic analysis would enhance our understanding of the underlying mechanisms. Proteomic analysis can reveal the protein composition, modifications, and interactions involved in electron transport, offering insights into post-transcriptional regulations, protein-protein interactions, and functional characterization. Moreover, incorporating metabolomic profiling techniques into the study would allow for the investigation of metabolic changes during electroactive growth, helping identify key metabolites involved in electron transfer. By integrating electrochemical experiments, proteomic analysis, and metabolomic profiling, a comprehensive understanding of the electron transport mechanisms, as well as potential redox mediators or electron shuttles, can be achieved.

REFERENCES

1. Abee, T., Knol, J., Hellingwerf, K.J. *et al.* A Kdp-like, high-affinity, K^+-translocating ATPase is expressed during growth of *Rhodobacter sphaeroides* in low potassium media. *Arch. Microbiol.* **158**, 374–380 (1992). https://doi.org/10.1007/BF00245368
2. Andrews, S. (2010). FastQC: A quality control tool for high throughput sequence data. [Online]. Available online at: https://www.bioinformatics.babraham.ac.uk/projects/fastqc/
3. Anthony M. Bolger and others, Trimmomatic: a flexible trimmer for Illumina sequence data, *Bioinformatics*, Volume 30, Issue 15, August 2014, Pages 2114–2120, https://doi.org/10.1093/bioinformatics/btu170
4. Argüello JM, González-Guerrero M, Raimunda D. Bacterial transition metal P(1B)-ATPases: transport mechanism and roles in virulence. Biochemistry. 2011 Nov 22;50(46):9940-9. doi: 10.1021/bi201418k. Epub 2011 Oct 31. PMID: 21999638; PMCID: PMC3224801.
5. Armitage, J.P. 2009. "Swimming and Behavior in Purple Non-Sulfur Bacteria." In The Purple Phototrophic Bacteria, 643–54. Springer, Dordrecht. https://doi.org/10.1007/978-1-4020-8815-5_32.
6. Axelrod, H., Miyashita, O., and Okamura, M. 2009. "Structure and Function of the Cytochrome c2: Reaction Center Complex from Rhodobacter Sphaeroides." Photosynth Res 85, 101–114 (2005). https://doi.org/10.1007/s11120-005-1368-8.
7. Axelsen, K., Palmgren, M. Evolution of Substrate Specificities in the P-Type ATPase Superfamily. *J Mol Evol* **46**, 84–101 (1998). https://doi.org/10.1007/PL00006286

8. Badger, M.R., and Bek, E.J. 2008. "Multiple Rubisco Forms in Proteobacteria: Their Functional Significance in Relation to CO_2 Acquisition by the CBB Cycle." Journal of Experimental Botany 59 (7): 1525–41. https://doi.org/10.1093/jxb/erm297.
9. Bick JA, Dennis JJ, Zylstra GJ, Nowack J, Leustek T. Identification of a new class of 5'-adenylylsulfate (APS) reductases from sulfate-assimilating bacteria. J Bacteriol. 2000 Jan;182(1):135-42. doi: 10.1128/JB.182.1.135-142.2000. PMID: 10613872; PMCID: PMC94249.
10. Bickle, M. J., *et al.* "Sulfur transport and sulfur isotope fractionations in ocean floor hydrothermal systems." Mineralogical Magazine, (1994) 58A, pp. 88-89.
11. Bird LJ, Coleman ML, Newman DK. Iron and copper act synergistically to delay anaerobic growth of bacteria. Appl Environ Microbiol. 2013 Jun;79(12):3619-27. doi: 10.1128/AEM.03944-12. Epub 2013 Apr 5. PMID: 23563938; PMCID: PMC3675935.
12. Blankenship, R.E. 2010. "Early Evolution of Photosynthesis." Future Perspectives in Plant Biology. http://www.plantphysiol.org/content/154/2/434.full
13. Boags AT, Samsudin F, Khalid S. Binding from Both Sides: TolR and Full-Length OmpA Bind and Maintain the Local Structure of the E. coli Cell Wall. Structure 27, 713-724.e2, (2019). PMID: 30713026
14. Breuer, M., Rosso, K.M., Blumberger, J., and Butt, J.N. 2015. "Multi-Haem Cytochromes in Shewanella Oneidensis MR-1: Structures, Functions and Opportunities." Journal of the Royal Society, Interface 12 (102). https://doi.org/10.1098/rsif.2014.1117.
15. Brune, D. 1995. "Sulfur Compounds as Photosynthetic Electron Donors." In: Blankenship, R.E., Madigan, M.T., Bauer, C.E. (eds) Anoxygenic Photosynthetic Bacteria. Advances in

Photosynthesis and Respiration, vol 2. Springer, Dordrecht. https://doi.org/10.1007/0-306-47954-0_39.

16. Buranaki, E., *et al.* "Voltammetric characterization of metal sulfide particles and nanoparticles in model solutions and natural waters." Analytica chimica acta, (2007), 594, pp. 44–51.
17. Caltech.edu. (2023, March 8). Unexpected Findings Change Picture of Sulfur on Early Earth. Caltech About News. Retrieved from https://www.caltech.edu/about/news/unexpected-findings-change-picture-sulfur-early-earth-44407
18. Cannell, A., Blamey, N., Brand, U., Escapa, I., & Large, R. (2022). A revised sedimentary pyrite proxy for atmospheric oxygen in the Paleozoic: Evaluation for the Silurian-Devonian-Carboniferous period and the relationship of the results to the observed biosphere record. Earth-Science Reviews, 231, 104062. https://doi.org/10.1016/j.earscirev.2022.104062
19. Carlson, H. K. *et al.* Surface multiheme c-type cytochromes from Thermincola potens and implications for respiratory metal reduction by Gram-positive bacteria. Proc. Natl Acad. Sci. USA 109, 1702–1707 (2012).
20. Chen, L., Fang, W., Chang, J., Liang, J., Zhang, P., & Zhang, G. (2022). Improvement of Direct Interspecies Electron Transfer via Adding Conductive Materials in Anaerobic Digestion: Mechanisms, Performances, and Challenges. Frontiers in Microbiology, 13, 860749. https://doi.org/10.3389/fmicb.2022.860749
21. Chen, Z.W., Koh, M., Van Driessche, G., Van Beeumen, J.J., Bartsch, R.G., Meyer, T.E., Cusanovich, M.A., and Mathews, F.S. 1994. "The Structure of Flavocytochrome c Sulfide

Dehydrogenase from a Purple Phototrophic Bacterium." Science 266 (5184): 430–32. https://doi.org/10.1126/science.7939681.

22. Chong, G.W., Karbelkar, A.A., and El-Naggar, M.Y. 2018. "Nature's Conductors: What Can Microbial Multi-Heme Cytochromes Teach Us about Electron Transport and Biological Energy Conversion?" Current Opinion in Chemical Biology 47 (December): 7–17. https://doi.org/10.1016/j.cbpa.2018.06.007.
23. Cohen-Bazire, G., Sistrom, W.R., and Stanier, R.Y. 1957. "Kinetic Studies of Pigment Synthesis by Non-Sulfur Purple Bacteria." Journal of Cellular and Comparative Physiology 49 (1): 25–68. https://doi.org/10.1002/jcp.1030490104.
24. Costa, N. L., Clarke, T. A., Philipp, L.-A., Gescher, J., Louro, R. O., & Paquete, C. M. (2018). Electron transfer process in microbial electrochemical technologies: The role of cell-surface exposed conductive proteins. *Bioresource Technology*, *255*, 308-317. doi:10.1016/j.biortech.2018.01.133
25. Costa, N. L., Clarke, T. A., Philipp, L.-A., Gescher, J., Louro, R. O., & Paquete, C. M. (2018). Electron transfer process in microbial electrochemical technologies: The role of cell-surface exposed conductive proteins. *Bioresource Technology*, *255*, 308-317. doi:10.1016/j.biortech.2018.01.133
26. Dahl C, Franz B, Hensen D, Kesselheim A, Zigann R. Sulfite oxidation in the purple sulfur bacterium Allochromatium vinosum: identification of SoeABC as a major player and relevance of SoxYZ in the process. Microbiology (Reading). 2013 Dec;159(Pt 12):2626-2638. doi: 10.1099/mic.0.071019-0. Epub 2013 Sep 12. PMID: 24030319.
27. Dahl, C. (2008). Inorganic Sulfur Compounds as Electron Donors in Purple Sulfur Bacteria. In: Hell, R., Dahl, C., Knaff, D., Leustek, T. (eds) Sulfur Metabolism in

Phototrophic Organisms. Advances in Photosynthesis and Respiration, vol 27. Springer, Dordrecht. https://doi.org/10.1007/978-1-4020-6863-8_15

28. Dahl, C. (2020). Bacterial Intracellular Sulphur Globules. In: Jendrossek, D. (eds) Bacterial Organelles and Organelle-like Inclusions. Microbiology Monographs, vol 34. Springer, Cham. https://doi.org/10.1007/978-3-030-60173-7_2
29. Dahl, C. 2015. "Cytoplasmic Sulfur Trafficking in Sulfur-Oxidizing Prokaryotes." IUBMB Life 67 (4): 268–74. https://doi.org/10.1002/iub.1371.
30. Dahl, C. 2017. "Sulfur Metabolism in Phototrophic Bacteria." In Modern Topics in the Phototrophic Prokaryotes, edited by Patrick C. Hallenbeck, 27–66. Cham: Springer International Publishing. https://doi.org/10.1007/978-3-319-51365-2_2.
31. Dahl, C., Engels S, Pott-Sperling As, Schulte A, Sander J, Lübbe Y, Deuster O, and Brune Dc. 2005. "Novel Genes of the *dsr* Gene Cluster and Evidence for Close Interaction of *dsr* Proteins during Sulfur Oxidation in the Phototrophic Sulfur Bacterium *Allochromatium vinosumAllochromatium vinosum*." Journal of Bacteriology 187 (4). https://doi.org/10.1128/JB.187.4.1392-1404.2005.
32. Daldal, *et al.* "Advances in Photosynthesis and Respiration, 28: Purple Phototrophic Bacteria." Springer, (2008).
33. Danza F, Ravasi D, Storelli N, Roman S, Lüdin S, Bueche M, Tonolla M. Bacterial diversity in the water column of meromictic Lake Cadagno and evidence for seasonal dynamics. PLoS One. 2018 Dec 26;13(12):e0209743. doi: 10.1371/journal.pone.0209743. PMID: 30586464; PMCID: PMC6306205.

34. Deng, R., Chen, Y., (2021). A Critical Review of Resistance and Oxidation Mechanisms of Sb-Oxidizing Bacteria for the Bioremediation of Sb(III) Pollution. Frontiers in Microbiology, 12, 738596. https://doi.org/10.3389/fmicb.2021.738596
35. Dincturk, Benan, *et al.* "*Bd* oxidase homologue of photosynthetic purple sulfur bacterium *Allochromatium vinosumAllochromatium vinosum* is co-transcribed with a nitrogen fixation related gene." Antonie van Leeuwenhoek, (2011), 99, pp. 211-220
36. Doyle, L. E., & Marsili, E. (2015). Methods for enrichment of novel electrochemically-active microorganisms. *Bioresource Technology*, 195, 273-282. https://doi.org/10.1016/j.biortech.2015.07.025
37. Drews, G. 1985. "Structure and Functional Organization of Light-Harvesting Complexes and Photochemical Reaction Centers in Membranes of Phototrophic Bacteria." Microbiological Reviews, March. https://doi.org/10.1128/mr.49.1.59-70.1985.
38. DTU Health Tech. (n.d.). SignalP 5.0. Retrieved August 15, 2023, from https://services.healthtech.dtu.dk/services/SignalP-5.0/
39. Dulay H, Tabares M, Kashefi K, Reguera G. Cobalt Resistance via Detoxification and Mineralization in the Iron-Reducing Bacterium *Geobacter sulfurreducens*. Front Microbiol. 2020 Nov 26;11:600463. doi: 10.3389/fmicb.2020.600463. PMID: 33324382; PMCID: PMC7726332.
40. Ehrenreich A, Widdel F. "Anaerobic oxidation of ferrous iron by purple bacteria, a new type of phototrophic metabolism." Appl. Environ, Microbiol., (1994), 12, 4517-4526
41. Epstein, W., Mattle, D., & Yagil, E. (1990). The bacterial Kdp K+-ATPase and its relation to other transport ATPases, such as the Na+/K+- and Ca2+-ATPases in higher organisms.

Philosophical Transactions of the Royal Society of London. Series B, Biological Sciences, 326, 479-487. https://doi.org/10.1098/rstb.1990.0026

42. Fantauzzi, M., Elsener, B., Atzei, D., Rigoldi, A., & Rossi, A. (2015). Exploiting XPS for the identification of sulfides and polysulfides. RSC Advances, 5, 75953-75963.
43. Findlay, A. J. (2016). Microbial impact on polysulfide dynamics in the environment. FEMS Microbiology Letters, 363(11), fnw103. https://doi.org/10.1093/femsle/fnw103
44. Franz, B., Gehrke T., Lichtenberg H., Hormes J., Dahl C., and Prange A. 2009. "Unexpected Extracellular and Intracellular Sulfur Species during Growth of *Allochromatium vinosumAllochromatium vinosum* with Reduced Sulfur Compounds." Microbiology (Reading, England) 155 (Pt 8). https://doi.org/10.1099/mic.0.027904-0.
45. Franz, B., Lichtenberg, H., Hormes, J., Modrow, H., Dahl, C., and Prange, A. 2007. "Utilization of Solid 'Elemental' Sulfur by the Phototrophic Purple Sulfur Bacterium *Allochromatium vinosumAllochromatium vinosum*: A Sulfur K-Edge X-Ray Absorption Spectroscopy Study." Microbiology 153 (4): 1268–74. https://doi.org/10.1099/mic.0.2006/003954-0.
46. Gahlot, Pallavi & Aboudi, Kaoutar & Ahmed, Banafsha & Tawfik, Ahmed & Khan, Abid & Khursheed, Anwar & Tyagi, Vinay & Aboudi, Kautar. (2021). Direct interspecies electron transfer (DIET) via conductive materials in anaerobic digestion of organic wastes. 10.1016/B978-0-323-85223-4.00024-5.
47. Garbini GL, Barra Caracciolo A, Grenni P. Electroactive Bacteria in Natural Ecosystems and Their Applications in Microbial Fuel Cells for Bioremediation: A Review. *Microorganisms*. 2023; 11(5):1255. https://doi.org/10.3390/microorganisms11051255

48. Gartman, Amy and George W.Luther. “Comparison of pyrite (FeS_2) synthesis mechanisms to reproduce natural FeS_2 nanoparticles found at hydrothermal vents.” Geochimica et Cosmochimica Acta, (2013), 120, pp. 447-458.
49. Gorby YA, *et al.* Electrically conductive bacterial nanowires produced by Shewanella oneidensis strain MR-1 and other microorganisms. Proc Natl Acad Sci U S A. 2006 Jul 25;103(30):11358-63. doi: 10.1073/pnas.0604517103. Epub 2006 Jul 18. PMID: 16849424; PMCID: PMC1544091.
50. Gorby, Y. A., Yanina, S., McLean, J. S., Fredrickson, J. K., *et al.* (2006). Electrically conductive bacterial nanowires produced by Shewanella oneidensis strain MR-1 and other microorganisms. Proceedings of the National Academy of Sciences, 103(30), 11358-11363. https://doi.org/10.1073/pnas.0604517103
51. Gregersen, L.H., Bryant, D.A., and Frigaard, N.U. 2011. “Mechanisms and Evolution of Oxidative Sulfur Metabolism in Green Sulfur Bacteria.” Frontiers in Microbiology 2 (May). https://doi.org/10.3389/fmicb.2011.00116.
52. Grein, F., Pereira, I.A.C., Dahl, C. 2010. “Biochemical Characterization of Individual Components of the *Allochromatium vinosumAllochromatium vinosum* DsrMKJOP Transmembrane Complex Aids Understanding of Complex Function In Vivo.” Journal of Bacteriology 192 (24). https://doi.org/10.1128/JB.00849-10.
53. Griesbeck, C., Schütz, M., Schödl, T., Bathe, S., Nausch, L., Mederer, L., Vielreicher, M., and Hauska, S. 2002. “Mechanism of Sulfide-Quinone Reductase Investigated Using Site-Directed Mutagenesis and Sulfur Analysis.” Research-article. ACS Publications. American Chemical Society. World. September 7, 2002. https://doi.org/10.1021/bi026032b.

54. Grimm, F., Dobler, N., and Dahl, C. 2010. "Regulation of *dsr* Genes Encoding Proteins Responsible for the Oxidation of Stored Sulfur in *Allochromatium vinosumAllochromatium vinosum*." Microbiology 156 (3): 764–73. https://doi.org/10.1099/mic.0.034645-0.

55. Grondelle, R., and Novoderezhkin, V.I. 2009. "Spectroscopy and Dynamics of Excitation Transfer and Trapping in Purple Bacteria." In The Purple Phototrophic Bacteria, 231–52. Springer, Dordrecht. https://doi.org/10.1007/978-1-4020-8815-5_13.

56. Guiral, M., Prunetti, L., Aussignargues, C., Ciaccafava, A., Infossi, P., Ilbert, M., Lojou, E., *et al.* 2012 "The Hyperthermophilic Bacterium Aquifex Aeolicus: From Respiratory Pathways to Extremely Resistant Enzymes and Biotechnological Applications." In Advances in Microbial Physiology, 61:125–94. Academic Press. https://doi.org/10.1016/B978-0-12-394423-8.00004-4.

57. Hacking, K.A. 2015 "Characterisation of the LH2 Complexes of *Allochromatium vinosumAllochromatium vinosum*." Doctoral dissertation.

58. Hallbeck L, Pedersen K. Culture parameters regulating stalk formation and growth rate of Gallionella ferruginea. Journal of General Microbiology. 1990;136:1675.

59. Han, D. S., Batchelor, B., & Abdel-Wahab, A. (2013). XPS analysis of sorption of selenium (IV) and selenium (VI) to mackinawite (FeS). Environmental Progress & Sustainable Energy, 32(1), 84-93. ISSN 1944-7442. https://doi.org/10.1002/ep.10609

60. *Handbook of Metalloproteins*. 2001. eds. Messerschmidt, A., Huber, R., Poulos, T. & Wieghardt, K. (Wiley, Chichester, U.K.)

61. Hanson, T.E., and Tabita F.R. 2003. "Insights into the Stress Response and Sulfur Metabolism Revealed by Proteome Analysis of a Chlorobium Tepidum Mutant Lacking

the Rubisco-like Protein." Photosynthesis Research 78 (3). https://doi.org/10.1023/B:PRES.0000006829.41444.3d.

62. Hanson, T.E., and Tabita, F.R. 2001. "A Ribulose-1,5-Bisphosphate Carboxylase/Oxygenase (RubisCO)-like Protein from Chlorobium Tepidum That Is Involved with Sulfur Metabolism and the Response to Oxidative Stress." Proceedings of the National Academy of Sciences 98 (8): 4397–4402. https://doi.org/10.1073/pnas.081610398.
63. Hashimoto, H., Fujii, R., Yanagi, K., Kusumoto, T., Gardiner, A.T., Cogdell, R.J., *et al.* 2006. "Structures and Functions of Carotenoids Bound to Reaction Centers from Purple Photosynthetic Bacteria." Pure and Applied Chemistry 78 (8): 1505–18. https://doi.org/10.1351/pac200678081505.
64. Hayashi, H., and Morita, S. 1980. "Near-Infrared Absorption Spectra of Light Harvesting Bacteriochlorophyll Protein Complexes from Chromatium Vinosum." Journal of Biochemistry 88 (5). https://doi.org/10.1093/oxfordjournals.jbchem.a133093.
65. Hayashi, N.R., Arai, H., Kodama, T., and Igarashi, Y. 1999. "The CbbQ Genes, Located Downstream of the Form I and Form II RubisCO Genes, Affect the Activity of Both RubisCOs." Biochemical and Biophysical Research Communications 265 (1). https://doi.org/10.1006/bbrc.1999.1103.
66. Hensen, D., Sperling, D., Trüper, H.G., Brune, D.C., and Dahl, C. 2006. "Thiosulphate Oxidation in the Phototrophic Sulphur Bacterium *Allochromatium vinosumAllochromatium vinosum*." Molecular Microbiology 62 (3): 794–810. https://doi.org/10.1111/j.1365-2958.2006.05408.x.

67. Hochella, *et al.* "Nanominerals, mineral nanoparticles, and Earth systems." Science, (2008), 21, pp. 1631-1635

68. Hoffman, P. F., Kaufman, A. J., Halverson, G. P., & Schrag, D. P. (1998). A Neoproterozoic Snowball Earth. Science, 281(5381), 1342-1346. DOI: 10.1126/science.281.5381.1342

69. Hu, S., Wu, Y., Ding, Z., Shi, Z., Li, F., & Liu, T. (2020). Facet-dependent reductive dissolution of hematite nanoparticles by Shewanella putrefaciens CN-32. Environmental Science: Nano, 7(2), 2522-2531. https://doi.org/10.1039/D0EN00555J

70. Hubas C, Jesus B, Ruivo M, Meziane T, Thiney N, Davoult D, *et al.* (2013) Proliferation of Purple Sulphur Bacteria at the Sediment Surface Affects Intertidal Mat Diversity and Functionality. PLoS ONE 8(12): e82329. https://doi.org/10.1371/journal.pone.0082329

71. Hunter, N.C., Daldal, F., Thurnauer, M.C., Beatty, J.T. (Eds.) 2009 "The Purple Phototrophic Bacteria." Springer, Dordrecht. https://link.springer.com/book/10.1007/978-1-4020-8815-5.

72. Hunter, Neil, *et al.* The Purple Phototrophic Bacteria. . Vol. 28, Springer, 2009.

73. Hurtgen, M. T., Arthur, M. A., & Prave, A. R. (2004). The sulfur isotope composition of carbonate-associated sulfate in Mesoproterozoic to Neoproterozoic carbonates from Death Valley, California. *SPECIAL PAPERS-GEOLOGICAL SOCIETY OF AMERICA*, 177-194.

74. James G. Ferry, Formate dehydrogenase, FEMS Microbiology Reviews, Volume 7, Issue 3-4, December 1990, Pages 377–382, https://doi.org/10.1111/j.1574-6968.1990.tb04940.x

75. Jing X, Wu Y, Shi L, Peacock CL, Ashry NM, Gao C, Huang Q, Cai P. Outer Membrane *c*-Type Cytochromes OmcA and MtrC Play Distinct Roles in Enhancing the Attachment of *Shewanella oneidensis* MR-1 Cells to Goethite. Appl Environ Microbiol. 2020 Nov

10;86(23):e01941-20. doi: 10.1128/AEM.01941-20. PMID: 32978123; PMCID: PMC7657618.

76. Kasai T, Kouzuma A, Nojiri H, Watanabe K. Transcriptional mechanisms for differential expression of outer membrane cytochrome genes omcA and mtrC in Shewanella oneidensis MR-1. BMC Microbiol. 2015 Mar 21;15:68. doi: 10.1186/s12866-015-0406-8. PMID: 25886963; PMCID: PMC4417206.
77. Kato S., *et al.* "Methanogenesis facilitated by electric syntropy via (semi) conductive iron-oxide minerals." Environ. Microbiol. (2012), 14, pp. 1646–1654.
78. Kawano Y, Suzuki K, Ohtsu I. Current understanding of sulfur assimilation metabolism to biosynthesize L-cysteine and recent progress of its fermentative overproduction in microorganisms. Appl Microbiol Biotechnol. 2018 Oct;102(19):8203-8211. doi: 10.1007/s00253-018-9246-4. Epub 2018 Jul 26. PMID: 30046857.
79. Kessler, D. 2006. "Enzymatic Activation of Sulfur for Incorporation into Biomolecules in Prokaryotes." FEMS Microbiology Reviews 30 (6): 825–40. https://doi.org/10.1111/j.1574-6976.2006.00036.x.
80. Kessler, N., Kraemer, S. M., Shaked, Y., & Schenkeveld, W. D. C. (2020). Investigation of Siderophore-Promoted and Reductive Dissolution of Dust in Marine Microenvironments Such as Trichodesmium Colonies. Frontiers in Marine Science, 7, Article 45. https://doi.org/10.3389/fmars.2020.00045
81. Kilby, B.A. 1979. "The Photosynthetic Bacteria: Edited by Roderick K Clayton and William R Sistrom, Pp 946. Plenum Press, New York and London. 1978. £53.55 or $85.00." Biochemical Education 7 (3): 73–73. https://doi.org/10.1016/0307-4412(79)90054-2.

82. Klaus Bosecker, Bioleaching: metal solubilization by microorganisms, *FEMS Microbiology Reviews*, Volume 20, Issue 3-4, July 1997, Pages 591–604, https://doi.org/10.1111/j.1574-6976.1997.tb00340.x

83. Kobayashi, H.A., *et al.* "Use of photosynthetic bacteria for hydrogen, sulfide removal from anaerobic waste treatment effluent". Water research, (1983) 17, pp. 579-587.

84. Koch, T., and Dahl, C. (2018). A novel bacterial sulfur oxidation pathway provides a new link between the cycles of organic and inorganic sulfur compounds. ISME J. 12, 2479–2491. doi: 10.1038/s41396-018-0209-7

85. Koch, T., and Dahl, C. 2018. "A Novel Bacterial Sulfur Oxidation Pathway Provides a New Link between the Cycles of Organic and Inorganic Sulfur Compounds." The ISME Journal 12 (10): 2479–91. https://doi.org/10.1038/s41396-018-0209-7.

86. Kramer, D.M., Nitschke, W., and Cooley, J.W. 2009. "The Cytochrome Bc 1 and Related Bc Complexes: The Rieske/Cytochrome b Complex as the Functional Core of a Central Electron/Proton Transfer Complex." In The Purple Phototrophic Bacteria, 451–73. Springer, Dordrecht. https://doi.org/10.1007/978-1-4020-8815-5_23.

87. Kunito T, Kusano T, Oyaizu H, *et al.* Cloning and sequence analysis of czc genes in Alcaligenes sp. strain CT14. Bioscience, Biotechnology, and Biochemistry. 1996 Apr;60(4):699-704. DOI: 10.1271/bbb.60.699. PMID: 8829543.

88. Langmead, B., & Salzberg, S. (2012). Fast gapped-read alignment with Bowtie 2. Nature Methods, 9(4), 357-359

89. Lavergne, J., Verméglio, A., and Joliot, P. 2009. "Functional Coupling Between Reaction Centers and Cytochrome Bc 1 Complexes." In The Purple Phototrophic Bacteria, 509–36. Springer, Dordrecht. https://doi.org/10.1007/978-1-4020-8815-5_26.

90. Lee Kump, *et al.* "Massive release of hydrogen sulfide to the surface ocean and atmosphere during intervals of ocean anoxia." Geology, (2005) 35, pp. 937-400

91. Li, B., Dewey, C., & Durbin, R. (2011). RSEM: accurate transcript quantification from RNA-Seq data with or without a reference genome. *BMC Bioinformatics*, 12(323). doi:10.1186/1471-2105-12-323

92. Liang, C., Qian, L., Li, H., Dong, X., Zheng, T., & Chen, M. (2023). New insight into the activation mechanism of hydrogen peroxide by greigite (Fe3S4) for benzene removal: The combined action of dissolved and surface bounded ferrous iron. Chemosphere, 321, 138111. https://doi.org/10.1016/j.chemosphere.2023.138111.

93. Light SH, Su L, Rivera-Lugo R, Cornejo JA, Louie A, Iavarone AT, Ajo-Franklin CM, Portnoy DA. A flavin-based extracellular electron transfer mechanism in diverse Gram-positive bacteria. Nature. 2018 Oct;562(7725):140-144. doi: 10.1038/s41586-018-0498-z. Epub 2018 Sep 12. PMID: 30209391; PMCID: PMC6221200.

94. Light, S.H., Su, L., Rivera-Lugo, R. *et al.* A flavin-based extracellular electron transfer mechanism in diverse Gram-positive bacteria. *Nature* 562, 140–144 (2018). https://doi.org/10.1038/s41586-018-0498-z

95. Liu, J., Chen, Q., Yang, Y., Wei, H., Laipan, M., Zhu, R., He, H., & Hochella, M. F. (2022). Coupled redox cycling of Fe and Mn in the environment: The complex interplay of solution species with Fe- and Mn-(oxyhydr)oxide crystallization and transformation. Earth-Science Reviews, 232, 104105. ISSN 0012-8252. https://doi.org/10.1016/j.earscirev.2022.104105

96. Liu, L.J., Stockdreher, Y., Koch, T., Sun, S.T., Fan, Z., Josten, J., *et al.* 2014. "Thiosulfate Transfer Mediated by DsrE/TusA Homologs from Acidothermophilic Sulfur-Oxidizing

Archaeon Metallosphaera Cuprina." Journal of Biological Chemistry 289 (39): 26949–59. https://doi.org/10.1074/jbc.M114.591669.

97. Love, M. I., Huber, W., & Anders, S. (2014). Moderated estimation of fold change and dispersion for RNA-seq data with DESeq2. Genome Biology, 15(12), 550. https://doi.org/10.1186/s13059-014-0550-8

98. Lovley DR, Nevin KP. Electrobiocommodities: powering microbial production of fuels and commodity chemicals from carbon dioxide with electricity. Curr Opin Biotechnol. 2013 Jun;24(3):385-90. doi: 10.1016/j.copbio.2013.02.012. Epub 2013 Mar 4. PMID: 23465755.

99. Lovley, D., Stolz, J., Nord, G. *et al.* Anaerobic production of magnetite by a dissimilatory iron-reducing microorganism. *Nature* 330, 252–254 (1987). https://doi.org/10.1038/330252a0

100. Lovley, D.R., and Walker, D.J.F. 2019. "Geobacter Protein Nanowires." Frontiers in Microbiology 10 (September). https://doi.org/10.3389/fmicb.2019.02078.

101. Lübbe, Y.J., Youn, H.S., Timkovich, R., and Dahl, C. 2006. "Siro(Haem)Amide in *Allochromatium vinosumAllochromatium vinosum* and Relevance of DsrL and DsrN, a Homolog of Cobyrinic Acid a,c-Diamide Synthase, for Sulphur Oxidation." FEMS Microbiology Letters 261 (2): 194–202. https://doi.org/10.1111/j.1574-6968.2006.00343.x.

102. Madigan MT. A novel photosynthetic purple bacterium isolated from a yellowstone hot spring. Science. 1984 Jul 20;225(4659):313-5. doi: 10.1126/science.225.4659.313. PMID: 17749561

103. Madigan, M.T., and Jung, D.O. 2009. “An Overview of Purple Bacteria: Systematics, Physiology, and Habitats.” In The Purple Phototrophic Bacteria, 1–15. Springer, Dordrecht. https://doi.org/10.1007/978-1-4020-8815-5_1.

104. Madigan, M.T., Jung, D.O. (2009). An Overview of Purple Bacteria: Systematics, Physiology, and Habitats. In: Hunter, C.N., Daldal, F., Thurnauer, M.C., Beatty, J.T. (eds) The Purple Phototrophic Bacteria. Advances in Photosynthesis and Respiration, vol 28. Springer, Dordrecht. https://doi.org/10.1007/978-1-4020-8815-5_1

105. Malik, K.A. 1983 “A Modified Method for the Cultivation of Phototrophic Bacteria.” Journal of Microbiological Methods 1 (6): 343–52. https://doi.org/10.1016/0167-7012(83)90011-8.

106. Mansor, M., Cantando, E., Wang, Y., Hernandez-Viezcas, J. A., Gardea-Torresdey, J. L., Hochella Jr., M. F., & Xu, J. (2020). Insights into the Biogeochemical Cycling of Cobalt: Precipitation and Transformation of Cobalt Sulfide Nanoparticles under Low-Temperature Aqueous Conditions. Environmental Science & Technology, 54(9), 5598–5607. https://doi.org/10.1021/acs.est.0c01363

107. Marques ELS, Dias JCT, Gross E, Silva ABCE, de Moura SR, Rezende RP. Purple Sulfur Bacteria Dominate Microbial Community in Brazilian Limestone Cave. Microorganisms. 2019 Jan 23;7(2):29. doi: 10.3390/microorganisms7020029. PMID: 30678083; PMCID: PMC6406701.

108. Mattis AN, Gumport RI, Gardner JF. J. Purification and characterization of bacteriophage P22 Xis protein. Bacteriol. 190, 5781-96, (2008).

109. Mechler, B., and Oelze, J. 1978. “Differentiation of the Photosynthetic Apparatus of Chromatium Vinosum, Strain D.” Archives of Microbiology 118 (1): 109–14. https://doi.org/10.1007/BF00406082.

110. Miller JM, Enemark EJ. Fundamental Characteristics of AAA+ Protein Family Structure and Function. Archaea. 2016 Sep 14;2016:9294307. doi: 10.1155/2016/9294307. PMID: 27703410; PMCID: PMC5039278.

111. Miller, D.J., Biesinger, M.C., & McIntyre, N.S. (2002). Surf. Interface Anal., 33, 2

112. Miranda-Brito, M., Silva, J. C., & Silva, L. S. (2021). Molecular characterization of Pseudomonas aeruginosa OmpA protein and its role in biofilm formation. Frontiers in Microbiology, 12, 727709. https://doi.org/10.3389/fmicb.2021.727709

113. Miranda-Brito, M., Silva, J. C., & Silva, L. S. (2023). Molecular characterization of Pseudomonas aeruginosa OmpA protein and its role in biofilm formation. **Journal of Bacteriology**, 225, e00776. doi: https://doi.org/10.1128/jb.00776

114. Mitchell AC, Peterson L, Reardon CL, Reed SB, Culley DE, Romine MR, Geesey GG. Role of outer membrane c-type cytochromes MtrC and OmcA in Shewanella oneidensis MR-1 cell production, accumulation, and detachment during respiration on hematite. Geobiology. 2012 Jul;10(4):355-70. doi: 10.1111/j.1472-4669.2012.00321.x. Epub 2012 Feb 23. PMID: 22360295.

115. Mueller, E.G. 2006. “Trafficking in Persulfides: Delivering Sulfur in Biosynthetic Pathways.” Nature Chemical Biology 2 (4): 185–94. https://doi.org/10.1038/nchembio779.

116. Müller, F. H., Bandeiras, T. M., Urich, T., Teixeira, M., Gomes, C. M., & Kletzin, A. (2004). Coupling of the pathway of sulfur oxidation to dioxygen reduction: Characterization of a novel membrane-bound thiosulfate:quinone oxidoreductase.

Molecular Microbiology, 53(4), 1147-1160. https://doi.org/10.1111/j.1365-2958.2004.04193.x

117. Mulligan, C., Fischer, M., & Thomas, G. H. (2011). Tripartite ATP-independent periplasmic (TRAP) transporters in bacteria and archaea. FEMS Microbiology Reviews, 35(1), 68-86. https://doi.org/10.1111/j.1574-6976.2010.00236.x

118. Muyzer, G. and Stams, A. J. "The ecology and biotechnology of sulphate-reducing bacteria". Nature Reviews Microbiology. (2008) 6, pp. 441–454.

119. Nagashima, S., and Nagashima, K.V.P. 2013. "Comparison of Photosynthesis Gene Clusters Retrieved from Total Genome Sequences of Purple Bacteria." In Advances in Botanical Research, 66:151–78. Elsevier. https://doi.org/10.1016/B978-0-12-397923-0.00005-9.

120. Nagashima, S., Shimada, K., Matsuura, K., and Nagashima, K.V.P. 2002. "Transcription of Three Sets of Genes Coding for the Core Light-Harvesting Proteins in the Purple Sulfur Bacterium, *Allochromatium vinosumAllochromatium vinosum*." Photosynthesis Research 74 (3): 269–80. https://doi.org/10.1023/A:1021280104053.

121. Niedzwiedzki, D.M., Bina, D., Picken, N., Honkanen, S.,Blankenship, R.E., Holten, D., Cogdell, R.J. 2012 "Spectroscopic Studies of Two Spectral Variants of Light-Harvesting Complex 2 (LH2) from the Photosynthetic Purple Sulfur Bacterium *Allochromatium vinosumAllochromatium vinosum*." Biochimica et Biophysica Acta (BBA) - Bioenergetics 1817 (9): 1576–87. .

122. Nyström, E.; Thomas, H.; Wanhainen, C.; Alakangas, L. Occurrence and Release of Trace Elements in Pyrite-Rich Waste Rock. *Minerals* 2021, *11*, 495. https://doi.org/10.3390/min11050495

123. OECD. (2010). The Bioeconomy to 2030: Designing a Policy Agenda. Retrieved from https://www.oecd-ilibrary.org/docserver/9789264096158-11-en.pdf?expires=1688762704&id=id&accname=guest&checksum=89CCD9CA833913CC4BBC313D0AC1F57C

124. Open Press. (2019, November 20). Isotopic Dating Methods 2. Open Press, University of Saskatchewan. Retrieved from https://openpress.usask.ca/physicalgeology/chapter/19-4-isotopic-dating-methods-2/

125. Ostroumov, E.E., Mulvaney, R.M., Anna, J.M., Cogdell, R.J. and Scholes, G.D. 2013. "Energy Transfer Pathways in Light-Harvesting Complexes of Purple Bacteria as Revealed by Global Kinetic Analysis of Two-Dimensional Transient Spectra." Research-article. ACS Publications. American Chemical Society. World. July 18, 2013. https://doi.org/10.1021/jp403028x.

126. Outten FW, Huffman DL, Hale JA, O'Halloran TV. The independent cue and cus systems confer copper tolerance during aerobic and anaerobic growth in Escherichia coli. The Journal of Biological Chemistry. 2001 Aug;276(33):30670-30677. DOI: 10.1074/jbc.m104122200. PMID: 11399769.

127. Outten FW, Huffman DL, Hale JA, O'Halloran TV. The independent cue and cus systems confer copper tolerance during aerobic and anaerobic growth in Escherichia coli. The Journal of Biological Chemistry. 2001 Aug;276(33):30670-30677. DOI: 10.1074/jbc.m104122200. PMID: 11399769.

128. Overmann, J., Beatty, J.T., and Hall, K.J. 1996. "Purple Sulfur Bacteria Control the Growth of Aerobic Heterotrophic Bacterioplankton in a Meromictic Salt Lake." Applied

and Environmental Microbiology 62 (9). https://doi.org/10.1128/aem.62.9.3251-3258.1996.

129. Overmann, J., Hall, K.J., Northcote, T.G., and Beatty J.T. 1999. "Grazing of the Copepod Diaptomus Connexus on Purple Sulphur Bacteria in a Meromictic Salt Lake." Environmental Microbiology 1 (3). https://doi.org/10.1046/j.1462-2920.1999.00026.x.

130. Overmann, J.J., Beatty, T., and Hall, K.J. 1994. "Photosynthetic Activity and Population Dynamics of Amoebobacter Purpureus in a Meromictic Saline Lake." FEMS Microbiology Ecology 15 (3–4): 309–19. https://doi.org/10.1111/j.1574-6941.1994.tb00254.x.

131. Overmann, Jorg (1997). Advances in microbial ecology. Advances in Microbial Ecology. Vol. 15. Boston, MA: Springer US. pp. 252–258, 278, 279. doi:10.1007/978-1-4757-9074-0

132. Parkes-Loach, P.S., Michalski, T.J., Bass, W.J., Smith, U., and Loach, P.A. 1990. "Probing the Bacteriochlorophyll Binding Site by Reconstitution of the Light-Harvesting Complex of Rhodospirillum Rubrum with Bacteriochlorophyll a Analogues." Biochemistry 29 (12). https://doi.org/10.1021/bi00464a010.

133. Parson, W.W., and Warshel, A. 2009. "Mechanism of Charge Separation in Purple Bacterial Reaction Centers." In The Purple Phototrophic Bacteria, 355–77. Springer, Dordrecht. https://doi.org/10.1007/978-1-4020-8815-5_19.

134. Pattaragulwanit, K., Brune, D.C., Trüper, H.G., and Dahl, C. 1998. "Molecular Genetic Evidence for Extracytoplasmic Localization of Sulfur Globules in Chromatium Vinosum." Archives of Microbiology 169 (5): 434–44. https://doi.org/10.1007/s002030050594.

135. Philippot, Pascal, *et al.* "Globally asynchronous sulphur isotope signals require re-definition of the Great Oxidation Event." Nature Communications, (2018), 9(1).

136. Pi H, Helmann JD. Ferrous iron efflux systems in bacteria. Metallomics. 2017 Jul 19;9(7):840-851. doi: 10.1039/c7mt00112f. PMID: 28604884; PMCID: PMC5675029.

137. Pott, A.S., and Dahl, C. 1998. "Sirohaem Sulfite Reductase and Other Proteins Encoded by Genes at the *dsr* Locus of Chromatium Vinosum Are Involved in the Oxidation of Intracellular Sulfur." Microbiology 144 (7): 1881–94. https://doi.org/10.1099/00221287-144-7-1881.

138. Poza-Carrión C, Jiménez-Vicente E, Navarro-Rodríguez M, Echavarri-Erasun C, Rubio LM. Kinetics of Nif gene expression in a nitrogen-fixing bacterium. J Bacteriol. 2014 Feb;196(3):595-603. doi: 10.1128/JB.00942-13. Epub 2013 Nov 15. PMID: 24244007; PMCID: PMC3911164.

139. Prange, A., Engelhardt, H., Trüper, H.G., and Dahl, C. 2004. "The Role of the Sulfur Globule Proteins of *Allochromatium vinosumAllochromatium vinosum*: Mutagenesis of the Sulfur Globule Protein Genes and Expression Studies by Real-Time RT-PCR." Archives of Microbiology 182 (2): 165–74. https://doi.org/10.1007/s00203-004-0683-3.

140. Rabaey, K., & Rozendal, R. A. (2010). Microbial electrosynthesis—revisiting the electrical route for microbial production. Nature Reviews Microbiology, 8(10), 706-716.

141. Ragsdale SW, Pierce E. Acetogenesis and the Wood-Ljungdahl pathway of CO(2) fixation. Biochim Biophys Acta. 2008 Dec;1784(12):1873-98. doi:

10.1016/j.bbapap.2008.08.012. Epub 2008 Aug 27. PMID: 18801467; PMCID: PMC2646786.

142. Reinartz, M., Tschäpe, J., Brüser, T., Trüper, H.G., and Dahl, C. 1998. "Sulfide Oxidation in the Phototrophic Sulfur Bacterium Chromatium Vinosum." Archives of Microbiology 170 (1). https://doi.org/10.1007/s002030050615.

143. Richardson DJ, Butt JN, Clarke TA. Controlling electron transfer at the microbe-mineral interface. Proc Natl Acad Sci U S A. 2013 May 7;110(19):7537-8. doi: 10.1073/pnas.1305244110. Epub 2013 Apr 29. PMID: 23630260; PMCID: PMC3651448.

144. Rickard, D., *et al.* "Sedimentary sulfides." Elements, (2017) 13(2), pp. 117–122.

145. Rickard, Marc

Mussmann, Jeffrey A. Steadman; Sedimentary Sulfides. *Elements* 2017;; 13 (2): 117–122. doi: https://doi.org/10.2113/gselements.13.2.117

146. Rowe, A.R., Salimijazi, F., Trutschel, L. *et al.* Identification of a pathway for electron uptake in *Shewanella oneidensis*. *Commun Biol* **4**, 957 (2021). https://doi.org/10.1038/s42003-021-02454-x

147. Ruey-an Doong and Bernhard Schink. (2002). Cysteine-Mediated Reductive Dissolution of Poorly Crystalline Iron(III) Oxides by Geobacter sulfurreducens. Environmental Science & Technology, 36(13), 2939-2945. DOI: 10.1021/es0102235.

148. Sander, J., Engels-Schwarzlose, S.,and Dahl, C. 2006. "Importance of the DsrMKJOP Complex for Sulfur Oxidation in *Allochromatium vinosumAllochromatium vinosum* and Phylogenetic Analysis of Related Complexes in Other Prokaryotes." Archives of Microbiology 186 (5): 357–66. https://doi.org/10.1007/s00203-006-0156-y.

149. Scheer, H., Svec, W.A., Cope, B.T., Studier, M.H., Scott, R.G., and Katz, J.J. 2002. "Structure of Bacteriochlorophyll b." ACS Publications. American Chemical Society. World. May 1, 2002. https://doi.org/10.1021/ja00818a092.

150. Seitz, A. P., Nielsen, T. H., & Overmann, J. (1993). Physiology of purple sulfur bacteria forming macroscopic aggregates in Great Sippewissett Salt Marsh, Massachusetts. FEMS Microbiology Ecology, 12(4), 225-235. ISSN 0168-6496.

151. Sharma, I., and Ghangrekar, M. M. "Screening anodic inoculums for microbial fuel cells by quantifying bioelectrogenic activity using tungsten trioxide quantum rods." Bioresource Technology, (2018), 252, pp. 66-71.

152. Shi, L., Dong, H., Reguera, G. *et al.* Extracellular electron transfer mechanisms between microorganisms and minerals. Nat Rev Microbiol 14, 651–662 (2016). https://doi.org/10.1038/nrmicro.2016.93

153. Shi, L., Dong, H., Reguera, G., Beyenal, H., Lu, A., Liu, J., Yu, H.Q., and Fredrickson, J.K. 2016. "Extracellular Electron Transfer Mechanisms between Microorganisms and Minerals." Nature Reviews Microbiology 14 (10): 651–62. https://doi.org/10.1038/nrmicro.2016.93.

154. Shi, Z., Zachara, J. M., Wang, Z., Shi, L., & Fredrickson, J. K. (2013). Reductive dissolution of goethite and hematite by reduced flavins. Geochimica et Cosmochimica Acta, 121, 139-154. ISSN 0016-7037. https://doi.org/10.1016/j.gca.2013.05.039.

155. Shin, D., Jeong, J., Lee, S., Pandey, B. D., & Lee, J. (2013). Evaluation of bioleaching factors on gold recovery from ore by cyanide-producing bacteria. Minerals Engineering, 48, 20-24. https://doi.org/10.1016/j.mineng.2013.03.019

156. Stockdreher, Y., Sturm, M., Josten, M., Sahl, H.G., Dobler, N., Zigann, R., and Dahl, C. 2014. “New Proteins Involved in Sulfur Trafficking in the Cytoplasm of *Allochromatium vinosumAllochromatium vinosum*.” Journal of Biological Chemistry 289 (18): 12390–403. https://doi.org/10.1074/jbc.M113.536425.

157. Sturgis, J.N., and Robert, B. 1996. “The Role of Chromophore Coupling in Tuning the Spectral Properties of Peripheral Light-Harvesting Protein of Purple Bacteria.” Photosynthesis Research 50 (1): 5–10. https://doi.org/10.1007/BF00018216.

158. Sun, Y., Wei, J., Liang, P. *et al.* Microbial community analysis in biocathode microbial fuel cells packed with different materials. AMB Expr 2, 21 (2012). https://doi.org/10.1186/2191-0855-2-21

159. Susanne Douglas , Terry J. Beveridge, Mineral formation by bacteria in natural microbial communities, *FEMS Microbiology Ecology*, Volume 26, Issue 2, June 1998, Pages 79–88, https://doi.org/10.1111/j.1574-6941.1998.tb00494.x

160. Szklarczyk D, Kirsch R, Koutrouli M, Nastou K, Mehryary F, Hachilif R, Gable AL, Fang T, Doncheva NT, Pyysalo S, Bork P, Jensen LJ, von Mering C. The STRING database in 2023: protein-protein association networks and functional enrichment analyses for any sequenced genome of interest. Nucleic Acids Res. 2023 Jan 6;51(D1):D638-D646. doi: 10.1093/nar/gkac1000. PMID: 36370105; PMCID: PMC9825434.

161. Takahashi, M., and Ichimura, S. 1968. “Vertical Distribution and Organic Matter Production of Photosynthetic Sulfur Bacteria in Japanese Lakes.” Limnology and Oceanography 13 (4): 644–55. https://doi.org/10.4319/lo.1968.13.4.0644.

162. Tejedor-Sanz S, Stevens ET, Li S, Finnegan P, Nelson J, Knoesen A, Light SH, Ajo-Franklin CM, Marco ML. Extracellular electron transfer increases fermentation in

lactic acid bacteria via a hybrid metabolism. Elife. (2022) Feb 11;11:e70684. doi: 10.7554/eLife.70684. PMID: 35147079; PMCID: PMC8837199.

163. Temirbekova A, Tekebayeva Z, Temirkhanov A, Yevneyeva D, Sadykov A, Meiramkulova K, Mkilima T, Abzhalelov A. Isolation and Characterization of Bacteria with High Electroactive Potential from Poultry Wastewater. *Biology*. 2023; 12(4):623. https://doi.org/10.3390/biology12040623

164. Teufel, F., Armenteros, J.J.A, Johansen, A.R., Gíslason, M.H., Pihl, S.I., Tsirigos, K.D., Winther, O., Brunak, S., Heijne, G., and Nielsen, H. 2022. "SignalP 6.0 Predicts All Five Types of Signal Peptides Using Protein Language Models." Nature Biotechnology 40 (7): 1023–25. https://doi.org/10.1038/s41587-021-01156-3.

165. Thermo Fisher Scientific. (n.d.). Transition Metals: Iron. Thermo Fisher Scientific. Retrieved June 6, 2023, from https://www.thermofisher.com/us/en/home/materials-science/learning-center/periodic-table/transition-metal/iron.html

166. Turro, N., Ramamurthy, V., and Scaiano, J. 2008. "Principles of Molecular Photochemistry: An Introduction." University Science Books, Mill Valley.

167. Utgikar, Vivek, Stephen M .Harmon, Navendu Chaudhary. "Inhibition of Sulfate-Reducing Bacteria by Metal Sulfide Formation in Bioremediation of Acid Mine drainage". Wiley periodicals, (2002), 17, 40-48

168. Verelst W, Asard H. A phylogenetic study of cytochrome b561 proteins. Genome Biol. 2003;4(6):R38. doi: 10.1186/gb-2003-4-6-r38. Epub 2003 May 28. PMID: 12801412; PMCID: PMC193617.

169. Viale, A., Kobayashi H., Akazawa T. 1989. “Expressed Genes for Plant-Type Ribulose 1,5-Bisphosphate Carboxylase/Oxygenase in the Photosynthetic Bacterium Chromatium Vinosum, Which Possesses Two Complete Sets of the Genes.” Journal of Bacteriology 171 (5). https://doi.org/10.1128/jb.171.5.2391-2400.1989.

170. Vredenberg, W.J., Amesz, J. 1966 “Absorption Bands of Bacteriochlorophyll Types in Purple Bacteria and Their Response to Illumination.” Biochimica et Biophysica Acta (BBA) - Biophysics Including Photosynthesis 126 (2): 244–53. https://doi.org/10.1016/0926-6585(66)90060-4.

171. Wang, H., Han, J., Manica, R., Qi, C., & Liu, Q. (2022). Effect of Cu(II) ions on millerite (β-NiS) flotation and surface properties in alkaline solutions. Minerals Engineering, 180, 107443. ISSN 0892-6875. https://doi.org/10.1016/j.mineng.2022.107443.

172. Wang, L.-Y., Nevin, K. P., Woodard, T. L., Mu, B.-Z., & Lovley, D. R. (2016). Expanding the Diet for DIET: Electron Donors Supporting Direct Interspecies Electron Transfer (DIET) in Defined Co-Cultures. Frontiers in Microbiology, 7. https://doi.org/10.3389/fmicb.2016.00236

173. Wang, W., & Lee, D.-J. (2021). Direct interspecies electron transfer mechanism in enhanced methanogenesis: A mini-review. Bioresource Technology, 330, 124980. https://doi.org/10.1016/j.biortech.2021.124980

174. Watanabe, T., Kojima, H., Fukui, M., & Nakagawa, S. (2019). Genomes of Neutrophilic Sulfur-Oxidizing Chemolithoautotrophs Representing 9 Proteobacterial Species From 8 Genera. Frontiers in Microbiology, 10, 316. https://doi.org/10.3389/fmicb.2019.00316

175. Weissgerber, T., Dobler, N., Polen, T., Latus, J., Stockdreher, Y., and Dahl, C. 2013. “Genome-Wide Transcriptional Profiling of the Purple Sulfur Bacterium *Allochromatium vinosumAllochromatium vinosum* DSM 180T during Growth on Different Reduced Sulfur Compounds.” Journal of Bacteriology 195 (18): 4231–45. https://doi.org/10.1128/JB.00154-13.

176. Weissgerber, T., Zigann, R., Bruce, D., Chang, Y.J., Detter, J.C., Loren Hauser, C.H., *et al.* 2011. “Complete Genome Sequence of *Allochromatium vinosumAllochromatium vinosum* DSM 180T.” Standards in Genomic Sciences 5 (3): 311. https://doi.org/10.4056/sigs.2335270.

177. Welte, C., Hafner, S., Krätzer, C., Quentmeier, A., Friedrich, C.G., Dahl, C. 2009 “Interaction between *sox* Proteins of Two Physiologically Distinct Bacteria and a New Protein Involved in Thiosulfate Oxidation.” FEBS Letters 583 (8): 1281–86. https://doi.org/10.1016/j.febslet.2009.03.020.

178. Wignall, P.B., Twitchett R.J. “Extend, duration, and nature of the Permian-Triassic super anoxic event.” Geological Society of America Special Papers, (2002) 356, 395-413.

179. Williams, J.C., and Allen, J.P. 2009. “Directed Modification of Reaction Centers from Purple Bacteria.” In The Purple Phototrophic Bacteria, 337–53. Springer, Dordrecht. https://doi.org/10.1007/978-1-4020-8815-5_18.

180. Wraight, C.A., and Gunner, M.R. 2009. “The Acceptor Quinones of Purple Photosynthetic Bacteria — Structure and Spectroscopy.” In The Purple Phototrophic Bacteria, 379–405. Springer, Dordrecht. https://doi.org/10.1007/978-1-4020-8815-5_20.

181. Xiong A, Jayaswal RK. Molecular characterization of a chromosomal determinant conferring resistance to zinc and cobalt ions in Staphylococcus aureus. Journal of

Bacteriology. 1998 Aug;180(16):4024-4029. DOI: 10.1128/jb.180.16.4024-4029.1998. PMID: 9696746; PMCID: PMC107394.

182. You, L.-X., Liu, L.-D., Xiao, Y., Dai, Y.-F., Chen, B.-L., Jiang, Y.-X., & Zhao, F. (2018). Flavins mediate extracellular electron transfer in Gram-positive Bacillus megaterium strain LLD-1. Bioelectrochemistry, 119, 196-202. ISSN 1567-5394. https://doi.org/10.1016/j.bioelechem.2017.10.005.

183. Yu H, Schut GJ, Haja DK, Adams MWW, Li H. Evolution of complex I-like respiratory complexes. J Biol Chem. 2021 Jan-Jun;296:100740. doi: 10.1016/j.jbc.2021.100740. Epub 2021 May 3. PMID: 33957129; PMCID: PMC8165549.

184. Zhan, Y., Yang, M., Zhang, S. *et al.* Iron and sulfur oxidation pathways of *Acidithiobacillus ferrooxidans*. *World J Microbiol Biotechnol* **35**, 60 (2019). https://doi.org/10.1007/s11274-019-2632-y

185. Zhang, Q., Ma, W., Peng, Q., Shu, X. 2020. "Stabilization and Utilization of Pyrite under Light Irradiation: Discussion of Photocorrosion Resistance." ACS Omega, 5: 28693−28701.

186. Zhang, Y., Ru, J., Hua, Y., Huang, P., Bu, J., & Wang, Z. (2021). Facile and controllable synthesis of NiS2 nanospheres in deep eutectic solvent. Materials Letters, 283, 128742. https://doi.org/10.1016/j.matlet.2020.128742.

187. Zhou N, Keffer JL, Polson SW, Chan CS. Unraveling Fe(II)-Oxidizing Mechanisms in a Facultative Fe(II) Oxidizer, Sideroxydans lithotrophicus Strain ES-1, via Culturing, Transcriptomics, and Reverse Transcription-Quantitative PCR. Appl Environ Microbiol. 2022 Jan 25;88(2):e0159521. doi: 10.1128/AEM.01595-21. Epub 2021 Nov 17. PMID: 34788064; PMCID: PMC8788666.

188. Zou, L., Zhu, F., Long, Ze. *Et al.* Bacterial extracellular electron transfer: a powerful route to the green biosynthesis of inorganic nanomaterials for multifunctional applications. J Nanobiotechnol 19, 120 (2021). https://doi.org/10.1186/s12951-021-00868-7

APPENDIX

Table 0-1 Appendix - Media composition of MS culture, negative, positive controls

Component	*Positive Control*	*Negative Control*	*MS Medium*
$CaCl_2 \cdot 2H_2O$	1.7 mM	1.7 mM	1.7 mM
Yeast	250 mg/L	250 mg/L	250 mg/L
NH_4Cl	6.5 mM	6.5 mM	6.5 mM
KCl	4.6 mM	4.6 mM	4.6 mM
MgCl2·6H2O	1 mM	1 mM	1 mM
HEPES	20 mM	20 mM	20 mM
$NaHCO_3$	35 mM	35 mM	35 mM
KH_2PO_4	5.1 mM	5.1 mM	5.1 mM
$Na_2S \cdot 9H2O$	6.1 mM	None	6.1mM equivalent mg/L of MS

Table Appendix - FeS_Hypothetical genes-homology percent. Table showing hypothetical genes in the transcriptome with log2FC above 2 or below -2

Gene locus	**log2FC**	Padj	**Annotation**	**g-protobacteria**
Upregulated Genes				
Alvin_0017	3.64	5.3E-05	hypothetical protein Alvin_0017	95%
Alvin_0016	3.60	1.3E-05	hypothetical protein Alvin_0016	83%
Alvin_0034	3.37	2.0E-04	hypothetical protein Alvin_0034	32%
Alvin_0893	3.21	4.3E-02	hypothetical protein Alvin_0893	59%
Alvin_1191	3.16	2.5E-09	hypothetical protein Alvin_1191	97%
Alvin_1447	3.08	1.2E-03	hypothetical protein Alvin_1447	95%
Alvin_1708	3.04	5.9E-01	hypothetical protein Alvin_1708	100%
Alvin_1190	2.90	1.2E-07	hypothetical protein Alvin_1190	27%

Alvin_0022	2.85	7.0E-02	Domain of unknown function DUF1924	80%
Alvin_1189	2.70	1.1E-08	hypothetical protein Alvin_1189	38%
Alvin_3202	2.68	1.3E-02	hypothetical protein Alvin_3202	82%
Alvin_1448	2.49	5.5E-03	putative transposase	39%
Alvin_0060	2.28	2.8E-06	hypothetical protein Alvin_0060	99%
Alvin_1686	2.06	4.1E-01	hypothetical protein Alvin_1686	100%
Alvin_3205	2.06	1.1E-01	hypothetical protein Alvin_3205	90%
Alvin_0937	2.02	1.3E-02	hypothetical protein Alvin_0937	28%
Downregulated Genes				
Alvin_0703	-10.67	1.2E-38	hypothetical protein Alvin_0703	99%
Alvin_0705	-8.06	1.4E-38	hypothetical protein Alvin_0705	98%
Alvin_3072	-7.25	2.6E-22	hypothetical protein Alvin_3072	63%
Alvin_1741	-6.81	1.3E-28	hypothetical protein Alvin_1741	29%
Alvin_2515	-5.78	1.3E-28	hypothetical protein Alvin_2515	99%
Alvin_2759	-4.95	2.6E-03	hypothetical protein Alvin_2759	99%
Alvin_0708	-4.70	1.8E-12	hypothetical protein Alvin_0708	98%
Alvin_2136	-4.66	1.6E-45	hypothetical protein Alvin_2136	99%
Alvin_2107	-4.03	3.0E-28	hypothetical protein Alvin_2107	97%
Alvin_1197	-3.72	9.6E-03	hypothetical protein Alvin_1197	100%
Alvin_1250	-3.63	1.6E-09	hypothetical protein Alvin_1250	93%
Alvin_2497	-3.61	1.4E-19	hypothetical protein Alvin_2497	84%
Alvin_2063	-3.36	1.7E-05	hypothetical protein Alvin_2063	66%
Alvin_3199	-3.28	1.8E-01	hypothetical protein Alvin_3199	6%

Alvin_1249	-3.24	2.5E-08	hypothetical protein Alvin_1249	95%
Alvin_1196	-3.14	7.6E-03	hypothetical protein Alvin_1196	100%
Alvin_3032	-3.01	2.8E-25	hypothetical protein Alvin_3032	96%
Alvin_2980	-2.86	5.2E-06	hypothetical protein Alvin_2980	98%
Alvin_1036	-2.65	3.7E-02	hypothetical protein Alvin_1036	100%
Alvin_2601	-2.55	9.3E-17	hypothetical protein Alvin_2601	100%
Alvin_0631	-2.43	1.0E-03	hypothetical protein Alvin_0631	
Alvin_2038	-2.26	1.3E-05	hypothetical protein Alvin_2038	99%
Alvin_3233	-2.23	1.9E-04	putative thiol-disulphide oxidoreductase DCC	90%
Alvin_2001	-2.19	5.7E-08	putative transcriptional regulator, Crp/Fnr family	87%
Alvin_0499	-2.09	5.8E-11	hypothetical protein Alvin_0499	99%
Alvin_2295	-2.02	9.9E-04	hypothetical protein Alvin_2295	

Table 0-2 Appendix - Negative control hypothetical genes-homology percent. Table showing hypothetical genes in the transcriptome with log2FC above 2 or below -2

Gene locus	**log2FC**	Padj	**Annotation**	**g-protobacteria**
Upregulated Genes				
Alvin_0893	4.24	4.4E-03	hypothetical protein Alvin_0893	59%
Alvin_3273	2.959434638	5.0E-04	hypothetical protein Alvin_3273	85%
Alvin_0116	2.75	4.0E-04	putative hemolysin	94%
Alvin_3202	2.73	1.1E-02	hypothetical protein Alvin_3202	82%
Alvin_2406	2.71	1.1E-06	hypothetical protein Alvin_2406	
Alvin_1708	2.44	6.8E-01	hypothetical protein Alvin_1708	100%

Alvin_3274	2.38	6.3E-03	hypothetical protein Alvin_3274	90%
Alvin_2558	2.37	6.5E-03	hypothetical protein Alvin_2558	50%
Alvin_3196	2.36	1.1E-02	hypothetical protein Alvin_3196	
Alvin_3272	2.35	1.7E-03	hypothetical protein Alvin_3272	96%
Alvin_1381	2.31	4.4E-08	hypothetical protein Alvin_1381	
Alvin_0022	2.28	1.7E-01	Domain of unknown function DUF1924	80%
Alvin_0159	2.27	5.0E-04	hypothetical protein Alvin_0159	
Alvin_1686	2.13	3.7E-01	hypothetical protein Alvin_1686	100%
Alvin_3195	2.06	1.2E-02	hypothetical protein Alvin_3195	47%
Alvin_1146	2.05	5.7E-03	hypothetical protein Alvin_1146	93%
Alvin_2812	2.03	7.6E-05	hypothetical protein Alvin_2812	
Downregulated Genes				
Alvin_3072	-6.52	3.5E-18	hypothetical protein Alvin_3072	63%
Alvin_2515	-5.70	6.7E-28	hypothetical protein Alvin_2515	99%
Alvin_1741	-5.47	7.6E-20	hypothetical protein Alvin_1741	29%
Alvin_0703	-5.38	2.4E-19	hypothetical protein Alvin_0703	99%
Alvin_0705	-5.25	7.9E-18	hypothetical protein Alvin_0705	98%
Alvin_2136	-5.24	7.3E-58	hypothetical protein Alvin_2136	99%
Alvin_2107	-4.01	1.7E-28	hypothetical protein Alvin_2107	97%
Alvin_2497	-3.96	1.5E-23	hypothetical protein Alvin_2497	84%
Alvin_1197	-3.73	5.9E-03	hypothetical protein Alvin_1197	100%
Alvin_2063	-3.14	9.0E-05	hypothetical protein Alvin_2063	66%
Alvin_1196	-3.08	6.0E-03	hypothetical protein Alvin_1196	100%

Alvin_2038	-3.04	1.4E-09	hypothetical protein Alvin_2038	99%
Alvin_0708	-3.00	1.9E-06	hypothetical protein Alvin_0708	98%
Alvin_1250	-2.90	2.7E-06	hypothetical protein Alvin_1250	93%
Alvin_1249	-2.70	8.2E-06	hypothetical protein Alvin_1249	95%
Alvin_2001	-2.13	1.8E-07	putative transcriptional regulator, Crp/Fnr family	87%

Table 0-3 Appendix - NiS_Hypothetical genes-homology percent. Table showing hypothetical genes in the transcriptome with log2FC above 2 or below -2

Gene locus	**log2FC**	Padj	**Annotation**	**g-protobacteria**
Upregulated Genes				
Alvin_0034	5.70	9.11E-12	hypothetical protein Alvin_0034	32%
Alvin_1447	5.42	3.84E-10	hypothetical protein Alvin_1447	95%
Alvin_1448	4.46	3.36E-08	putative transposase	39%
Alvin_1191	3.49	1.85E-11	hypothetical protein Alvin_1191	97%
Alvin_1686	3.26	1.13E-01	hypothetical protein Alvin_1686	100%
Alvin_3263	3.24	3.74E-04	hypothetical protein Alvin_3263	86%
Alvin_3205	3.24	3.82E-03	hypothetical protein Alvin_3205	90%
Alvin_0937	3.24	1.13E-05	hypothetical protein Alvin_0937	28%
Alvin_1449	3.10	5.32E-05	hypothetical protein Alvin_1449	36%

Alvin_1190	3.05	1.43E-08	hypothetical protein Alvin_1190	27%
Alvin_0893	2.94	5.80E-02	hypothetical protein Alvin_0893	59%
Alvin_3264	2.87	2.14E-04	virulence protein, putative	48%
Alvin_1189	2.82	1.36E-09	hypothetical protein Alvin_1189	38%
Alvin_3212	2.81	4.05E-07	hypothetical protein Alvin_3212	90%
Alvin_3220	2.79	1.23E-03	hypothetical protein Alvin_3220	100%
Alvin_3202	2.79	7.16E-03	hypothetical protein Alvin_3202	82%
Alvin_3273	2.69	1.35E-03	hypothetical protein Alvin_3273	85%
Alvin_3229	2.68	4.23E-04	hypothetical protein Alvin_3229	67%
Alvin_0941	2.66	1.75E-05	hypothetical protein Alvin_0941	49%
Alvin_0016	2.65	1.90E-03	hypothetical protein Alvin_0016	83%
Alvin_3278	2.61	8.83E-04	hypothetical protein Alvin_3278	2%
Alvin_3274	2.60	1.72E-03	hypothetical protein Alvin_3274	90%
Alvin_1702	2.51	6.35E-05	hypothetical protein Alvin_1702	40%
Alvin_0770	2.47	1.51E-06	hypothetical protein Alvin_0770	32%

Alvin_0895	2.42	1.87E-03	hypothetical protein Alvin_0895	40%
Alvin_3279	2.28	8.37E-05	hypothetical protein Alvin_3279	3%
Alvin_0060	2.24	3.57E-06	hypothetical protein Alvin_0060	99%
Alvin_0116	2.23	4.01E-03	putative hemolysin	94%
Alvin_0896	2.23	1.01E-03	hypothetical protein Alvin_0896	100%
Alvin_0017	2.19	2.08E-02	hypothetical protein Alvin_0017	95%
Alvin_1146	2.04	4.35E-03	hypothetical protein Alvin_1146	93%
Downregulated Genes				
Alvin_0703	-9.67	4.92E-42	hypothetical protein Alvin_0703	99%
Alvin_0705	-8.45	1.68E-41	hypothetical protein Alvin_0705	98%
Alvin_1741	-8.25	2.84E-36	hypothetical protein Alvin_1741	29%
Alvin_3072	-7.43	1.93E-23	hypothetical protein Alvin_3072	63%
Alvin_1197	-5.80	3.14E-03	hypothetical protein Alvin_1197	100%
Alvin_2515	-5.57	1.07E-26	hypothetical protein Alvin_2515	99%
Alvin_1250	-4.93	8.95E-17	hypothetical protein Alvin_1250	93%
Alvin_0708	-4.82	5.45E-13	hypothetical protein Alvin_0708	98%

Alvin_2136	-4.49	2.37E-42	hypothetical protein Alvin_2136	99%
Alvin_1196	-4.09	1.34E-03	hypothetical protein Alvin_1196	100%
Alvin_2107	-3.97	1.46E-27	hypothetical protein Alvin_2107	97%
Alvin_1249	-3.96	2.39E-12	hypothetical protein Alvin_1249	95%
Alvin_2063	-3.55	3.71E-06	hypothetical protein Alvin_2063	66%
Alvin_2497	-3.53	8.42E-19	hypothetical protein Alvin_2497	84%
Alvin_2980	-3.37	3.50E-08	hypothetical protein Alvin_2980	98%
Alvin_1743	-3.19	7.95E-09	hypothetical protein Alvin_1743	94%
Alvin_3233	-2.86	4.91E-07	putative thiol-disulphide oxidoreductase DCC	90%
Alvin_3032	-2.82	2.63E-22	hypothetical protein Alvin_3032	96%
Alvin_3291	-2.80	1.16E-03	hypothetical protein Alvin_3291	100%
Alvin_2038	-2.79	2.70E-08	hypothetical protein Alvin_2038	99%
Alvin_3201	-2.78	1.04E-12	hypothetical protein Alvin_3201	
Alvin_2011	-2.57	7.42E-10	hypothetical protein Alvin_2011	100%
Alvin_3070	-2.54	2.40E-05	hypothetical protein Alvin_3070	95%

Alvin_2601	-2.45	1.29E-15	hypothetical protein Alvin_2601	100%
Alvin_3199	-2.19	3.01E-01	hypothetical protein Alvin_3199	6%
Alvin_2414	-2.17	2.97E-05	hypothetical protein Alvin_2414	38%
Alvin_1860	-2.10	1.42E-11	hypothetical protein Alvin_1860	
Alvin_2034	-2.09	1.17E-09	hypothetical protein Alvin_2034	53%
Alvin_2001	-2.07	2.68E-07	putative transcriptional regulator, Crp/Fnr family	87%

Table 0-4 Appendix - Pyrite hypothetical genes-homology percent. Table showing hypothetical genes in the transcriptome with log2FC above 2 or below -2

Gene locus	**log2FC**	Padj	**Kegg or Strindb annotation**	**pBlast %**
Upregulated genes				
Alvin_0431	2.805207117	1.90E-17	hypothetical protein	100
Alvin_1556	2.456845372	5.89E-31	hypothetical protein	98.57
Alvin_1150	2.116093655	9.47E-16	conserved hypothetical protein	100
Alvin_0900	2.174872911	2.07E-14	hypothetical protein	52.38
Alvin_3291	3.201406084	4.82E-30	hypothetical protein	100
Alvin_0492	2.184299786	6.21E-19	conserved hypothetical protein	98.21
Alvin_1524	2.29922231	0.002293	Protein of unknown function DUF1920	87.13
Alvin_3196	2.808525533	3.32E-07	hypothetical protein	100
Alvin_1154	2.004335109	7.41E-08	conserved hypothetical protein	71.76
Alvin_0016	2.934227017	3.20E-15	conserved hypothetical protein	87.21
Alvin_0022	7.104148889	7.80E-116	Domain of unknown function DUF1924	81.76
Alvin_1146	2.238967162	4.43E-19	hypothetical protein	93.33

Alvin_2704	2.039542999	1.12E-12	conserved hypothetical protein	96.3
Alvin_0107	2.045940556	3.87E-13	conserved hypothetical protein	98.9
Alvin_0929	2.750084318	4.79E-13	hypothetical protein	100
Alvin_2092	2.500312024	3.30E-13	conserved hypothetical protein	91.93
Alvin_1094	4.828489714	4.22E-62	uncharacterized protein	97.62
Alvin_1152	2.264056063	3.85E-20	uncharacterized conserved protein UCP029693	96.41
Downregulated genes				
Alvin_2759	-3.154620377	0.007983	hypothetical protein	98.75
Alvin_0708	-3.027398638	2.25E-07	hypothetical protein	98.64
Alvin_0703	-6.828681509	3.27E-10	hypothetical protein	99.15
Alvin_3072	-4.692102625	3.19E-68	conserved hypothetical protein	59.63
Alvin_0705	-6.622226895	1.51E-78	hypothetical protein	98.51
Alvin_3032	-3.044955173	7.99E-33	conserved hypothetical protein	95.72
Alvin_1741	-6.216786076	3.70E-36	hypothetical protein	100
Alvin_1711	-3.277756991	1.76E-08	hypothetical protein	100
Alvin_2254	-2.557752055	2.15E-14	conserved hypothetical protein	44.03
Alvin_3195	-2.156967974	0.001211	hypothetical protein	48.06
Alvin_1122	-2.730331129	2.51E-16	conserved hypothetical protein	83.95
Alvin_1712	-2.481727529	2.14E-12	conserved hypothetical protein	48.15
Alvin_2497	-3.958402498	1.66E-52	conserved hypothetical protein	84.85
Alvin_2136	-5.228498883	9.42E-76	hypothetical protein	99.4
Alvin_2415	-2.014921119	8.42E-09	conserved hypothetical protein	34.59
Alvin_1841	-3.126809614	1.25E-64	Protein of unknown function	100
Alvin_0500	-3.270204044	6.79E-27	protein of unknown function DUF150	98.4

Alvin_0749	-3.171302926	0.000522	hypothetical protein	17.99
Alvin_1734	-2.12492807	9.49E-08	Protein of unknown function DUF2269	37.89
Alvin_2601	-2.091473724	2.03E-20	conserved hypothetical protein	98.45
Alvin_0962	-5.752529934	6.48E-108	uncharacterized protein	98.41
Alvin_1896	-2.167797768	6.99E-19	protein of unknown function DUF177	99.44
Alvin_2515	-4.055405065	9.34E-94	hypothetical protein	98.15
Alvin_0499	-2.18866098	1.16E-14	hypothetical protein	98.25
Alvin_0746	-2.150323876	4.29E-10	hypothetical protein	41.43

Table 0-5 Appendix - Negative control photosynthetic gene expression of *puc* and *puf* genes

No.	Gene locus	log2FC	Padj	Annotation
***puf* genes**				
1	Alvin_2547	-1.016969301	0.409852575	puf/LH1
2	Alvin_2548	-0.792069371	0.480607695	puf/LH1
3	Alvin_2549	-0.890936016	0.451954303	puf/LH1
4	Alvin_2550	-1.498039832	0.162794192	puf/LH1
5	Alvin_2551	-1.976106521	0.02529796	puf/LH1
6	Alvin_2552	-2.649277514	0.061689939	puf/LH1
7	Alvin_2553	-2.611817172	0.064065548	puf/LH1
8	Alvin_2554	-1.2944821	0.471555869	puf/LH1
9	Alvin_2555	-1.325814676	0.246577339	puf/LH1
10	Alvin_2634	-0.109867924	0.883949019	puf/LH1
11	Alvin_2635	-1.106659761	0.080922671	puf/LH1
12	Alvin_2636	-1.726528895	0.010759542	puf/LH1

13	Alvin_2637	-1.316278811	0.171470147	puf/LH1
***puc* genes**				
14	Alvin_0703	-5.382469814	2.44E-19	pucA6
15	Alvin_0704	-5.528479994	6.96E-16	pucB6
16	Alvin_0705	-5.253038008	7.89E-18	pucA5
17	Alvin_0706	-4.948448257	5.57E-14	pucB5
18	Alvin_0708	-3.003892623	1.89E-06	pucA4
19	Alvin_0709	-3.864599126	0.013577369	pucB4
20	Alvin_2759	0.297924177	0.90082339	pucA3
21	Alvin_2760	-0.017334684	0.995574316	pucB3
22	Alvin_2576	-0.575460813	0.767511646	Lux/LH2
23	Alvin_2577	-0.762006219	0.712279602	Lux/LH2
24	Alvin_2578	-1.044325136	0.595912514	Lux/LH2
25	Alvin_2579	-1.236321989	0.503230468	Lux/LH2
26	Alvin_2580	-0.13022492	0.790826784	Lux/LH2

Table 0-6 Appendix Negative control sulfur oxidation gene expression for *sox* and *dsr* genes

		NEG	
Gene	**Protein**	**log2FCChange**	Padj
***dsr* genes**			
Alvin_1251	DsrA	-6.1322	2.50E-11
Alvin_1252	DsrB	-6.89731	1.48E-09
Alvin_1253	DsrE	-6.29671	3.12E-14
Alvin_1254	DsrF	-5.11243	2.25E-10
Alvin_1255	DsrH	-2.00428	0.000203
Alvin_1256	DsrC	-2.92513	4.78E-08
Alvin_1257	DsrM	-3.43621	8.87E-06
Alvin_1258	DsrK	-4.40475	3.56E-15
Alvin_1259	DsrL	-4.26736	2.11E-18
Alvin_1260	DsrJ	-3.89936	7.20E-19
Alvin_1261	DsrO	-3.57439	6.21E-12
Alvin_1262	DsrP	-3.03167	6.27E-13

Alvin_1263	DsrN	-1.23237	3.79E-05
Alvin_1264	DsrR	-0.61788	0.196365
Alvin_1265	DsrS	-0.73341	0.027678
***sox* genes**			
Alvin_2111	SoxY	0.499286	0.257625
Alvin_2112	SoxZ	0.263714	0.500839
Alvin_2167	SoxB	0.019786	0.983959
Alvin_2168	SoxX	0.111759	0.799777
Alvin_2169	SoxA	-0.09267	0.826892
Alvin_2170	SoxK	0.16211	0.789931
Alvin_2171	SoxL	-0.02045	0.970003

Table 0-7 Appendix Negative control transcriptome. Gene table showing only genes with log2FC above 2 or below -2.

No.	**Gene locus**	**log2FC**	Padj	**Annotation**
Upregulated Genes				
1	Alvin_1095	5.242	7.7E-55	NapC/NirT cytochrome c domain protein
2	Alvin_1094	5.112	4.7E-38	Ankyrin
3	Alvin_1093	4.623	5.3E-27	cytochrome c class I, FccA
4	Alvin_0893	4.243	4.4E-03	hypothetical protein Alvin_0893
5	Alvin_1092	4.194	1.1E-14	Flavocytochrome c sulphide dehydrogenase flavin-binding protein, FccB
6	Alvin_2307	3.464	6.3E-14	Ni/Fe-hydrogenase, b-type cytochrome subunit
7	Alvin_2309	3.212	3.0E-13	hydrogenase (NiFe) small subunit HydA
8	Alvin_2306	3.178	5.9E-12	hydrogenase expression/formation protein
9	Alvin_2451	3.034	1.2E-31	molybdopterin oxidoreductase Fe4S4 region
10	Alvin_2453	3.030	1.4E-30	formate dehydrogenase, beta subunit
11	Alvin_3273	2.959	5.0E-04	hypothetical protein Alvin_3273

12	Alvin_2308	2.874	4.5E-12	nickel-dependent hydrogenase large subunit
13	Alvin_0116	2.752	4.0E-04	putative hemolysin
14	Alvin_3202	2.727	1.1E-02	hypothetical protein Alvin_3202
15	Alvin_2406	2.712	1.1E-06	hypothetical protein Alvin_2406
16	Alvin_2454	2.683	4.4E-17	formate dehydrogenase, gamma subunit
17	Alvin_1145	2.488	2.1E-03	protein of unknown function Spy-related protein
18	Alvin_1708	2.440	6.8E-01	hypothetical protein Alvin_1708
19	Alvin_3274	2.379	6.3E-03	hypothetical protein Alvin_3274
20	Alvin_2558	2.369	6.5E-03	hypothetical protein Alvin_2558
21	Alvin_3196	2.356	1.1E-02	hypothetical protein Alvin_3196
22	Alvin_3272	2.346	1.7E-03	hypothetical protein Alvin_3272
23	Alvin_1381	2.315	4.4E-08	hypothetical protein Alvin_1381
24	Alvin_3275	2.312	5.6E-03	phage recombination protein Bet
25	Alvin_0022	2.284	1.7E-01	Domain of unknown function DUF1924
26	Alvin_0159	2.272	5.0E-04	hypothetical protein Alvin_0159
27	Alvin_1143	2.165	5.5E-03	twin-arginine translocation pathway signal
28	Alvin_2446	2.162	1.4E-06	nitrite and sulphite reductase 4Fe-4S region
29	Alvin_1686	2.131	3.7E-01	hypothetical protein Alvin_1686
30	Alvin_0284	2.129	5.9E-04	peptidase M61 domain protein
31	Alvin_2557	2.065	2.3E-02	Protein of unknown function DUF2442
32	Alvin_3195	2.060	1.2E-02	hypothetical protein Alvin_3195
33	Alvin_1699	2.057	4.2E-02	DNA binding domain protein, excisionase family
34	Alvin_1146	2.052	5.7E-03	hypothetical protein Alvin_1146

35	Alvin_1723	2.045	2.0E-03	positive regulator of sigma E, RseC/MucC
36	Alvin_2812	2.027	7.6E-05	hypothetical protein Alvin_2812
Downregulated Genes				
37	Alvin_1006	-7.017	2.2E-07	Peroxiredoxin
38	Alvin_1252	-6.897	1.5E-09	DsrB
39	Alvin_3072	-6.520	3.5E-18	hypothetical protein Alvin_3072
40	Alvin_1253	-6.297	3.1E-14	DsrE
41	Alvin_1251	-6.132	2.5E-11	DsrA
42	Alvin_3073	-5.699	5.2E-14	C4-dicarboxylate transporter/malic acid transport protein
43	Alvin_2515	-5.697	6.7E-28	hypothetical protein Alvin_2515
44	Alvin_0704	-5.528	7.0E-16	antenna complex alpha/beta subunit
45	Alvin_1741	-5.470	7.6E-20	hypothetical protein Alvin_1741
46	Alvin_0703	-5.382	2.4E-19	hypothetical protein Alvin_0703
47	Alvin_1740	-5.302	7.6E-20	Dinitrogenase iron-molybdenum cofactor biosynthesis protein
48	Alvin_0705	-5.253	7.9E-18	hypothetical protein Alvin_0705
49	Alvin_2136	-5.239	7.3E-58	hypothetical protein Alvin_2136
50	Alvin_1254	-5.112	2.3E-10	DsrF
51	Alvin_0706	-4.948	5.6E-14	antenna complex alpha/beta subunit
52	Alvin_1739	-4.900	6.9E-16	Cobyrinic acid ac-diamide synthase
53	Alvin_0962	-4.672	1.3E-35	Ankyrin
54	Alvin_0440	-4.611	1.4E-09	Chaperonin Cpn10

55	Alvin_1258	-4.405	3.6E-15	DsrK
56	Alvin_0441	-4.305	9.4E-12	chaperonin GroEL
57	Alvin_1259	-4.267	2.1E-18	DsrL
58	Alvin_1508	-4.147	8.3E-25	sulfur relay protein, TusE/DsrC/DsvC family
59	Alvin_2107	-4.008	1.7E-28	hypothetical protein Alvin_2107
60	Alvin_2497	-3.960	1.5E-23	hypothetical protein Alvin_2497
61	Alvin_1260	-3.899	7.2E-19	DsrJ
62	Alvin_0709	-3.865	1.4E-02	antenna complex alpha/beta subunit
63	Alvin_1738	-3.784	3.5E-09	Cobyrinic acid ac-diamide synthase
64	Alvin_2498	-3.740	6.8E-31	nitrogen fixation-related protein
65	Alvin_1197	-3.727	5.9E-03	hypothetical protein Alvin_1197
66	Alvin_0853	-3.686	4.5E-07	chaperonin GroEL
67	Alvin_0316	-3.628	8.3E-25	transketolase
68	Alvin_1365	-3.618	5.6E-29	Ribulose-bisphosphate carboxylase
69	Alvin_1261	-3.574	6.2E-12	DsrO
70	Alvin_1257	-3.436	8.9E-06	DsrM
71	Alvin_0009	-3.418	2.4E-05	heat shock protein Hsp20
72	Alvin_1853	-3.310	8.9E-06	efflux transporter, RND family, MFP subunit
73	Alvin_0854	-3.302	8.6E-07	Chaperonin Cpn10
74	Alvin_1737	-3.199	3.6E-05	Dinitrogenase iron-molybdenum cofactor biosynthesis protein
75	Alvin_1530	-3.175	1.0E-05	transcriptional regulator, ArsR family

76	Alvin_2037	-3.154	7.6E-20	protein of unknown function DUF224 cysteine-rich region domain protein
77	Alvin_2063	-3.136	9.0E-05	hypothetical protein Alvin_2063
78	Alvin_1323	-3.082	4.8E-07	glutathione-disulfide reductase
79	Alvin_1196	-3.080	6.0E-03	hypothetical protein Alvin_1196
80	Alvin_1434	-3.080	5.4E-02	Protein of unknown function DUF2061, membrane
81	Alvin_1386	-3.046	6.9E-07	chaperone protein DnaK
82	Alvin_2038	-3.045	1.4E-09	hypothetical protein Alvin_2038
83	Alvin_1262	-3.032	6.3E-13	DsrP
84	Alvin_0708	-3.004	1.9E-06	hypothetical protein Alvin_0708
85	Alvin_2039	-2.990	4.4E-08	hydrogenase (NiFe) small subunit HydA
86	Alvin_1734	-2.980	1.5E-07	Protein of unknown function DUF2269, transmembrane
87	Alvin_1324	-2.978	2.4E-04	Redoxin domain protein
88	Alvin_1121	-2.946	4.4E-15	AprA
89	Alvin_1256	-2.925	4.8E-08	DsrC
90	Alvin_0707	-2.918	1.4E-06	regulatory protein LuxR
91	Alvin_1250	-2.900	2.7E-06	hypothetical protein Alvin_1250
92	Alvin_0358	-2.880	7.8E-05	Sulfur globule protein SgpB
93	Alvin_2661	-2.863	1.3E-07	protein of unknown function DUF323
94	Alvin_1385	-2.843	2.3E-06	GrpE protein
95	Alvin_1120	-2.827	2.1E-12	AprB
96	Alvin_1435	-2.810	2.4E-03	Ferritin Dps family protein

97	Alvin_0804	-2.738	6.8E-08	pyruvate dehydrogenase complex dihydrolipoamide acetyltransferase
98	Alvin_0345	-2.727	8.9E-06	sulfur relay protein, TusE/DsrC/DsvC family
99	Alvin_1249	-2.695	8.2E-06	hypothetical protein Alvin_1249
100	Alvin_1359	-2.688	6.7E-08	ATP-dependent chaperone ClpB
101	Alvin_0805	-2.677	9.5E-09	2-oxo-acid dehydrogenase E1 subunit, homodimeric type
102	Alvin_2552	-2.649	6.2E-02	photosynthetic reaction center, M subunit
103	Alvin_2499	-2.649	9.9E-13	cytochrome bd ubiquinol oxidase subunit I
104	Alvin_1202	-2.636	1.0E-07	ATPase-like, ParA/MinD
105	Alvin_1119	-2.624	5.9E-13	AprM
106	Alvin_0315	-2.615	2.5E-14	glyceraldehyde-3-phosphate dehydrogenase, type I
107	Alvin_1531	-2.614	7.9E-05	permease
108	Alvin_2553	-2.612	6.4E-02	photosynthetic reaction center L subunit
109	Alvin_0010	-2.582	6.5E-03	membrane protein-like protein
110	Alvin_0502	-2.573	1.7E-05	translation initiation factor IF-2
111	Alvin_1318	-2.539	7.6E-08	4Fe-4S ferredoxin iron-sulfur binding domain protein
112	Alvin_1395	-2.501	1.4E-11	cytochrome c family protein
113	Alvin_2043	-2.499	2.7E-06	methionine aminopeptidase, type I
114	Alvin_1112	-2.498	3.1E-01	transposase IS4 family protein
115	Alvin_0313	-2.471	2.4E-16	pyruvate kinase
116	Alvin_0312	-2.470	1.3E-09	fructose-bisphosphate aldolase, class II, Calvin cycle subtype

117	Alvin_2036	-2.451	5.3E-20	nickel-dependent hydrogenase large subunit
118	Alvin_1366	-2.429	2.2E-13	Ribulose-bisphosphate carboxylase
119	Alvin_1384	-2.425	2.6E-05	heat-inducible transcription repressor HrcA
120	Alvin_0314	-2.402	3.3E-09	Phosphoglycerate kinase
121	Alvin_0766	-2.399	5.5E-05	protein of unknown function DUF198
122	Alvin_3000	-2.389	1.5E-09	glutamine synthetase, type I
123	Alvin_2660	-2.365	7.8E-06	methyltransferase
124	Alvin_0258	-2.344	1.1E-04	Rhodanese domain protein
125	Alvin_0739	-2.337	1.2E-05	FeS assembly protein SufB
126	Alvin_0140	-2.320	5.6E-05	UDP-3-0-acyl N-acetylglucosamine deacetylase
127	Alvin_1852	-2.305	7.3E-07	acriflavin resistance protein
128	Alvin_1118	-2.265	9.6E-14	sulfate adenylyltransferase
129	Alvin_0741	-2.263	4.3E-10	FeS assembly protein SufD
130	Alvin_1387	-2.261	1.5E-03	chaperone protein DnaJ
131	Alvin_2572	-2.237	7.6E-03	RNA polymerase, sigma 32 subunit, RpoH
132	Alvin_1079	-2.229	1.0E-14	cytochrome B561
133	Alvin_0740	-2.229	5.2E-10	FeS assembly ATPase SufC
134	Alvin_0503	-2.228	1.9E-04	ribosome-binding factor A
135	Alvin_2042	-2.214	4.5E-05	UTP-GlnB uridylyltransferase, GlnD
136	Alvin_3241	-2.214	1.0E-03	protein of unknown function DUF302
137	Alvin_2040	-2.211	2.1E-05	HupH hydrogenase expression protein
138	Alvin_1468	-2.199	6.2E-05	YceI family protein
139	Alvin_2600	-2.181	5.3E-07	SirA family protein

140	Alvin_0803	-2.176	3.6E-07	dihydrolipoamide dehydrogenase
141	Alvin_1951	-2.153	3.9E-03	flagellin domain protein
142	Alvin_2001	-2.128	1.8E-07	putative transcriptional regulator, Crp/Fnr family
143	Alvin_1688	-2.122	9.2E-03	Antibiotic biosynthesis monooxygenase
144	Alvin_1735	-2.119	1.0E-03	transcriptional coactivator/pterin dehydratase
145	Alvin_0501	-2.118	3.7E-05	NusA antitermination factor
146	Alvin_1248	-2.111	7.9E-05	CRISPR-associated protein, Cas6-related protein
147	Alvin_2899	-2.046	1.2E-03	porin Gram-negative type
148	Alvin_0504	-2.039	6.1E-05	tRNA pseudouridine synthase B
149	Alvin_1733	-2.030	5.0E-04	peptidase M15D vanX D-ala-D-ala dipeptidase
150	Alvin_1317	-2.021	1.3E-06	molybdopterin oxidoreductase Fe4S4 region
151	Alvin_1255	-2.004	2.0E-04	DsrH
152	Alvin_0008	-2.004	3.4E-03	ABC transporter related protein

Table 0-8 Hypothetical proteins gene expression in pyrite transcriptome analysis

Gene locus	*log2FC*	Padj	*Kegg or Strindb annotation*	*pBlast %*	*AA length*	*Sequence protein domains*	*Protein motifs (AA locus)*	*Transmembrane domains (AA locus)*	*Hydropathicity*
									Upregulated genes
Alvin_0431	2.805207117	1.90E-17	hypothetical protein	100	59	none	none	none	-0.912
Alvin_1556	2.456845372	5.89E-31	hypothetical protein	98.57	59	none	none	none	-0.712
Alvin_1150	2.116093655	9.47E-16	conserved hypothetical protein	100	62	none	none	TM (4-26 & 33-52)	1.6
Alvin_0900	2.174872911	2.07E-14	hypothetical protein	52.38	64	none	none	none	-0.0783
Alvin_3291	3.201406084	4.82E-30	hypothetical protein	100	71	none	none	none	-1.165
Alvin_0492	2.184299786	6.21E-19	conserved hypothetical protein	98.21	76	none	none	none	-0.641
Alvin_1524	2.29922231	0.002293	Protein of unknown function DUF1920	87.13	84	FeoC	none	none	-0.506
Alvin_3196	2.808525533	3.32E-07	hypothetical protein	100	85	none	none	none	-0.667
Alvin_1154	2.004335109	7.41E-08	conserved hypothetical protein	71.76	96	none	coiled-coil (9-36)	none	-1.034
Alvin_0016	2.934227017	3.20E-15	conserved hypothetical protein	87.21	101	DUF-3430	none	TM (60-80)	0.17
Alvin_0022	7.104148889	7.80E-116	Domain of unknown function DUF1924	81.76	118	DUF-1924	signal peptide (1-23)	TM (5-25)	-0.403
Alvin_1146	2.238967162	4.43E-19	hypothetical protein	93.33	130	none	none	none	-0.358
Alvin_2704	2.039542999	1.12E-12	conserved hypothetical protein	96.3	154	none	none	none	-0.271
Alvin_0107	2.045940556	3.87E-13	conserved hypothetical protein	98.9	171	DUF5063	none	none	-0.214
Alvin_0929	2.750084318	4.79E-13	hypothetical protein	100	198	none	none	TM (60-80)	-0.234
Alvin_2092	2.500312024	3.30E-13	conserved hypothetical protein	91.93	219	sulfotransfer_2 domain	none	none	-0.519

Alvin_1094	4.828489714	4.22E-62	uncharacterized protein	97.62	320	Ankyrin repeats	signal peptide (1-27)	none	0.05
Alvin_1152	2.264056063	3.85E-20	uncharacterized conserved protein UCP029693	96.41	357	DUF2333	TM	TM (33-55)	-0.262
									Downregulated genes
Alvin_2759	-3.154620377	0.007983	hypothetical protein	98.75	52	LHC	TM (29-51)	TM (29-51)	0.679
Alvin_0708	-3.027398638	2.25E-07	hypothetical protein	98.64	52	LHC	TM (24-49)	TM (21-43)	0.862
Alvin_0703	-6.828681509	3.27E-10	hypothetical protein	99.15	53	LHC	TM (25-50)	TM (28-50)	0.692
Alvin_3072	-4.692102625	3.19E-68	conserved hypothetical protein	59.63	61	DUF2892	TM (7-25 & 31-52)	TM (30-52)	0.793
Alvin_0705	-6.622226895	1.51E-78	hypothetical protein	98.51	69	LHC	TM (26-46)	M (24-46)	0.648
Alvin_3032	-3.044955173	7.99E-33	conserved hypothetical protein	95.72	74	none	Coiled-coil (4-31 & 47-67)	none	-0.611
Alvin_1741	-6.216786076	3.70E-36	hypothetical protein	100	78	none	coiled-coil (51-71)	none	-0.735
Alvin_1711	-3.277756991	1.76E-08	hypothetical protein	100	95	none	none	none	-0.784
Alvin_2254	-2.557752055	2.15E-14	conserved hypothetical protein	44.03	104	none	TM (1-21)	none	-0.052
Alvin_3195	-2.156967974	0.001211	hypothetical protein	48.06	106	none	none	none	-0.842
Alvin_1122	-2.730331129	2.51E-16	conserved hypothetical protein	83.95	116	none	none	none	-0.318
Alvin_1712	-2.481727529	2.14E-12	conserved hypothetical protein	48.15	129	none	none	none	-0.409
Alvin_2497	-3.958402498	1.66E-52	conserved hypothetical protein	84.85	135	none	none	none	0.076
Alvin_2136	-5.228498883	9.42E-76	hypothetical protein	99.4	138	none	signal peptide (1-24)	TM (7-24)	-0.107

Alvin_2415	-2.014921119	8.42E-09	conserved hypothetical protein	34.59	146	none	Coiled-coil (68-88)	none	-0.072
Alvin_1841	-3.126809614	1.25E-64	Protein of unknown function	100	149	YqeY	none	none	-0.168
Alvin_0500	-3.270204044	6.79E-27	protein of unknown function DUF150	98.4	151	DUF150	RimP C and N terminal	none	-0.175
Alvin_0749	-3.171302926	0.000522	hypothetical protein	17.99	154	none	none	none	-0.348
Alvin_1734	-2.12492807	9.49E-08	Protein of unknown function DUF2269	37.89	155	DUF2296	TM (12-31, 52-70, 82-104 & 132-152)	TM (10-32, 52-74, 84-106, & 133-152)	0.939
Alvin_2601	-2.091473724	2.03E-20	conserved hypothetical protein	98.45	159	DsrE_2	coiled-coil (103-123) Transmembrane (21-44 &72-91)	TM (21-43 & 72-91)	0.236
Alvin_0962	-5.752529934	6.48E-108	uncharacterized protein	98.41	176	Ankyrin repeats	Ankyring repeats signal peptide 1-22	1-20TM	-0.067
Alvin_1896	-2.167797768	6.99E-19	protein of unknown function DUF177	99.44	184	YceD	none	none	0.329
Alvin_2515	-4.055405065	9.34E-94	hypothetical protein	98.15	202	none	TM (1-22) Coiled-coil (35-55 & 126-160)	TM (7-26)	-0.902
Alvin_0499	-2.18866098	1.16E-14	hypothetical protein	98.25	277	none	TM (16-34) coiled-coil (211-238)	TM (13-35)	-0.325
Alvin_0746	-2.150323876	4.29E-10	hypothetical protein	41.43	381	Putative MetA	signal peptide (1-31) coiled-coil (41-61)	TM (12-34)	-0.152

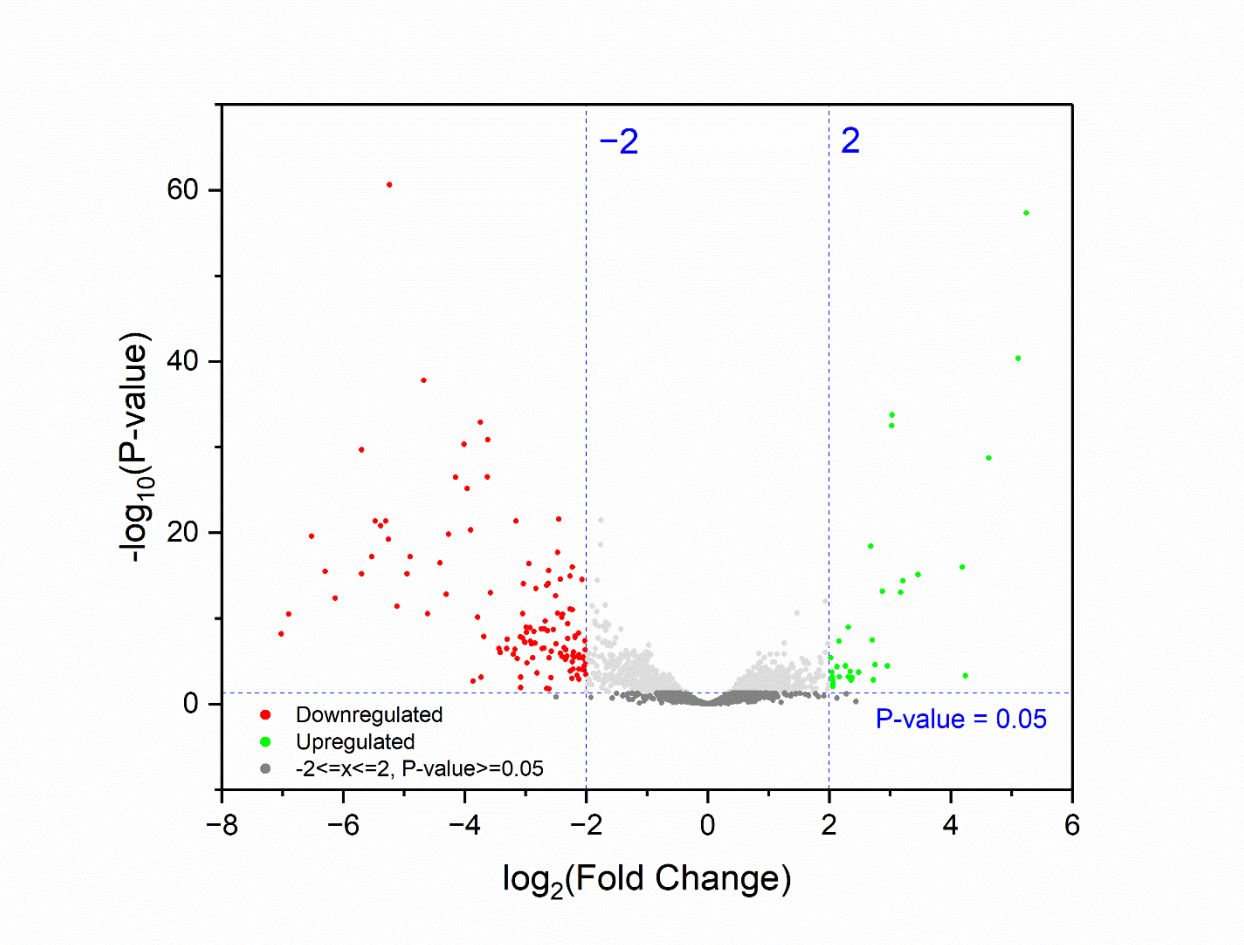

Figure A-1 Volcano plot of the transcriptome of the negative control

Table 0-8 Most upregulated and downregulated hypothetical genes for Negative control transcriptome

Gene locus	log2FC	Padj	Kegg or Strindb annotation	pBlast %	AA length	Sequence protein domains	Protein motifs (AA locus)	Transmembrane domains (AA locus)	Hydropathicity
Upregulated genes									
Alvin_0893	4.2432	0.0044	hypothetical protein Alvin_0893	59	86	HTH_17	none	none	-0.459
Alvin_3273	2.9594	0.0005	hypothetical protein Alvin_3273	85	122	Gly-zipper_OmpA, UPF0547	signal peptide (39-40)	TM (20-44 & 48-82)	0.352
Alvin_0116	2.7523	0.0004	putative hemolysin	94	253	Acetyltransf_5, Autoind_synth	none	none	-0.142
Alvin_3202	2.7271	0.0111	hypothetical protein Alvin_3202	82	85	none	none	TM (10-22)	0.236
Downregulated genes									
Alvin_3072	-6.5204	3.52E-18	hypothetical protein Alvin_3072	63	61	DUF2892, Pox_P21	none	TM (11-27 & 30-52)	0.793
Alvin_2515	-5.6970	6.65E-28	hypothetical protein Alvin_2515	99	202	Mod_r, GBP_C	signal peptide (22-23)	TM (06-25)	-0.902
Alvin_1741	-5.4702	7.63E-20	hypothetical protein Alvin_1741	29	78	DUF5320, FoP_duplication	none	none	-0.735
Alvin_0703	-5.3825	2.44E-19	hypothetical protein Alvin_0703	99	53	LHC	none	TM (23-51)	0.692
Alvin_0705	-5.2530	7.89E-18	hypothetical protein Alvin_0705	98	69	DUF5989, LHC	none	TM (24-46)	0.648
Alvin_2136	-5.2393	7.29E-58	hypothetical protein Alvin_2136	99	138	none	none	TM (06-22)	-0.107

Table 0-8 Hypothetical proteins gene expression in pyrite transcriptome analysis

Gene locus	*log2FC*	Padj	*Kegg or Strindb annotation*	*pBlast %*	*AA length*	*Sequence protein domains*	*Protein motifs (AA locus)*	*Transmembrane domains (AA locus)*	*Hydropathicity*
									Upregulated genes
Alvin_0431	2.805207117	1.90E-17	hypothetical protein	100	59	none	none	none	-0.912
Alvin_1556	2.456845372	5.89E-31	hypothetical protein	98.57	59	none	none	none	-0.712
Alvin_1150	2.116093655	9.47E-16	conserved hypothetical protein	100	62	none	none	TM (4-26 & 33-52)	1.6
Alvin_0900	2.174872911	2.07E-14	hypothetical protein	52.38	64	none	none	none	-0.0783
Alvin_3291	3.201406084	4.82E-30	hypothetical protein	100	71	none	none	none	-1.165
Alvin_0492	2.184299786	6.21E-19	conserved hypothetical protein	98.21	76	none	none	none	-0.641
Alvin_1524	2.29922231	0.002293	Protein of unknown function DUF1920	87.13	84	FeoC	none	none	-0.506
Alvin_3196	2.808525533	3.32E-07	hypothetical protein	100	85	none	none	none	-0.667
Alvin_1154	2.004335109	7.41E-08	conserved hypothetical protein	71.76	96	none	coiled-coil (9-36)	none	-1.034
Alvin_0016	2.934227017	3.20E-15	conserved hypothetical protein	87.21	101	DUF-3430	none	TM (60-80)	0.17
Alvin_0022	7.104148889	7.80E-116	Domain of unknown function DUF1924	81.76	118	DUF-1924	signal peptide (1-23)	TM (5-25)	-0.403
Alvin_1146	2.238967162	4.43E-19	hypothetical protein	93.33	130	none	none	none	-0.358
Alvin_2704	2.039542999	1.12E-12	conserved hypothetical protein	96.3	154	none	none	none	-0.271
Alvin_0107	2.045940556	3.87E-13	conserved hypothetical protein	98.9	171	DUF5063	none	none	-0.214
Alvin_0929	2.750084318	4.79E-13	hypothetical protein	100	198	none	none	TM (60-80)	-0.234
Alvin_2092	2.500312024	3.30E-13	conserved hypothetical protein	91.93	219	sulfotransfer_2 domain	none	none	-0.519

Alvin_1094	4.828489714	4.22E-62	uncharacterized protein	97.62	320	Ankyrin repeats	signal peptide (1-27)	none	0.05
Alvin_1152	2.264056063	3.85E-20	uncharacterized conserved protein UCP029693	96.41	357	DUF2333	TM	TM (33-55)	-0.262
									Downregulated genes
Alvin_2759	-3.154620377	0.007983	hypothetical protein	98.75	52	LHC	TM (29-51)	TM (29-51)	0.679
Alvin_0708	-3.027398638	2.25E-07	hypothetical protein	98.64	52	LHC	TM (24-49)	TM (21-43)	0.862
Alvin_0703	-6.828681509	3.27E-10	hypothetical protein	99.15	53	LHC	TM (25-50)	TM (28-50)	0.692
Alvin_3072	-4.692102625	3.19E-68	conserved hypothetical protein	59.63	61	DUF2892	TM (7-25 & 31-52)	TM (30-52)	0.793
Alvin_0705	-6.622226895	1.51E-78	hypothetical protein	98.51	69	LHC	TM (26-46)	M (24-46)	0.648
Alvin_3032	-3.044955173	7.99E-33	conserved hypothetical protein	95.72	74	none	Coiled-coil (4-31 & 47-67)	none	-0.611
Alvin_1741	-6.216786076	3.70E-36	hypothetical protein	100	78	none	coiled-coil (51-71)	none	-0.735
Alvin_1711	-3.277756991	1.76E-08	hypothetical protein	100	95	none	none	none	-0.784
Alvin_2254	-2.557752055	2.15E-14	conserved hypothetical protein	44.03	104	none	TM (1-21)	none	-0.052
Alvin_3195	-2.156967974	0.001211	hypothetical protein	48.06	106	none	none	none	-0.842
Alvin_1122	-2.730331129	2.51E-16	conserved hypothetical protein	83.95	116	none	none	none	-0.318
Alvin_1712	-2.481727529	2.14E-12	conserved hypothetical protein	48.15	129	none	none	none	-0.409
Alvin_2497	-3.958402498	1.66E-52	conserved hypothetical protein	84.85	135	none	none	none	0.076
Alvin_2136	-5.228498883	9.42E-76	hypothetical protein	99.4	138	none	signal peptide (1-24)	TM (7-24)	-0.107

Alvin_2415	-2.014921119	8.42E-09	conserved hypothetical protein	34.59	146	none	Coiled-coil (68-88)	none	-0.072
Alvin_1841	-3.126809614	1.25E-64	Protein of unknown function	100	149	YqeY	none	none	-0.168
Alvin_0500	-3.270204044	6.79E-27	protein of unknown function DUF150	98.4	151	DUF150	RimP C and N terminal	none	-0.175
Alvin_0749	-3.171302926	0.000522	hypothetical protein	17.99	154	none	none	none	-0.348
Alvin_1734	-2.12492807	9.49E-08	Protein of unknown function DUF2269	37.89	155	DUF2296	TM (12-31, 52-70, 82-104 & 132-152)	TM (10-32, 52-74, 84-106, & 133-152)	0.939
Alvin_2601	-2.091473724	2.03E-20	conserved hypothetical protein	98.45	159	DsrE_2	coiled-coil (103-123) Transmembrane (21-44 &72-91)	TM (21-43 & 72-91)	0.236
Alvin_0962	-5.752529934	6.48E-108	uncharacterized protein	98.41	176	Ankyrin repeats	Ankyring repeats signal peptide 1-22	1-20TM	-0.067
Alvin_1896	-2.167797768	6.99E-19	protein of unknown function DUF177	99.44	184	YceD	none	none	0.329
Alvin_2515	-4.055405065	9.34E-94	hypothetical protein	98.15	202	none	TM (1-22) Coiled-coil (35-55 & 126-160)	TM (7-26)	-0.902
Alvin_0499	-2.18866098	1.16E-14	hypothetical protein	98.25	277	none	TM (16-34) coiled-coil (211-238)	TM (13-35)	-0.325
Alvin_0746	-2.150323876	4.29E-10	hypothetical protein	41.43	381	Putative MetA	signal peptide (1-31) coiled-coil (41-61)	TM (12-34)	-0.152

Table 0-9 Expression of Rubisco genes in FeS, NiS and negative control

	NiS		FeS		NEG		
	log2FC	Padj	log2FC	Padj	log2FC	Padj	Annotation
Alvin_1365	-3.00554	3.14E-20	-3.13352	7.34E-22	-3.61826	5.59E-29	Rubisco large subunit
Alvin_1366	-3.28575	7.89E-24	-2.88041	1.88E-18	-2.42851	2.21E-13	Rubisco large subunit
Alvin_2545	0.076773	0.9102	-0.64058	0.255647	-0.33946	0.591298	Rubisco small subunit
Alvin_2749	0.528408	0.591445	0.536256	0.599362	1.344067	0.11582	Rubisco small subunit
Alvin_2750	1.482846	0.007065	1.357515	0.018632	1.132088	0.058904	Rubisco-like protein

Table 0-10: This table presents the transcriptome analysis of FeS, highlighting the expression of genes related to carotenoid photosynthetic pigments and RubisCo, which is associated with the carbon fixation of carbon dioxide.

	FeS		NEG	
	log2FC	Padj	**log2FC**	Padj
Carotenoid genes				
Alvin_1182	-0.53384	0.176606	-0.59267	0.130041
Alvin_1183	-0.59113	0.266203	-0.87452	0.081364
Alvin_2556	0.203823	0.824421	0.731031	0.360703
Alvin_2561	-0.56101	0.116528	-0.60523	0.090463
Alvin_2562	-0.30297	0.26393	-0.93617	3.79E-05
Alvin_2563	-0.34477	0.277753	-0.3656	0.246537
Alvin_2638	-1.16827	0.078172	-0.54764	0.476026
Alvin_2639	-1.2673	0.025327	-0.65211	0.304761
Alvin_2640	-1.05481	0.026595	-0.78373	0.120189
Alvin_2641	-0.47265	0.399694	-0.13044	0.846393
Alvin_2642	-0.32715	0.648024	0.019173	0.983665
Alvin_2643	-0.32516	0.678	0.256851	0.759158
Alvin_2564	-0.30298	0.456328	0.439109	0.252448
Alvin_2565	-0.54524	0.0536	0.074591	0.844777
Alvin_2566	1.507832	0.000491	0.853465	0.075561
Alvin_2567	0.62748	0.212876	0.642328	0.20456
Alvin_2568	-0.11427	0.897623	1.19522	0.060306
Alvin_2569	-1.17484	0.246855	0.523737	0.658284
Alvin_2570	-1.12361	0.191021	-0.16309	0.882999
RubisCo genes				
Alvin_1365	-3.13352	7.34E-22	-3.61826	5.59E-29

Alvin_1366	-2.88041	1.88E-18	-2.42851	2.21E-13
Alvin_2749	0.536256	0.599362	1.344067	0.11582
Alvin_2750	1.357515	0.018632	1.132088	0.058904

Table 0-11 This table presents the transcriptome analysis of NiS, highlighting the expression of genes related to carotenoid photosynthetic pigments and RubisCo, which is associated with the carbon fixation of carbon dioxide.

	NiS		**NEG**	
	log2FC	Padj	**log2FC**	Padj
Carotenoid genes				
Alvin_1182	-0.38433	0.332795	-0.59267	0.130041
Alvin_1183	-0.71651	0.137245	-0.87452	0.081364
Alvin_2556	1.463517	0.031261	0.731031	0.360703
Alvin_2561	-0.76922	0.019255	-0.60523	0.090463
Alvin_2562	-0.41132	0.091901	-0.93617	3.79E-05
Alvin_2563	-0.35918	0.225394	-0.3656	0.246537
Alvin_2638	-1.11731	0.08037	-0.54764	0.476026
Alvin_2639	-1.08303	0.051056	-0.65211	0.304761
Alvin_2640	-0.82348	0.080846	-0.78373	0.120189
Alvin_2641	-0.01882	0.978544	-0.13044	0.846393
Alvin_2642	0.12132	0.876559	0.019173	0.983665
Alvin_2643	0.156895	0.850238	0.256851	0.759158
Alvin_2564	0.161518	0.706401	0.439109	0.252448
Alvin_2565	-0.54572	0.04348	0.074591	0.844777
Alvin_2566	1.477827	0.000523	0.853465	0.075561
Alvin_2567	0.575332	0.232003	0.642328	0.20456
Alvin_2568	-0.16812	0.838281	1.19522	0.060306
Alvin_2569	-0.16624	0.89189	0.523737	0.658284
Alvin_2570	-0.21611	0.838681	-0.16309	0.882999
RubisCo genes				
Alvin_1365	-3.00554	3.14E-20	-3.61826	5.59E-29
Alvin_1366	-3.28575	7.89E-24	-2.42851	2.21E-13
Alvin_2749	0.528408	0.591445	1.344067	0.11582
Alvin_2750	1.482846	0.007065	1.132088	0.058904

Table 0-12 d-spacing values of high-resolution transmission electron microscopy metal sulfide samples

Py_AV	FeS_AV (FOV1)	FeS_AV (FOV2)	FeS_CONTROL (FOV_1)	FeS_CONTROL (FOV_2)	NiS_AV (FOV1)	NiS_AV (FOV2)	NiS_CONTROL
				d-spacing			
0.74389	1.61856	1.62779	1.22565	0.97769	1.45704	1.00076	1.63735
0.80705	1.76187	1.74471	1.55174	1.22123	1.59654	1.13086	2.76862
0.83870	1.87934	1.84674	1.95537	1.39785	3.03183	1.24727	
0.89570	2.11425	2.10528	2.48736	1.54466	3.84809	1.46231	
0.97210	2.21098	2.46712	2.77279	1.94414	3.53117	1.60785	
1.02760	2.46919	2.72234		2.39916		3.02908	
1.11820	2.77278	3.18981		3.25270		3.60912	
1.23980	3.25270	5.54021					
1.30110	5.63801						
1.49428							
1.89401							
2.25125							
2.57280							
4.44400							

Vita

Hugo Alarcón Valenzuela was born in Mexico City and came to the United States for the completion of superior education. Their basic education from elementary to high school was completed in Ciudad Juarez, Chihuahua. With bachelor's in microbiology and a Master of Science in Chemistry graduate from UTEP, he completed his thesis on "Study of coordination complexes as DNA carriers for their use in the improvement of gene therapy and vaccination."

Hugo's research experience spans several significant projects, spanning ten years working in Chemistry, Geomicrobiology and Health Science laboratories. Until recently served as a Research Assistant at the University of Texas at El Paso, working on a Geomicrobiology project studying Purple Sulfur Bacteria and elucidating their interaction mechanisms with solid sulfide substrates that culminated in this dissertation. He also served as a Research Assistant in the Chemistry Department and the Health Sciences Department at UTEP, where he conducted extensive work on the synthesis, purification, and spectral characterization of coordination complexes as transfection agents in eukaryotic cells, in vitro and in vivo, for their use as gene vaccine carriers.

His list of publications showcases his valuable contributions to scientific advancements. Notable manuscripts include "Alkyl length effects on the DNA transport properties of Cu (II) and Zn (II) metallovesicles: an in vitro and in vivo study," "Current and emergent analytical methods for monitoring the behavior of agricultural functional nanoparticles in relevant matrices: a review," "Interaction of Sulfate-Reducers with Hydrous Sulfate Minerals in Water-Restricted Terrestrial Gypsic Settings: Implication for the Habitability of Martian Gypsic Environments," and "Simultaneous insight into dissolution and aggregation of metal sulfide nanoparticles through Single-Particle Inductively Coupled Plasma Mass Spectrometry." Additionally, Hugo is on a manuscript titled "Autotrophic Growth of Purple Sulfur Bacteria Enabled by Solid-Phase Metal Sulfide as Sulfur and Electron Donor Source," which is currently under review in Frontiers in Microbiology. Moreover, Hugo Alarcón Valenzuela is listed as a co-inventor on patent: "Rapid Gene Sensors from Carbon Nanotube-DNA Systems," registered in 2017.

As an accomplished educator, Hugo has valuable teaching experience, with a commendable dedication to each institution. He served as a Medical Laboratory Instructor at Southwest University for four years, from January 2015 to December 2018. During this time, he taught a range of courses, including Anatomy & Physiology, General Biology, General Chemistry, Microbiology, and Clinical Microbiology, contributing significantly t the students' learning experiences. Before his successful stay at Southwest University, Hugo served as a Chemistry Professor at El Paso Community College for five years, from January 2013 to December 2017. Throughout these five years, he brought his expertise to the Chemistry department, teaching laboratory and classes as a part-time instructor. His commitment to educational excellence was evident in his contributions to the development of the first printed laboratory manual for the college, enhancing the learning resources available to students.With his academic achievements, diverse research experience, and valuable teaching background, Hugo Alarcón Valenzuela is a committed and knowledgeable Science Researcher, well-equipped to contribute significantly to various scientific endeavors. For contact, please reach out via email at hvalarcon@miners.utep.edu.